FORMATION FLIGHT CONTROL FOR AERIAL REFUELING

THESIS

Steven M. Ross, Captain, USAF

AFIT/GAE/ENY/06-M35

DEPARTMENT OF THE AIR FORCE
AIR UNIVERSITY

AIR FORCE INSTITUTE OF TECHNOLOGY

Wright-Patterson Air Force Base, Ohio

AFIT/GAE/ENY/06-M35

FORMATION FLIGHT CONTROL FOR AERIAL REFUELING

THESIS

Presented to the Faculty

Department of Aeronautics and Astronautics

Graduate School of Engineering and Management

Air Force Institute of Technology

Air University

Air Education and Training Command

In Partial Fulfillment of the Requirements for the

Degree of Master of Science in Aeronautical Engineering

Steven M. Ross, BS

Captain, USAF

March 2006

AFIT/GAE/ENY/06-M35

FORMATION FLIGHT CONTROL FOR AERIAL REFUELING

Steven M. Ross, BS
Captain, USAF

Approved:

/signed/
_____ 2 Feb 06
David R. Jacques (Co-Chairman) Date

/signed/
_____ 2 Feb 06
Meir Pachter (Co-Chairman) Date

/signed/
_____ 2 Feb 06
Brian Kish (Member) Date

Abstract

A controller is designed for an aircraft to autonomously fly formation during aerial refueling. Requirements for a refueling autopilot are stated. A six-degree-of-freedom model is developed for an F-16 lead aircraft and a Learjet LJ-25 wing aircraft. Bare airframe stability of both aircraft is investigated, and stability augmentation is performed. A Matlab Simulink® simulation is built to reproduce the sensor inputs that will be available to the wing aircraft in flight, including disturbances. Control frames are investigated to determine the optimum presentation of the error vector for control during the task of air refueling. Control laws are developed from the initial premise of proportional-plus-integral control on position error only, and made more complex until desired performance is achieved.

Tanker flight profiles are designed for the lead aircraft, and simulations are accomplished to estimate controller performance. Stability and robustness are investigated through the addition of noise, turbulence, and time delays while exploring the capability limits during increasingly aggressive profiles.

Modifications for flight test are described, and flight test results are reviewed from 7 formation flights of a USAF C-12 and a Learjet LJ-25 under fully autonomous control in an operationally representative refueling environment. Actual controller performance is analyzed and compared to predictions, and suggestions are made for future controllers.

To my wife, thanks for your amazing patience.

Acknowledgments

The scope of what was accomplished in this work far exceeded my own vision, and would not have been possible without the patient instruction of many along the way. I would like to express my sincere appreciation to my faculty advisors, Dr. David Jacques and Dr. Meir Pachter for their advice at key points, and for the learning experience of being allowed so much latitude in decision making along the way. Thank you for your trust, even if I didn't think I merited it at the time. I would also like to thank Dr. Brad Liebst, for the knowledge of the industry passed along and my instruction in aircraft control from the ground up.

A special note of thanks is due to Dr. John Raquet, who first introduced the concept to me as a thesis, and who was the supplier of everything GPS related for the project. I am indebted to the patient instruction and mentorship you and your family have provided, inside the classroom and out.

On the flight test side, I would like to acknowledge the instruction and experienced eye of Mr. Russ Easter of Calspan, who pointed me in the right direction several times to get the controller adapted to the Learjet, and was a source of sound advice and leadership throughout the program.

Most importantly, I would like to acknowledge my God and creator, and my wonderful wife, who both provide constant help in all things, both great and small. I am indebted to them for the love and patience shown to someone who learns life's most important lessons so slowly.

Steven M. Ross

Table of Contents

Page

Page

Page

List of Figures

Page

Page

Page

Page

List of Tables

Table Page

List of Symbols

Symbol	Definition
$\mathbf{A}$, $\mathbf{A}_{lat}$, $\mathbf{A}_{long}$	Stability Derivative Matrices
b	Wing Span
$\mathbf{B}$, $\mathbf{B}_{lat}$, $\mathbf{B}_{long}$	Stability Derivative Matrices
C_D	Coefficient of Drag
C_l	Rolling Moment Coefficient
C_L	Coefficient of Lift
C_m	Pitching Moment Coefficient
C_n	Yawing Moment Coefficient
C_Y	Coefficient of Side Force
$\bar{c}$	Mean Aerodynamic Chord
da_c	Commanded Wing Aircraft Aileron Deflection
de_c	Commanded Wing Aircraft Elevator Deflection
dr_c	Commanded Wing Aircraft Rudder Deflection
dxl_c, dxr_c	Commanded Wing Aircraft Thrust, Left, Right
deg	Degrees
$\mathbf{F}$, F_x, F_y, F_z	Force Vector
ft	Feet
g	Gravitational Constant

Symbol	Definition
h, h_L	Altitude, Lead Altitude
Hz	Hertz
H	Angular Momentum Vector
I_{xx}, $I_{yy,}$ I_{zz}, I_{xy}, I_{xz}, I_{yz}	Mass Moment and Products of Inertia
k	Gain (subscript denotes which one)
L	Scale Length
L	Aerodynamic and Thrust Moment, x-body axis
$L_p, L_r, L_v, L_\beta, L_{\delta a}, L_{\delta r}$	Lateral Stability Derivatives
m	Mass
M	Aerodynamic and Thrust Moment, y-body axis
M	Moment Vector
M_u, $M_{w,}$ $M_{q,}$ $M_{\dot{w}}$, $M_{\delta e}$	Longitudinal Stability Derivatives
N	Aerodynamic and Thrust Moment, z-body axis
$N_p, N_r, N_v, N_\beta, N_{\delta a}, N_{\delta r}$	Lateral Stability Derivatives
p	Roll Rate
q, q_L	Pitch Rate, Lead Pitch Rate
$\bar{q}$	Dynamic Pressure
r	Yaw Rate
r	Inertial Position Vector
s, sec	Seconds
S	Wing Area

Symbol	Definition
t	Time
u	Velocity, x-body axis
v	Velocity, y-body axis
$\mathbf{v}$	Velocity Vector
$\mathbf{v_c}$	Velocity Vector at the Center of Mass
vel_L	Desired Lead Velocity
V_T	Velocity, True Airspeed
w	Velocity, z-body axis
W	Airframe Weight + Fuel
x_b, x_f , $x_{NED,}$ x_1	Longitudinal Aircraft Axis (subscript denotes frame)
x_e	Position Error, Longitudinal Axis
$\mathbf{x}, \mathbf{x_{lat}}$, $\mathbf{x_{long}}$	Longitudinal State Vector
X	Force, x-body axis
X_u, X_w	Longitudinal Stability Derivatives
y_b, y_f , $y_{NED,}$ y_1	Lateral Aircraft Axis (subscript denotes frame)
y_e	Position Error, Lateral Axis
$Y_p , Y_r , Y_\beta , Y_{\delta a} , Y_{\delta r}$	Lateral Stability Derivatives
z_b, z_f , $z_{NED,}$ z_1	Vertical Aircraft Axis (subscript denotes frame)
z_e	Position Error, Vertical Axis
Z_u, Z_w, $Z_{\delta e}$	Longitudinal Stability Derivatives

Symbol	Definition
α, α_L	Angle of Attack, Lead
α_{Turb}	Random Disturbance in Angle of Attack
β	Angle of Sideslip
γ	Flight Path Angle
δa_{L_cmd}	Commanded Lead Aileron Deflection
$\delta e_{L,} \delta e_w$	Elevator Deflection; Lead, Wing
$\delta e_{L\_cmd,} \delta e_{w\_cmd}$	Commanded Elevator Deflection; Lead, Wing
δr_{L_cmd}	Commanded Lead Rudder Deflection
$\delta_{T\_L\_cmd}$	Commanded Lead Throttle Setting
δ_{T_L0}	Lead Equilibrium Throttle Setting
Δ	Perturbation Value
ε	Zero Mean, Unity Covariance White Noise
ζ	Damping Ratio
$\boldsymbol{\eta}_{\mathbf{lat}}$, $\boldsymbol{\eta}_{\mathbf{long}}$	Control Vectors
θ, $\theta_{L,} \theta_w$	Pitch Angle, Lead Pitch Angle, Wing Pitch Angle
ρ	Density
σ	Turbulence Intensity Constant
φ, φ_L, φ_{L_cmd}	Roll Angle, Lead Roll Angle, Commanded Lead Roll Angle
ψ, ψ_L , ψ_w	Heading Angle, Lead Heading Angle, Wing Heading Angle
ψ_{L_est}	Estimated Lead Heading Angle
$\boldsymbol{\omega}$	Angular Velocity Vector

List of Abbreviations

Abbreviation Page

Abbreviation Page

FORMATION FLIGHT CONTROL FOR AERIAL REFUELING

I. Introduction and Overview

Motivation

The subject of automated air refueling (AAR) has multiple applications that will be used in future developments of the United States Air Force. It is conceivable that all types of air-refuelable aircraft will someday have a refueling mode installed on their autopilot, but the short-term applications center around unmanned aerial vehicles (UAVs) such as the Joint Unmanned Combat Air System (J-UCAS). Development of unmanned combat systems is a high priority for the Air Force, and the ability to refuel will be imperative for its mission accomplishment. The Air Force Research Laboratory (AFRL) has been developing a control system for AAR since 2003 [1].

Automated air refueling capability will greatly enhance the effectiveness of future unmanned vehicles. Force projection capability for the Air Force will be improved in speed, attainable distances, and the number of staging destinations in deployed locations that are suitable for employment of unmanned systems. AAR will also increase airborne flexibility, range, and station time, critical factors in all extensive air campaigns.

Pilot fatigue is currently a major planning factor and limitation of US global strike capability. For 24 hour operations such as covering the No-Fly Zone over Iraq in

OPERATION NORTHERN WATCH and OPERATION SOUTHERN WATCH, pilot rotation required extensive manpower and equipment with a fragile, complicated work cycle. The Air Force is developing technologies to have fewer pilots airborne at any one point in time, each armed with several unmanned wingmen. This greatly eases the task of supporting 24 hour operations. Future situations that require a show-of-force or defensive stance, such as unrest across North Korea, could quickly require such air coverage again. Offensive missions will be greatly enhanced as well, especially in light of today's emerging target capability mindset. Future attack assets need to be on station for unknown periods waiting for time-critical taskings. Autonomous air refueling will provide that capability by greatly extending the endurance of future UAVs, a valuable force multiplier.

Previous Research

In its simplest form, a formation flight controller must start by receiving information about an aircraft's actual position relative to a lead aircraft. The controller must then derive the desired position to fly to--again, relative to the leader. This position may change from time to time, or may even be fluid, depending on the purpose of the controller. For air refueling, the primary position is below and behind the tanker, as shown in Figure 1. Lastly, a formation flight controller must generate commands to minimize the difference between the actual and desired positions. Several research groups are currently attempting to solve pieces of the problem. None of the research studied dealt with the specific task of air refueling, but this is merely a subset of

formation control. Some previous work did address the very similar problem of formation flight control at close ranges.

Figure 1. F-15Cs Refueling from a KC-135

Previous AFIT Thesis Work

The Air Force Institute of Technology (AFIT) has a long history of thesis research that focuses on some or all of the functions of a formation flight controller. Early theses worked with extremely simplified aircraft models which were restricted to move only in certain axes. Each new thesis brought fresh perspective on the problem, and increased the complexity and fidelity of the aircraft modeling. The research has continued to develop and expand into this thesis, which culminated in the first ever completely autonomous formation flight that was flown close enough, and controlled well enough, to perform air refueling. The AFIT research leading up to this accomplishment started 15 years ago with the work of Rohs.

In 1991, Rohs began what became a series of theses on control algorithms designed to be used on C-130s or HH-53s for Special Operations Forces (SOF). Several theses followed, the driving concept being a minimization of pilot workload in intensive situations, such as night formation low-level sorties in the weather. Each simulated wing aircraft was assumed to have perfect knowledge of their relative position from lead, and an autopilot capable of matching a commanded flight path was assumed. Simplified, first order, planar models of aircraft were used and loose formation positions (the closest being 500 feet away) were simulated [19]. Dargan continued the work by using a proportional-plus-integral (PI) controller to ensure zero steady state position error as the wing aircraft loosely followed the leader through turns or changed wide formation positions [4]. In 1992, Buzogany stepped the research up to include second order aircraft models, and added the freedom to change the wing aircraft's altitude, though to this point the lead aircraft still performed changes of heading and airspeed only. For this and each prior controller, when the lead aircraft turned, the wingman sought to hold position 500 feet aft and 500 feet either inside or outside of the turn with a large change in airspeed. Buzogany attempted to minimize the required throttle excursions by allowing the wingman to vary altitude in order to change speed, but did not track the lead aircraft's altitude or velocity changes [3].

In 1994, Reyna added the knowledge of the lead aircraft states by incorporating heading error and velocity error into the wing aircraft's controller. Using the first-order models, he enabled the controller to minimize specific energy excursions as the wing aircraft changed altitude to assist in velocity control [18]. Veth expanded that research

with the second order models and used a decomposition of the energy problem to further optimize energy tracking, in addition to introducing a circular path autopilot to fly around a fixed point [24]. The last in the long line of C-130 formation research was McCamish, who investigated a new control law that fed the lead's velocity forward, without heading information, alleviating some rate saturation effects on the wing aircraft [10].

In 1999, Proud changed the direction of the research. He initially used the C-130 model with Dargan's controller, but moved the wing aircraft into a close formation (60 feet aft, 32 feet to the side) in order to reduce fuel consumption by flying in the upwash of the wingtip wake vortex. Proud showed that the gains selected by the previous authors were inadequate for close formation control, and adjusted them before applying the same controller to a simple F-16 model [16].

Hall continued Proud's research toward minimization of fuel flow. Hall developed a controller around a point-mass model (no moments of inertia considered), in coordinated flight (no sideslip permitted). The models were still simple, and Hall controlled with thrust, lift, and roll rate instead of going the next step of finding the actual control surface positions required to achieve the requested forces and rotation. Hall created a proportional-plus-integral-plus-derivative (PID) control law on position error (3-axis), adding a second derivative on separation error and a proportional heading error to his roll rate command to compensate for the dynamics of the lateral maneuvers. His controller was simulated in close formation during 15 degree bank turns and held position in simulation to within 9 feet [8].

Osteroos used Hall's research as a stepping stone toward a new controller, and attempted the dramatic next step of actually implementing it in a formation flight test with the Variable-Stability In-Flight Simulator Test Aircraft (VISTA) F-16 following a lead aircraft. Osteroos modified Hall's controller by adding the ability to control angle of attack (α) and angle of sideslip (β) instead of lift [13]. Because the premise of the thesis was formation control for fuel savings, his formation position was in the upwash of the lead's wingtip vortex. Commanding α and β gave him the ability to either crab or slip into the wind of the modified airflow. Osteroos modified the control laws to effectively follow the lead aircraft during close formation by matching the lead aircraft velocities in each direction. The thrust control law was PI control on forward-aft position error and velocity error. The angle of attack control law was PI control on vertical error and vertical flight path error. The roll rate control law was PI control on lateral separation error and velocity vector roll angle error. The control law for sideslip was a complex function designed to limit the use of the rudder to situations where the wing aircraft was nearly in position and the heading error was small [13].

Moving from theory and simulation to flying actual hardware is a huge step. Osteroos had planned on controlling α and β, but these were not available options in the stability computer of the VISTA F-16. An external autopilot had to be built around the control laws to command pitch angle, bank angle, and velocity. Inner loops of control also had to be built to stabilize the F-16. Osteroos planned on using the lead aircraft bank angle for feedback into his controller, but that parameter was not available in real-time. In the end, the project was changed into a single ship flight test, following a simulated

lead aircraft. As happens in all of flight test, Osteroos was plagued with problems. Datalink dropouts unfortunately ruined many of his attempted maneuvers. A missed aircraft position update at the high speeds of flight test leads to instant, large position errors being fed into the controller. Wind effects are typically strong at higher altitudes and were experienced by the real aircraft, but not the lead model. Osteroos used the velocity vectors for damping, and the differences caused by the wind made stable control impossible unless aligned to negate its effects [14].

The maneuver attempted by Osteroos that was most similar to those performed in this thesis was a turn for 30 degrees of heading change with a heading rate of about 1 to 1.5 degrees per second. Ignoring the attempts with obvious problems, the maximum position errors ranged between 50 and 132 feet in each axis direction for this maneuver [14]. To his credit, Osteroos made the first attempt at fully autonomous close formation flight, and several of his lessons learned were heeded for this research.

On the theoretical side, Osteroos used a completely different paradigm of control than was selected for this research. Osteroos worked in the wing wind axis frame, moving the wing aircraft until the lead aircraft was located at a desired position that was defined *relative to the wing aircraft.* This is the opposite of the fundamental perspective of this research, which sought to move until the wingman reached a desired position relative to the leader. One of the most positive aspects of Osteroos' approach was noise rejection. With Osteroos' technique, variations in lead attitude have no impact on the position the controller is attempting to fly to, theoretically eliminating all noise from the

lead aircraft's attitude sources. In reality, most of the noise from those sources was eliminated, but Osteroos ended up needing lead bank angle and roll rate for control.

The downsides of Osteroos' approach are in the form of steady state errors in position and overall difficulty of control. The control laws were of a balancing nature, and position error was balanced with velocity error. If either was not zero, control was applied until the sum was zero. For straight and level flight, this is very effective, but in turning flight, the turning radius is different for the lead and wing aircraft. The result is a steady state error in velocities if the two aircraft stay together. This velocity error could not be held to zero without dropping aft if outside of the turn. The controller then balanced the errors by accepting a steady state position error in the opposite direction. The difference in bank angles during turns led to the same problem in lateral position error. If precise positioning was critical, such as during air refueling, a continuously computing trim function or set of look-up tables would have been required to inject a compensation term into the desired wingman position algorithm to truly fly the correct position.

Other Research

Outside of AFIT, formation flight control is also an item of interest. The National Aeronautics and Space Administration (NASA) Dryden Flight Research Autonomous Formation Flight project demonstrated semi-autonomous station keeping capability with two F/A-18 research aircraft. Blended inertial navigation system (INS) and global positioning system (GPS) measurements sent across a data link gave the wing aircraft a

position error signal. A control frame was defined to avoid the inevitable problems with inaccuracies and noise on the lead aircraft's attitude measurements [9].

The trail aircraft determines where to fly based on the attitude of the lead aircraft. As the lead aircraft maneuvers, so does the desired formation position. With the large lever arm of wider formations, small changes in the lead aircraft attitude can have a large impact on the location that the wing aircraft is trying to fly to. The control frame used by NASA did not rotate automatically with the lead aircraft, but was level with the ground and steered in heading between straight test runs by a flight test engineer (FTE). This technique eliminated any undesired motion in the desired position that could be caused by sensor noise from the lead aircraft's attitude indicator, but at the cost of not holding formation geometry when the lead aircraft rolled into bank. In addition, the controller was not capable of turning away from the initial course, but did accomplish small "s" turns around the heading set by the FTE. The NASA controller was also not fully automated. The heading of the lead aircraft had to be manually set, and the throttle channel of the trail aircraft was also manually controlled by a pilot. The remaining control was accomplished automatically via PID control on position and velocity error with normal acceleration and bank angle used for damping [9].

In more current research, two Boeing X-45A aircraft achieved the first unmanned formation flight in August of 2004. Both aircraft followed commands generated by a simulated leader. These tests, and several follow on tests, were done at a range greater than a mile [5]. The flight control algorithm required to fly at the close range of air

refueling is fundamentally different, but the requirement to be capable of it is on the near horizon.

Besides NASA and AFIT, the Air Force Research Laboratory is also currently investigating the automated air refueling for J-UCAS development. The program has a high level of attention with several corporate partners and a 30 million dollar budget, and has been under development since 2003 [1]. Like this research, AFRL is planning on using a differential GPS (DGPS) for position awareness, and they are investigating supplementing that with an optical sensor for additional position and rate feedback. The Naval Air Systems Command is developing the GPS technology, while Northrop is investigating the sensor-based positioning approach and Boeing is working the control laws. Pilot-flown test flights have been accomplished to investigate optical sensor reception as well as horizon shielding of the GPS antenna on the receiver aircraft by the tail of the tanker. Though only linked in purpose, the core difficulty of AFRL's program is the same problem investigated in this research. According to the AAR program manager, "The technical focus of the program is how you do close formation flight. That's the hardest problem we're dealing with" [1].

Lessons from Previous Research

The results of previous research on the subject of formation flight control shaped the direction of this thesis in one manner or another. Most notably, this research took a different direction to attack the problem of formation control than the recent work of Osteroos. The fundamental control frame perspective and top tier command strategy were completely changed. This will be shown to solve some of Osteroos' control

challenges, but at the cost of potential noise difficulties explained in Chapter III. The lessons about the difficulties of real aircraft integration were heavily heeded. The simulator built for this thesis contained the exact controller that was used in the test aircraft. The controller was built for only one specific aircraft with its stability derivatives and flight characteristics, and the bare airframe was stabilized by the controller. The signals for the controller in simulation traveled the full path, from the exact format of inputs all the way through to the degrees of control desired for each control surface. These efforts eliminated the requirement for the late addition of inner and outer loop autopilots.

Another lesson heeded was the critical nature of simulator fidelity in reducing the number of flight test surprises. The simulator was built to mirror all of the disturbances that were known to exist before flight test as faithfully as possible, including considerations such as sampling problems specific to this system, noise, turbulence, time delays, and actuator rate limits. The aircraft models used in simulation were also as complete as possible, including non-linear effects and six degrees of freedom. Lastly, several of the concepts of control frames, an idea expanded in Chapter IV, were taken from previous research, including the wing wind frame used by Osteroos and the formation frame used by NASA. These were not ultimately used, but they provided valuable lessons in control. Control law concepts were experimented with that reflected some of the early AFIT work on wide formation control, as well. Each author that was studied contributed toward the achievement of fully autonomous close formation flight. This effort undertook the goal of moving the research forward to actually autonomously

controlling a real aircraft in close formation well enough to perform the task of air refueling.

Air Refueling Problem Statement

To accomplish the mission of air refueling, a controller must have the capability of autonomously holding three formation positions relative to a tanker within narrow position tolerances during operationally representative maneuvers. The maneuvers are simple, including straight and level flight, and relatively benign turns. The controller must also be able to change between the three positions autonomously at the request of a pilot or UAV commander at any point in the maneuvering. The remaining elements of refueling, including the rejoin to and departure from the tanker were not considered. The controller was designed to be integrated into a specific test aircraft and flown in formation in the context of a Test Management Project at the Test Pilot School (TPS) with constraints of a limited budget and compressed flying window.

Formation Positions.

The three standard formation positions for air refueling are contact, pre-contact, and wing observation, and are shown in Figure 2. The separation requirements for each position are defined in the tanker body frame, where the x-axis runs from the center of gravity (cg) through the nose of the tanker, the z-axis orthogonally through the floor of the tanker, and the y-axis orthogonal to both, in the direction of the right wingtip.

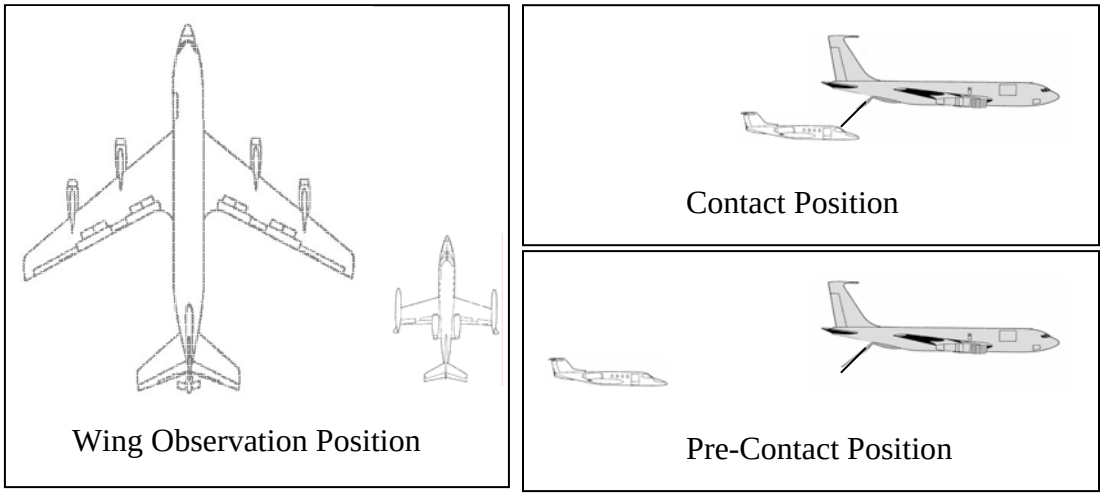

Figure 2. Required Refueling Formation Positions

The distances for the required positions were calculated from a proposed rear GPS antenna on a KC-135 tanker, which sits just forward of the tail on the upper surface of the empennage, to the proposed location of the central GPS antenna on the J-UCAS. The distances were adjusted only slightly when applied to the flight test aircraft, a USAF C-12 and a Calspan LJ-25 Learjet. Obviously, with the smaller test aircraft, the distances between the antennae could have been decreased slightly, but were maintained for realism. The level of effort required to maintain the geometry of the formation and the impact of sensor noise actually increase with formation range if the performance tolerances remain the same. Therefore, the distances for the formation positions were retained as a better test of controller capability. The perspective of the wing aircraft in the contact position is shown in Figure 3, and a view from the lead aircraft with the Learjet in the wing observation position is shown in Figure 4.

Figure 3. View of Lead Aircraft from Contact Position

Figure 4. Receiving Aircraft in Wing Observation Position

The formation positions actually flown and simulated are defined in Table 1, and this formation geometry was held constant with respect to the simulated tanker during all maneuvers.

Table 1. Formation Position Offsets Between GPS Antennae

Formation Position	X-Axis Offset (ft)	Y-Axis Offset (ft)	Z-Axis Offset (ft)
Contact	-26	0	31
Pre-Contact	-85	0	40
Wing Observation	-15	112	6

Tolerances.

There are no objective safety limits of deviation from each position. Instead, acceptable formation position deviation is subjective and varies with the potential for collision. For instance, in the pre-contact position, well aft of the tanker and other receivers, there is wide latitude for excursion in the lateral and vertical directions, but the longitudinal channel should be controlled in a manner that does not approach the boom without clearance. Conversely, in the wing observation position, very little room for position error is available laterally without danger of collision with the tanker or other receivers on the tanker's wing, but no close danger exists longitudinally. To meet all requirements without an exhaustive list of acceptable tolerances, a tight design goal of no more than 10 feet of position error in any direction during all maneuvers was set for this research. This goal was applied whether collision potential existed or not, as an overall goal of precise formation station keeping capability. In the contact position, 10 feet is not tight enough, and the station keeping goal was further restricted based on the well defined limits of the refueling boom envelope, shown in Figure 5.

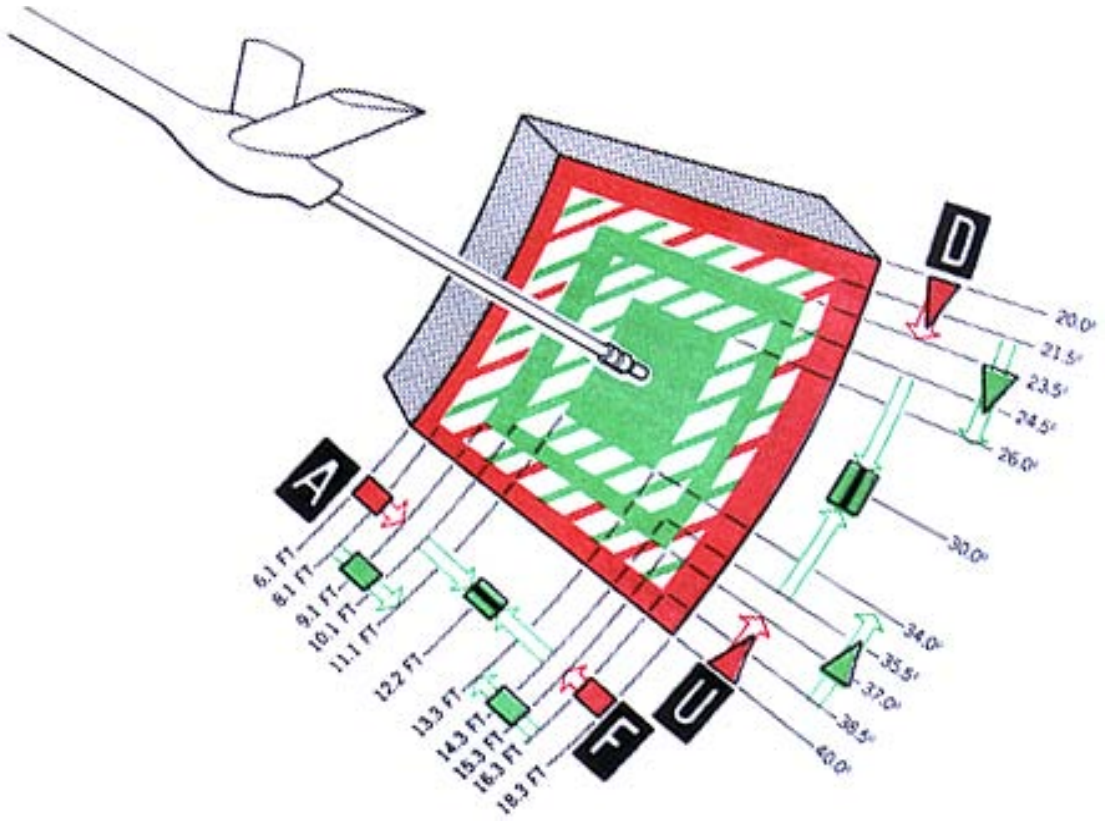

Figure 5. Boom Envelope Limits

In practice, experienced pilots seldom exceed the boom envelope limits. Pilots who are inexperienced, however, will likely exceed them as they are learning, and will continue to from time to time, especially when faced with challenging circumstances such as turbulence, reduced visibility, darkness, or fatigue. The boom envelope does not represent a safety limit, but a desired performance goal. When an aircraft approaches boom envelope limits, the refueling receptacle is automatically or manually disengaged until the aircraft is again inside the boom envelope. Once reasonably stable, the boom operator reestablishes the connection between the aircraft.

For actual boom limit ranges, the X-Z plane in the tanker body axis is shown in Figure 6 with the sign of the axes reversed to generate a side view.

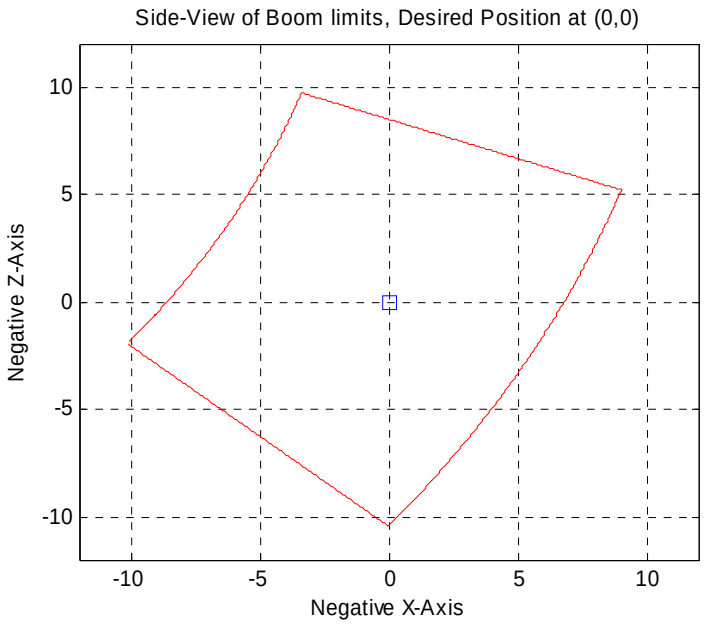

Figure 6. Side View of Boom Limits

The top view is shown in Figure 7. The distances in Figure 7, however, are measured in the boom plane, and then projected into the horizontal X-Y plane, so it can be later compared with position errors of the wing aircraft. As can be seen in Figure 6, there is no simple representation for X-Y front-aft limits, which change based on the height of the boom. The simple average projection method selected is more restrictive in the front-aft distances when the wing aircraft is in the heart of the vertical envelope, and less restrictive when the wing aircraft is high or low. As will be shown in the simulation and flight test results, however, the wing aircraft has excellent station keeping capability along the x-axis, so the exact front-aft limits are of little concern.

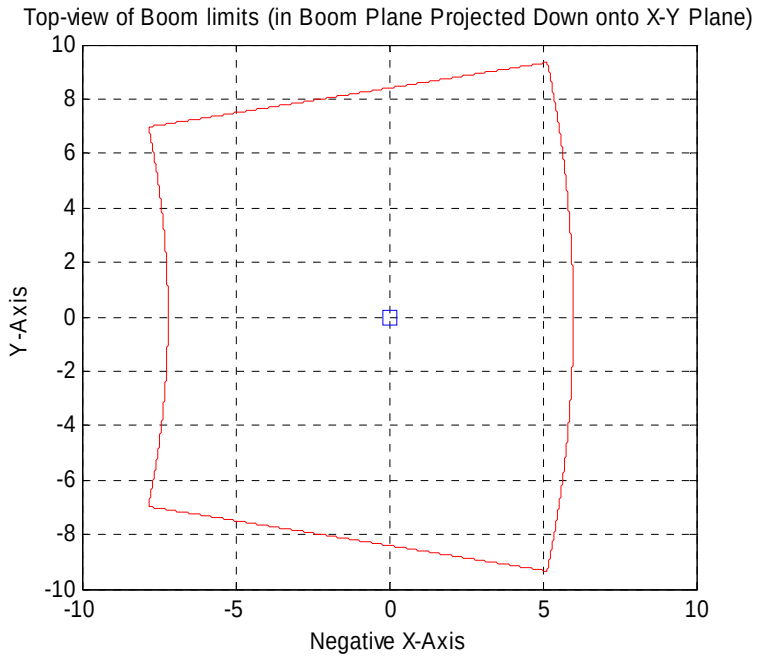

Figure 7. Top View of Boom Limits

Tanker Maneuvers.

The maneuvers required to perform air refueling by the tanker are very simple. The tanker flies a level, constant speed and altitude profile in an oval "race track" pattern, as shown in Figure 8.

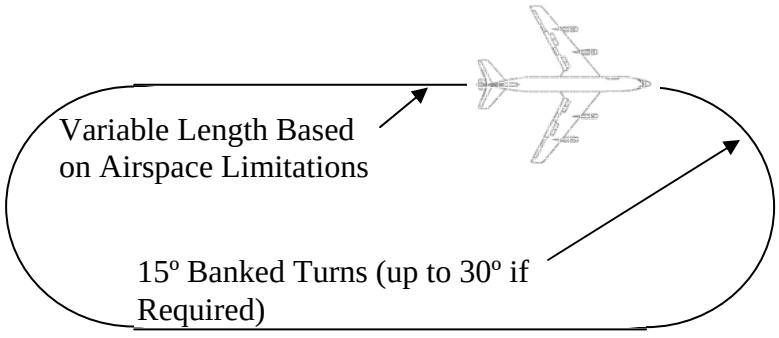

Figure 8. Typical Tanker Pattern

The tanker's turns are planned with 15 degrees of bank, but may be increased to 30 degrees of bank for correction if the airspace changes or other unexpected limitations arise. Therefore, the design point for turning in this thesis was optimized around 15 degree bank turns, but still capable of turns at 30 degrees of bank.

Limitations.

The primary driver of this thesis was the requirement for actual flight test in the context of a test management project (TMP). As such, a large portion of the work was directed beyond just the theory of control, down to the myriad of details that must be worked out in order to integrate that theory into an actual flying hardware system. This system had to accommodate a specific platform and all of the quirks associated with it. This effort was found not to be trivial. Several of the integration techniques and lessons that were not specific to the test aircraft are presented in this work to assist future designers that will undoubtedly be faced with the same problems to solve. As a further consequence of the cost, safety, and equipment availability constraints associated with actually flying a thesis, some design compromises were made up front. The selection of test aircraft drove the two largest design impacts, a simulator limitation and a design point compromise.

The perfect test of the controller would obviously be installed on an unmanned vehicle, but that was not realistic for the scope of the project. The Test Pilot School's VISTA F-16 was planned as a substitute, but this was later changed to the Calspan Lear 2 Learjet (LJ-25), resulting in a redesign of the control system. Likewise, scheduling and

cost constraints precluded the use of an actual tanker for the lead aircraft, as well as considerations of GPS horizon shielding by the tanker's tail, a topic not investigated in this research. Originally, an F-16 was proposed as a surrogate leader. The simulator was therefore designed around an F-16 lead aircraft. Relatively late in the design process, the lead aircraft plan was also changed for monetary considerations, but the model of an F-16 was left as the lead aircraft in simulation as a known limitation. For the actual test, the Test Pilot School's C-12C Huron (Beechcraft King Air) was adopted as a low-cost alternative, and both test aircraft are shown in Figure 9.

Figure 9. C-12 and Learjet in Fully Autonomous Formation Flight, Contact Position

The C-12 could not reach the intended design refueling point of 250 Knots Indicated Airspeed (KIAS) at 20,000 feet Mean Sea Level (MSL). The design point was therefore changed to 190 KIAS at 10,000 feet MSL, a less realistic point, but one in the flight envelope of both the Learjet and the C-12. This change impacted performance in

the simulator, a factor that increased the difficulty of design. The lower speed is in the flap regime for the Learjet, a business jet that is not intended for tight position control even at normal speeds. At 190 KIAS, the Learjet is slightly sluggish, requires larger control deflections to produce desired rates, and the impacts of increased angle of attack such as adverse yaw are magnified. This was not insurmountable, as humans can refuel in much more sluggish aircraft such as tankers and bombers. However, the lags in the system, increased relative moments of inertia, and slower response dictate less performance for the same stability margin than a fighter or potentially a UAV. On the positive side, as a variable stability demonstrator, the Learjet's actuators have a higher bandwidth and higher saturation rates than a production representative Learjet.

General Approach and Thesis Overview

The path to a working flight controller is long and complicated. A simulator must first be created to determine flight control laws. To make the simulator, several different pieces must be independently developed before complete integration. The most basic pieces of the simulator are the individual aircraft models. Chapter II covers the model requirements and the equations of motion behind them. The actual wing aircraft model used in simulation is proprietary, but the basic lead aircraft modeling technique is identical. The work of this thesis may be closely repeated if the same model is used for both aircraft, with the exception of specific stability derivatives.

Once both aircraft models are created, the lead aircraft must be controlled. In actual flight, the lead aircraft is independently controlled by the tanker pilot, but representative profiles must be created for simulations. To be able to command these

profiles, the lead aircraft is first stabilized, and then control laws are built for a autopilot in the simulator. This process is also developed in Chapter II, so that the work performed in this thesis may be fully reproduced.

With a lead aircraft that is ready for simulated flight, and a wing aircraft model awaiting a controller, the next step in development is to create a method to track their relative separation in formation. This process is detailed in Chapter III. The inputs to the controller, DGPS derived relative separation and lead attitude signals, are produced in this tier of the simulator and conditioned with disturbances of noise, turbulence, time delay, and sampling time errors to make them appear to the controller exactly as they would during flight. Each of these disturbances is modeled, and the integration of the individual models to the complete formation simulator is detailed.

When the simulator is developed to this point, investigation of the concept of the type of control desired for the wing aircraft can begin. The question of which control frame to use when presenting position error to the controller is explored in Chapter IV. All of the close formation flight controllers studied prior to this research came up with a different answer to this fundamental question, and this thesis did as well. Each of the control frames are defined, and the most positive and negative aspects of control in each of the frames are found through simulation.

Once a fundamental concept of control has been determined, actual control of the wing aircraft is developed in Chapter V. This includes not only the control laws, but the control questions of wing aircraft stability, desired position assignment, control theory for position changes, and the transfer of control to the refueling autopilot when it is

engaged. Each of these problems is addressed, and the implementation of each of the solutions in the controller is explained in enough detail that they may be re-created for future controllers. Simulations of the controller's performance are presented in Chapter VI.

For flight test, many modifications were required to integrate the entire control system, including attitude and position sensors and a datalink to pass their signals. These modifications are explained in Chapter VII. The software also required several modifications, as hardware failures during flight test necessitated patches and estimators to be built to compensate for information sources that were not working properly. Software filtering requirements were also underestimated in the design of the controller and were worked during the flight test. The results of the flight test are presented in Chapter VIII, and conclusions from the controller's performance are included with the lessons learned for future work in Chapter IX.

II. Individual Aircraft Models

Aircraft Modeling Approach

The goal of a refueling autopilot is to take position and attitude signals from the tanker and to determine appropriate flight control surface deflections and throttle settings to maintain formation flight and change positions in the formation. The decisions on how much control to apply are based on a model of the formation, which consists of the interactions between two independent aircraft models. At the outset of this research, the lead aircraft model simply consisted of a manually created trajectory with constant altitude and airspeed for the wing aircraft to follow. The lead aircraft's attitude was not considered. As the control laws were developed and the wing aircraft could maintain a simple offset during straight and level flight, the lead model grew in complexity to introduce new problems and fidelity.

The model of the formation is inherently non-linear. The entire premise of control rests on maintaining angles and relative motion of aircraft moving and rotating in separate coordinate axis systems. The trigonometry is unavoidable, and multiple transformations are required with angles that are not necessarily small. For the individual aircraft, saturation effects of the throttle and control surface positions and rates must be included for realistic modeling. In addition, the goal of the autopilot is control of an aircraft in a dynamic environment to a level where inches count. Smaller effects that are normally linearized or neglected such as moments of inertia, axis coupling, and nose droop during roll-ins are now significant. As a result, full, non-linear models with six-

degrees-of-freedom were used for both aircraft. In this section, the fundamentals of the models themselves are discussed, and the stabilization and control is developed for the lead aircraft.

The lead aircraft model is an F-16. After the simulator was constructed, the lead aircraft available for the flight test was changed from an F-16 to a USAF C-12 Huron, but with insufficient time to change the model. The fact that the lead model is not a C-12 is a significant limitation. For the benign maneuvers required of the lead aircraft, however—gentle rolls to 15 or 30 degrees of bank while holding altitude—a full model of any aircraft should provide a reasonable flight path and sampling of the coupling problems the wing aircraft will be faced with, if the bank angles and rates are the same.

The model of the wing aircraft, with some small modifications, was supplied by Calspan and is proprietary. The Learjet model does, however, have a high degree of correlation to that used for the F-16 lead aircraft. The basic modeling approach is identical, and the work of this thesis may be faithfully reproduced if the following modeling approach is followed for both aircraft, as long as the individual stability derivatives are maintained.

Six-Degree-of-Freedom Model Development

The computer code for the lead model was developed from the baseline model in Stevens and Lewis [22]. Specific values for stability derivatives, moments of inertia, weight, etc. are retrieved in the main program with table look-ups and can be found in the text. The entire derivation used to create that code from the equations of motion will not

be repeated here, but a sample outline of the logic flow in this entire section is presented from excerpts of Nelson [11] to allow the reader understanding of the concept.

The rigid body equations of motion are obtained from Newton's second law, considering an axis fixed to the Earth to be an inertial reference frame:

$$\Sigma \mathbf{F} = \frac{d}{dt}(m\mathbf{v}) \tag{1}$$

where the vectors for force (**F**) and velocity (**v**) are expressed in the inertial frame.

Considering the airplane as a collection of elements of finite mass, summing all of the elements, and assuming the mass of the vehicle (m) is constant, the force equation can be expressed:

$$\mathbf{F} = m\frac{d\mathbf{v}_c}{dt} \tag{2}$$

where $\mathbf{v}_c$ is the velocity of the center of mass. In order to keep the moments of inertia constant, we allow the body frame of reference (noted with subscript b) to rotate with the aircraft. Adding the Coriolis terms:

$$\mathbf{F} = m\left.\frac{d\mathbf{v}_c}{dt}\right|_b + m(\boldsymbol{\omega} \times \mathbf{v}_c) \tag{3}$$

where angular velocity (**ω**) is defined as:

$$\boldsymbol{\omega} = p\mathbf{i} + q\mathbf{j} + r\mathbf{k}$$

Applying the cross product, expanding to three scalar equations, and adding the effects of the force of gravity in the body axis:

$$(F_x)_{gravity} = -mg\sin\theta \tag{4}$$
$$(F_y)_{gravity} = mg\cos\theta\sin\phi \tag{5}$$
$$(F_z)_{gravity} = mg\cos\theta\cos\phi \tag{6}$$

Yield the force equations:

$$X - mg\sin\theta = m(\dot{u} + qw - rv) \tag{7}$$
$$Y + mg\cos\theta\sin\phi = m(\dot{v} + ru - pw) \tag{8}$$
$$Z + mg\cos\theta\cos\phi = m(\dot{w} + pv - qu) \tag{9}$$

where *u*, *v*, and *w* are velocities, *p*, *q*, and *r* are rotations, and *X*, *Y*, and *Z* are forces—all defined in the respective body frame directions.

Newton's equation for the moments (**M**) and the angular momentum (**H**):

$$\Sigma\mathbf{M} = \frac{d}{dt}\mathbf{H} \tag{10}$$

can be considered in a similar manner when combined with the inertial position vector, **r**:

$$\mathbf{r} = x\mathbf{i} + y\mathbf{j} + z\mathbf{k} \tag{11}$$

and the mass moment and products of inertia about the x, y, and z axes I_{xx}, I_{yy}, I_{zz}, I_{xy}, I_{xz}, and I_{yz}. When the body axis is selected such that I_{yz} and I_{xy} are zero, the body angular velocities defined in terms of Euler angles (ψ, θ, φ) and Euler rates are:

$$p = \dot{\phi} - \dot{\psi}\sin\theta \tag{12}$$
$$q = \dot{\theta}\cos\phi + \dot{\psi}\cos\theta\sin\phi \tag{13}$$
$$r = \dot{\psi}\cos\theta\cos\phi - \dot{\theta}\sin\phi \tag{14}$$

reducing the moment equations to:

$$L = I_{xx}\dot{p} - I_{xz}\dot{r} + qr(I_{zz} - I_{yy}) - I_{xz}pq \tag{15}$$
$$M = I_{yy}\dot{q} + rp(I_{xx} - I_{zz}) + I_{xz}(p^2 - r^2) \tag{16}$$
$$N = -I_{xz}\dot{p} + I_{zz}\dot{r} + pq(I_{yy} - I_{xx}) + I_{xz}qr \tag{17}$$

where *L*, *M*, and *N* are the aerodynamic and thrust moments around each body x, y, and z axis, respectively.

Linearization.

The equations of motion can now be solved for the motion of the aircraft given the forces and moments, but the question remains open of exactly how to find those forces and moments. Toward that end, the force and moment equations are first linearized with small disturbance theory by assuming a steady reference flight condition and replacing each variable with a reference value plus a disturbance:

$$u = u_0 + \Delta u\,; \quad p = p_0 + \Delta p\,; \quad X = X_0 + \Delta X \ldots \text{etc.}$$

Assuming a symmetric flight condition with constant propulsive forces and the x-axis aligned with the airplane's velocity vector:

$$v_0 = p_0 = q_0 = r_0 = \phi_0 = \psi_0 = w_0 = 0 \tag{18}$$

The small disturbance variables are substituted into each of the six equations of motion, and then the equations are simplified by assuming small disturbance angles and neglecting products of disturbances. For instance, the X-force equation reduces to:

$$\Delta X - mg\Delta\theta\cos\theta_0 = m\Delta\dot{u} \tag{19}$$

The perturbation variables are the instantaneous changes from the reference conditions of the translational velocities, angular velocities, control deflections, and their derivatives, and can be expressed with a Taylor series expansion of all of the perturbation variables:

$$\Delta X\left(u,\dot{u},v,\dot{v}\ldots\delta_e,\dot{\delta}_e\right) = \frac{\partial X}{\partial u}\Delta u + \frac{\partial X}{\partial \dot{u}}\Delta\dot{u} + \cdots + \frac{\partial X}{\partial \delta_e}\Delta\delta_e + \text{higher order terms} \tag{20}$$

Each term such as $\frac{\partial X}{\partial u}$ is called a stability derivative, and usually noted in shorthand as X_u. Derivatives that are insignificant are disregarded.

For the models used in this thesis, the longitudinal derivatives that were retained are shown in Table 2 in terms of their dimensionless coefficients.

Table 2. Retained Longitudinal Derivatives

$X_u = \frac{-(C_{D_u} + 2C_D)\bar{q}S}{mu_0} (\text{s}^{-1})$	$M_u = C_{m_u} \frac{\bar{q}S\bar{c}}{u_0 I_{yy}} \left(\frac{1}{ft \cdot s}\right)$
$X_w = \frac{-(C_{D_\alpha} - C_L)\bar{q}S}{mu_0} (\text{s}^{-1})$	$M_w = C_{m_\alpha} \frac{\bar{q}S\bar{c}}{u_0 I_{yy}} \left(\frac{1}{ft \cdot s}\right)$
$Z_u = \frac{-(C_{L_u} + 2C_L)\bar{q}S}{mu_0} (\text{s}^{-1})$	$M_{\dot{w}} = C_{m_{\dot{\alpha}}} \frac{\bar{c}}{2u_0} \frac{\bar{q}S\bar{c}}{u_0 I_{yy}} (\text{ft}^{-1})$
$Z_w = \frac{-(C_{L_\alpha} + C_D)\bar{q}S}{mu_0} (\text{s}^{-1})$	$M_q = C_{m_q} \frac{\bar{c}}{2u_0} \frac{\bar{q}S\bar{c}}{I_{yy}} (\text{s}^{-1})$
$Z_{\delta e} = \frac{C_{Z_{\delta e}} \bar{q}S}{m} (\text{ft/s}^2)$	$M_{\delta e} = C_{m_{\delta e}} \frac{\bar{q}S\bar{c}}{I_{yy}} (\text{s}^{-2})$

The dimensional lateral directional derivatives retained are shown in Table 3.

Table 3. Retained Lateral Derivatives

$Y_\beta = \frac{\bar{q}SC_{y_\beta}}{m} (\text{ft/s}^2)$	$N_\beta = \frac{\bar{q}SbC_{n_\beta}}{I_{zz}} (\text{s}^{-2})$	$L_\beta = \frac{\bar{q}SbC_{l_\beta}}{I_{xx}} (\text{s}^{-2})$
$Y_p = \frac{\bar{q}SbC_{y_p}}{2mu_0} (\text{ft/s})$	$N_p = \frac{\bar{q}Sb^2C_{n_p}}{2I_{zz}u_0} (\text{s}^{-1})$	$L_p = \frac{\bar{q}Sb^2C_{l_p}}{2I_{xx}u_0} (\text{s}^{-1})$
$Y_r = \frac{\bar{q}SbC_{y_r}}{2mu_0} (\text{ft/s})$	$N_r = \frac{\bar{q}Sb^2C_{n_r}}{2I_{zz}u_0} (\text{s}^{-1})$	$L_r = \frac{\bar{q}Sb^2C_{l_r}}{2I_{xx}u_0} (\text{s}^{-1})$
$Y_{\delta a} = \frac{\bar{q}SbC_{y_{\delta a}}}{m} (\text{ft/s}^2)$	$N_{\delta a} = \frac{\bar{q}SbC_{n_{\delta a}}}{I_{zz}} (\text{s}^{-2})$	$L_{\delta a} = \frac{\bar{q}SbC_{l_{\delta a}}}{I_{xx}} (\text{s}^{-2})$
$Y_{\delta r} = \frac{\bar{q}SbC_{y_{\delta r}}}{m} (\text{ft/s}^2)$	$N_{\delta r} = \frac{\bar{q}SbC_{n_{\delta r}}}{I_{zz}} (\text{s}^{-2})$	$L_{\delta r} = \frac{\bar{q}SbC_{l_{\delta r}}}{I_{xx}} (\text{s}^{-2})$

where:

S = Wing Area
b = Wing Span (ft)
W= Airframe Weight + fuel (lbs)
g = Gravitational Const (32.2 ft/s^2)
$\bar{c}$ = Mean Aerodynamic Chord (ft)
u_0= Equilibrium Velocity, x_b direction (ft/s)
$m = Wg$
$\bar{q}$ = ½ ρV^2, Dynamic Pressure (psf)
I_{xx}, I_{yy}, I_{zz}, I_{xz} =Moments and Products of Inertia

Note: For simulation, the actual value for air density, ρ, was calculated using the standard atmosphere equations. These equations were corrected to a surface temperature of 80° F to compensate for the likely hotter than standard day for testing at Edwards Air Force base.

For the lead aircraft, the actual values for the dimensional derivatives were obtained from Stevens and Lewis [22]. These derivatives originated from NASA-Langley wind tunnel tests on a subscale F-16 model. The derivatives were given in terms of the non-dimensional coefficients in Table 4, re-dimensionalized for the real aircraft at the flight condition selected for the tanker via table look-ups. For the Learjet, the non-dimensional coefficients in Table 4 were provided by Calspan from flight test data near the test condition for this thesis, and were considered linear in the range between the data test point and the thesis test point.

Table 4. Learjet Non-Dimensional Coefficients

$C_L = \frac{L}{\bar{q}S}$	$C_D = \frac{D}{\bar{q}S}$	$C_{l_r} = \frac{\partial C_l}{\partial(rb/2u_0)}$ (rad^{-1})
$C_{L_\alpha} = \frac{\partial C_L}{\partial \alpha}$ (rad^{-1})	$C_{D_\alpha} = \frac{\partial C_D}{\partial \alpha}$ (rad^{-1})	$C_{l_\beta} = \frac{\partial C_l}{\partial \beta}$ (rad^{-1})
$C_{L_{\delta e}} = \frac{\partial C_L}{\partial \delta e}$ (rad^{-1})	$C_{D_{\delta e}} = \frac{\partial C_D}{\partial \delta e}$ (rad^{-1})	$C_{l_{\delta a}} = \frac{\partial C_l}{\partial \delta a}$ (rad^{-1})
$C_{L_u} = M\frac{\partial C_L}{\partial M}$	$C_{D_u} = M\frac{\partial C_D}{\partial M}$	$C_{l_{\delta r}} = \frac{\partial C_l}{\partial \delta r}$ (rad^{-1})
$C_m = \frac{M}{\bar{q}S\bar{c}}$	$C_Y = \frac{Y}{\bar{q}S}$	$C_n = \frac{N}{\bar{q}Sb}$
$C_{m_\alpha} = \frac{\partial C_m}{\partial \alpha}$ (rad^{-1})	$C_{Y_r} = \frac{\partial C_Y}{\partial(rb/2u_0)}$ (rad^{-1})	$C_{n_p} = \frac{\partial C_n}{\partial(pb/2u_0)}$ (rad^{-1})
$C_{m_q} = \frac{\partial C_m}{\partial(q\bar{c}/2u_0)}$ (rad^{-1})	$C_{Y_p} = \frac{\partial C_Y}{\partial(pb/2u_0)}$ (rad^{-1})	$C_{n_r} = \frac{\partial C_n}{\partial(rb/2u_0)}$ (rad^{-1})
$C_{m_{\dot\alpha}} = \frac{\partial C_m}{\partial(\dot\alpha\bar{c}/2u_0)}$ (rad^{-1})	$C_{Y_\beta} = \frac{\partial C_Y}{\partial \beta}$ (rad^{-1})	$C_{n_\beta} = \frac{\partial C_n}{\partial \beta}$ (rad^{-1})
$C_{m_{\delta e}} = \frac{\partial C_m}{\partial \delta e}$ (rad^{-1})	$C_{Y_{\delta r}} = \frac{\partial C_Y}{\partial \delta r}$ (rad^{-1})	$C_{n_{\delta a}} = \frac{\partial C_n}{\partial \delta a}$ (rad^{-1})
$C_{m_u} = M\frac{\partial C_m}{\partial M}$	$C_l = \frac{L}{\bar{q}Sb}$	$C_{n_{\delta r}} = \frac{\partial C_n}{\partial \delta r}$ (rad^{-1})
	$C_{l_p} = \frac{\partial Cl}{\partial(pb/2u_0)}$ (rad^{-1})	

Smaller terms were thrown out, and forces from the flaps, gear, and (in the Learjet's case) direct side-force generators were disregarded as unnecessary for this thesis, leaving the non-dimensional lift, drag and side-force equations:

$$C_L = C_{L_0} + C_{L_q} q\left(\frac{\bar{c}}{2u_0}\right) + C_{L_\alpha}\alpha + C_{L_{\delta e}}\delta e \tag{21}$$

$$C_D = C_{D_0} + C_{D_q} q\left(\frac{\bar{c}}{2u_0}\right) + C_{D_\alpha}\alpha + C_{D_{\delta e}}\delta e \tag{22}$$

$$C_Y = C_{Y_0} + C_{Y_r} r\left(\frac{1}{u_0}\right) + C_{Y_\beta}\beta + C_{Y_{\delta r}}\delta r \tag{23}$$

which led to the solution for the aerodynamic forces on the aircraft--lift, drag, and side-force:

$$Lift = \bar{q}SC_L \tag{24}$$
$$Drag = \bar{q}SC_D \tag{25}$$
$$Y = \bar{q}SC_Y \tag{26}$$

When expressed as forces in the body frame,

$$X = -Drag \tag{27}$$
$$Z = -Lift \tag{28}$$

The roll, pitch, and yawing moment coefficients were found in the same manner:

$$C_l = C_{l_p}\left(\frac{pb}{2u_0}\right) + C_{l_r}\left(\frac{rb}{2u_0}\right) + C_{l_\beta}\beta + C_{l_{\delta a}}\delta a + C_{l_{\delta r}}\delta r \tag{29}$$

$$C_n = C_{n_p}\left(\frac{pb}{2u_0}\right) + C_{n_r}\left(\frac{rb}{2u_0}\right) + C_{n_\beta}\beta + C_{n_{\delta a}}\delta a + C_{n_{\delta r}}\delta r \tag{30}$$

$$C_m = C_{mq}\left(\frac{q\bar{c}}{2u_0}\right) + C_{m\dot{\alpha}}\left(\frac{\dot{\alpha}\bar{c}}{2u_0}\right) + C_{m\alpha}\alpha + C_{m\delta e}\delta e \tag{31}$$

The coefficients were then dimensionalized to the moments around the body frame x_b, y_b, and z_b axes:

$$L = C_l\bar{q}Sb \tag{32}$$
$$M = C_m\bar{q}S\bar{c} \tag{33}$$
$$N = C_n\bar{q}Sb \tag{34}$$

With the actual aerodynamic forces and moments solved for, the total forces on the aircraft were found by adding in thrust and gravity effects. In the case of the Learjet, the force from thrust can be assumed to be completely in the x_b direction and through the center of gravity. With the values of stability derivatives provided by Stevens and Lewis [22] for the lead aircraft, and from Calspan for the Learjet, equations 7-9 (force

equations) and 15-17 (moment equations) can now be used to solve for $\dot{u}$, $\dot{v}$, $\dot{w}$, $\dot{p}$, $\dot{q}$, and $\dot{r}$, completing the bare airframe model with known values. Both the lead and wing bare airframes require augmentation for stability and control.

Lead Aircraft Stability and Control

Lead Aircraft Stability Augmentation.

The lead aircraft F-16 model was stabilized primarily with classical techniques of root locus design. In order to accomplish this, the entire model was first linearized. Again, the technique is taken from Nelson [11]. The lead aircraft linearized longitudinal equations of motion in state space form are now:

$$\dot{\mathbf{x}}_{\mathbf{long}} = \mathbf{A}_{\mathbf{long}}\mathbf{x}_{\mathbf{long}} + \mathbf{B}_{\mathbf{long}}\boldsymbol{\eta}_{\mathbf{long}} \tag{35}$$

where the longitudinal **A** and **B** matrices are:

$$\mathbf{A}_{\mathbf{long}} = \begin{bmatrix} X_u & X_w & 0 & -g \\ Z_u & Z_w & u_0 & 0 \\ M_u + M_{\dot{w}}Z_u & M_w + M_{\dot{w}}Z_w & M_q + M_{\dot{w}}u_0 & 0 \\ 0 & 0 & 1 & 0 \end{bmatrix}$$

$$\mathbf{B}_{\mathbf{long}} = \begin{bmatrix} X_{\delta e} & X_{\delta_T} \\ Z_{\delta e} & Z_{\delta_T} \\ M_{\delta e} + M_{\dot{w}}Z_{\delta e} & M_{\delta_T} + M_{\dot{w}}Z_{\delta_T} \\ 0 & 0 \end{bmatrix}$$

and the state and control vectors are given by:

$$\mathbf{x}_{\mathbf{long}} = \begin{bmatrix} \Delta u \\ \Delta w \\ \Delta q \\ \Delta \theta \end{bmatrix}, \quad \boldsymbol{\eta}_{\mathbf{long}} = \begin{bmatrix} \Delta \delta e \\ \Delta \delta_T \end{bmatrix}$$

The linearized lateral equations of motion are formulated in the same manner with:

$$\mathbf{A}_{\mathbf{lat}} = \begin{bmatrix} \frac{Y_\beta}{u_0} & \frac{Y_p}{u_0} & -\left(1 - \frac{Y_r}{u_0}\right) & \frac{g \cos\theta_0}{u_0} \\ L_v^* + \frac{I_{xz}}{I_{xx}} N_v^* & L_p^* + \frac{I_{xz}}{I_{xx}} N_p^* & L_r^* + \frac{I_{xz}}{I_{xx}} N_r^* & 0 \\ N_v^* + \frac{I_{xz}}{I_{xx}} L_v^* & N_p^* + \frac{I_{xz}}{I_{xx}} L_p^* & N_r^* + \frac{I_{xz}}{I_{xx}} L_r^* & 0 \\ 0 & 1 & 0 & 0 \end{bmatrix}$$

$$\mathbf{B}_{\mathbf{lat}} = \begin{bmatrix} 0 & Y_{\delta r} \\ L_{\delta a}^* + \frac{I_{xz}}{I_{xx}} N_{\delta a}^* & L_{\delta r}^* + \frac{I_{xz}}{I_{xx}} N_{\delta r}^* \\ N_{\delta a}^* + \frac{I_{xz}}{I_{xx}} L_{\delta a}^* & N_{\delta r}^* + \frac{I_{xz}}{I_{xx}} L_{\delta r}^* \\ 0 & 0 \end{bmatrix}$$

$$\mathbf{x}_{\mathbf{lat}} = \begin{bmatrix} \Delta \beta \\ \Delta p \\ \Delta r \\ \Delta \phi \end{bmatrix}, \quad \boldsymbol{\eta}_{\mathbf{lat}} = \begin{bmatrix} \Delta \delta a \\ \Delta \delta r \end{bmatrix}$$

where

$$L_v^* = \frac{L_v}{\left[1 - \left(I_{xz}^{\ 2} / (I_{xx} I_{zz})\right)\right]} \quad , \quad N_v^* = \frac{N_v}{\left[1 - \left(I_{xz}^{\ 2} / (I_{xx} I_{zz})\right)\right]} \quad \text{and so on.}$$

The systems are appended to form the decoupled, linearized equations of motion:

$$\dot{\mathbf{x}} = \mathbf{A}\mathbf{x} + \mathbf{B}\boldsymbol{\eta} \tag{36}$$

with

$$\mathbf{A} = \begin{bmatrix} \mathbf{A}_{\mathbf{long}} & \mathbf{0} \\ \mathbf{0} & \mathbf{A}_{\mathbf{lat}} \end{bmatrix}$$

$$\mathbf{B} = \begin{bmatrix} \mathbf{B}_{\mathbf{long}} & \mathbf{0} \\ \mathbf{0} & \mathbf{B}_{\mathbf{lat}} \end{bmatrix}$$

The final state vector **x** and control vector **η** produced are:

$$\mathbf{x} = \begin{bmatrix} \Delta u \\ \Delta w \\ \Delta q \\ \Delta \theta \\ \Delta \beta \\ \Delta p \\ \Delta r \\ \Delta \phi \end{bmatrix}, \quad \boldsymbol{\eta} = \begin{bmatrix} \Delta \delta e \\ \Delta \delta_T \\ \Delta \delta a \\ \Delta \delta r \end{bmatrix}$$

The linear model was used for lead stability augmentation only. Classical root locus techniques were employed, feeding back successive loops of angle of attack(α), angle of pitch (θ), and pitch rate (q), and adjusting gains until the poles of the system were acceptable. Actual perturbation elevator position ($\Delta\delta e_L$) was found by modeling the elevator dynamics as a first order response:

$$\frac{\Delta \delta e_L(s)}{\Delta \delta e_{L\_cmd}(s)} = \frac{20.2}{s + 20.2} \tag{37}$$

This first order lag model was also used for the actual positions of the rudder and aileron. The final command for the elevator was then found by simply adding the delta to the equilibrium state.

The only lateral stabilization implemented on the lead aircraft model was in the form of PID feedback of sideslip to the rudder to keep the turns coordinated. The rudder gains were selected by trial and error with the non-linear model to keep sideslip near zero while using a small amount of rudder deflection. All lead aircraft gains are listed in Table 5 of the next section.

Lead Aircraft Control.

With the lead aircraft model stabilized, the control algorithm can now be developed. The concept of the air-refueling flight is that of leader-follower. That is, the lead aircraft has no information about the wing aircraft, and is controlled independently. The duties of keeping the formation geometry fall completely to the wing aircraft. For the simulator, an autopilot for the lead aircraft was designed to hold altitude and velocity, coordinate turns, and fly profiles representative of a tanker track. The Simulink® model for the lead control algorithm is shown in Figure 113, Appendix A. The core of the model is the non-linear F-16 equation block and look-up tables found in Stevens and Lewis [22]. Using the equations of motion, the derivative of each state is first solved for and the states are then propagated forward. Control surface deflections are solved for by adding equilibrium conditions to commands, which are generated from the control loops.

The elevator control law uses the stability augmentation system (SAS) feedback of perturbation angle of attack ($\Delta\alpha_L$), pitch angle ($\Delta\theta_L$), and pitch rate (Δq_L), with an altitude hold loop that feeds back deviation from desired altitude (Δh_L).

The result is the lead elevator control law:

$$\Delta\delta e_{L\_cmd} = k_{\alpha_L}\Delta\alpha_L + k_{q_L}\Delta q_L + k_{\theta_L}\Delta\theta_L + k_{h_L}\Delta h_L \tag{38}$$

Actuator dynamics are applied to the command to find the actual change in angle as discussed in the previous section, and the equilibrium value is added to find the true surface deflection.

For the throttle control law, a simple airspeed hold technique is used to determine lead throttle command ($\delta_{T\_L\_cmd}$) away from equilibrium (δ_{T_L0}) by feeding back the lead aircraft deviation from desired velocity (Δvel_L):

$$\delta_{T\_L\_cmd} = \delta_{T\_L0} + k_{vel_L}\Delta vel_L \tag{39}$$

A saturation block is used in the Simulink® model to ensure the throttle command stays within the capabilities of the aircraft. Throttle spool up time is included as a lag state in the Stevens and Lewis model, but was considered negligible and not used for this research. The only lead aircraft throttle change required during air refueling is a minor increase in thrust for gentle turns. In addition, the engine response of the actual test aircraft, a C-12 turboprop, is faster than the turbofan engines of the F-16.

The rudder command channel consists only of the PID control on sideslip angle for turn coordination as discussed in the stabilization of the lead aircraft. The same actuator dynamics are applied for all channels of control. The control law for commanded rudder deflection (δr_{L_cmd}) is:

$$\delta r_{L\_cmd} = k_{\beta_L}\beta + k_{I_{\beta\_L}}\int \beta\, dt + k_{D_{\beta\_L}}\dot{\beta} \tag{40}$$

The aileron channel is set up to mimic a tanker with a bank angle (φ) hold system. To properly simulate a tanker track, the simulated lead aircraft needs to slowly bank to 15

or 30 degrees for a period of time, usually through 180 degrees of turn. A roll rate (p_L) loop was added after experimentation. This feedback gives the capability to keep the roll rate from building too much over time while also minimizing bank overshoot. Aileron command (δa_{L_cmd}) is determined, therefore, with the following control law:

$$\delta a_{L\_cmd} = k_{phi_L}\left(\phi_{L\_cmd} - \phi_L\right) + k_{p_L} p_L \tag{41}$$

The actual aileron position is again found after applying the actuator dynamics.

The values selected for all lead aircraft gains are shown in Table 5 with altitude in feet, speed in ft/s, and all angles in degrees. The gain on lead aircraft roll rate (k_{PL}) is altered depending on the magnitude of the bank command to achieve desired rates:

Table 5. Lead Aircraft Gains

k_{α_L}	k_{q_L}	k_{θ_L}	k_{h_L}	k_{vel_L}	k_{ϕ_L}	k_{p_L}	k_{β_L}	$k_{I_{\beta\_L}}$	$k_{D_{\beta\_L}}$
-0.56	-0.192	-3	-0.8	0.1	-.5	-2.3	-4	-1	-5

The implementation of these control laws can be seen in the lead aircraft model schematic, Figure 113 of Appendix A.

Lead Aircraft Profiles.

For the simulation, profiles were designed for left and right turns to both 15 and 30 degrees, as well as straight and level flight. Prior to flight test, the desired roll rate was predicted to be near 10 deg/s, and this rate was used during optimization of the gains for the wing aircraft autopilot. During flight test, however, this rate was found to be excessive. A roll rate of less than 3 deg/s was found to be closer to actual tanker

performance with receivers in formation, and future research should use this rate for gain optimization. For investigation of robustness and sensitivity, lead aircraft profiles were also designed with even faster roll rates (up to 40 deg/s), bank angles up to the controller limits, and turn reversals (15 degrees to 15 degrees as well as 30 degrees to 30 degrees).

With the lead aircraft bare airframe model stabilized and control profiles designed for simulation of tanker operations, the independent aircraft models were ready to be connected into the full formation model.

III. Formation Simulation

The formation simulation is created by connecting the two aircraft models and tracking their relative position. Initial simulations did not include a full lead aircraft model or any coordinate transformation work, just the aforementioned manual trajectory to follow with a determined offset. As the control laws became advanced enough to work with turning and changing formation positions, the lead aircraft model was added and several control frames were experimented with. The simulator was designed to work with multiple control frames simultaneously, so that the results could be compared directly. The simulator also allowed several options from the developing control laws. Once the decisions on the control frame and control laws were final, the simulator was greatly simplified. The basic concept is shown in Figure 10.

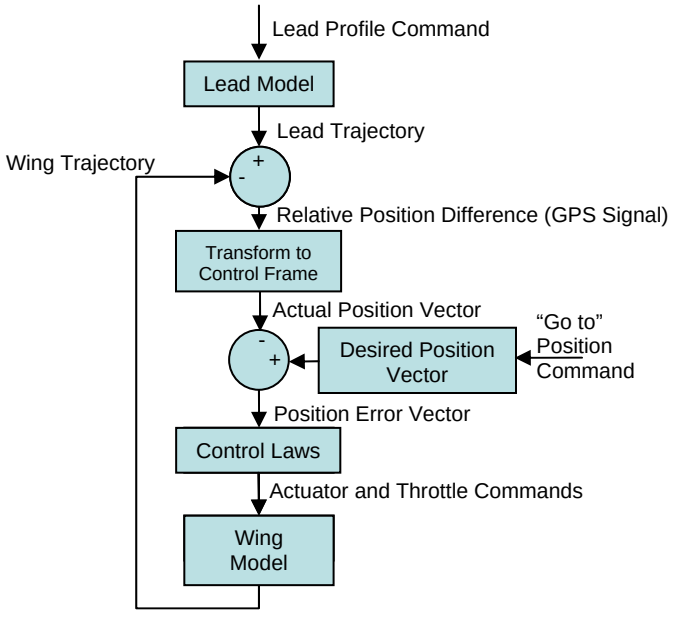

Figure 10. Formation Simulation Concept

Top Tier Control

The top tier of the real simulator is shown in final form in Figure 112, Appendix A. The top tier encompasses everything that is required for simulation that is external to the actual controller block, referred to as the second tier. The top tier of simulation propagates both aircraft models, adds disturbances and environmental considerations, and generates all of the inputs that are available to the actual controller during flight. This design technique allowed the controller block to be cut directly from the top tier of the simulator and installed into the test aircraft with no changes. Modifications to the controller for flight test could then be made and tested with assurance that the system tested in simulation was exactly the same as the test article.

The top tier of simulation begins with open loop control of the simulated tanker. The "Lead_cmd" command is set to designate which profile the lead aircraft will follow. The attitude and flight path for that profile are generated in the lead aircraft model, which has the control laws shown in full form in Figure 113, Appendix A. The heading of the lead aircraft is used to split the state of velocity into east and north components. These components are integrated to find the change in position that has occurred since the initialization of the model, and propagated as states. The states of east position (delta pe), north position (delta pn), and altitude (h) are then passed to the main simulation. All propagation is performed with a first order differential (Euler) solver using a fixed time step of 0.01 seconds. The time step mirrors the speed of the Variable Stability System (VSS) computer on the Learjet where the controller was installed for flight test.

The lead aircraft's attitude is taken directly from the states in the lead model. Heading angle (ψ), pitch angle (θ), bank angle (φ) and roll rate (p) are the attitude inputs that the real wing aircraft receives from a small Inertial Measurement Unit (IMU) in the lead aircraft. The rate and angles are required for coordinate transformations and wing aircraft control. Disturbances are added to the position and attitude signals in the form of pure time delays, sampling errors, sensor noise, turbulence, and a units error that was added after the first test sortie. These are described in the next section. The conditioned attitude signals are then added to several other inputs to the controller, including the GPS differential position vector, a selection of what formation position to fly to, definitions of where each formation position is, controller gains, autopilot engagement commands, and wing feedback states of bank angle, roll rate, and sideslip angle (β). The controller takes all of these inputs and determines the commands of elevator (de_c), aileron (da_c), rudder (dr_c), and thrust for both motors (dxl_c and dxr_c). These commands, with the turbulence disturbance input, drive the wing aircraft model.

The wing aircraft model takes the inputs and produces the velocity components and altitude of the aircraft receiving fuel from the tanker. The wing aircraft velocity components are integrated just as the lead's, and are combined with an offset that simulates the receiver's position at initialization. The result is a position vector delta from the start of the simulation that is propagated with the simulation in the same manner as the lead aircraft position information. In early simulations, each position vector was then translated to the Earth-Centered, Earth Fixed (ECEF) coordinate system, in order to exercise the controller's ability to convert the signals back into a local reference frame.

As the test plan developed, however, the conversion to the local frame was moved from the controller into the DGPS, and the requirement was removed from the simulator.

With the position of both aircraft known by the simulator, the two vectors are differenced, resulting in a vector from the lead aircraft to the wing aircraft, which is transformed into components of north, east, and down. This vector is a reproduction of the signal that is currently produced by the AFIT Relnav system used for flight test (after transformation from ECEF). This signal closes the loop and completes the top tier of control.

Disturbances

Several disturbances are added to the signals to increase simulator fidelity. Each of these disturbances is toggled with an on/off switch, allowing the changes in performance due to each disturbance to be isolated. Since the disturbances are for signals external to the controller, they are all applied in the top tier of control. The implementation of the disturbances is shown in Appendix A, with turbulence in Figure 115 and the remainder of the disturbances in Figure 114.

Time Delay.

Time delays are added to several signals. The values for each delay are estimates, and each was varied in the investigation of sensitivity and robustness that is discussed in Chapter VI. For the primary simulations, a delay of 0.1 seconds was added to the DGPS and the IMU signals. These signals must travel from the source (either the GPS antenna or the IMU on the C-12) to the Relnav system in the Learjet via a datalink, and the

differential position solution must be solved before translation into a 1553 bus signal usable by the VSS computer. An additional 0.06 seconds was also added for VSS computational time on signals within the Learjet.

Sampling Errors.

The Learjet VSS operates at 100 Hz, and therefore the positions of the control surfaces are scheduled 100 times each second. Unfortunately, the datalink that was affordable for this test was only capable of passing the satellite pseudoranges and ephemeris data from the C-12 at 20 Hz. Since the IMU data was passed on the same datalink, it was also only available to the VSS at 20 Hz. The resulting sampling error has the potential to wreak havoc on the controller, which uses the derivative of several signals for damping. The VSS samples the signal 5 times before seeing any change in the data. When the change occurs, it is 5 times larger than expected for one time step. This zero-order-hold effect is incompatible with derivative control without filtering.

This problem was known about prior to testing, and to test the controller's ability to handle such signals, the effect was duplicated in the simulator. Each value of attitude or position data is held for 5 time epochs, and then the current signal is sampled again and held for another 5 epochs. The technique to accomplish this is shown in Figure 114, Appendix A. Essentially, a sine wave is used as a timer, and each time the sine wave reaches its peak the current values for attitude and position are held in memory and repeatedly passed on until the sine wave again peaks and the information is replaced by new values.

Noise.

Signal noise is also added to increase the fidelity of the simulation as well as to give insight to the sensitivity and robustness of the system. Actual noise in the IMU and the DGPS systems was recorded and reproduced. In the case of the position data, the only DGPS noise available was from a static condition. The errors were very small, on the centimeter level. Errors of this magnitude in position data are completely washed out by the noise in the attitude channels, and were eventually discarded. Small variances in the attitude of the lead aircraft, however, can have a large impact on the performance of the controller.

The desired position for the wing aircraft to fly to is based on the position of the refueling boom, considered as a rigid part of the tanker. As the lead aircraft rotates in any direction, or as sensor noise makes it appear that the lead aircraft is rotating, the desired position moves as well. When not in the contact position, the controller still determines its desired position as if it were connected in a rigid manner to the tanker. The farther away the desired position is then, the greater effect small changes in angles have. In the pre-contact position, with about 94 feet between the antennae of the two aircraft, a change of 1 degree of heading moves the desired position over 1.6 feet. The gains on the controller are sensitive, and inches count. Obviously, small amounts of noise in the attitude system can be detrimental to control, especially with derivative control magnifying the effects of the apparent rapid changes in the desired position.

There are ways to reduce the effects of lead attitude sensor noise. Osteroos used the wingman's perspective for control. In essence, his controller did not minimize the

error between the wing aircraft and a point in space moving with the tanker, but it minimized the error between the tanker and a point moving with the wing aircraft [13]. The concept behind the technique is to remove the requirement for lead attitude information at all, including the noise that goes with it. There are other problems with the wing wind frame control that drove this research in another direction, but the concept of noise cancellation by removing the requirement for heading, pitch angle, bank angle, and roll rate should be considered in future research. Unfortunately, Osteroos was not able to adequately control the wing aircraft without the addition of lead bank angle and roll rate anyway. Ironically, the two sets of attitude inputs for actual flight test ended up being exactly the same (an attitude source failure removed the intended inputs of heading and pitch angle from flight test for this research).

The prospect of a noise problem was accepted for the benefits of the selected style of control. The key that makes it work is the low amount of angular maneuvering from the lead aircraft, which allows for heavy filtering on the attitude signals which could have a large adverse effect on control. A tanker with receivers will not turn faster than a standard rate turn of 3 degrees per second of heading change (accepting perhaps an extreme case, which wouldn't be much faster). Sensor attitude noise typically has a much higher frequency. Therefore, a heavy noise filter on heading angle at the high frequencies has minimal impact on the controller. Roll rates for a tanker with receivers are also typically around 3 degrees per second, again allowing heavy filtering on both bank angle and rate. The steady state pitch angle of the tanker must be known, but changes are negligible for the shallow turns of air refueling.

For early simulations, attitude sensor noise used was provided by the MIDG II Micro-Electrical Mechanical System Inertial Measurement Unit (MEMS IMU) manufacturer, Microbiotics, Inc. The IMU data were recorded on a flight of a Cessna 172, and a representative time slice was reproduced for all of the simulations prior to flight test. Figure 11 shows a sample of the data.

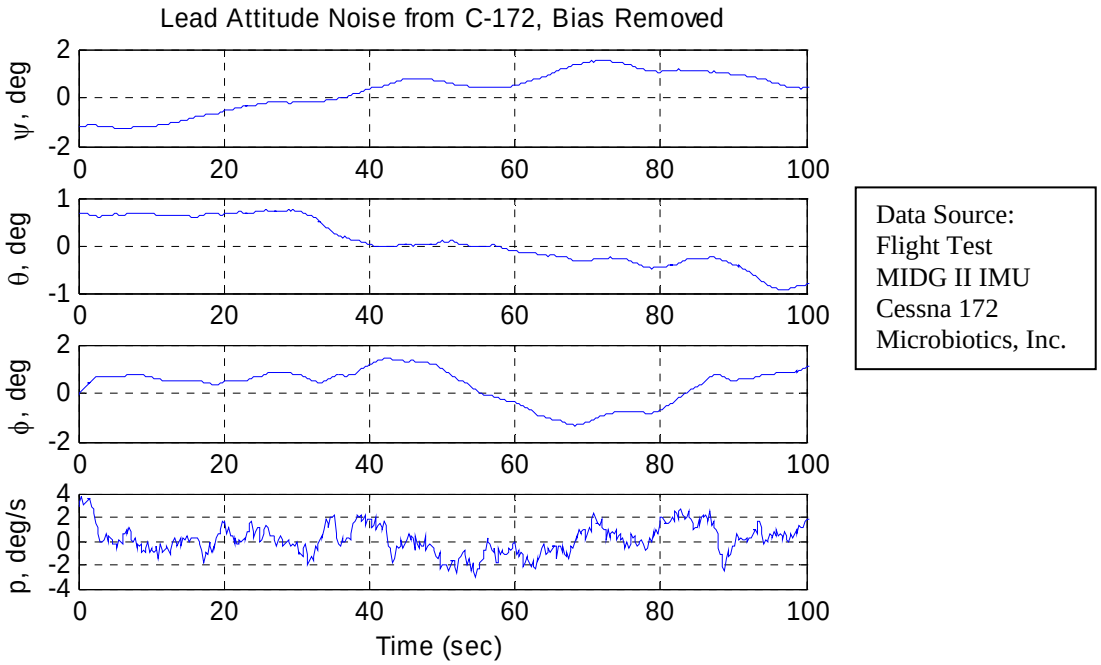

Figure 11. Noise Added to IMU Signals for Simulation (from Cessna 172 Flight)

The rate of change in the angles is of much higher concern than the bias from zero. Recall that the desired position moves (erroneously) as the attitude changes with angle errors, as if on the end of a stick. As the angles have errors slowly introduced, the controller can adjust to the moving desired position, albeit with some amount of error from the true position that the controller knows nothing about. The final position relative

to the boom will obviously only be as accurate as the sensors allow. The controller cannot, however, keep up with a rapidly changing position, and these rapid changes are magnified by the derivative control on position error. The rates from the Cessna 172 flight in Figure 11 are very low, as shown by the smooth lines with no sharp edges that would excite the derivative control. This fact led to a much lower emphasis on filtering during the design portion of the controller than was truly required. Once the first flight was performed, data from the IMU were recorded on the C-12 and the bias was removed. The results were not as smooth as the data from the manufacturer, and made worse by the rounding done in the conversion to the 1553 format. A sample is shown in Figure 12. Even though the magnitudes of the errors are similar, the rapid changes and corners in the data found during flight test led to last minute scrambling to design appropriate filters.

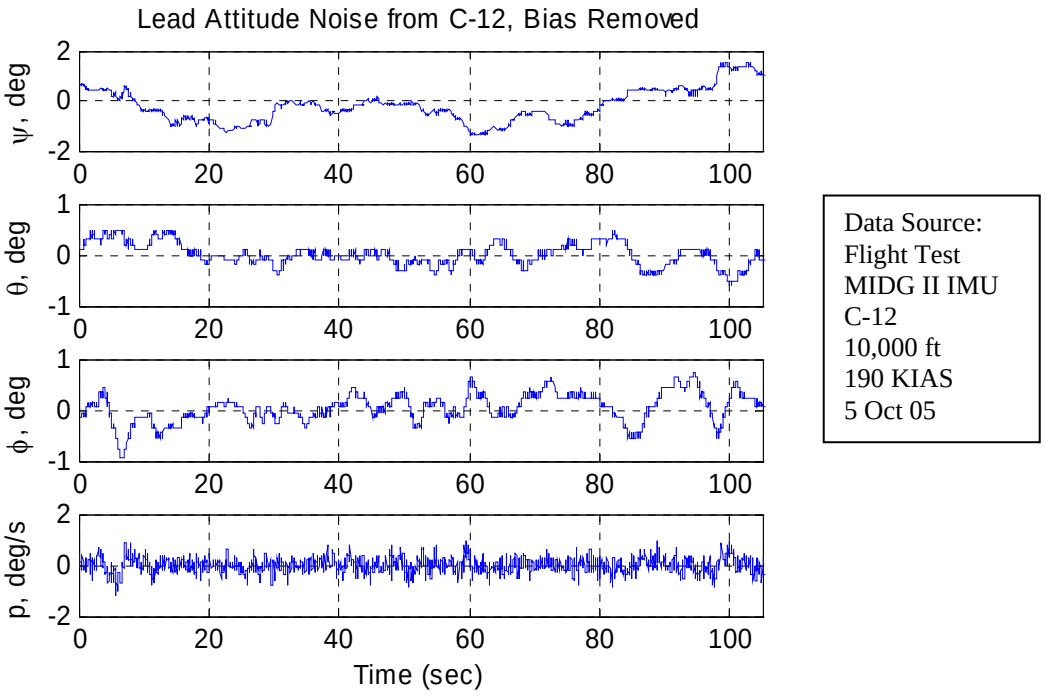

Figure 12. Noise Added to Lead Aircraft IMU for Simulation (from C-12 Flight)

Turbulence Model [1].

The final environmental consideration in the simulator for sensitivity and robustness investigation is the addition of turbulence. An approximation of the Von Karman model for wind disturbances is applied to both the lead and the wing aircraft. Normalized states are created for a random disturbance in angle of attack and sideslip, generated with:

$$\dot{\alpha}_{Turb}(t) = -2\left(\frac{u_0}{L}\right)\alpha_{Turb}(t) + \frac{2\sigma}{\sqrt{\pi L u_0}}\varepsilon(t) \tag{42}$$

Where α_{Turb} = Random disturbance in angle of attack, radians (the same technique is used to generate sideslip disturbance)
u_0 = Airspeed, ft/s
ε = Zero mean, unity covariance white noise

scale length, L is determined by altitude:

$$L = \begin{cases} 200\ ft\ at\ sea\ level \\ 200 \rightarrow 2500\ ft\ when\ altitude\ is\ below\ 2500\ ft\ (Linearly\ Interpolate) \\ 2500\ ft\ when\ altitude > 2500\ ft \end{cases} \tag{43}$$

and

$$\sigma = \begin{cases} 6\ ft/s\ normal \\ 15\ ft/s\ in\ cumulous\ clouds \\ 30\ ft/s\ in\ thunderstorms \end{cases} \tag{44}$$

The turbulence was considered as a velocity field disturbance, applied to the lead aircraft first, and delayed to the trailing aircraft. The Matlab Simulink® model implemented is shown in Figure 115, Appendix A. The upper half of the model generates the disturbances, and the lower half is logic to apply the delay. The GPS differential vector is used to determine the distance from the lead aircraft GPS antenna to

that of the wing aircraft in the direction of flight. A correction term is added to find the spacing from nose to nose. This spacing is used with the airspeed of the formation to determine the appropriate amount of time to delay the application of the field disturbances to the trailing aircraft. The disturbances are then added to the actual values of angle of attack and angle of sideslip for each aircraft model. The effects of the turbulence are discussed in the sensitivity and robustness section of Chapter VI.

IV. Control Frame Investigation

One of the major design decisions required for a formation flight controller is that of the control frame. The control frame determines the components of position error that the controller will seek to minimize. How that information is presented to the controller has a large impact on the controller's performance in terms of maximum position errors, stability, and settling time. The overall strategy of control depends on which control frame is used, and the majority of efforts toward controller refinement are determined by the strengths and weaknesses of the strategy selected. Osteroos looked at the formation control problem from the wing aircraft's perspective with the wing wind frame [13]. NASA accomplished formation flight from the lead aircraft's perspective with a non-rotating formation frame that was realigned prior to each data run [9]. This research investigated each of these frames and more, and eventually selected the lead aircraft's perspective, but with a fully rotating frame attached to the tanker instead of the wingman. This chapter will define each control frame and highlight some of their strengths and weaknesses.

Axes Definitions

Beyond just the final frame of control, several intermediate reference frames were required in the development of the formation simulation. The final simulation requires only three. Most of the reference and control frames have been introduced in previous student theses, and an excellent exposition is available in Miller, but some were modified with differences such as the polarity of the angle β and the introduction of the GPS

frame. As these transformations are critical to the model of two maneuvering aircraft, each of the reference frames used and the transformations between them are briefly reviewed here for clarity.

Earth Centered, Earth Fixed (ECEF) Frame.

DGPS information on relative position is solved for in the ECEF Frame. When the simulator was originally built, the DGPS signal was to be converted into MIL-STD 1553 data bus format and fed directly into the controller. As such, a transformation from ECEF into a local navigation frame was required up front. A second transformation was required after the aircraft models to again reproduce the simulated differential input in ECEF. This transformation was in the formation model, but outside of the actual controller. As the actual flight test approached, the ECEF to local transformation was moved earlier in the data stream (prior to conversion to the MIL-STD 1553 formatting). The transformation was therefore removed from the controller and will not be discussed here, but the methods used are retained in Appendix C for follow on research that will likely again require the technique.

North, East, Down (NED) Frame.

The ECEF coordinates are not geographically intuitive, so a North, East, Down (NED) frame is utilized for ease of analysis of aircraft motion. Two NED frames are used, attached to each aircraft's center of gravity. The NED z-axis, z_{NED}, points from the center of mass of the aircraft toward the center of mass of the Earth. The x_{NED} and y_{NED} axes are orthogonal to the z-axis and each other and point true north and east,

respectively, as shown in Figure 13. The NED frame moves with the aircraft, and rotates as the aircraft flies around the Earth. In the top tier of control shown in Figure 112, Appendix A, the NED frame is used for the DGPS signal that is conditioned in the signal errors block and proceeds into the actual controller.

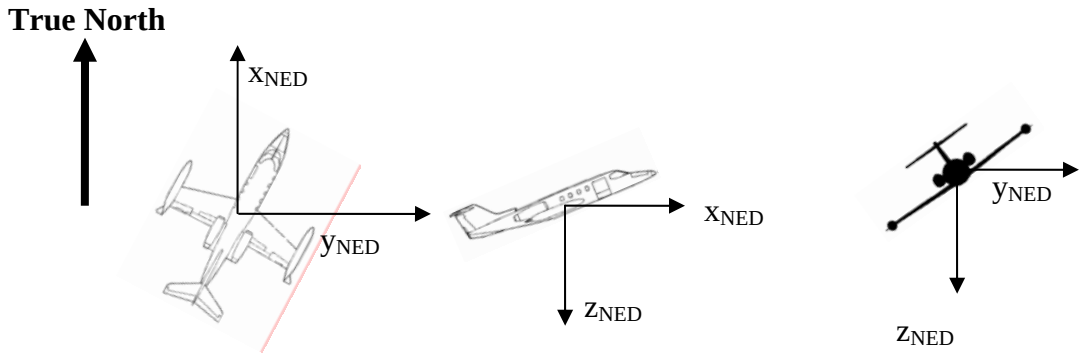

Figure 13. North, East, Down Frame Definition

Local Position--East, North, Up (ENU) Frame.

Similar to the NED frame but stationary (with respect to the surface of the Earth), a local frame is used in the simulation for position propagation in the East, North, Up (ENU) frame, with its origin at the latitude and longitude of Edwards Air Force Base, but at zero feet MSL. Technically, for transformations between ENU and ECEF, the height is at zero feet from the World Geodetic System-84 geoid, but the difference is not critical for this thesis as long as both the wing and lead aircraft are initialized the same way.

The ENU frame was selected for convenience in navigation. The ENU z-axis points away from the center of the Earth, and the x and y axes complete an orthogonal, right hand x-y-z system with x pointing north and y pointing east. The simulation of the

wing and lead aircraft will provide east and north velocities as states, as well as altitude. With integration of the velocities and the assumption of initialization over Edwards Air Force Base, the position information of both aircraft is automatically in the ENU frame. The positions are then differenced and transformed to the NED frame to produce the DGPS signal that will be available in flight.

Body Frames.

Aircraft specific reference frames are also required. During aerial refueling, the proper formation position of the receiving aircraft is determined by the location of their boom receptacle. The desired position vector that describes this location is a differential vector found from the GPS antenna on the tanker to the GPS antenna on the receiver when the aircraft are connected and the refueling boom of the tanker is centered in azimuth, elevation, and extension. This vector is considered part of the rigid body of the tanker, moving with the center of mass and rotating with changes in heading, pitch, and roll. It is therefore expressed in the tanker body axis. The body axis has the origin at the center of gravity of the aircraft, with the x-axis, x_b, directed along the waterline through the nose of the aircraft, y_b out of the right wing, and z_b through the floor of the aircraft at the axis of symmetry in another right-hand x-y-z orthogonal system as shown in Figure 14.

The orientation of the body axis is found by starting with the NED frame and rotating through the Euler angles, which define the intermediate axes. From true north, the NED frame is rotated about the z_{NED} axis by the heading angle (ψ) to establish the formation axes. The formation axes will be discussed shortly and for the time being is

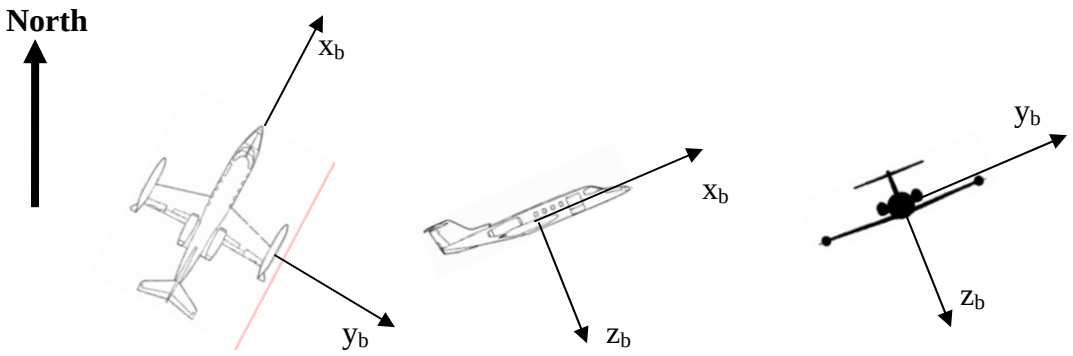

Figure 14. Body Axes Definition

labeled as the intermediate 1-axes. This axes set is then rotated about the y_1-axis by the pitch angle (θ) to the intermediate 2-axes, which is finally rotated about the x_2-axis by the roll angle (φ) as shown in Figure 15. The wing body frame is defined in the same manner as the tanker body frame, using the wing aircraft Euler angles and center of gravity.

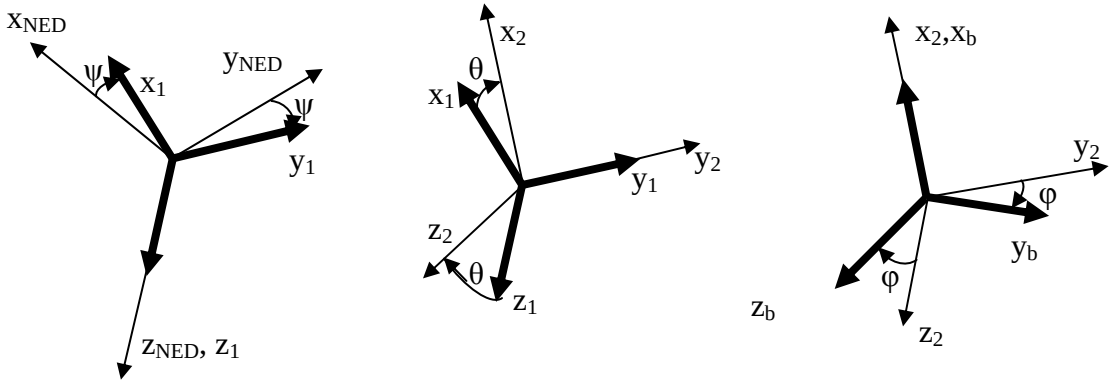

Figure 15. Euler Angle Rotations From NED Frame to Body Frame

The transformation from the NED frame to the body frame can be derived from Figure 15. The rotations:

$$\mathbf{C}_{\psi} = \begin{bmatrix} \cos\psi & \sin\psi & 0 \\ -\sin\psi & \cos\psi & 0 \\ 0 & 0 & 1 \end{bmatrix}$$

$$\mathbf{C}_{\theta} = \begin{bmatrix} \cos\theta & 0 & -\sin\theta \\ 0 & 1 & 0 \\ \sin\theta & 0 & \cos\theta \end{bmatrix}$$

$$\mathbf{C}_{\phi} = \begin{bmatrix} 1 & 0 & 0 \\ 0 & \cos\phi & \sin\phi \\ 0 & -\sin\phi & \cos\theta \end{bmatrix}$$

Combine to form the NED to body transformation matrix:

$$\mathbf{C}^{b}_{NED} = \mathbf{C}_{\phi} \cdot \mathbf{C}_{\theta} \cdot \mathbf{C}_{\psi} \tag{45}$$

Thus:

$$\mathbf{C}^{b}_{NED} = \begin{bmatrix} \cos\theta\cos\psi & \cos\theta\sin\psi & -\sin\theta \\ \sin\phi\sin\theta\cos\psi - \cos\phi\sin\psi & \sin\phi\sin\theta\sin\psi + \cos\phi\cos\psi & \sin\phi\cos\theta \\ \cos\phi\sin\theta\cos\psi + \sin\phi\sin\psi & \cos\phi\sin\theta\sin\psi - \sin\phi\cos\psi & \cos\phi\cos\theta \end{bmatrix} \tag{46}$$

Formation Frame.

The formation frame mentioned in the preceding paragraph as the intermediate 1-axes is the control frame that was used by NASA in the Formation Flight Autopilot project [9]. The x-axis is in the direction of the nose of the lead aircraft and perpendicular to the z-axis, which remains straight down from the center of gravity to the center of the Earth. No consideration is given for bank or pitch angle.

Therefore:

$$\mathbf{C}_{NED}^{Form} = \mathbf{C}_{\psi} \tag{47}$$

The formation frame is depicted in Figure 16. As used by NASA, the frame was not adjusted for heading changes while collecting data. It was initialized to the lead aircraft's heading prior to each data run, and the only heading changes were small "s" turns centered on the original heading. For this research, the heading of the aircraft was available and used to rotate the frame to always align with the nose of the lead aircraft, making continuous turns possible.

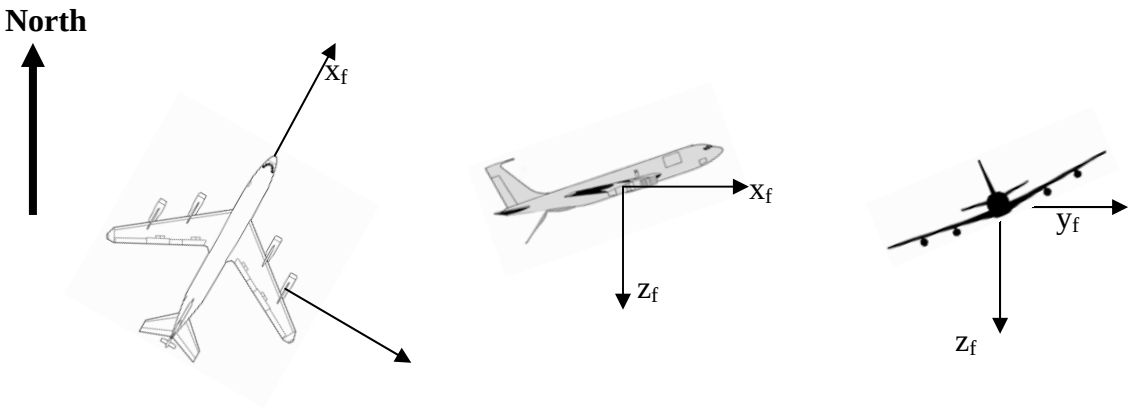

Figure 16. Formation Frame Definition

Wind Frame.

The body frame of the wing aircraft essentially shows where the aircraft is pointing. Another control frame investigated in this thesis was the wind axis, which shows the direction the aircraft is actually moving through the air mass. The wind axes differ from the body axes by the angle of attack (α), and the angle of sideslip (β). To

rotate vectors into the wind axis from the body axis, a negative rotation around the y_b-axis by the angle of attack (α) introduces an intermediate frame known as the stability axes, x_s, y_s, z_s. A positive rotation around z_s by the angle of sideslip (β) then moves into the wind axis as shown in Figure 17.

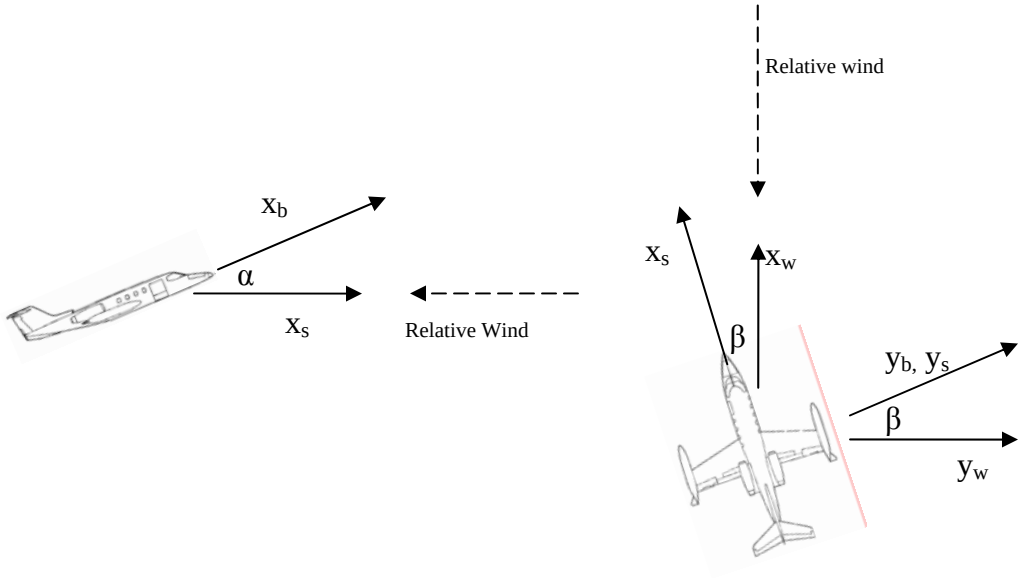

Figure 17. Wind Axes Definition

The following rotation matrices are derived from: Figure 17:

$$\mathbf{C}_b^s = \begin{bmatrix} \cos(\alpha) & 0 & \sin(\alpha) \\ 0 & 1 & 0 \\ -\sin(\alpha) & 0 & \cos(\alpha) \end{bmatrix} \tag{48}$$

$$\mathbf{C}_s^w = \begin{bmatrix} \cos(\beta) & \sin(\beta) & 0 \\ -\sin(\beta) & \cos(\beta) & 0 \\ 0 & 0 & 1 \end{bmatrix} \tag{49}$$

Yielding the direction cosine matrix to rotate from body to wind:

$$\mathbf{C}_b^w = \begin{bmatrix} \cos\alpha\cos\beta & \sin\beta & \sin\alpha\cos\beta \\ -\cos\alpha\sin\beta & \cos\beta & -\sin\alpha\sin\beta \\ -\sin\alpha & 0 & \cos\alpha \end{bmatrix} \tag{50}$$

Control Frame Selection

The control strategy investigated for this research was viewed from the lead aircraft's perspective. That is, the position the wing aircraft is attempting to fly to is defined relative to the lead aircraft. As the lead aircraft moves and rotates, this desired position is relocated as if it were a rigid part of the tanker. This concept was used whether there was a physical connection between the aircraft such as the refueling boom, or whether the wing aircraft was merely assigned to hold a position out near the wing of the tanker. The formation geometry is always maintained.

This technique is certainly not the only way to solve the refueling problem. Osteroos chose the complete opposite perspective, moving until the tanker was at a desired relative position from the receiver vice the other way around. There are also questions to be answered about where to fly. For example, it would be much simpler to design a controller that always maintains altitude with the tanker instead of climbing and descending during rolls while assigned to the wing observation position (the drawback would be turning the tanker into a co-altitude aircraft that may experience a control problem or delay). As unmanned vehicles will most likely follow fighter-type procedures, the goal of this research was to mirror the current method used by Air Force fighter pilots exactly.

With the overall paradigm determined, the control strategy is simple: determine the difference between the actual position of the wing aircraft and the desired position, and apply the control surfaces to drive that position error vector to zero. The position error vector is first broken into three components. Each frame investigated was oriented such that the x-component of error was applied to the throttle channel, the y-component to the aileron, and the z-component to the elevator. The question remained open, however, of which reference frame to express the error in before applying the control. Figure 18 highlights the differences.

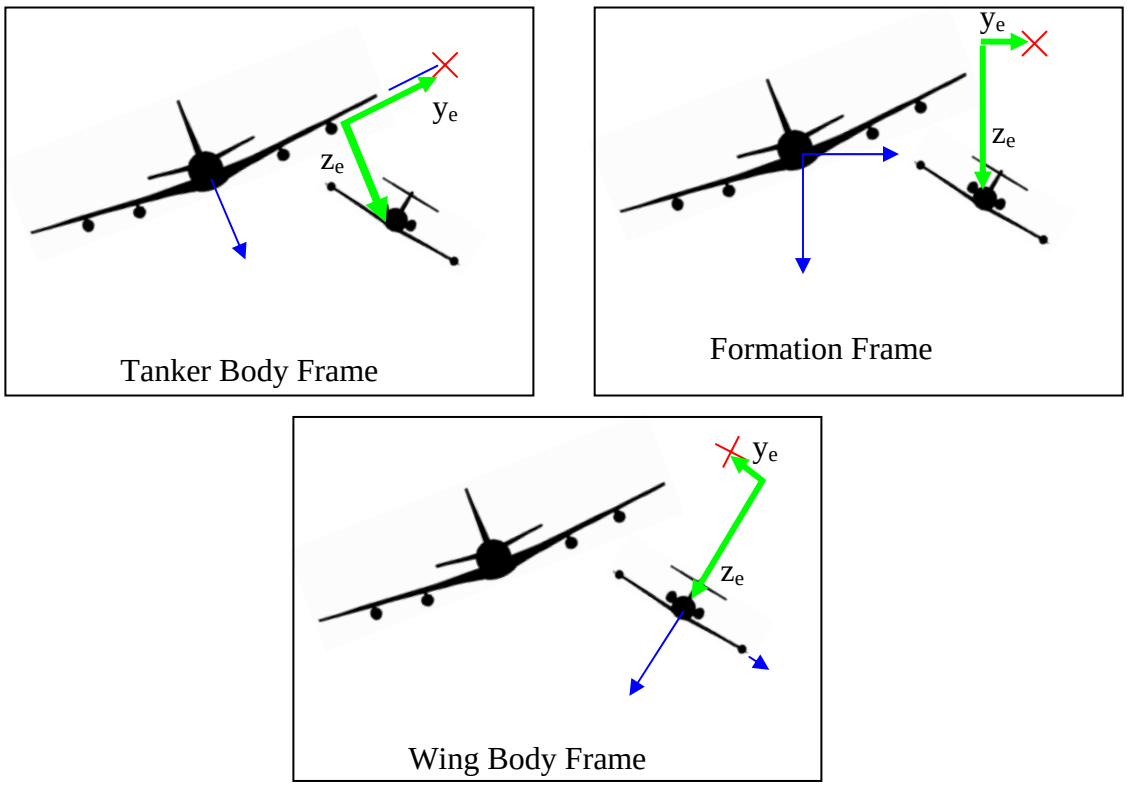

Figure 18. Control Frame Differences

In each case, the wing aircraft has error between the current position and the desired position—on the wing of the tanker marked with an "x". The three frames shown demonstrate that the control frame selected will determine not only what proportion of the error goes into each channel of the controller, but in extreme circumstances it can determine the direction of control as well. Several frames of control were investigated, and some of the lessons learned are repeated here in an effort to assist future research along the same lines.

From Figure 18, the seemingly obvious conclusion drawn is that the wing body frame (or the similar wing wind axis) is the control frame of choice. It is the only frame which generates the correct direction of control for this condition (left aileron).

Wing Wind Frame Control.

The wing body frame is the most intuitive, as it is aligned with the direction that the controls are physically mounted onto the airplane. In addition, the error is seen from the wing aircraft pilot's perspective. From the pilot's viewpoint, a move in the "up" direction is made with back stick and resulting tip-up elevator. Which direction the aircraft actually moves in inertial (or near-inertial) space is irrelevant for control application. As a small note, the wing body axis shows where the aircraft is pointed, and not necessarily where it is going, so the similar wing wind frame is used instead.

Consider the exaggerated situation shown in Figure 19. In this case, an error vector in the body axis would control the elevator to move the aircraft down, but an error vector in the wind axis would correctly move the aircraft up. This difference is minor as the angle of attack will usually be less than 10 degrees. The differences between the

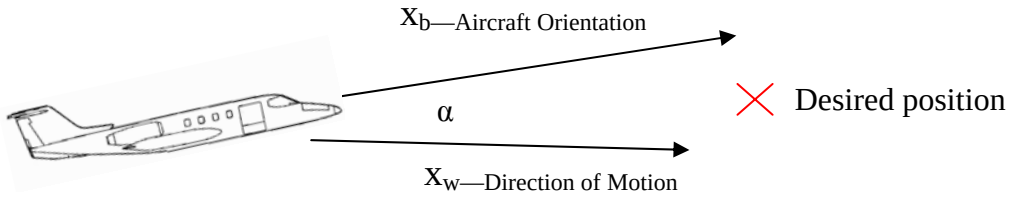

Figure 19. Wing Wind vs. Body Axes

wind and body frames could potentially be ignored if future control designers do not have access to a clean angle of attack signal.

Wing Wind Frame Difficulty.

Though intuitive, several factors decrease the effectiveness of control in the wing wind frame. In simulation, the wing aircraft was completely controllable during straight and level flight, and responded well to step response errors in each axis. Difficulty, however, was encountered during more aggressive turns. As will be developed in the next chapter, the control laws will contain proportional, integral, and derivative control in each axis, with a few additions in the pitch and roll axes. The components of wind axis error vary with the attitude of the wing aircraft. Consider the simple turn in Figure 20.

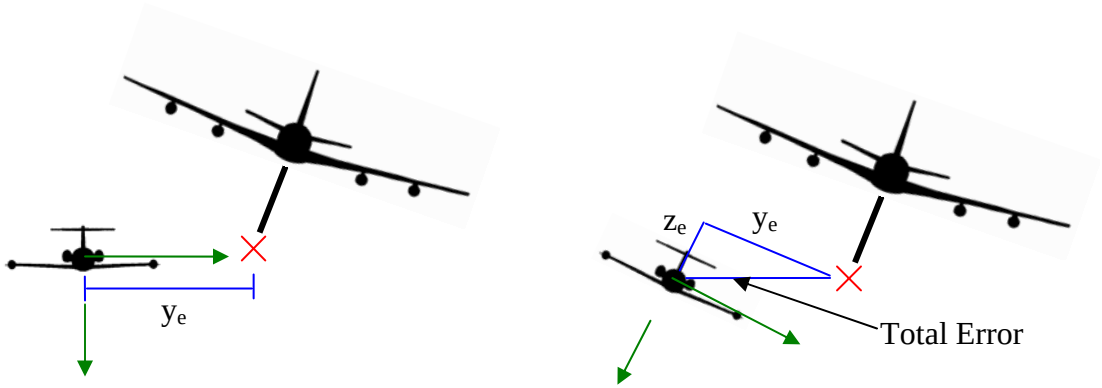

Figure 20. Error Components in the Wing Wind Frame

As the tanker begins a turn and moves away from the wing aircraft, error develops in the y-channel, commanding roll to compensate. The greatest errors obviously occur when the lead aircraft moves away briskly, or when there is a reversal in direction of turn. As shown in Figure 20, when the wing aircraft rolls to begin its turn, the error is translated into components of the y and z-axes. As the wing aircraft's bank continues to increase, the size of the error component in the wind axis z-direction continues to increase and the component in the y-direction decreases (in the extreme, if you rolled to 90° of bank you would have 100% z-axis, and no y-axis error resulting in all elevator control).

The proportional effect is to increase control from the elevator and to decrease control from the aileron. While a steady state increase of elevator control is desirable for the turn, the effect in simulation was delayed. The elevator was not added until the wing aircraft reached a level of bank large enough to make the z-component of error significant. At the slow roll rates of a tanker (exacerbated by an adverse control input to be explained in the control law development), the elevator blended in somewhat late and caused more lag outside of the turn than other frames of control.

Some oscillation and a minor settling time increase was also noted when controlling with the wing wind frame. As a turn was initiated by the tanker, lateral error developed that was again partially transferred to the elevator as the wing aircraft banked to correct the initial lateral error. As before, the steady state position of the wing aircraft's elevator will have to increase to continue the turn. With wing frame control, however, the proper steady state amount of error signal to the elevator is only seen when

the wing body frame is aligned with the tanker body frame. As the wing aircraft initially over-banks to "catch up" with a tanker that has begun a turn, the amount of elevator commanded is more than required for steady state. This is the most efficient way to get *to* the desired position, but when *arriving* there the heading of the wing aircraft is slightly inside the turn, as a result of the position correction. Heading feedback was not an option for this research as one of the possible test aircraft did not have heading information accessible on the data bus. The heading mismatch is corrected by using less bank angle than the tanker, but this leads to an insufficient amount of steady state elevator, which drops the wing aircraft slightly outside the turn again. The cycle would continue for some minor settling until the body frames of both aircraft were nearly aligned. This effect was not dramatic, and it should be noted that the research accomplished with the control frames was performed relatively aggressively. After reconsideration in the light of the low rates experienced during actual flight test, there is potential that the slow maneuvers of refueling may be acceptably controlled with the wing wind frame.

Another negative effect of wind frame control occurs as a result of the derivative control applied to each channel. Referring again to Figure 20, as the wing aircraft begins to roll, the component of y-axis error is reduced. While the amount of bank desired should be a function of true lateral error to be corrected, now it is strongly dependent on the wing aircraft's attitude—even with zero relative motion. This problem is compounded by the effect of derivative control, as $\dot{y}_e$ and $\dot{z}_e$ are now also strong functions of bank angle, not merely reflections of position error. With derivative control, $\dot{y}_e$ is negative (the controller thinks lateral error is being corrected) while rolling into the turn.

The controller therefore commands roll in the opposite direction for damping, even if there has been no real change in the actual lateral error relative to the tanker. The opposite effect is seen in the elevator channel. The y and z-axis error components continue to swap channels as the wing aircraft fights to find the right bank angle, and some oscillation develops. The effects of this coupling are small as long as the changes in bank angle are small, but in simulation, for 30° turns and turn reversals, wind axis control resulted in lateral control that pilots would refer to as "ratchety".

Formation Frame.

The formation frame designed for the NASA F-18 flights was investigated next. The formation frame eliminates the y and z coupling by not rotating with the pitch or roll of the tanker [9]. The frame is completely independent of the wing aircraft's attitude. Figure 21 shows that the problem of error components swapping control channels when the wing aircraft fights to stay in position is solved with formation frame control.

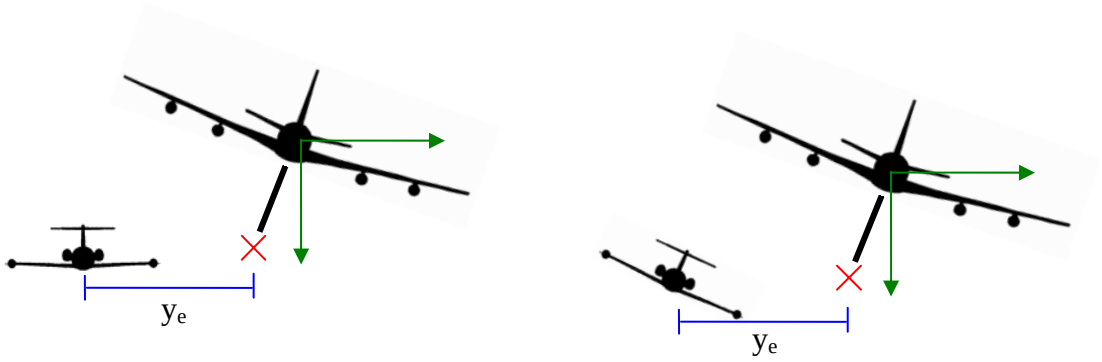

Figure 21. Formation Frame Solution to Wing Error Channel Coupling

The result was a much more stable lateral system. Obviously, if the wing aircraft is grossly misaligned, the control inputs would be completely inappropriate (consider the extreme case of being inverted; all of the corrective commands are backwards). A controller operating in the formation frame must assume that the wing aircraft will be relatively near wings level. A final benefit of the formation frame was the correlation of the elevator to a common altitude hold system, which is relatively easy to design.

Formation Frame Difficulty.

A major portion of the design was accomplished with formation frame control, including all of the work with step errors in each direction for initial gain tuning during straight and level flight. When NASA designed the formation frame, however, they did not intend their controller to be capable of turns. Simulation shows that the formation frame is less effective when the lead aircraft is in a bank. Conceptually, consider the two cases presented in Figure 22.

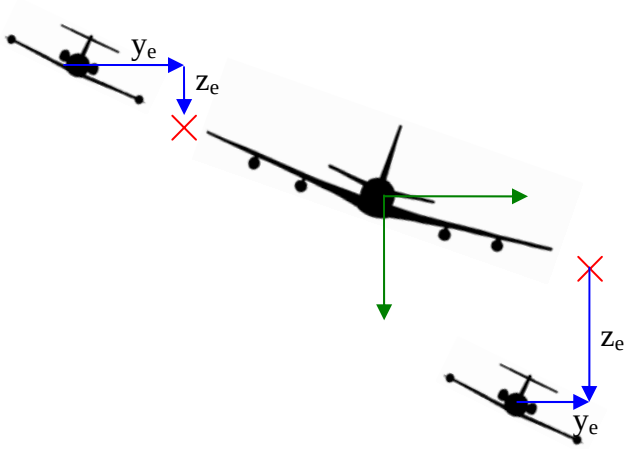

Figure 22. Formation Frame Misalignment in a Bank

A pilot trying to fly formation on the left wing of the tanker would fix the position error with an application of right aileron alone. After moving into position, the rates would be arrested with left aileron, but the elevator would not be used. Conversely, the pilot on the right wing of the tanker would correct position error with elevator alone and no aileron. An automatic controller working in the formation frame would erroneously command control in both channels for both cases.

This effect of misapplying some amount of control between the y and z axes worsens with increased bank angles. A portion of the error vector is put into the wrong channel any time the lead aircraft is not wings level. The effect on control is long settling times, as shown in Figure 23.

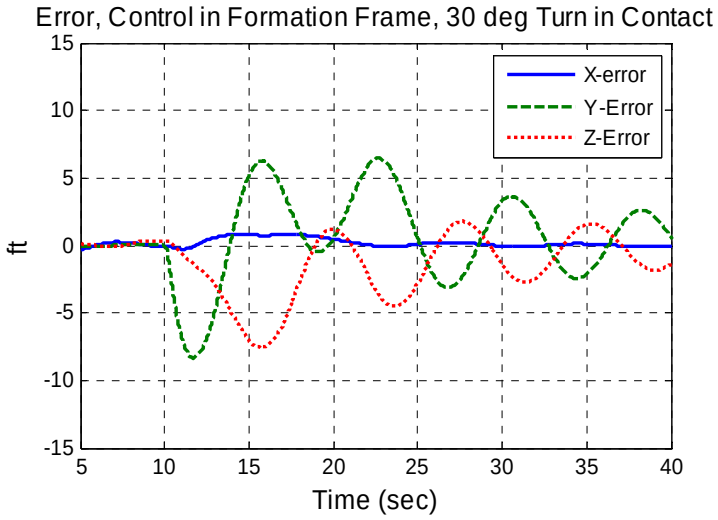

Figure 23. Formation Control Frame Settling Time

Figure 23 shows formation frame control for a wing aircraft in the contact position during a 30 degree bank right turn initiated at 10 seconds. The roll rate of the

tanker was increased to 12 deg/s to accentuate the problem. The initial error of -8 feet (8 feet left) is a function of geometry (as the tanker rolls into bank to the right, the boom of the tanker, if held rigid, would go to the left). As the turn stabilizes, the coupling effect can be seen between the y and z axes. The extended settling time is a function of applying small amounts of control in the wrong channels, caused by the misalignment of the formation frame from the actual tanker attitude. In contrast, consider Figure 24, the exact same turn presented to a controller operating in the tanker body frame.

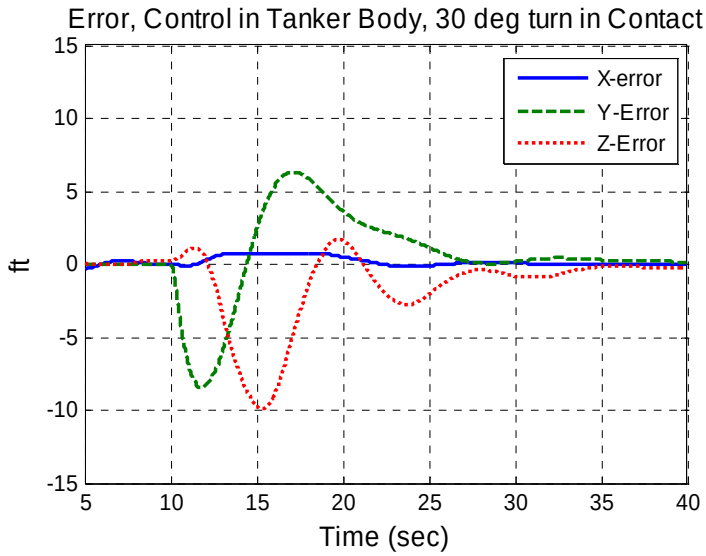

Figure 24. Tanker Body Frame Control Settling Time

When the control was applied in the tanker body frame, the elevator channel is not as effective at maintaining altitude control. The wing aircraft gets 10 feet high (recall z is positive downward), but the ability to settle toward steady state is greatly enhanced. Note that this turn, with a roll rate of 12 deg/s, is not representative of real tanker maneuvers, but is exaggerated to highlight the control frame effects.

Tanker Body Frame.

The final frame investigated, and eventually selected for control, was the tanker body frame. As an observation from personal refueling experience and experience as a formation flight instructor, pilots think in terms of a primary frame of reference in the lead aircraft's body frame, though pilots mentally decouple motion in separate axes. Pilots use this to solve flight geometry problems sequentially (prioritizing one axis at a time) when it is beneficial, eliminating some weaknesses of this frame.

In most fighter aircraft, the pilot cannot see the actual boom while refueling, though some jets do have canopy mirrors allowing a backward view. Regardless, it is difficult to precisely estimate position. To assist them, pilots visually receive position feedback in the tanker body frame through a set of lights on the belly of the tanker. These lights derive and display the receiver location based on the position of the boom. On a KC-135 tanker, two scales of lights with the commands down/up and forward/aft are graduated to show how far to move in the commanded direction to center the boom. Lateral control is accomplished by lining up directly under a reference point on the belly of the tanker. The KC-10 tanker goes further to solve some of the proportional response overshoot problems by providing trend information instead of position alone (proportional-plus-derivative control). By providing the same style of information to the autonomous controller, the intent is to make the system fly the way a pilot would.

Tanker Body Frame Difficulty.

The tanker frame is not the perfect solution to formation flight control, but simulation showed it to be the best choice of imperfect options for this purpose. The

downside is giving up the alignment with the flight controls that the wing body frame has exclusively when the tanker bank angle does not match the wing aircraft's bank angle. This tradeoff is in exchange for the stability that comes with the tanker body frame over any wing frame. The tanker only rotates between two positions (straight, or turning), with very small overshoots and none of the "fighting" for position that the wing aircraft will experience. As a result, the tanker body frame is much more stable and error commands to the controls are swapping axis channels far less. However, the concept of cross channel inputs still exists, as the controls will be misapplied to some degree any time that the wing aircraft's bank angle does not match that of the lead aircraft. Since the simulations showed the wing aircraft's bank angle to almost always match the lead aircraft's bank within a few degrees (with some settling around a steady state bank angle), the stability of the tanker frame was considered the better choice. Flight test also confirmed that the wing aircraft stays within about 5 degrees of the bank angle of the lead aircraft. This made the tanker body frame effectively operate as an *average* wing body frame—oriented in the right direction, without all the bank corrections that cause position error to swap channels.

As a side note, sensor quality plays a role in the soundness of this decision. If the sensors on the lead aircraft provide inaccurate, jumpy attitude data, this frame will provide poor control. In contrast, the formation frame would fix most of the problems with poor attitude data from the lead aircraft, but has poor performance compared to the tanker frame when the lead aircraft is in a bank.

Final Control Frame Selection.

The control frame investigation and control law development occurred simultaneously. As such, no frame was initially sufficient for control, as the control laws were still deficient. As the controller became more capable, even the less stable frames became acceptable. By the time the control laws could hold the wing aircraft to small errors that were quickly corrected, any frame of control could be effectively used. The main differences in the frames manifested themselves during more aggressive maneuvers, and in settling time. For air refueling, however, even small performance increases are important. Control with the tanker body frame produced the best results.

It is the characteristics of the air refueling problem that make the control frame selection the most appropriate. The tanker body frame provides a very stable frame for control that does not cause position error to continually swap control channels during maneuvering. The weakness is that it is not always fully aligned with the wing aircraft's control surfaces, and will therefore sometimes misapply control. For the air refueling problem, however, the angular difference between the tanker and the wing aircraft's body frames will be small enough to ignore this deficiency. The tanker body frame works as an effective average wing body frame. Taken together with the fact that the refueling problem also has slow angular attitude rates that allow for heavy filtering, the overall strategy of controlling from the tanker's perspective, in the tanker body frame, holds the most promise for successful employment. The concept demonstrated the highest level of performance in simulation, and was subsequently prepared for flight test.

V. Control of the Receiver Aircraft

The modeling concepts developed in chapters II and III were implemented into the Simulink® diagrams that are presented in Appendix A. Simulations were performed with a twofold intent. The simulator was used in research and development of the best strategy for control, and the best control laws. At the same time, the simulator was an active test of the evolving controller that would be installed for flight test validation of the theoretical work. As such, control of the receiver consisted not only of the basic control laws themselves, but it also included all of the initialization, position assignment, control during position changes, and stability augmentation that was required to fully control the Learjet for flight test.

Initialization

When a controller such as the one designed in this work is installed on real aircraft, it will only be activated for the period of time when the wing aircraft is flying in close formation with another aircraft. For the majority of the flight, a completely different style of autopilot will be in control that is designed to take the UAV from one location to another. In the case of a refueling autopilot installed on a manned aircraft, it will only be engaged for a small portion of the flight. To be able to engage the system at all, the problem of how to smoothly transition between the two types of control must be solved.

Position Error Jumps.

The control laws will be discussed shortly, but for now, proportional, derivative, and integral elements exist in each axis. Transitioning from hand flying to a "go to" point when the system is engaged presents a problem. As the system is engaged, it sees a large jump in position error that happens in an instant of time. This error will always be there, unless you can fly *exactly* to the right place before engaging the system, an impossibility. Even if you could get very close, the jump in position error occurs in one time epoch for the controller, in this case, $1/100^{th}$ of a second. Any non-trivial amount of position error presented across that short of a time span will appear to have been caused by a huge rate of motion. This rate will be sensed by the derivative portion of the controller, and an unacceptable pulse will be commanded in each control axis.

There are several methods to avoid this. The method developed for this research was to create a new formation position. The Simulink® implementation can be found in the section of the controller that determines the position the wing aircraft should fly to, shown in the lower left corner of Figure 128, Appendix A. Along with contact, pre-contact, and wing-observation positions, a "hold position" option was created as position number 5 (positions 1 through 4 are shown in Figure 25 will be explained shortly). The current position vector, from the DGPS information transformed into the tanker body frame, is continually passed into the "hold position" coordinate definitions. At autopilot engagement, or any time when position number 5 is manually selected by the flight crew, the current coordinates are locked into a memory block and passed as the coordinates to hold. These coordinates are refreshed any time the crew selects position 5, allowing the

crew to stop moving at any time during a position change. This initialization solution avoids the large control spikes from the derivative control, allowing the system to engage without tripping one of the safety features on the Learjet that would disengage the autopilot after receiving such an abrupt command. Once position 5 is established, position change logic is invoked to move the aircraft from wherever it was when it was engaged to the desired formation position of contact, pre-contact, or wing observation, even if that spot is only inches away.

A similar initialization problem arises with the integral control in each axis. The controller always sees the position error vector that it is trying to drive to zero, whether the autopilot is engaged or not. When the autopilot is not engaged, the integral portion of control in each axis will continue to add up error and drive unbounded as the corrective action the controller is commanding is not followed. The simple solution is shown on the left side of Figure 136, Appendix A. Error enters the control law section of the controller, and a logic signal is used to reset the values in the integrators to zero when the system is not engaged.

These changes solve the initialization problems that come from the desired position jumping system engagement. When the autopilot is turned on, the controller is essentially told to fly to the position it is already at. Zero position error is seen by the proportional and derivative portions of control, and the integrator is reset to zero. The result is that zero control surface position command comes from the proportional, integral, or derivative portions of the control laws at the moment the system is engaged.

Control Trimming.

The Learjet VSS computer receives control surface position commands as deltas from an equilibrium point, but expects a full value for throttle commands. To avoid a pulse in the controls, the first commands that must come from the controller at initialization must all be zero with the exception of the throttle commands, which should be the same as they were just prior to initialization. Some of the control inputs were driven to zero in the previous section, but there are other additions to the control laws that will be developed shortly. These additions formulate control inputs based on a difference between the lead and wing aircraft's bank angle, roll rate and some pitch considerations. If all of these parameters are perfectly aligned, the control command at engagement will be zero. In reality, of course, the aircraft frames and rates will never perfectly match, and a residual command will exist that must be eliminated. If it is not, the residual commands will most likely trip the safety features of the Learjet when they are abruptly applied at initialization. The solution is regularly used by Calspan.

To solve the problem, a "balance and hold" technique is used that is shown in Figure 117, Appendix A, as the control signals leave the third control tier. The actual surface commands at the moment of initialization are trapped in memory and subtracted from future commands. The effort makes the initial commands zero, and makes future commands deltas from the actual surface positions at the moment of engagement.

For the thrust channels, a similar "freeze and hold" technique is used to add the settings at initialization to the delta command. The same technique is applied to the control surfaces deltas external to the controller to find their actual value. Working with

actual positions eliminates equilibrium estimate errors that may occur from mis-rigging of the flight controls or changes in true equilibrium elevator position due to fuel state or other weight distribution changes. In addition, there is a high likelihood that the pilot won't actually be in perfect equilibrium when the system is engaged, and the technique of working from deltas based on actual surface positions eliminates this concern as well.

Formation Position Assignment and Position Changes

Once the flight controller is initialized in "hold position" mode, it needs to be moved to the real formation positions. The Simulink® model that assigns those positions and contains the logic that controls moves between them is presented in Figure 128 of Appendix A. The contact, pre-contact, wing observation, and a "back corner" position created for position changes are presented to the controller via a constants block shown in Figure 116 of Appendix A. Avoiding hard-coding the positions allowed the flexibility of changing the position definitions during flight test, an option that was used to move the contact position farther away from the lead aircraft during the safety buildup. Each of these positions was defined relative to the lead aircraft in Figure 2 of Chapter I, and is presented to the controller in the tanker body frame.

Position Change Concept.

In the course of normal refueling operations, the wing aircraft will have to move between each of the assigned formation positions. Position changes from contact to pre-contact and back are accomplished directly, but moves to and from the wing observation position are done in the horseshoe pattern shown in Figure 25 to avoid potential collision.

Vertically, when moving from contact to wing observation, the aircraft moves down on the way to pre-contact, stays level across to the back corner, and climbs back up on the way to wing observation. For simplicity, and to correlate with the Simulink® model, the formation positions will be referred to by the numbers shown in Figure 25.

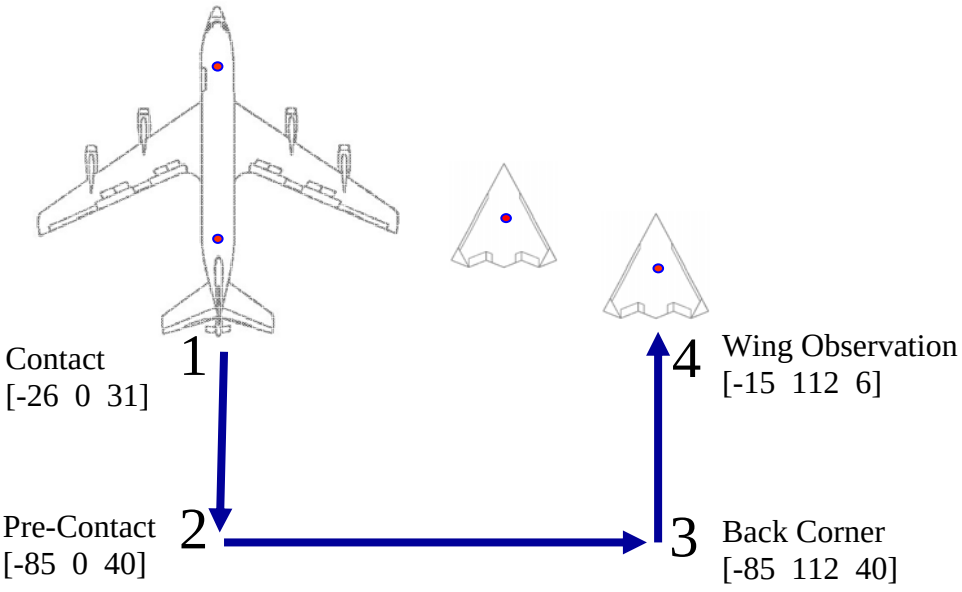

Figure 25. Formation Position Change Overview

Several methods can be used to accomplish this position change. The first technique experimented with was a waypoint method that was the most obvious. The desired position command was simply changed instantly from position 1 to position 2. The controller saw the distance to the new position as error, and the wing aircraft flew there as if it was a new waypoint to hold. Several drawbacks to this technique emerged as lessons. First, the large change in desired position over a short period of time caused a large, instantaneous change in position error. The derivative control responds with an undesirable spike to the flight controls. Even if a rate limiter is used to get around the

flight control spike, the position error is so large and takes so long to fix that a large tendency exists to over-control. The controller is designed to care about inches in position error. When moving from 2 to 3, the lateral move is 112 feet. Finally, the integral action continually adds up error until the position change is complete. For the long periods that it takes to move from one position to another, this results in large overshoots, especially in the longitudinal axis.

The second method investigated to command the position change was to step through several waypoints between each position. While this minimizes some of the previous problems, they still exist in smaller form. Stepping through several waypoints is complicated to implement, and results in choppy control if a low number of waypoints are used, but it is a step in the right direction.

Drawing this to the extreme, a third solution was attempted with an infinite number of waypoints. A set of ramp commands was generated for each of the 6 possible position changes in each axis. For instance, Figure 26 shows the position commands for a move from position 1 (contact) to position 4 (wing observation).

This technique showed a major improvement in the smoothness of control between points, but the sharp turns of the linear ramp inputs led to overshoots at each corner. In addition, the aircraft was moving at the same speed until the very end of the position change, which was then followed by the overshoot. From a safety perspective, the most critical position change is from pre-contact to contact, and the wing aircraft was not slowed down as it approached the refueling boom until it passed the contact position

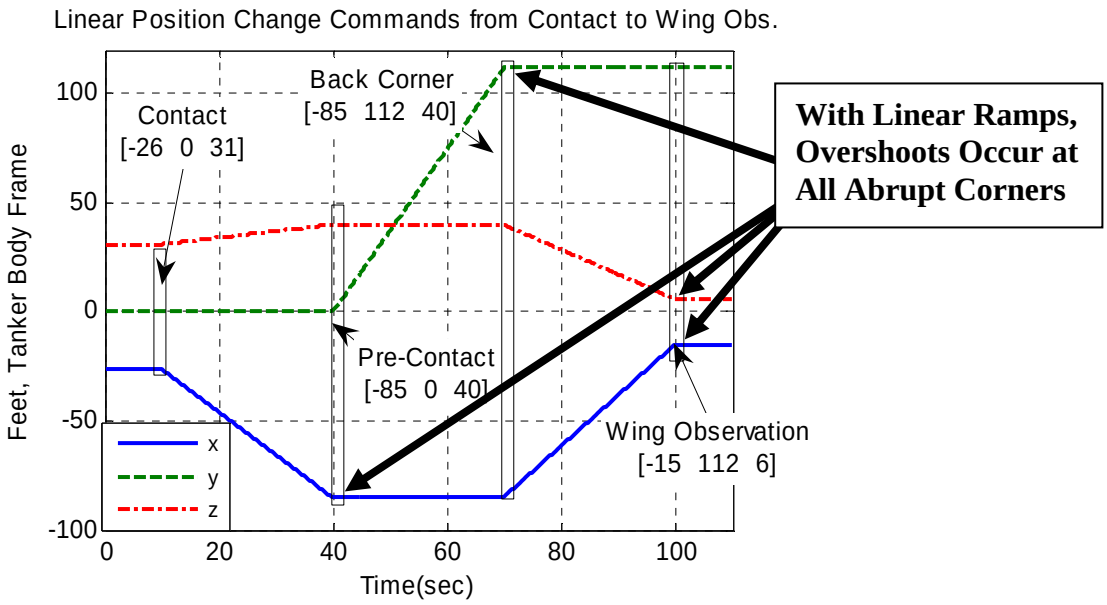

Figure 26. Linear Position Change Command Ramps

in an overshoot directly at the tanker. Justifiably, this has the potential to make the boom operator slightly nervous.

To work on the end points, a pre-programmed input was used as a fourth technique that was similar to the ramp commands with slightly rounded corners. This solution was effective, and used for the majority of simulation development. Unfortunately, there was no way to command the pre-programmed input to start while installed in the Learjet (in the simulator it was pre-programmed to automatically start after some delay from initialization). For future research, a rounded corner ramp input is sufficient for control, if you can implement it. For this flight test, the requirement to be able to command the rounded input to start at any time in any commanded direction led to an even better solution of position blending.

Position Blending.

The final solution, and the one that is recommended for further research, is to slowly blend the old position command into the new one, with a cosine wave to round the corners. To accomplish this, a timer must be built that can be reset in flight. The timer should be reset any time a new position is commanded and will control how fast the position blending takes place. Toward that end, a pulse is created when the position command is changed as shown in Figure 27.

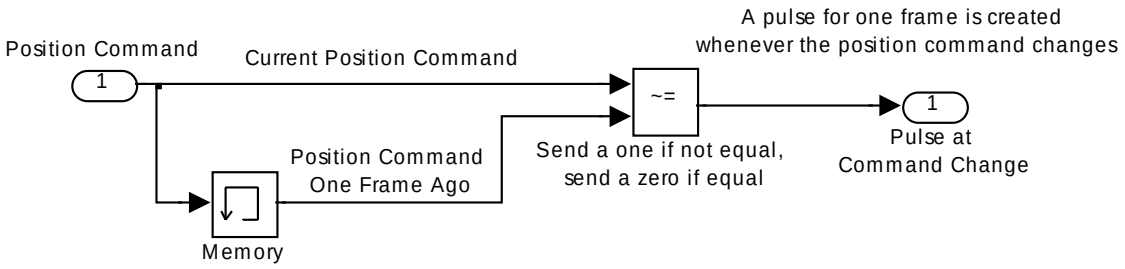

Figure 27. Pulse Logic

This pulse is used to reset an integrator which creates a ramp that operates as the timer. The number that is integrated determines how fast each old position is blended into a new one by adjusting the slope of the ramp. For flight test, the speed was left as a variable to allow in-flight adjustment of position change timing, but 30 seconds between positions was used as an estimate of an operationally representative speed. With a ramp function that can be commanded to start while in flight, the position blending can be accomplished by first saturating the ramp from zero to one. This number is then multiplied by each component of the new position command. The reverse of the ramp,

from one to zero, is multiplied by the components of the old position command. The sum of both products is a linear blend from the old command to the new.

The lesson already learned, however, was that linear position change commands have sharp corners that are undesirable. To alleviate this, the ramp is used to create a cosine wave to round the corners of the command. The implementation is show in Figure 28.

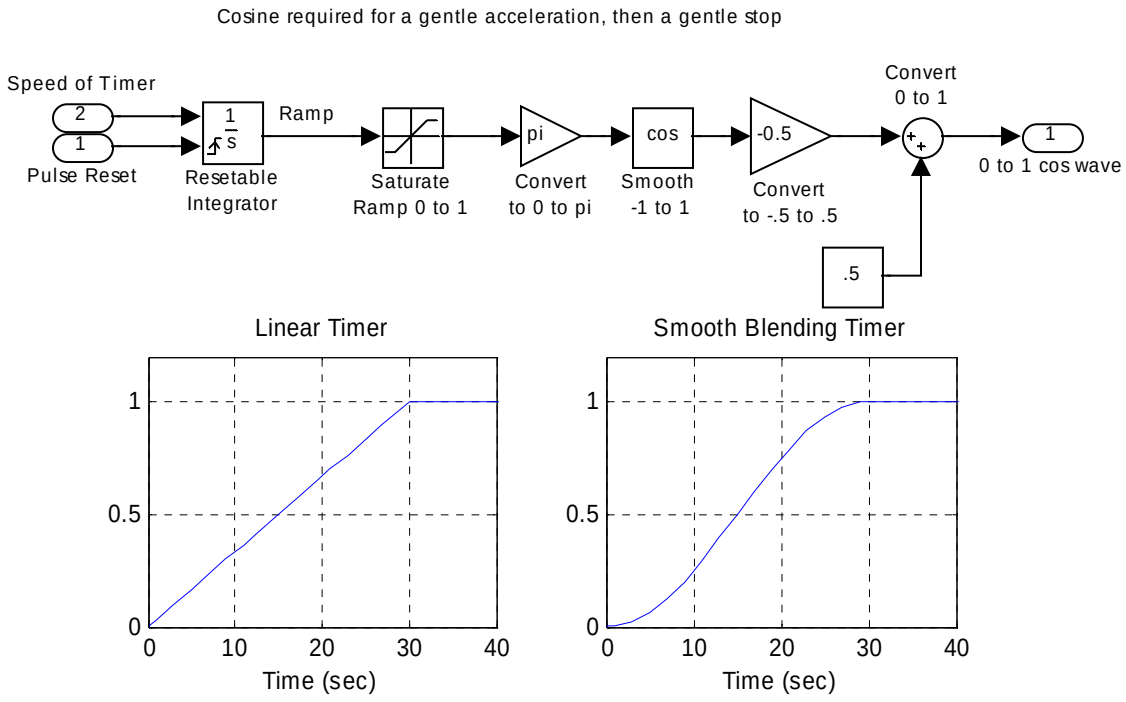

Figure 28. Smooth Timing Curve Creation for Position Blending

It is important to use a cosine function (or a phase shifted sine function) in order to put the smooth parts of the curve in the right places. The position change should start slowly, and end slowly. The output of the cosine function is shifted to move between zero and one. The opposite effect is created from one to zero, and the numbers are

applied to the old and new commands for smooth position blending. The full implementation for the simulator is shown in Figure 128 and Figure 135 in Appendix A. An example of the actual position commands is shown in Figure 29.

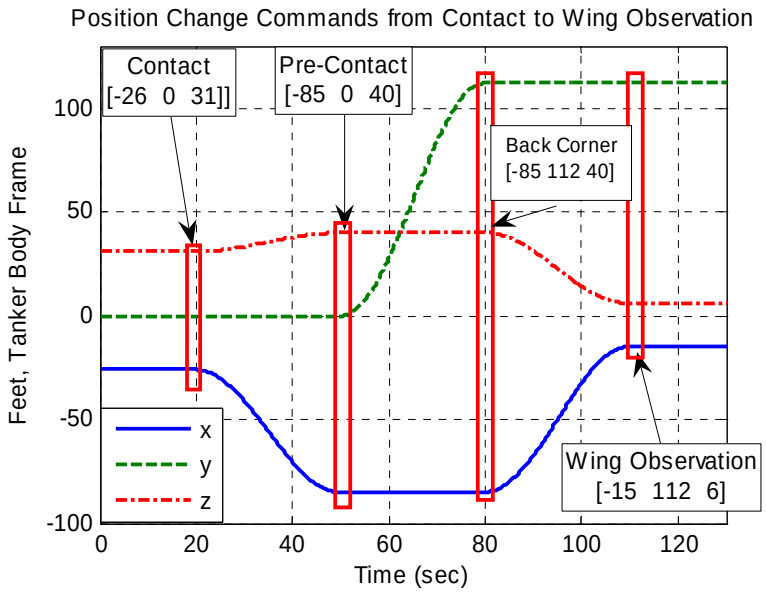

Figure 29. Smoothly Blended Position Change Commands

Two other considerations are required to complete the position change logic. First, one of the position options is “hold position”. When this is selected by the crew in flight, it is not desirable to blend in a solution, but to stop immediately and hold the current coordinates. An extra logic switch is provided to allow selection of position 5, the hold option, to bypass the timing logic. The implementation is also shown in Figure 128 of Appendix A.

The final piece of the position change logic is a safety consideration. Referring back to Figure 25, if a position change is commanded from the wing observation position

directly to the contact position, without first commanding changes through the back corner and pre-contact positions, the two aircraft will likely collide. The potential for a mistaken number to be entered in the "go to" command over the lifespan of the controller is extremely high. For the case of an unmanned vehicle, the mistake might not be noticed until it was too late. A control system should be designed at a minimum to not accept a request that was not entered in the correct sequence. Better yet, the controller should know to automatically sequence positions in the right order, allowing the flight crew or UAV commander to freely select any position. This is accomplished with horseshoe logic.

Horseshoe Logic.

Horseshoe logic was the name given to the software built to correctly sequence formation position commands. Again using the numbers for positions that were defined in Figure 25, a selection from position 1 to position 4 should be presented to the controller as 1, 2, 3, 4. The timing between numbers must be synchronized to coincide with the position blending timing that determines how long each leg of the position change will take. The full implementation of the horseshoe logic is presented in Figure 129 of Appendix A and an example of the options existing from position 1 will be presented to assist in understanding the full system.

An integrator is again used for timing, integrating the same number as the position blending timer to synchronize efforts. As with the position blending, a pulse is created whenever the "go to" command is changed in order to reset the timer. The value from the integrator is then reduced by 0.5 to compensate for a quantizer block that will be

explained shortly. One of the 5 step logic blocks shown in Figure 129 is then invoked, based on the current position that the wing aircraft is holding. Figure 30 shows the first step logic block, which is invoked when the wing aircraft receives a new "go to" command while in the contact position.

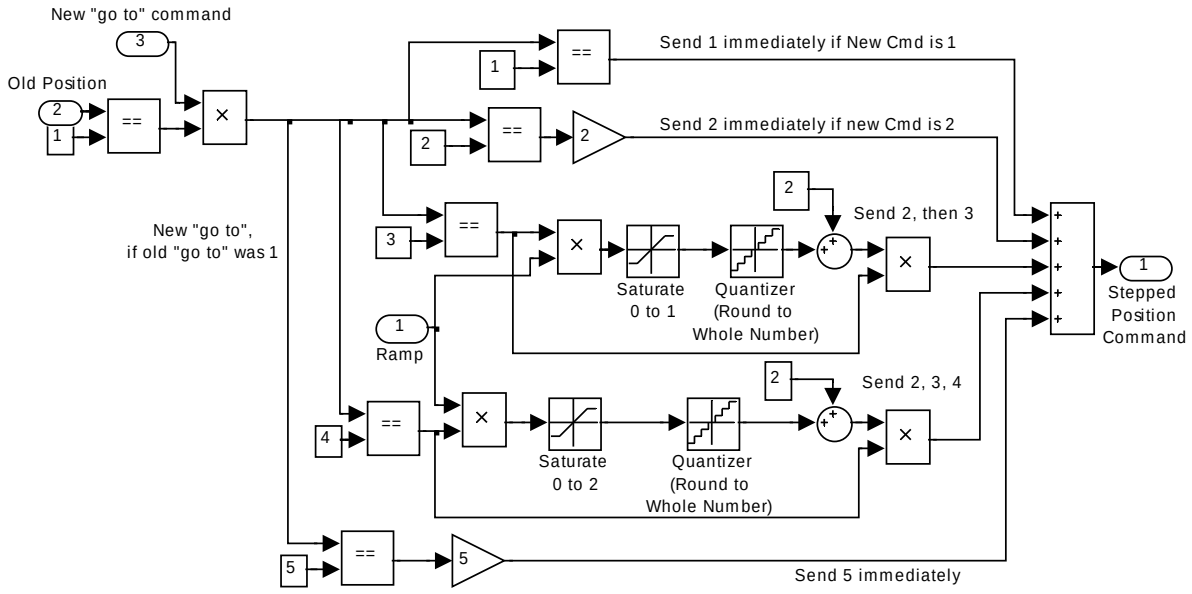

Figure 30. Step Logic for Formation Position Commands

The first portion of logic in the upper left hand corner of Figure 30 ensures that no signal is sent through the block unless the wing aircraft is being commanded from position 1. If the wing aircraft is in any other position, one of the other step logic blocks will be used instead. For the majority of time, the command of position 1 is sent through the top line of Figure 30. When the position command changes, one of the other 4 logic lines is used, based on the new command (2,3,4, or 5). The other options are again set to zero with the first logic block in each line. If the new command is position 2, the

number 2 proceeds straight through, as the contact position moves directly to the pre-contact position. The horseshoe logic sequences the order of the commands only, the blending of the old position to the new one happens after this block. If the new command is position 3, the output of the logic block should move first to 2, then to 3, with the standard position change timing between each step as the wing aircraft moves all the way to pre-contact before being commanded to the back corner.

Figure 30 shows the implementation. The ramp that was created to climb from -0.5 is saturated between two values, sent though a quantizer to round the signals to whole numbers, and then added to an initial condition (2 in this case). The position change timing will expire in the amount of time the ramp moves from -0.5 to 0.5. At that point, the quantizer will round up the signal from 0 to 1, moving the final stepped command from position 2 to position 3. For the case where position 4 is selected from position 1, the exact same logic is followed on the next horizontal line, except the ramp is not saturated until the value of 2, providing an extra step from position 3 to position 4 after another time period. If position 5, “hold position”, is ever selected, the command passes straight through without step logic.

Each of the other four step logic blocks work on the same principles, and can be reconstructed from the above explanation and the implementation shown in Figure 130 through Figure 134 of Appendix A. Building horseshoe logic, or another solution which allows carefree selection of any formation position at any time, is suggested for any future controllers as protection from an easy in-flight error that could result in severe consequences.

Second and Third Tier Control

The infrastructure of initialization occurs on the second tier of control, shown in Figure 117 of Appendix A. This is the block that is actually cut out of the simulator and installed into the test aircraft, as the top layer of the real controller. Position assignment, position changes, and the horseshoe logic are brought into the simulator in the third tier, shown in Figure 126 of Appendix A.

Several key events happen on the third control tier. The relative position signal that is provided to the controller is in the NED frame. The attitude information of heading angle, pitch angle, and bank angle is used to transform the position error into the tanker body frame, which was selected for control. This is accomplished via the direction cosine matrix shown in equation 46 of Chapter II and implemented in Figure 127 of Appendix A. The actual position vector is now subtracted from the desired position vector, which is produced by the position change logic previously explained. The result is the position error vector in the tanker body frame, the required driver for the control laws. However, before the control can be developed, the wing aircraft must first be stabilized.

Wing Aircraft Stability Augmentation

Unlike the lead aircraft model, the real Learjet is inherently stable. The longitudinal motion of the aircraft when disturbed from its equilibrium flight condition is characterized by a return to the equilibrium condition with a smooth damping, as shown in Figure 31, where an elevator doublet provides a disturbance to the angle of attack, α.

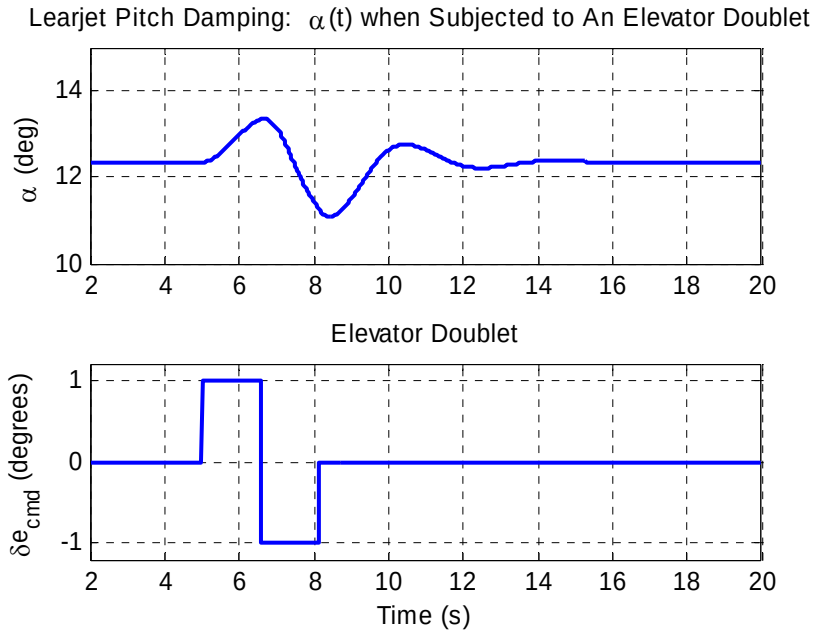

Figure 31. Learjet Longitudinal Stability

The longitudinal bare airframe characteristics were found then to be acceptable without control augmentation.

The lateral channel of the Learjet, however, was characterized by excessive Dutch roll oscillation. Figure 32 shows a rudder doublet of 2 radians per second used to excite the Dutch roll mode of the Learjet. Yaw rate and roll rate are poorly damped.

There are several methods to dampen Dutch roll. Calspan uses sideslip rate ($\dot{\beta}$) feedback. There is no sensor on the aircraft to measure sideslip rate, but the value is obtained from a filter designed to attenuate high frequency noise off of the sideslip sensor vane.

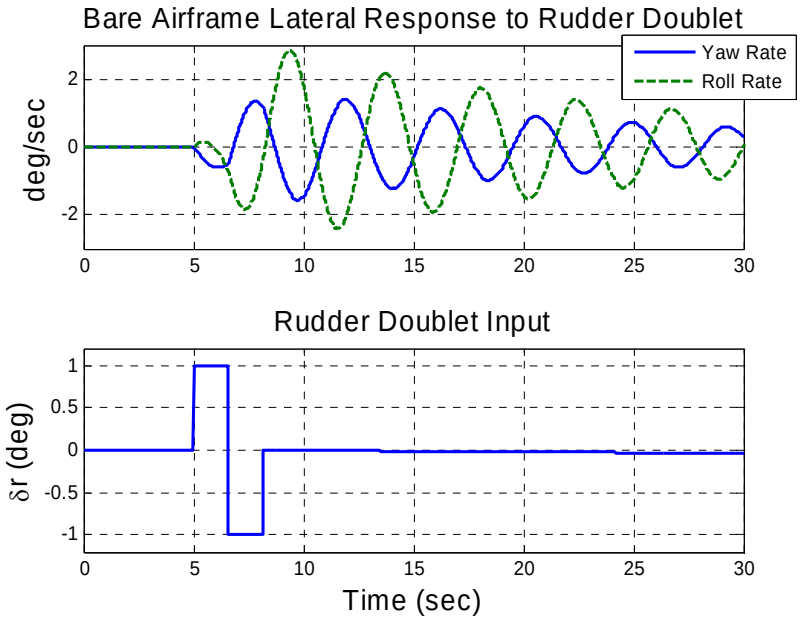

Figure 32. Learjet Bare Airframe Lateral Response

In order to keep the analysis of the data as simple as possible after the actual flight test, an effort was made to design the Dutch roll Stability Augmentation System (yaw SAS) as close to the model already in use by the industry as possible. In this spirit, the sideslip rate feedback technique was reproduced with some minor differences in methodology. The angle of sideslip measured from the beta-vane on the Learjet was differentiated to obtain $\dot{\beta}$. To attenuate the high frequency noise from the beta-vane, the following filter was used:

$$\frac{\dot{\beta}(s)}{\beta(s)} = \frac{100^2 s}{(s+100)^2}$$

The Bode plot of this filter is shown in Figure 33.

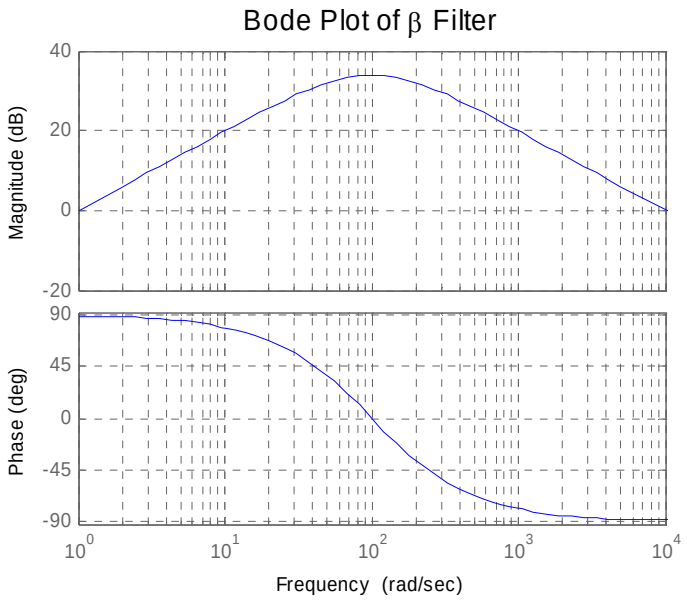

Figure 33. Bode Diagram of Differentiating Filter

As shown, the use of this filter provides the required differentiation at low frequencies, while attenuating the higher frequency noise disturbances that are too fast to be actual aircraft motion. To be the most effective, an analysis of the body modes of the aircraft and the beta-vane would be required to determine the best time constant for the filter. For simplicity, however, the attenuation point was selected through comparison to the time constants of the actuators. The actual values are proprietary, but it can be said that the break point of this filter is at a higher frequency than the actuator bandwidth. Therefore, the filter will supply the needed derivative for usable control signals, and will attenuate all signals that would be too fast for the attenuators to apply control for.

With the above filter in place and a $\dot{\beta}$ signal now available, the yaw-SAS was

implemented to command rudder deflection (δr_{w_cmd}) with the following control law:

$$\delta r_{w\_cmd} = k_{sas}\dot{\beta} \tag{51}$$

where

$$k_{sas} = -1.2$$

The value of k_{sas} was selected for adequate handling qualities. MIL-STD 1797 requires aircraft in category A flight to have a damping factor of at least 0.19 for a Level 1 rating [6]. The value for the damping ratio was found from the time response in Figure 32 with the following logarithmic decrement method from Ogata [12]:

$$\zeta = \frac{\frac{1}{n-1}\left(\ln\frac{x_1}{x_n}\right)}{\sqrt{4\pi^2 + \left[\frac{1}{n-1}\left(\ln\frac{x_1}{x_n}\right)\right]^2}} \tag{52}$$

where ζ represents the damping ratio, x_1 and x_n are peak amplitudes, and n is the number of the peak of interest. Without a yaw-SAS, the Learjet had a damping ratio of 0.03. With $\dot{\beta}$ feedback and k_{sas} gain of -1.2, the damping ratio has been raised to 0.43, calculated from Figure 34. The Dutch roll damping was the only stabilization required for the Learjet test aircraft. After much development to this point, the control laws can now be investigated.

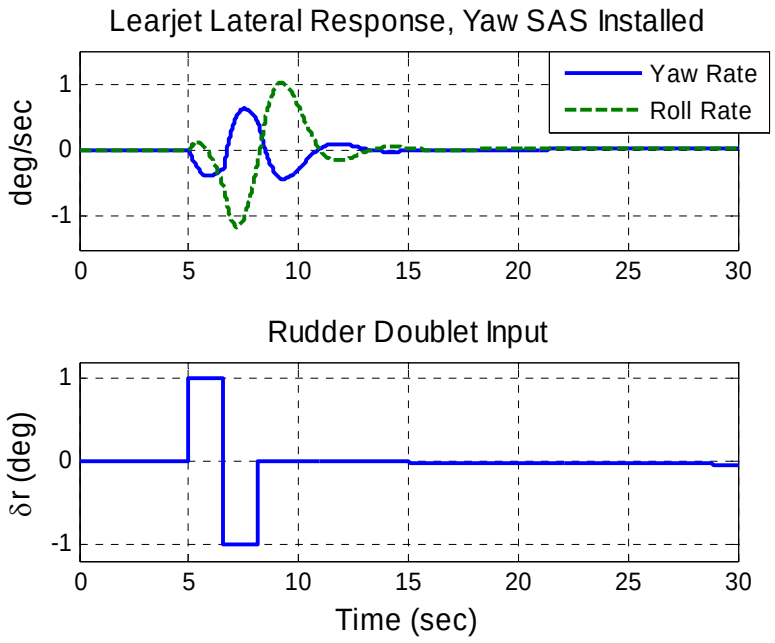

Figure 34. Learjet Lateral Response with Yaw Damper

Control Law Development

The original intent of this thesis, as presented to the author as a reachable goal, was to build a controller to fly formation based on proportional-plus-integral control on position error only. For this specific situation and these aircraft, however, that proposal proved untenable. An effort was made to keep the control laws as close to the original intent as possible. Extra control elements for damping and feed-forward (FFD) control were required to achieve the desired level of performance.

Elevator Channel.

The controller design method turned to elevator control first. The lateral control channel is by far the most complicated, and elevator control must first be in place to sustain a turn in order to investigate it. Likewise, without the elevator control to hold

altitude, investigation of the throttle control channel causes altitude excursions that change the geometry of the formation and ruin the attempt. The methodology followed for this research was to first hold ailerons, rudder, and throttle at equilibrium while tuning the elevator in straight and level flight. Next, the throttle constraints were released for complete longitudinal tuning, and finally the model was completely freed for the lateral work. Obviously, each new change in configuration brought changes to the prior work, and an iterative approach was used.

The initial elevator control design centered on PI control of position error only (specifically, the z-axis error was fed to the elevator channel). However, with the dynamic flying environment and high sensitivity of the aircraft altitude to very small changes in elevator angle, PI control was found to be too oscillatory at an acceptable rate of response. Figure 35 shows the vertical response of the aircraft when subjected to an initial altitude disturbance of one foot at 6 seconds (step input) with PI control only.

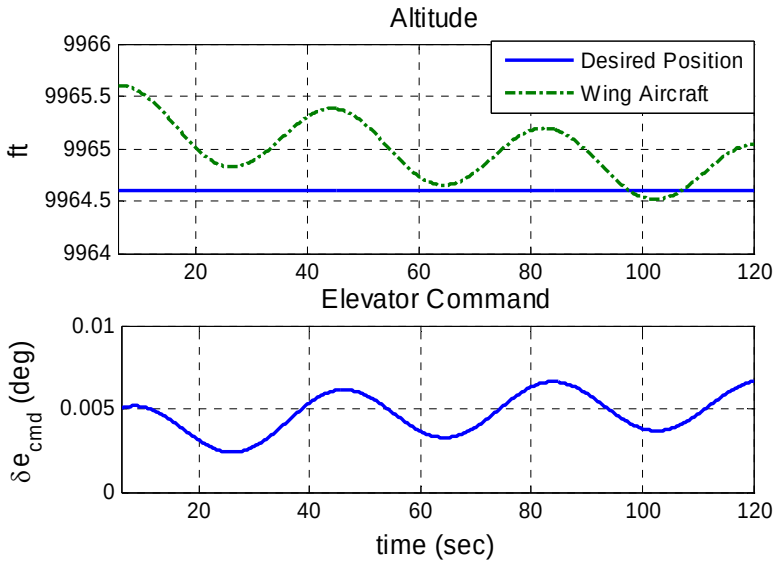

Figure 35. Simulated PI Control on Z-Axis Step Disturbance

As can be seen by the slow speed of response, the gains are set extremely low. The correction is so slow that the phugoid mode dominates the response. However, at even slightly higher gains, the system is unstable. This was investigated with proportional control only and PI. The gain margin of the system is extremely low due to the system sensitivity and inherent lag time. Other combinations of control are certainly possible, but the response of the system without some damping is inadequate. Derivative control was added, which enabled the gains to be increased. As a result, the speed of response and stability increased, and larger step disturbances were investigated (a potential factor for non-linear simulation). Figure 36 shows a three foot step disturbance applied at 6 seconds.

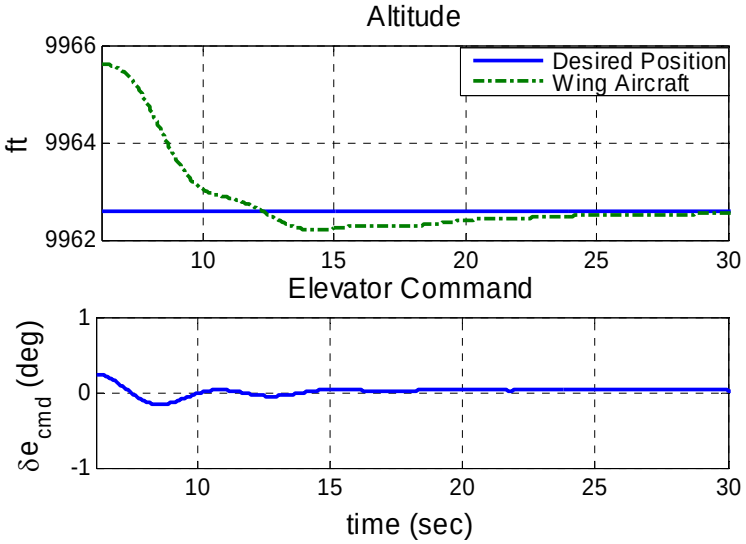

Figure 36. Simulated PID Control on Z-Axis Step Disturbance

A small overshoot is due to the impact of the integral control, but the response is acceptable and efficient. Later experimentation in simulation, however, showed a greater requirement for response during turns was required to eliminate nose droop on the roll in.

Any increase in gain, however, required a correlating increase in damping. Higher levels of derivative control began to result in decreased stability margin, and another form of damping was found in the form of pitch angle perturbation ($\Delta\theta$) feedback.

Pitch angle is not the traditional damper. Normally, one would dampen with pitch rate (q), flight path angle (γ), or vertical velocity ($\dot{h}$). Though not intuitive, it was found that for this formation flight simulation pitch angle feedback worked better than pitch rate feedback. Unlike the traditional flight control system, the goal is not to dampen a θ command system, but to dampen z-axis error. The derivative control on z-axis error is already a part of the control laws, and changes in θ provide the maximum lead for the system because the pitch changes before the resulting changes in γ or $\dot{h}$ (effectively telling the controller when it was *about* to change altitude). The key for pilots in maintaining formation flight is to match the attitude of the leader as much as possible, allowing only small deviations for position corrections. Since the pitch angle feedback is a delta from equilibrium, it acts as a penalty for straying from the nominal position. Any time the elevator control seeks to correct vertical position error, the penalty on moving the nose from equilibrium works against that command, effectively damping the vertical channel. The result was the following control law to determine the wing elevator command (δe_{w_cmd}):

$$\delta e_{w\_cmd} = k_{z_P} z_e + k_{z_D} \dot{z}_e + k_{z_I} \int z_e \, dt + k_{z_\theta} \Delta\theta_w \tag{53}$$

where the quantity $\Delta\theta_w$ was determined with the following relationship:

$$\theta_w = \theta_{w\_eq} + \Delta\theta_w$$

The angle θ_w is available from a sensor in the Learjet, but θ_{w_eq} is not. An estimate was used for θ_{w_eq} that was from the Learjet simulator obtained from Calspan. The estimate was taken at the design flight condition of 10,000 ft MSL and 190 KIAS and the likely weight for the flight test. Due to the flight test location of Edwards AFB, a slightly warmer than standard day temperature of 80 degrees on the ground was assumed with a standard temperature lapse rate. The true value for equilibrium pitch angle will depend on numerous variables such as weight, cg, and density altitude on the test day. In hindsight, it would be easy to capture the value for pitch angle at initialization into a memory block instead of using an estimate. However, any error in the estimate will likely be very small, and will be set to zero anyway when the system is engaged by the techniques discussed in the initialization section.

With the elevator control law established, implementation was performed using the same differentiation technique as the yaw damper design for high frequency noise cancellation. Figure 37 shows the Simulink® model.

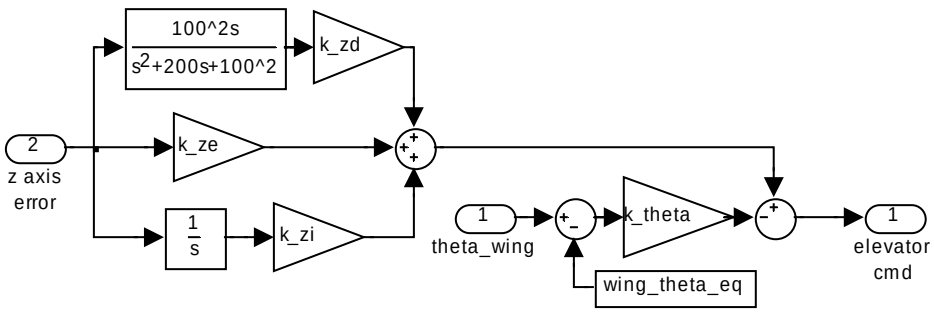

Figure 37. Z-Axis Control Law Implementation

The corresponding gains and constants used in the model are shown in Table 6, with all angles in degrees, all distances in feet.

Table 6. Elevator Channel Gains

k_zd	k_ze	k_zi	k_theta	wing_theta_eq
0.25	0.6	.08	-2	9.05

Throttle Channel.

With the elevator control in place to hold altitude during forward and aft excursions, control of the throttle channel was developed. An auto-throttle capability for the Learjet was installed for this flight test, but was not operational until the second week of testing. Obviously, no data about the characteristics of the system were available for modeling ahead of time. An estimate was provided by Calspan using a first order lag model with a time constant of $\tau = 1/5$ and a 0.3 second pure time delay. The wing aircraft model was amended to include the thrust model effects.

While the throttle was by far the simplest channel to achieve desired performance in, PI control was again found to be insufficient for formation flight control. Figure 38 shows the wing aircraft with a one foot step error in the x-axis with PI control. The aircraft were initialized heading north, and the error value shown is the difference in north position, in feet. The controller was turned on at 6 seconds.

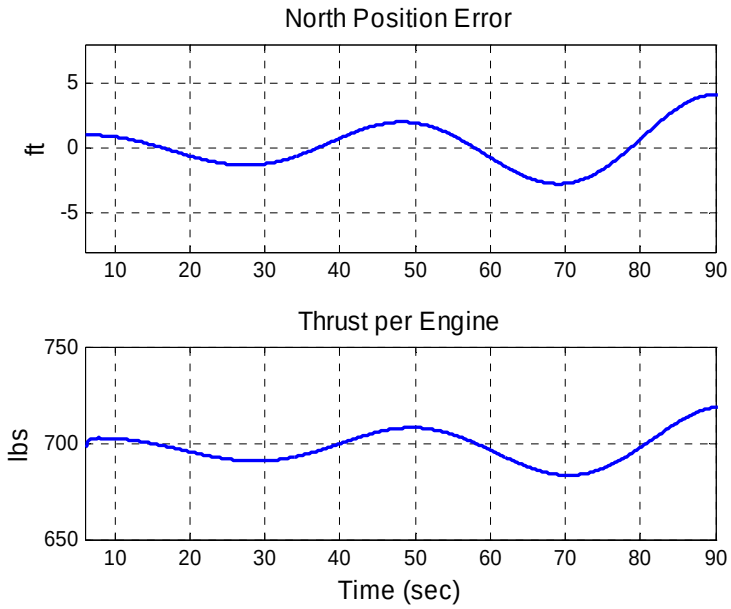

Figure 38. Simulated PI Control on X-Axis

As shown in Figure 38, even with extremely low feedback gain (note the time scale), the system is unstable. This is the case with or without integral control, and is again due to the nature of formation flight. When flying formation, the aircraft is moving through a fluid. For illustration, if you want to stop a boat in a particular place, pulling the engine back to idle by the time you reach that place (proportional control) will not stop the boat. The boat has continued to amass inertia for the entire time you approached the stopping point, and has very little friction to slow it down. Aircraft in formation move the same way. Unless the control is reversed prior to reaching the desired position, it will be overshot. This effect is exacerbated in the elevator and aileron channels, where the entire aircraft must rotate after the overshoot before the direction of travel reverses. For the duration of the overshoot, the integral control is adding up position error and

making corrections which are added to the proportional corrections and unchecked, making another overshoot likely. Instability is nearly inevitable without anticipation.

Without the auto-throttle delay, the system is stabilizable. For the real system, however, PI control is grossly insufficient and derivative control is added to make a PID control law for the left engine perturbation thrust command (Δdxl_{w_cmd}):

$$\Delta dxl_{cmd\_w} = k_{x_P} x_e + k_{x_D} \dot{x}_e + k_{x_I} \int x_e \, dt \tag{54}$$

An identical control law was provided for the right engine, Δdxr_{w_cmd} (no split throttle control). Figure 39 shows the system time response to a 3 foot step disturbance at 6 seconds.

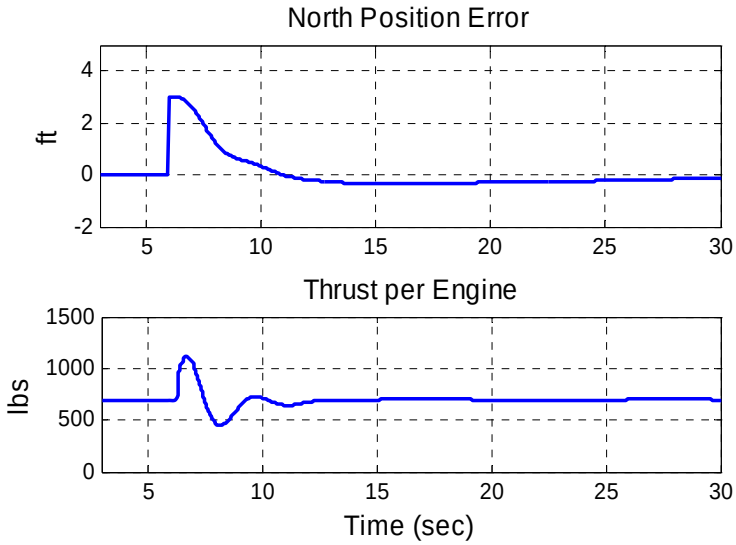

Figure 39. Simulated PID Control on X-Axis

For implementation, the proportional, integral, and derivative components of control were summed for a delta command, and this was added to the total thrust at the moment the autopilot was engaged for the total throttle command, as discussed in the

initialization section of this chapter. The thrust command was then saturated to stay within the physical capabilities of the aircraft in the second tier of control, shown in Figure 117 of Appendix A. The final gains selected for the throttle channel are shown in Table 7, with command thrust in pounds and distances in feet:

Table 7. Throttle Channel Gains

k_xd	k_xe	k_xi
300	100	10

Aileron Channel.

The lateral error is by far the most difficult to control. Movement of the ailerons does not directly translate into lateral position corrections, but instead induces roll rate. Roll rate integrated over time creates changes in bank angle, and the new bank angle then produces a turn rate which over time laterally moves the aircraft. Only after the wing aircraft begins turning is lateral position affected. From the pilot's perspective, a greater amount of anticipation and lead is required for aileron control. Roll occurs quickly, but there is a relatively long delay before lateral movement occurs. Adverse yaw exacerbates the problem. This is what makes quickly lining up with a runway centerline from a low altitude challenging. Nevertheless, pilots become experienced with aileron control and generally do not use any rudder when refueling. To reflect actual pilot technique, the lateral control for this project was performed with ailerons alone and the rudder was used only for stability augmentation. After the experience of watching the controller fly during actual testing, however, this decision was reconsidered. In hindsight, future

research should consider experimenting with the rudder for small lateral position error assistance, as rudder deflection directly causes a change in turn rate, skipping an entire integration required by aileron control.

For this research, finding acceptable lateral gains when the controller needed only to correct small disturbances in straight and level flight turned out to be relatively easy. Designing a controller that could maintain relative formation geometry during the dynamics of rolling maneuvers, however, proved to be much more difficult. Several control schemes were experimented with and simulated. Since this is the most challenging part of the control problem, some of the better concepts and the lessons learned are presented here to assist future designers.

PI control on lateral error applied to the ailerons was again attempted and discarded as inadequate. The addition of derivative control made the system stable, and a PID controller was designed that worked for small errors, feeding PID control on position error directly to the ailerons. Position error damping worked toward rolling the wing aircraft out when moving toward the desired position, but simulation showed that the commanded wing roll rate was too fast when position errors were large, causing large desired bank angle overshoots and subsequent oscillation. A roll rate feedback loop was added, essentially building a roll rate command system, driven by PID control on position error.

This control system was effective for small errors and turbulence disturbances, but inadequate for large errors or position changes using a changing waypoint method as described in the position change concepts section of this chapter. The lateral distance

from the centerline of the tanker to the wing observation position is 112 feet. A roll rate command system will continue to add bank until the position error is corrected. If an unlimited rate controller sees error for the entire time it takes to make the position change there is potential to actually roll the wing aircraft inverted. This extreme is all but impossible when using the blending technique for position changes, but there is a strong potential to over-control even with small position errors if they are not quickly corrected. The difficulty of maintaining formation increases greatly with higher bank angle differences between the two aircraft. This is compounded by the fact that any bank that is put in must be taken back out, and the aircraft will continue to overshoot until banked opposite the direction of motion to stop drift. When teaching new pilots to fly in formation during maneuvers, the first rule is to match the lead aircraft's attitude as closely as possible and to only allow small deviations for position correction.

To limit the potential for over-controlling, the design turned toward a bank command system to allow the capability of saturating the commanded bank angle difference between the two aircraft. The actual bank angle must be allowed to vary considerably, since the lead aircraft may be in up to 30° of bank. Dynamic saturation limits were set on the bank angle command to keep it near that of the lead aircraft. Limits were set to keep the controller from commanding more than a 20° difference in the aircrafts' bank angles. Obviously, saturation limits can lead to limit cycles and instability, but if the controller needs more than 20° of difference in bank during refueling (even during position changes) it most likely has other instability problems originating from the high level of aggressiveness. In hindsight, the aircraft during actual

flight test never had more than about 5 degrees of bank angle difference, so the saturation limits are liberal.

Figure 40 shows the control implementation to this point in the development for ease of understanding. PID control on y-axis error generates a bank command which is saturated to stay near the lead aircraft's bank angle. A gain on error between commanded and actual bank angle converts the signal to commanded bank rate, and a gain is applied to the bank rate error signal to achieve the desired commanded aileron deflection.

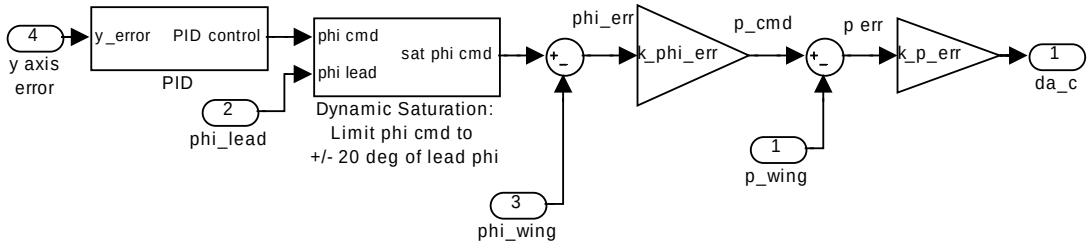

Figure 40. Interim Implementation of Bank Command System on Y-Axis Error

The bank command idea is solid, and sufficient for straight and level flight, even during position changes. The limitations of this type of control arise when the lead aircraft is in a bank. Figure 41 illustrates the point. As the lead aircraft begins a turn to the right, y-axis error is developed. The PID control commands a bank angle to compensate, and the error is eliminated. The problem with changing to a commanded bank angle instead of a rate is that when there is no position error, the bank command is zero. This obviously causes a roll out until more error develops and an oscillatory pattern of poor settling time is established. Eventually, integral control will compensate, but the effect is delayed.

Figure 41. Requirement for Lead Bank Angle Feed Forward Control

To alleviate this problem, the bank command system was changed to the same technique taught to young pilots--match the leader first, then add or subtract bank to compensate for error. This is accomplished by feeding the lead aircraft's bank angle forward into the bank command junction prior to the saturation, as shown in Figure 42.

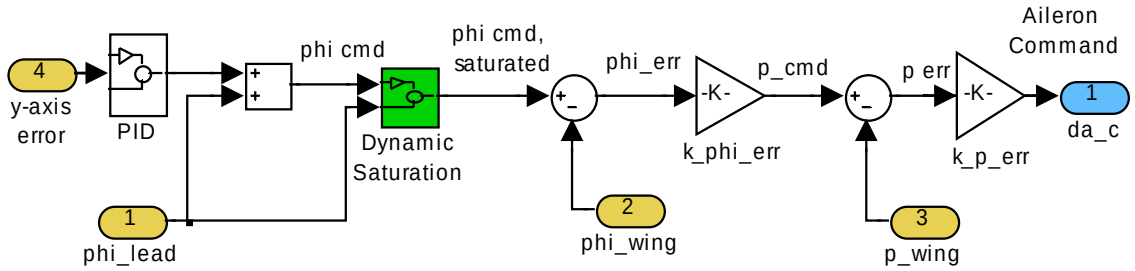

Figure 42. Addition of Lead Bank Angle FFD to Aileron Control

The controller was now capable of flying solid formation in established turns.

The final problem addressed in the design process was an "adverse command" present during the most dynamic portion of the profile, the roll in and roll out. The exaggerated picture in Figure 43 illustrates the problem.

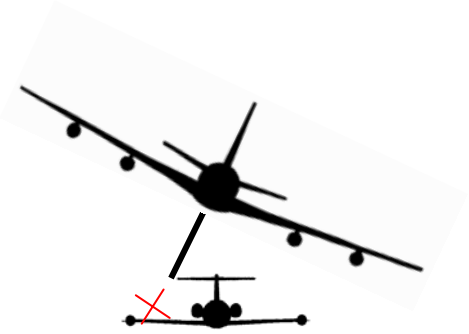

Figure 43. Adverse Lateral Command at Turn Initiation

At the roll in, the desired position of the wing aircraft moves toward the outside of the turn, the wrong direction to be commanding the wing aircraft to go. The size of the adverse change in position error depends on the roll rate of the tanker. From pure geometry, if the wing aircraft was in the contact position and the tanker rolled 30 degrees without moving, there would be about 16 feet of position error in the wrong direction. Only a portion of this is communicated to the controller, however, as the tanker begins to move toward the inside of the turn before reaching full bank. As the tanker rolls faster, more of the error is seen by the wing aircraft. Roll rates were investigated that allowed up to 8 feet of adverse command (anything greater than this and you would break the boom if the pilot didn't initially turn to the outside). For a controller tuned to hold position within inches while refueling, errors of this magnitude cause a large response. Even slow banked turns to small bank angles produce undesirable behavior. The bank command generated by a gentle turn to 15° of bank can be seen in Figure 44, which shows the non-minimum phase behavior commanded into the roll channel.

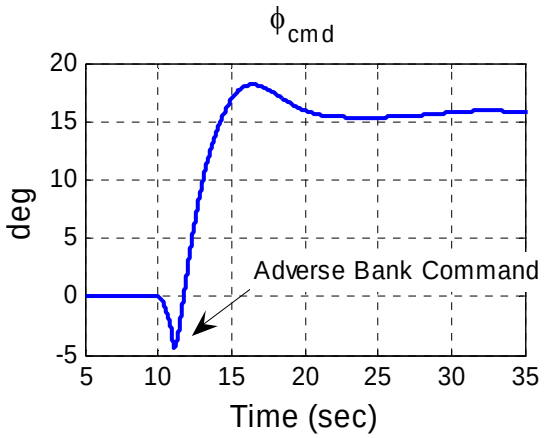

Figure 44. Adverse Bank Command

The impact of this command is not merely a delayed roll. The situation is compounded by the fact that the wing aircraft starts rolling the wrong way. The controller must now overcome the roll inertia that is building and reverse the turn. Meanwhile, the tanker is well established into the turn and steadily moving away. The delay involved in getting the aircraft rolling the correct direction results in large overshoots to the outside of turns.

The controller needs to anticipate the correct turn direction. This is provided by feeding the lead aircraft's roll rate forward into the rate command signal. The only time a tanker should have any roll rate (with good sensors and a well flown aircraft) is while entering and exiting turns. A pilot in formation does not wait until lateral position error or significant bank angle difference has developed before starting his turn, and would not consider rolling in the wrong direction as suggested by the adverse command. At the start of a tanker's roll, the pilot blends in just under the amount of bank used by the tanker and slowly drifts to the outside of the turn, then uses a small over-bank to arrest

the line of sight rate that developed from the small bank mismatch. Cueing on the roll rate of the tanker allows a correction to be started before a significant difference in the bank angle develops. Figure 45 shows the final control law implementation. Some filtering is added to the real controller, and the full implementation of the all control laws used in flight test is shown in Figure 136 of Appendix A.

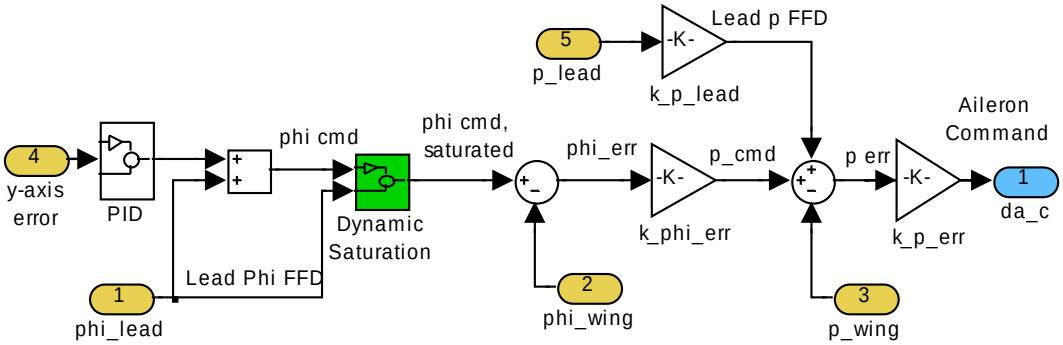

Figure 45. Final Control Law on Y-Axis Error

The corresponding gains are shown in Table 8, with distance in feet, angles in degrees, and rates in degrees per second:

Table 8. Aileron Channel Gains

k_yd	k_ye	k_yi	k_phi_err	k_p_lead	k_p_err
.8	.3	.03	2.5	1.5	-3

The amount of lead aircraft roll rate fed forward into the wing bank rate command channel was tuned for a design roll rate of 7.5 degrees per second. This rate was based on an estimate for a likely tanker roll rate with receivers. During flight test, however, operationally representative rolls were measured, and a realistic rate was found to be

much slower. Future research should tune the controller to a roll rate between 2.5 and 3 degrees per second at the fastest portion of the roll.

To tune the controller, the gain should be increased just enough to eliminate the non-minimum phase command in bank angle. Unfortunately, it is optimized only for the design position and roll rate. In the pre-contact position, for example, there is a larger vertical lever arm which exacerbates the adverse command problem. Being farther away, the controller sees more lateral position error for the same bank rate. The now larger position error overcomes the unchanged feed forward rate input, resulting in some adverse roll which causes a greater overshoot to the outside of turns. Since no other receivers are near the wing aircraft while in the pre-contact position, and the strict boom envelope position limits do not need to be maintained, this lateral error has little significance. If future designers wish to eliminate it, the feed forward roll rate gain needs to be scheduled based on vertical distance from the tanker.

The initial roll in portion of a turn now is a reasonable approximation of a pilot's technique. Figure 46 shows the error during a normal 15 degree turn to the right, with the wing aircraft maintaining the contact position. As the error plots are not initially intuitive, exaggerated aircraft drawings have been added to illustrate error progression.

The desired position is plotted from the tail view in Figure 47, with the wing position in the center of each graph. As the turn begins at 10 seconds, there is no error. By 12 seconds, adverse bank command is driving the controller to bank left, but the lead roll rate feed forward offsets this command, causing the wing aircraft to roll with the tanker, but slightly delayed as shown in the lower graph of Figure 46.

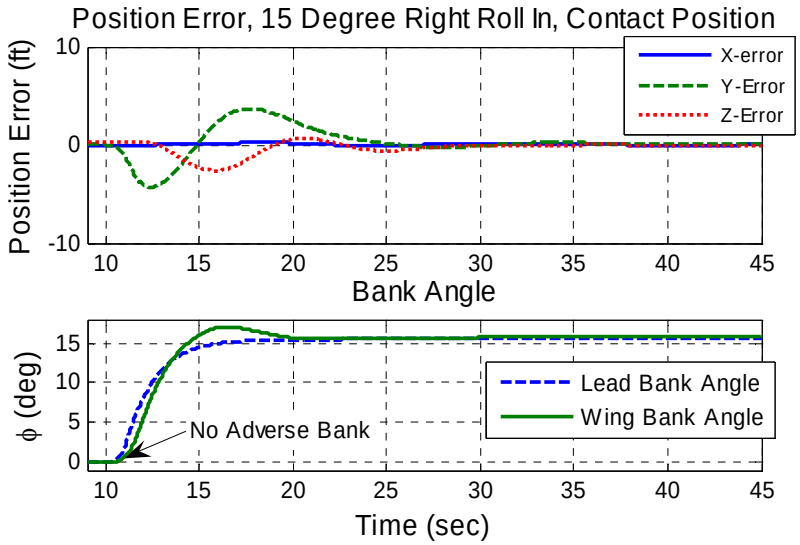

Figure 46. Position Error, Roll Rate FFD Canceling Adverse Roll

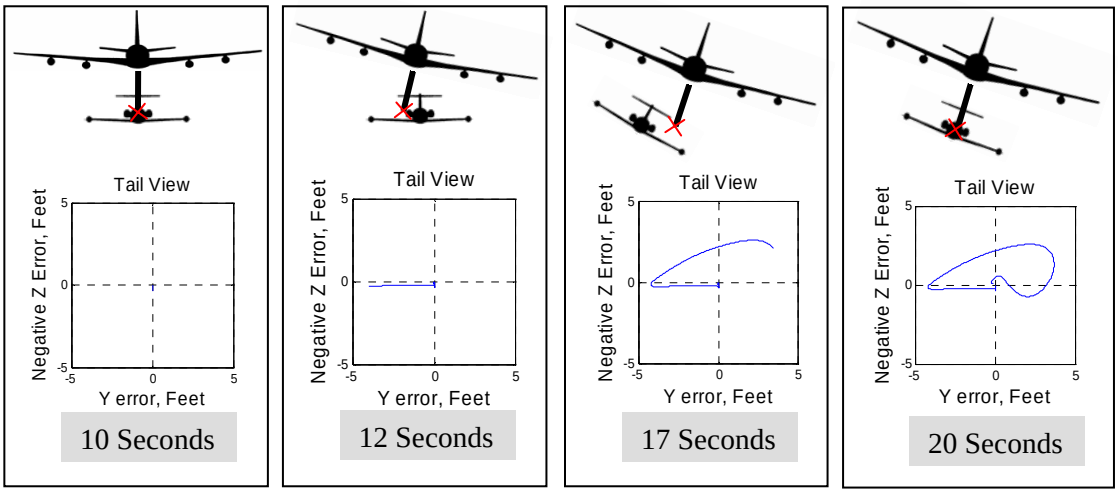

Figure 47. Sequence of Initial Roll Settling

At 15 seconds the wing is again centered laterally, but still sliding toward the outside of the turn. Some of this is natural inertia that must be checked with an over-bank, but some contribution comes from the integral control that has been adding up the perceived but false error to the left of the wing aircraft, resulting in some overshoot and

delay in getting settled into the turn. The extent of this overshoot is shown at 17 seconds and is considered acceptable. By 25 seconds the wing aircraft is stabilized in the turn, never having exited the center of the boom envelope by more than approximately 4 feet.

Several other methods were experimented with, that will not be listed here for space and clarity reasons, but one technique should briefly be mentioned. Heading error between the lead and wing aircraft is an excellent damper in simulation, and if using the waypoint method for changing formation positions, it provides a way to limit the rate of position correction as the wing aircraft moves laterally to the wing observation position. The most positive aspects of heading difference feedback are seen during large, aggressive maneuvers when there has been some lateral overshoot. The controller will guide the wing aircraft back into position but will require oscillation to achieve alignment. Figure 48 illustrates the situation where lateral error has been corrected and the bank angles are fairly closely matched as dictated by the control laws, but the headings are not lined up due to the wing aircraft's latest correction.

Figure 48. Heading Misalignment

The heading mismatch will soon develop into position error and there will be some oscillation. Feeding a small amount of heading error into the aileron control law dampens this effect and decreases settling time. Some heading mismatch is expected in turns, but this is a steady state effect which is eliminated by the integral control.

Despite potentially promising results in simulation, heading error was not added to the control laws. The backup test aircraft, Calspan's Lear 1, does not have heading information available in real time on the data bus. It was therefore removed to retain flight test flexibility. Adequate performance was achievable without heading feedback.

Rudder Channel.

The only rudder control applied was the Dutch roll damper designed during the stabilization process. During refueling, pilots normally do not apply rudder for station keeping, and the only rudder actuation occurs as part of the normal stabilization and coordination of the aircraft. In hindsight, two considerations should be investigated in future controllers. First, feeding the lateral position error into the rudder should be explored. As mentioned in the aileron channel section, the rudder influences turn rate directly, fixing later error faster than aileron control. Use of rudder for large position errors is not recommended due to the undesirable impacts of large sideslip angles, and a promising technique to blend out rudder correction for large errors was presented by Osteroos [13].

The second consideration that would be simple to implement and assist with turn coordination and adverse yaw effects is an aileron-rudder-interconnect (ARI). Since the

controller has only one design airspeed and altitude, the process is greatly simplified to only a proportional gain on the aileron defection added into the rudder channel.

Summary of Wing Aircraft Control

Several concepts of control have been experimented with and were presented in order to guide future designers who are currently working on the autonomous air refueling problem. The final configuration is briefly summarized here. A simulation was designed with two individual aircraft models. The ground track of the models was recorded, and a differential position vector was produced to mimic the DGPS relative position signal available in flight. The attitude signals of the lead and wing aircraft also available were likewise reproduced from states tracked in the simulator. The controller portion of the formation simulation received these inputs and determined the appropriate settings for control. The controller was an exact copy of what was installed in the aircraft for flight test.

Inside the controller, the desired position vector was created based on the position the wing aircraft should be in during refueling for contact, pre-contact, the wing observation position, and a back corner required for position changes. The difference of the desired and actual position vectors was the position error vector. The position error vector was transformed into components of the tanker body frame, and these components were acted upon by the control laws. X-axis error was applied to the throttle channel, y-axis error to the aileron channel, and z-axis error to the elevator channel. Each channel determined a delta position for control and applied that to the equilibrium positions of the control surfaces and throttles at initialization.

The throttle channel control consisted of PID control on forward-aft position error. The elevator channel consisted of PID control on vertical error, with an additional penalty term for allowing the wing aircraft to deviate from an equilibrium pitch attitude. The rudder channel consisted only of a stability augmentation system that minimized sideslip rate. The lateral channel consisted of a feed forward system that commanded the wing aircraft to match the lead aircraft's bank rate and bank angle, and then applied additional PID control to minimize position error. All feedback gains were tuned manually to achieve desired performance.

In order to change formation positions, the controller applied a blending technique that slowly changed the original position into a new position. Logic was applied to correctly sequence the order of maneuvers to accomplish any position change. To initialize the system, the current position at autopilot engagement was selected as the desired position. This ensured that the position error seen by the controller was zero, and all integrators were reset. A technique was used to balance and hold the trim positions of the control surfaces and throttles at engagement to avoid any transients. The position held at engagement was then blended into one of the standard formation positions to begin testing.

VI. Simulation Results

Lead Profiles

For operational aerial refueling, the racetrack pattern shown in Figure 8 of Chapter I is the most common flight profile. A design altitude and airspeed is determined for each type of aircraft, and allowances are made to change altitude when required. For the simulation and flight test, the design flight condition was 10,000 ft MSL and 190 KIAS, estimated with 220.1 knots true airspeed. The tanker's turns are planned for 15 degrees of bank, but may increase in bank up to 30 degrees if required for unforeseen circumstances. If traveling great distances, refueling is simply accomplished along the way in straight and level flight. To encompass all options, the controller needs to be able to maintain formation position while straight and level, and while accomplishing level turns. How the turns are accomplished is significant, both for an automated controller or a real pilot. Flying in formation precisely becomes increasingly difficult as the roll rates and bank angles of the lead aircraft increase.

During the design of the simulator and tuning of the feedback gains, the lead aircraft profiles commanded a maximum roll rate of 7.5 degrees per second when rolling to 15 degrees of bank, and 10 degrees per second when rolling to 30 degrees of bank based on a poor estimate. During actual flight test, a roll rate of 2.5 to 3 degrees per second was found to be much more realistic. In addition, a tanker, like any good flight leader, "telegraphs" turns by slowly building in roll rate vice going immediately to or from the maximum rate. The 7.5 and 10 degree per second "old" lead profiles were used for simulator tuning were found to be too abrupt and too fast for a realistic simulation of

a tanker. As such, the final gains were optimized for a flight condition more difficult than the controller should encounter. Presentation of the results found from the old lead profiles could be misleading. All of the position errors are within tolerances for the mission, but are not what should expected from this system. The old profiles do, however, demonstrate that the controller capability is not restricted to the very benign roll rates that are realistic for operational refueling. To keep the information gained from both sets of data, "new" lead profiles were created with more realistic rates and the simulations were re-accomplished. Position error results are shown for both new and old lead profiles for all 30 degree turn simulations, where the roll rate effects are the greatest. The old profiles are shown without noise, as the rate effects are of interest. Comparisons of the lead profiles used for the basic turns are shown in Figure 49 and Figure 50.

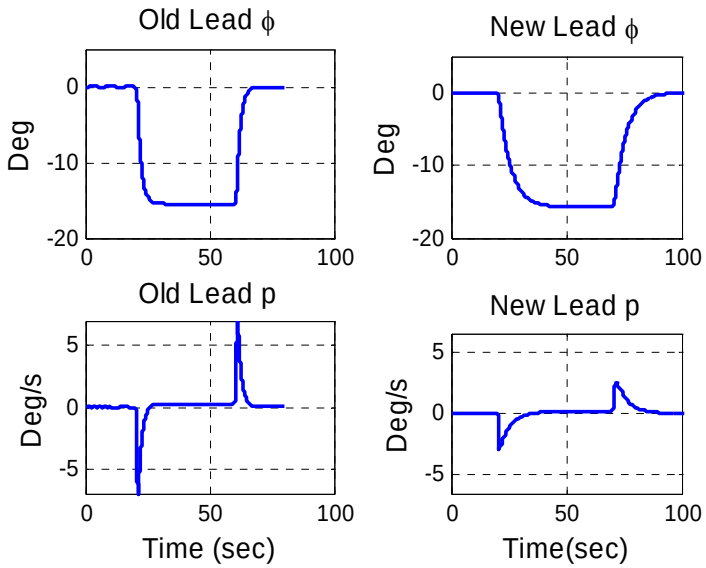

Figure 49. Comparison of Original Design and More Realistic Profiles for 15 Degree Banked Turns

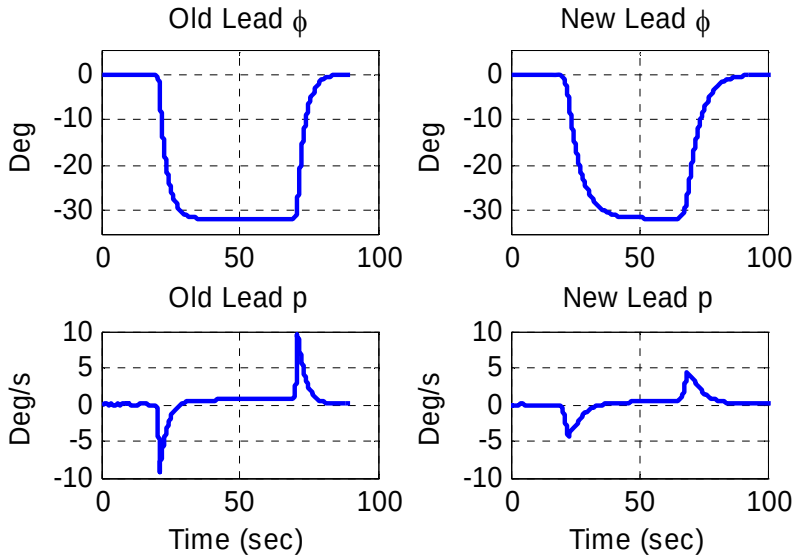

Figure 50. Comparison of Original and New Lead Profiles for 30 Degree Banked Turns

For turn direction, symmetry was assumed in the contact and pre-contact positions. Turns in both directions were accomplished in the wing observation position and during position changes, where the effects of being either inside or outside of the turn were significant. Other lead aircraft profiles were also created, including reversals of turn direction without stopping at level flight, continuous turns, and increases of bank angle and rate to the controller limits. Each variation only altered the types of turn. The additional profiles were used to highlight control characteristics, assist with gain selection, and to investigate the sensitivity and robustness of the system.

Wing Aircraft Initialization

Both aircraft were initialized heading true north, flying parallel at the design altitude and airspeed. A random offset was assigned to the wing aircraft to put distance

between the two antenna points. The initialization process took time, so most result plots are not presented from zero seconds. To get to the point where a test point could be simulated, the wing aircraft simulator first required 10 seconds to find the trim settings for the control surfaces and throttles. From there, the process mirrored that of flight test. The autopilot was engaged and commanded to perform a 30 second position blend from the start point to the first desired formation position. Some settling was allowed, and the test points were simulated after that. To eliminate confusion between controller performance and initialization procedures, plots are displayed only with the time slices of the maneuver of interest.

Contact Position

Straight and Level Simulation and Noise Effects.

Since straight and level flight requires simple station keeping in a non-dynamic environment, the controller performs identically in any formation position, regardless of offset. With no disturbances, the system has zero position error. Sampling errors, time delays, and noise, however, are considered normal difficulties for operations and are included as described in Chapter III for all simulation results unless specifically noted. Turbulence was only added during the robustness section. With these disturbances, Figure 51 shows the controller's performance in straight and level flight.

The lateral channel in Figure 51 shows the largest position errors, up to a maximum of 8 inches. This trend will be shown to exist for all simulations, including when the level of error becomes much more significant. There are two reasons that the

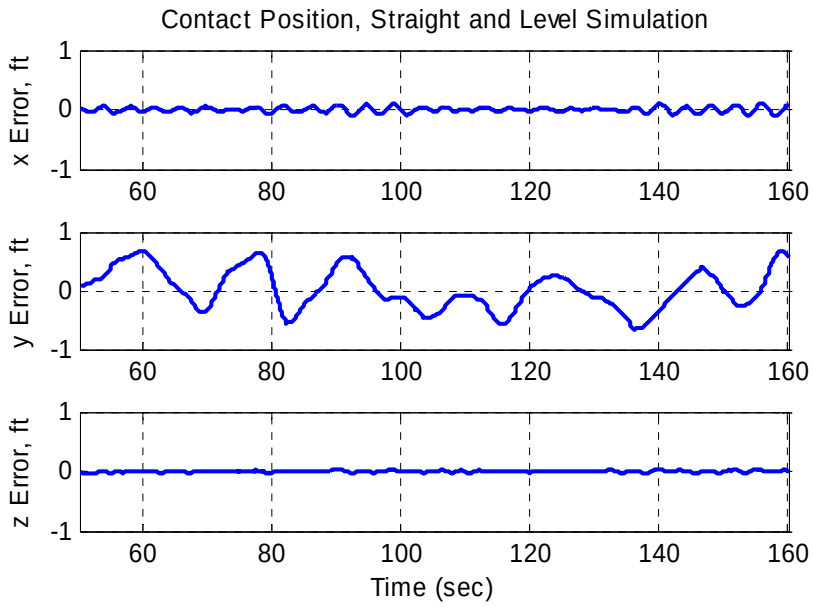

Figure 51. Simulated Straight and Level Simulation in Contact Position

lateral error dominates. First, the lateral channel is the most difficult to control, and corrections take longer. The correction is initiated with ailerons, and the aircraft must rotate to a bank angle before any turn rate begins to accrue. It is only after turn rate begins that lateral error starts to be corrected. Adverse yaw can exacerbate this if rudder is not used, actually moving the nose of the aircraft in the wrong direction as bank is initiated. The time required to overcome the nature of the lateral problem is greater than what is required for applying throttle or elevator control, which both begin to correct the position error immediately. The additional delay and phase lag complicate the control. Second, the lateral channel has twice the noise inputs of the other channels. When noise is seen from the lead aircraft attitude source in the pitch channel, it is interpreted by the controller as vertical movement of the desired position, and the elevator seeks to correct

it. In the lateral channel, however, both bank angle and heading angle noise from the lead aircraft are seen as lateral excursions. This gives the lateral channel twice the noise to contend with. To further degrade the situation, the noise is magnified by the derivative feedback gain, which is the highest in the lateral channel. The simulated noise effects on the control surfaces can be seen in Figure 52.

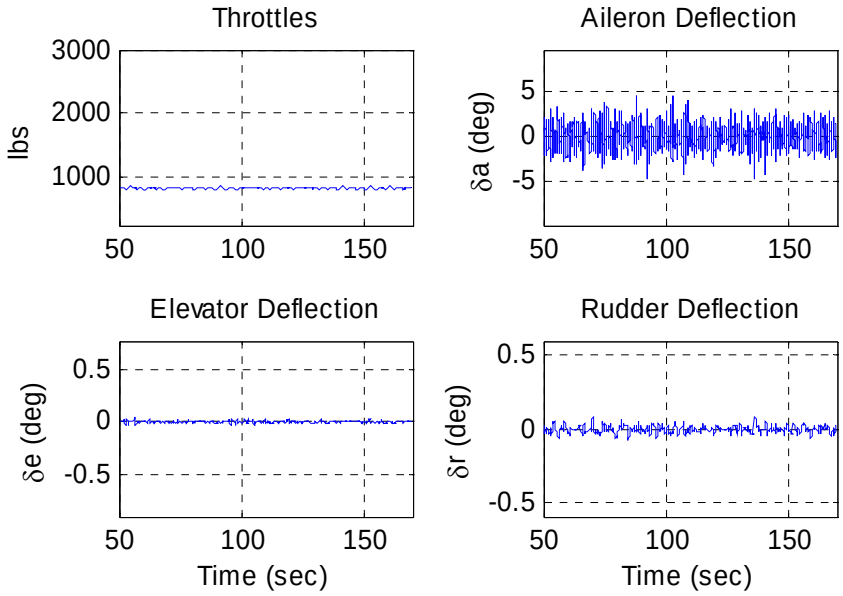

Figure 52. Control Surfaces, Straight and Level Simulation

As the vertical limits on the throttle plot are representative of the entire throttle range, the only significant noise effects are in the aileron channel. Most of the noise seen in the aileron channel is due to the very noisy MEMS IMU roll rate signal that is being fed forward directly into the aileron command without filtering. The noise effects seen in these results represent the early filtering configuration of the simulator and the controller, using the flight test noise that was obtained from a Cessna 172 and provided by the

company that made the IMU. As discussed in the noise section of Chapter III, the noise recorded during our flight test was much more significant.

The same simulation was performed with the noise recorded on the real lead aircraft by our test team, the noise effects in Figure 52 increased to command aileron deflections between 5 and 15 degrees, with lateral position errors increasing to a maximum of 2.5 feet. The later errors are still acceptable, but the amount of commanded control deflection is completely unsatisfactory. Filters were designed during testing and amended to the controller; the process is discussed in Chapter VII. At this point in the development of the control gains, however, none of this information was available. The information in Figure 52 was the data the decisions were based on, noting the spikes in the aileron channel. It was assumed that these spikes would not impact control, since the effects were over before the aircraft had time to move appreciably and the noise did not manifest itself in significant position error. The mass of the aircraft acts as a damper. The spikes seen in simulation were therefore ignored.

In hindsight, this was a reflection of inexperience and poor judgment. The first time the actual controller was engaged during a ground test, the noise effects were obvious in control stick vibrations and the aileron deflections could be physically seen. It was immediately clear that the amount of noise was not negligible. Again, the real noise was significantly higher than the noise used for the simulation, and the only filtering performed on the raw MEMS IMU signals was an averaging filter to compensate for the sampling error problem discussed in Chapter III. Based on the experience of seeing and feeling the noise effects, even the levels of noise that were expected from Figure 52

would cause excessive wear on the control actuators, and would detract from smooth control whether they had time to physically move the aircraft or not. As a reference point for future designers, it was found that noise effects to the control surfaces below ±1 degree were not noticeable through the controls or in flight.

In the simulations presented in this chapter, the original (lower) values of noise are retained, and the filters are not installed. Though this is not as strong of a controller as the final configuration, it reflects the conditions seen during design and highlights the reasons decisions were made. After filtering was installed, even the full C-12 flight noise has a dramatically smaller effect than the worst case that is shown in these simulation results.

Turns with 15 degrees of bank.

The core of the refueling task is maintaining the contact position during straight and level flight and turns with 15 degrees of bank. Figure 53 shows the position error vector from the lead aircraft to the wing aircraft during the maneuver. The roll in is performed at 55 seconds, and the roll out is at 100 seconds. The dashed lines represent the approximate boom limits (which change based on the aircraft's position in the envelope). For the heart of the refueling envelope, the controller is well within desired parameters.

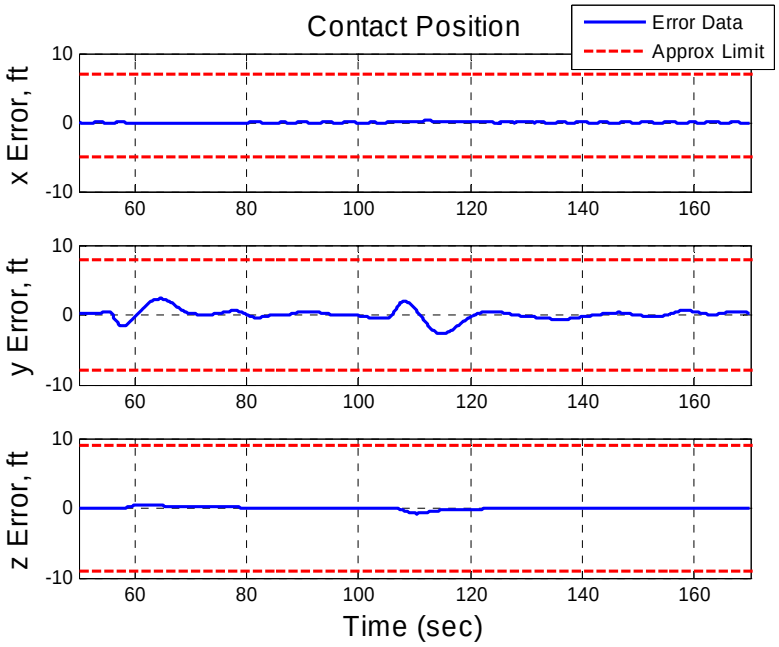

Figure 53. Simulated 15 Deg Left Turn, Contact Position

Turns with 30 Degrees of Bank.

For turns of 30 degrees of bank, a greater amount of lateral error can be seen in the left turn simulated in Figure 54. Again, the roll in is at 55 seconds and the roll out at 100 seconds. The maximum single axis error is 4 feet.

The sine wave appearance of the lateral error in Figure 54 is due to adverse command explained in the control law section of Chapter V. Recall that the y-axis error is positive out of the right wing of the receiving aircraft. Therefore, as the lead aircraft banks to the left, the desired position moves to the right (in the error plots it appears that the wing aircraft "moved" to the left). The wing aircraft slowly banks into the left turn, sliding outward to, and eventually overshooting, the desired position. This is also highlighted in Figure 54.

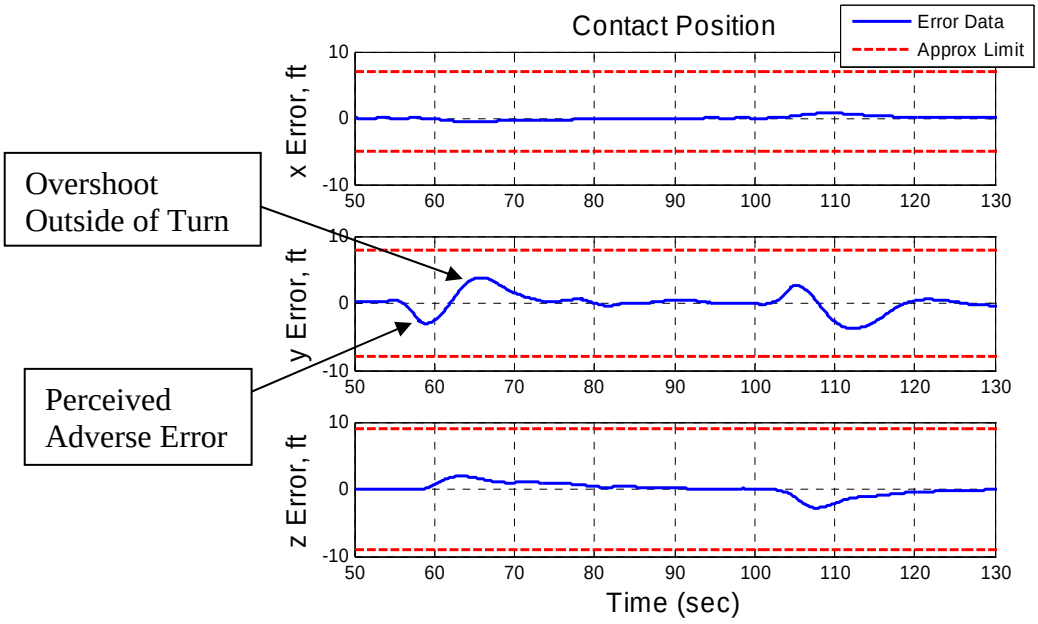

Figure 54. Simulated Left Turn, 30 Deg Bank, Contact Position

The following consideration may assist future designers with controlling this overshoot. The initial perceived adverse error is unavoidable with this paradigm of control. The roll rate FFD in the control laws is what keeps the wing aircraft from banking the wrong direction, as shown in Figure 55. If the effects of the adverse command were overcoming the FFD input, the initial move of the wing aircraft would have been to the right, as was shown in the control law development section of Chapter V.

Figure 55 shows that the wing aircraft is flying exactly the way it should, but as soon as the lead aircraft banks, the integrator on the lateral channel begins to add up the perceived position error on the inside of the turn. This greatly contributes to the amount of overshoot to the outside of the turn. A simple fix that should be investigated for the future would be to freeze the integrator any time that the lead aircraft's roll rate exceeded

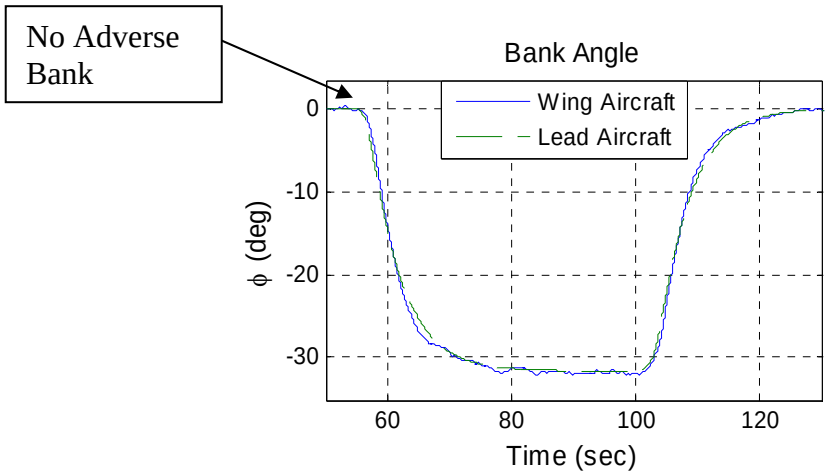

Figure 55. Bank Angle, Simulated 30 Deg Left Turn, Contact Position

a reasonable threshold. This would allow the integrator to work normally at all times, except when rolling into and out of turns, where the adverse error creates an erroneous input to the integrator.

Recall that each of these simulations is performed with a roll rate that is very low, but representative of what can be expected while refueling. Returning to the old lead aircraft profiles, Figure 56 shows a compilation of the errors for a turn to and from 30 degrees of bank that was performed at a maximum roll rate of 10 degrees per second. Comparing Figure 56 to Figure 54, an increase in lead roll rate from a maximum of 4 deg/s to 10 deg/s resulted in a y-axis error increase from 4 feet to over 6 feet, and a z-axis error increase from 4 feet to 7 feet. This was the limiting design condition during gain tuning. Figure 57 shows a side and top view of the position error track displayed with the maximum boom limits.

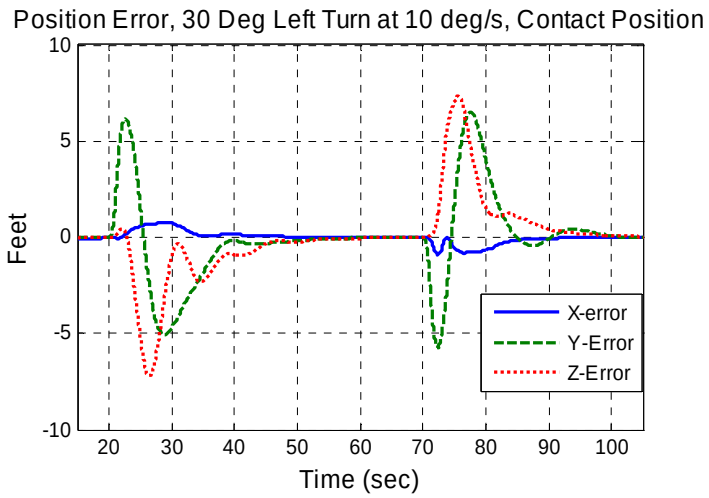

Figure 56. Left Turn to 30 Deg Bank at 10 Deg/s, Contact Position

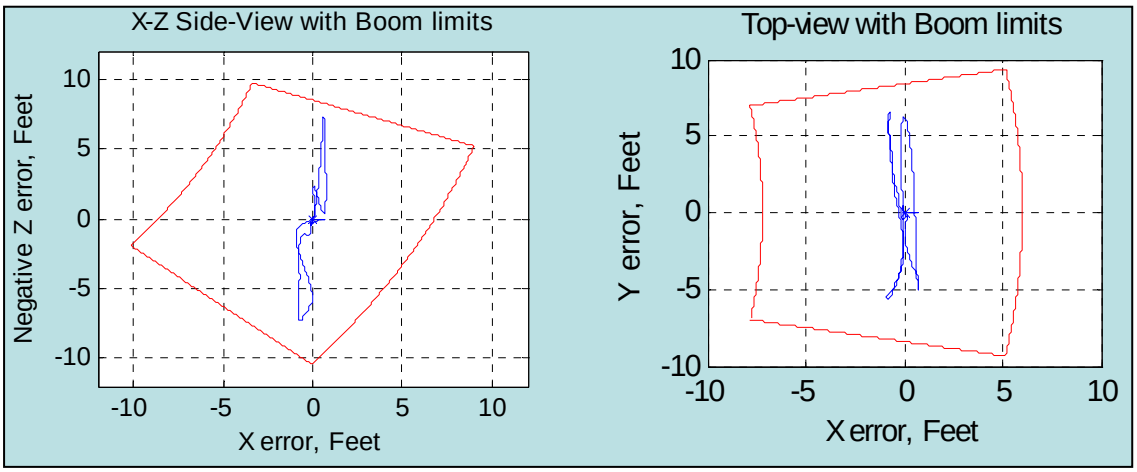

Figure 57. Position Error Relative to Boom Limits, 30 Degree Turn at 10 Deg/s

The gains for the controller were increased until performance for this condition was acceptable, with a very small amount of room left for unknowns. Again, the roll rate used for this simulation ended up being about 3 times faster than operationally representative turns, but it is a good indicator of sensitivity to the lead aircraft's roll rate in the contact position.

Pre-Contact

Turns with 15 Degrees of Bank.

The pre-contact position has the greatest vertical lever arm (85 feet between GPS antennae), causing the greatest challenge in the lateral control axis. Figure 58 shows the wing aircraft response to a left turn with 15 degrees of bank at 55 seconds, with a roll out at 105 seconds, while maintaining the pre-contact position.

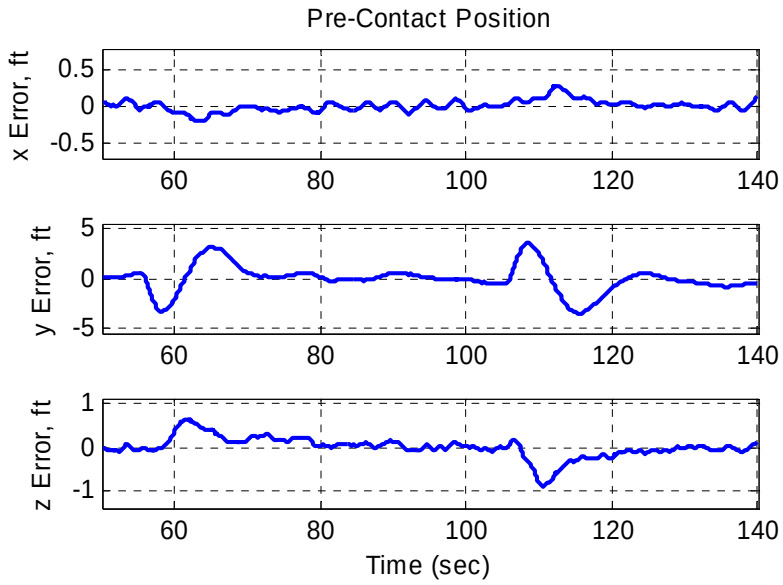

Figure 58. Simulated Left Turn, 15 Deg Bank, Pre-Contact Position

The controller is well within desired parameters for safe, stable close formation flying, and easily meets the design goal of 10 feet in all directions when not constrained by the boom limits in the contact position.

Turns with 30 Degrees of Bank.

As expected, increasing the turn to 30 degrees of bank slightly increases the position errors. The position errors during a right turn are shown in Figure 59.

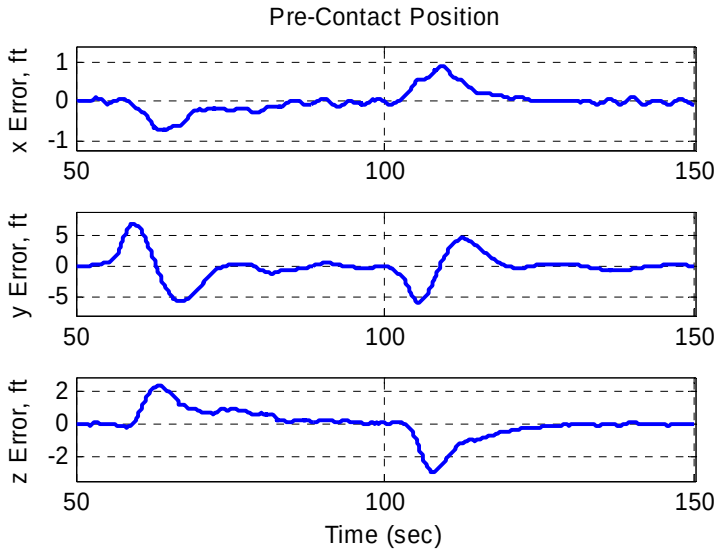

Figure 59. Simulated Right Turn, 30 Deg Bank, Pre-Contact Position

The effect of the roll rate being fed forward can be seen in a comparison of the bank angles, as shown in Figure 60. The wing aircraft does not roll to the left (negative) as suggested by the adverse command effect, but instead slightly delays the roll in for about 1 second, and uses less bank than the tanker to correct to the desired position. Upon reaching it, a slight over-bank is used to arrest the line-of-sight motion of the lead aircraft. The wing aircraft does float outside of the turn slightly, which, as mentioned, could be partly alleviated by turning off the lateral integrator during rolling maneuvers.

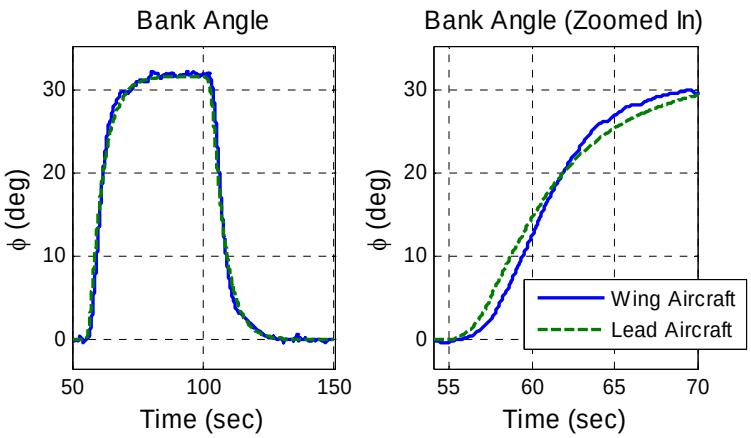

Figure 60. Comparison of Bank Angles, Right 30 Deg Turn, Pre-contact Position

Increasing the roll rate greatly increases the difficulty of station-keeping, as the controller attempts to keep up with a desired position that is essentially moving on a 100 ft stick attached to the lead aircraft. When the lead aircraft roll rate is increased to a maximum of 10 deg/s, the position errors increase to those shown in Figure 61.

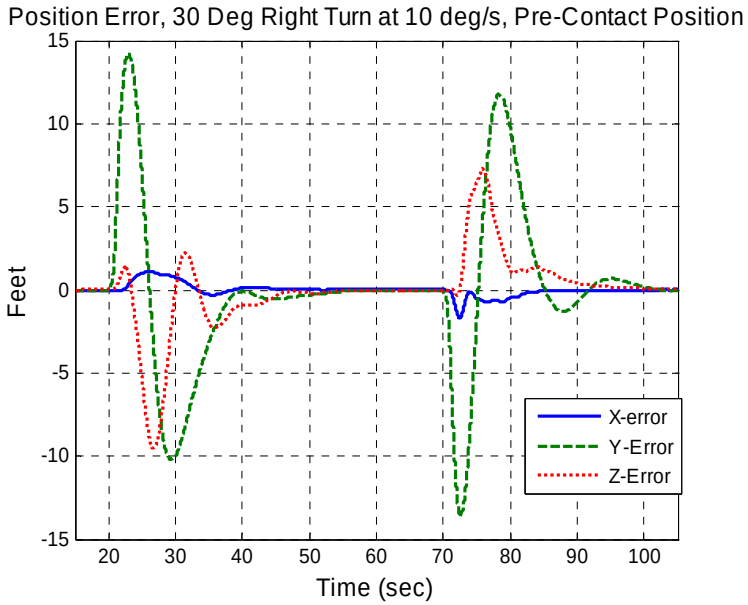

Figure 61. Simulated Right Turn, 30 Deg Bank at 10 Deg/s, Pre-Contact Position

Again, the initial error of 14 feet in the lateral axis is not real, but perceived error from adverse command effect of the lead aircraft rolling to the right. The wing aircraft should make no attempt to correct this, and because the lead aircraft roll rate is fed forward, it does not. The second overshoot of 10 feet for the roll in and 12 feet for the roll out, however, represents position error outside of the turn that would not be allowed if flying perfect formation. The pre-contact position, however, doesn't really exist as a place to fly, but a transition point to stabilize in before moving into the contact position. This position is also returned to when there are problems refueling. As such, the exact position is undefined, and the only true requirement is to ensure safety from collision with the tanker or any other receivers. The tight control of the forward-aft channel ensures plenty of clearance. Laterally, a ten foot error is less than ¼ of the wingspan of an F-15, and as such is an extremely desirable tolerance window, especially for the unrealistically high roll rate for a tanker with receivers. Real pilots exceed these tolerances daily.

Wing Observation Position

Turns with 15 Degrees of Bank.

For the simulations shown at the wing observation position, the wingman was always placed on the right side. As the geometry problem and required airspeed change varies greatly between turns into and away from the wingman, both left and right turns were performed. These are representative of performance on the opposite tanker wing.

The wing observation position has the greatest horizontal lever arm (112 feet), and as such presents the most challenge in the vertical direction. Recall that the formation geometry is maintained during the turns, as shown in Figure 62.

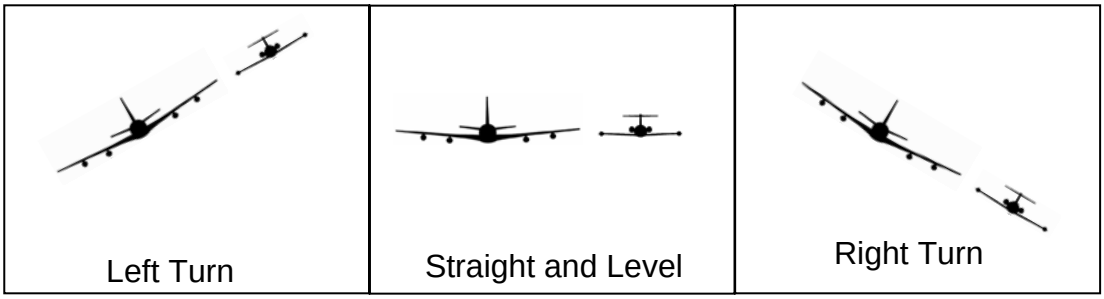

Figure 62. Wing Observation Position During Turns

For a 30 degree turn, the desired formation position moves 56 feet in the few seconds of roll in. Unlike the lateral command, however, the vertical command is not adverse and the controller can immediately attempt correction. This makes the control much easier. The position errors during a simulated left turn with 15 degrees of bank are shown in Figure 63.

Noting that the z-axis is positive downward, in Figure 63 the wing aircraft was 4 feet low during the roll in, and approximately 3 feet high during the roll out. A turn with the wingman on the inside of the formation is shown in Figure 64.

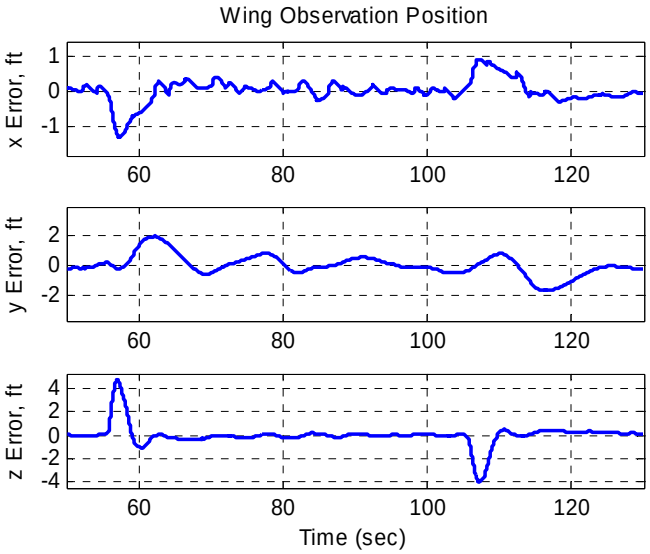

Figure 63. Simulated Left Turn, 15 Deg Bank, Wing Obs. Position

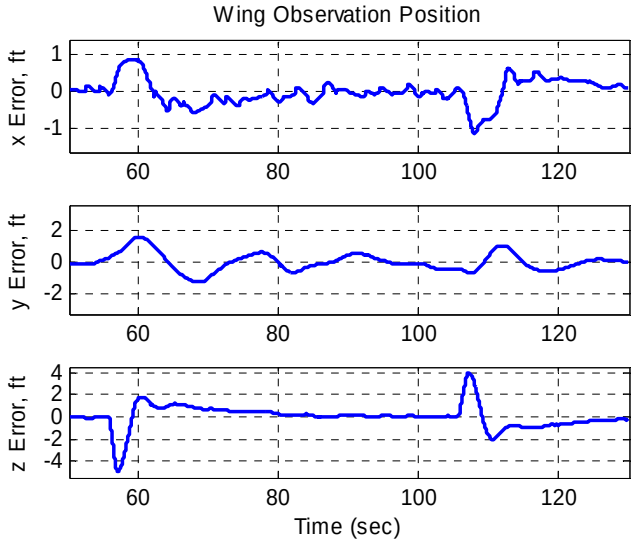

Figure 64. Simulated Right Turn, 15 Deg Bank, Wing Obs. Position

Again, the controller exhibits safe tendencies throughout, and maintains tolerances well within desired parameters during 15 degree turns—the heart of the refueling envelope.

Turns with 30 Degrees of Bank.

Increasing the bank angle to 30 degrees in a left turn with the wingman on the outside can be seen in the position error trace of Figure 65, and a right turn with the wingman on the inside is shown in Figure 66.

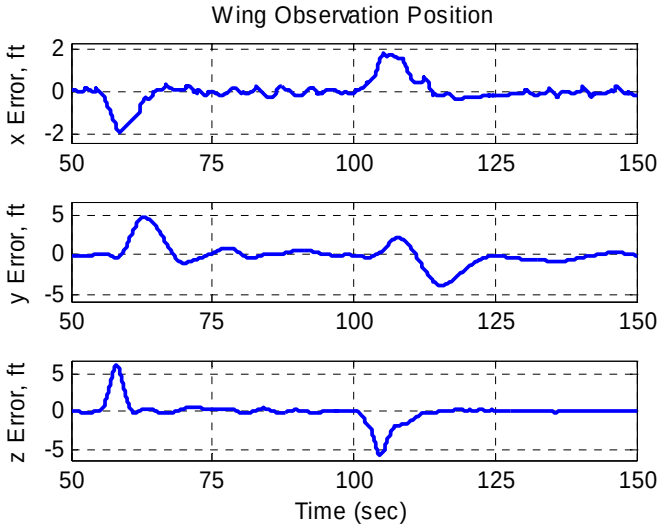

Figure 65. Simulated Left Turn, 30 Deg Bank, Wing Obs. Position

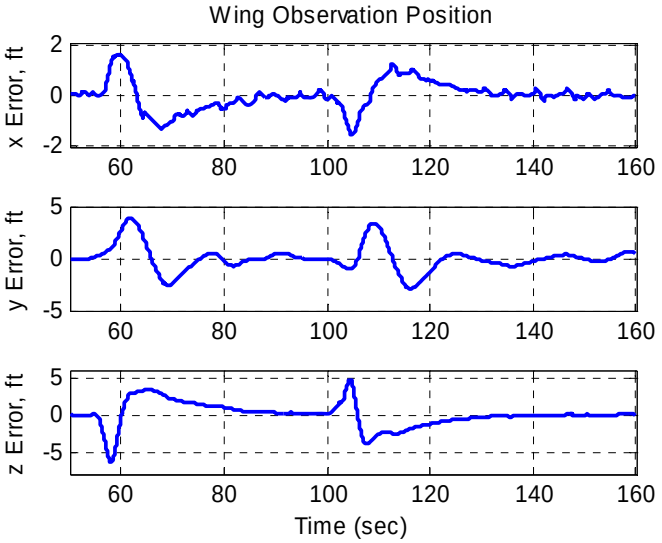

Figure 66. Simulated Right Turn, 30 Deg Bank, Wing Obs. Position

The control is stable and slow, as it should be for close formation corrections. Figure 67 shows that the system is controlling as a pilot does. Inside the turn to the right, an appropriately small decrease in pitch angle is used to correct the initial position error, followed by a minor increase in steady state pitch angle to create the additional lift required to sustain the turn.

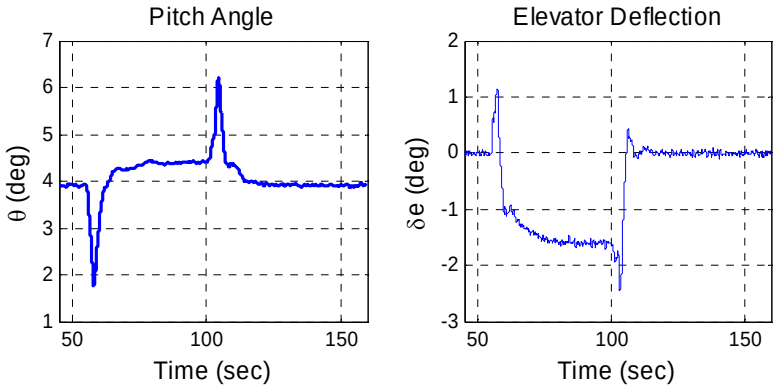

Figure 67. Pitch Angle and Elevator Control, 30 Deg Left Turn, Wing Obs. Position

Elevator control is likewise correct, predictable, and efficient (positive elevator deflection is defined as trailing edge down). Throughout these simulations, attention remained on the rates required of the actuators. The actuators on the test aircraft are larger and faster than production representative Learjets, and were estimated by Calspan to have a rate limit of 75 deg/s for the elevator, and 220 deg/s for the ailerons. The greatest rate demand seen without noise on the system was 30 deg/s on the aileron channel. Obviously, if noise effects are large enough in real flight, they may saturate any

control channel in rate. The nature of these inputs, however, should be of small enough magnitude and duration that no effects from rate limiting were expected.

Returning to the 10 deg/s lead profile, increases in roll rate again dramatically increase the difficulty of control, as shown in Figure 68 without noise. This roll rate is not representative of a real refueling problem, but it demonstrates the difficult flight condition that the feedback gains were tuned for. The right turn is shown, as it is the most difficult geometry problem for the pilot to solve, and the results have the largest errors.

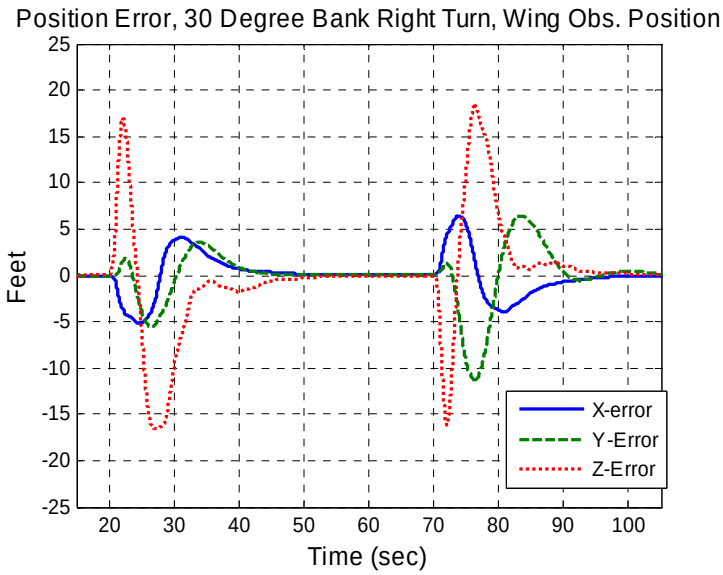

Figure 68. Simulated Right Turn, 30 Deg Bank at 10 Deg/s, Wing Obs. Position

The increased roll rate complicates smooth control for the wingman. Again, as the lead aircraft banks, the desired position moves down 56 feet vertically in a few seconds. The wingman is initially left 16 feet high during the correction. Just as the wing aircraft builds up enough vertical speed to catch up with the moving desired

position, the tanker completes its roll, and the inertia of the wing aircraft carries it into a large overshoot. Though the error is large, it is displayed in the tanker body frame, and therefore is pure vertical from the tanker's perspective. This means that there is no collision potential from vertical error with the tanker or other receivers, and the error is efficiently corrected. More concerning for the wing observation position, however, is the lateral error, where collision potential exists with other receivers. If this were a realistic turn, an 11 foot lateral error in the wing observation position is still relatively small, but if other receivers happen to have the same amount of error in the opposite direction, the distance between them is greatly reduced. This scenario is highly unlikely, as the lateral error is caused by the tanker either pulling away from or into the wingman, and all receivers would likely be impacted the same way. Nevertheless, it stands as a good measure of capability that at a 10 deg/s roll rate the control from the wing observation position is stable and solid, but the total errors are beginning to reach the tolerance goals.

Position Changes

Simulations were performed for all possible position changes in straight and level flight, and turns with 15 and 30 degrees of bank. Other position change simulations were performed with the lead aircraft rolling while the wing aircraft was moving between positions, and while in differing levels of turbulence. The second group of results is presented in the sensitivity and robustness section. Recall that position changes are commanded by blending the current position into the new position, and repeating this for each corner from contact (position 1), to pre-contact (position 2), to the back corner (position 3), and finally up to the wing observation position (position 4). The reverse is

true for position changes from the wing observation position to the contact position. The timing set for each segment was 30 seconds, an operationally representative time that provides a slow, controlled pace from one position to another. A full position change takes 90 seconds. Any individual segment may also be commanded independently. This occurs operationally, as occasionally aircraft that are refueling are asked to back up and hold to the pre-contact position while the tanker cycles its system. When the system is fully operational again, the wing aircraft performs only the position change segment from pre-contact to contact.

If all directions and all segments are considered, there are 12 possible position changes that can be commanded (1 to 2, 2 to 1, 1 to 3, etc.). All of these combinations, however, are simply segments of the two largest command changes, from contact all the way out to wing observation, or the return trip. As such, and since no surprises were found during position change simulations, only the two largest position changes are presented.

Position Changes During Straight and Level Flight.

A position change during straight and level simulation is shown in Figure 69. The change is initiated at 60 seconds, and can be seen by the command moving down (positive z direction) and back (negative x direction) from the tanker. At 90 seconds, the command is established at the pre-contact position, and the lateral change to the back corner begins. The final segment from the back corner up and forward to the wing observation position starts at 120 seconds.

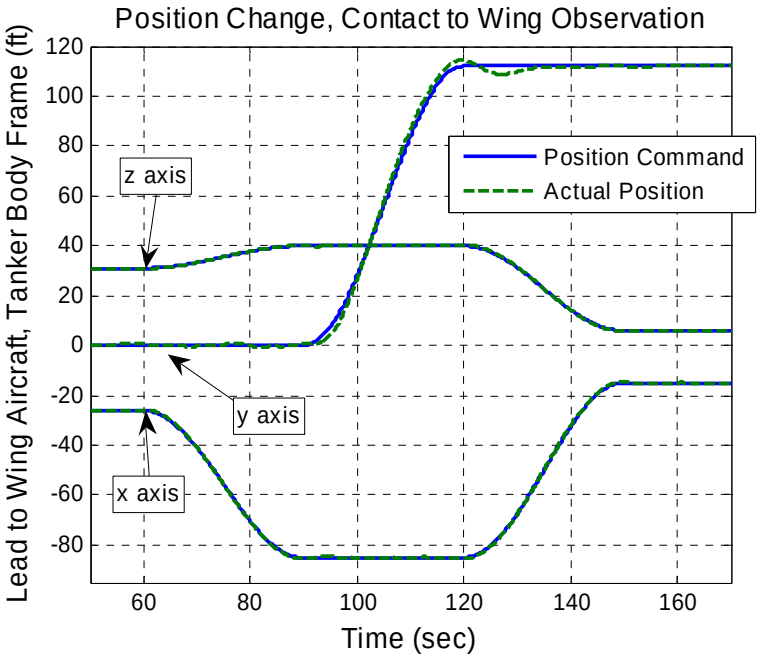

Figure 69. Simulated Position Change, Contact to Wing Observation

It is difficult to break out the difference between the actual and commanded position, so the radial position error of all three axes is combined and plotted in Figure 70.

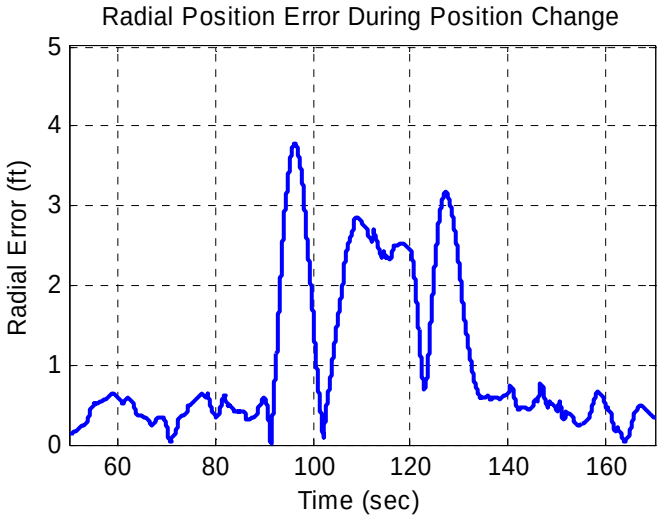

Figure 70. Radial Position Error During Position Change, Contact to Wing Observation

The radial position error is less than a foot except during the lateral move from the pre-contact position out to the back corner. The lateral move is the fastest, as the position blending of each leg takes 30 seconds and the lateral move of 112 feet is the longest path. The wing aircraft is moving very slowly in relation to the lead aircraft for the first and last portions of each 30 second interval. At its highest rate, the desired position command is moving at 6 ft/s. The lateral channel also has the highest control difficulty, as previously discussed. Nevertheless, the error magnitudes during position changes are small enough to be inconsequential. The full position change from the wing observation position to the contact position is shown in Figure 71.

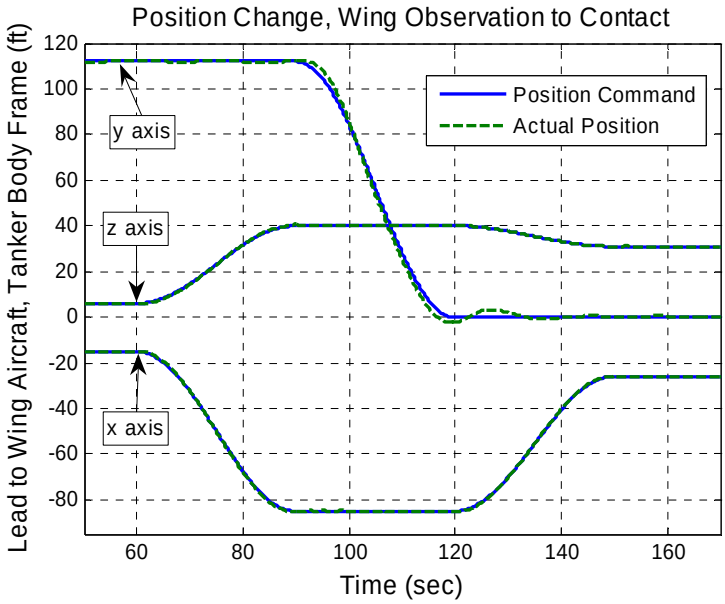

Figure 71. Simulated Position Change, Wing Observation to Contact

Position Changes During Turns.

Position changes during turns were simulated with 15 and 30 degrees of bank. The results were predictable, and for brevity only the more difficult 30 degree banked

turns are displayed in Figure 72 and Figure 73. The only change was an insignificant increase in position error. No significant changes exist between left and right turns.

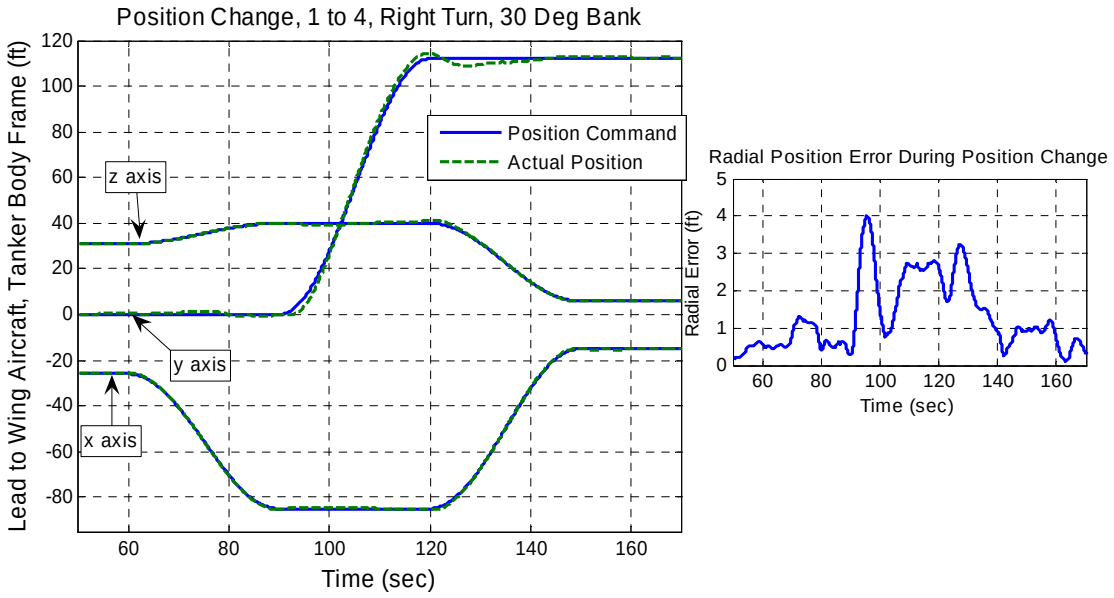

Figure 72. Position Change, Contact to Wing Obs., Right Turn, 30 Deg Bank

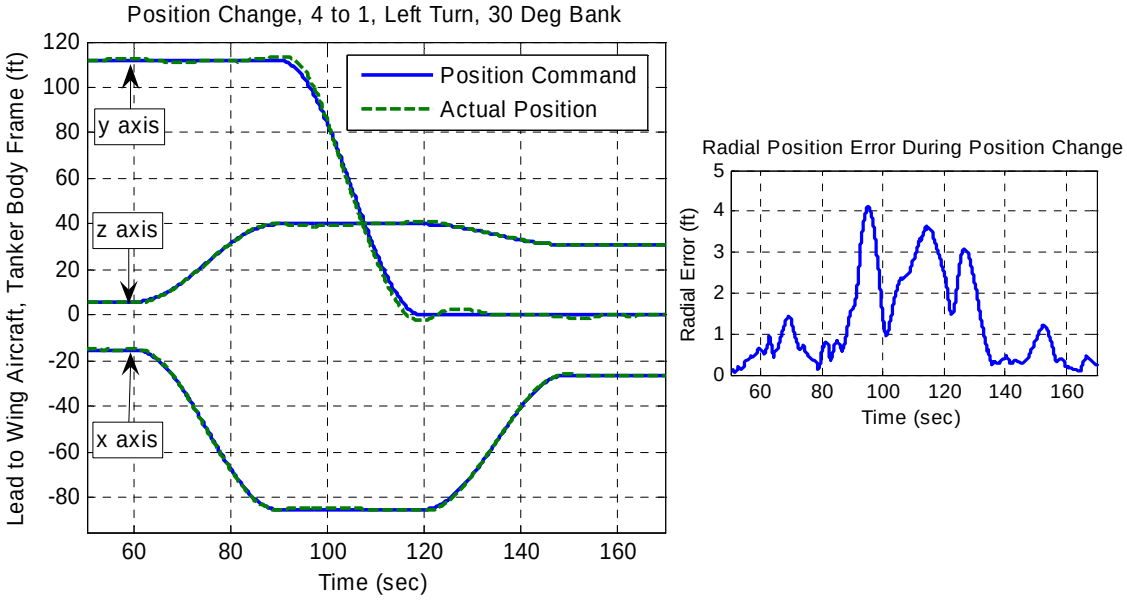

Figure 73. Position Change, Wing Obs. to Contact, Left Tun, 30 Deg Bank

The bank angle results during the position change of Figure 73 are shown in Figure 74.

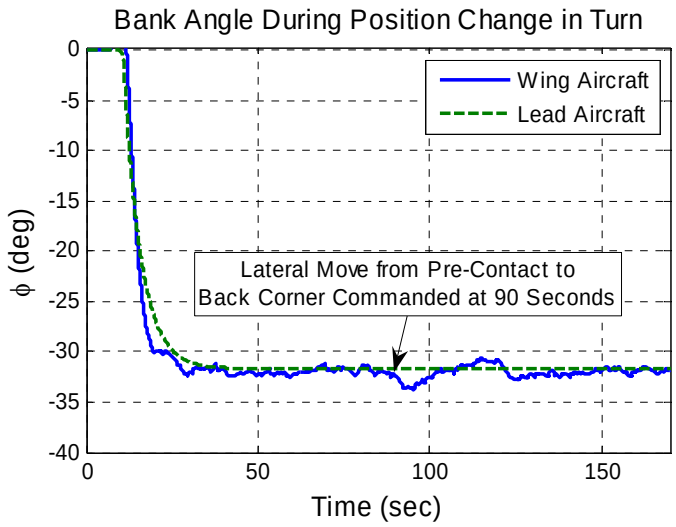

Figure 74. Bank Angle Comparison During Position Change in Turn

The lead aircraft banks to approximately 30 degrees, and the wing aircraft essentially matches the lead aircraft's bank angle throughout the maneuver. The exception to this is at 90 seconds, when the wing aircraft is commanded to laterally move from the back corner to the pre-contact position. To achieve the heading difference required for the necessary rate of relative closure, only 2 degrees of differential bank are required. This illustrates the sensitivity of the system to very small changes in bank.

Sensitivity and Robustness

Due to the non-linear nature of the entire formation model, evaluating sensitivity and robustness is difficult. The classical technique of cutting loops and checking the gain margins does not apply. As a substitute, sensitivity and robustness were investigated with the increase of disturbances and an exploration of the limits of the controller. The gap between what the controller can do at its limit and what it is expected to do to fulfill its mission gives some indication of the stability of the system.

Time Delays.

Unexpected time delays have a reputation for catching flight control designers by surprise, and small amounts of delay will drive many systems unstable. For the simulation results, a delay of 0.1 seconds was estimated for the time required to first transport GPS and IMU data from the lead aircraft to the wing aircraft and then to solve the carrier phase DGPS position solution and present the data in the proper bus format to the controller. Another delay of 0.06 seconds was allotted for the sensor lag and transport time for signals within the test aircraft. The true delays were never measured. The sensitivity of the system to an increase in estimated time delay was investigated. The GPS and IMU sensor data are packaged and delivered together across the same datalink. Following the DGPS position calculation, both sets of data are then formatted together. As such, the delay for both signals was increased simultaneously.

To excite the system and bring out instabilities while increasing the amount of time delay, the wing aircraft was commanded to perform a position change. During the position change, the lead aircraft rolls to 30 degrees of bank. The combination of

formation geometry changes caused by the roll and the position change make flight path of the desired position cue somewhat erratic and more difficult to follow, resulting in increased requirements for control, which excite the modes of motion.

As the time delay on the GPS and IMU data is increased to 0.3 seconds, a small sustained oscillation is noted in the longitudinal channel while moving back to pre-contact, and again after the roll out, as shown in Figure 75.

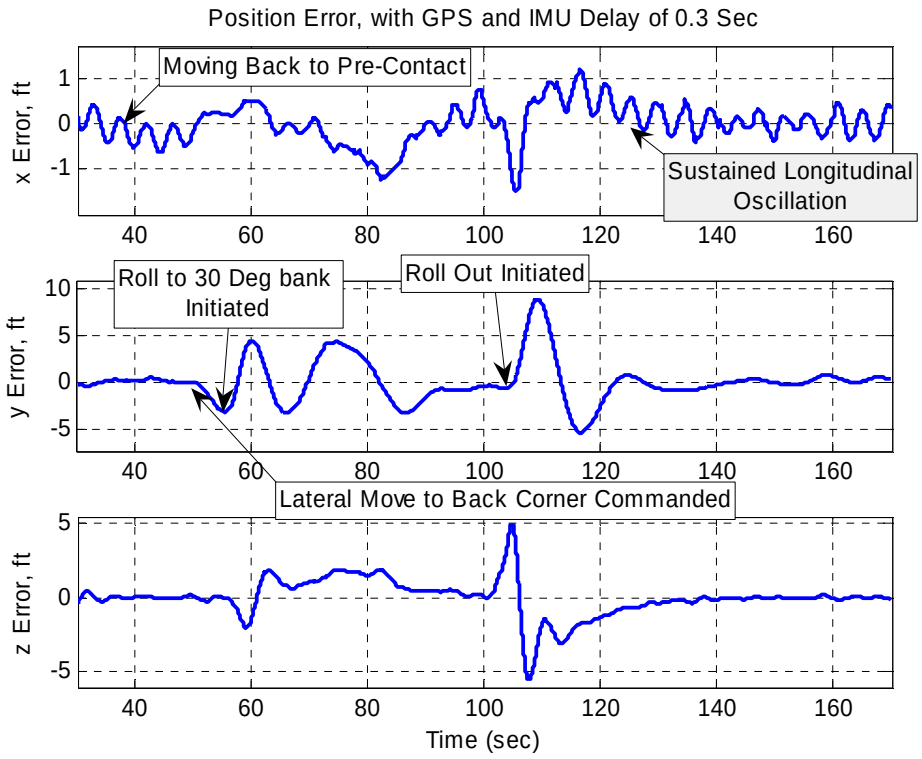

Figure 75. Complex Commands with GPS and IMU Delay Increased to 0.3 Sec

The position error due to the sustained oscillation is still on the order of inches, but impact of the GPS and IMU delay combined with the 0.3 second delay that already exists in the throttle model is obvious. The throttle response during the maneuver of

Figure 75 is shown in Figure 76. Again, the vertical limits of the plot represent the available range of throttle motion. The sustained oscillation is noticeable, and this was considered the edge of acceptable delay.

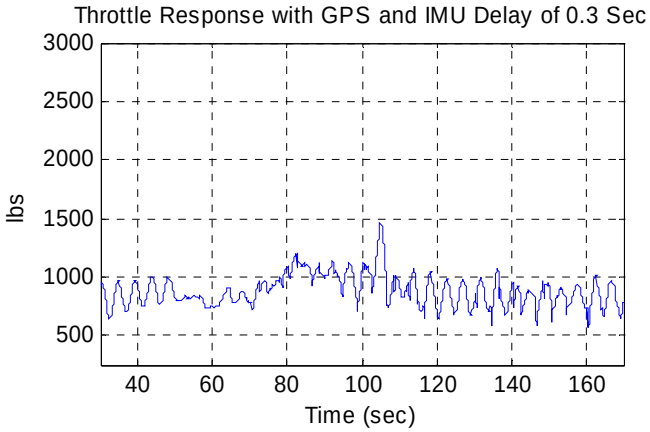

Figure 76. Throttle Response with GPS and IMU Delay of 0.3 Sec

Any further delay continues to degrade performance. With a delay of 0.35 seconds, the same maneuver is performed in Figure 77.

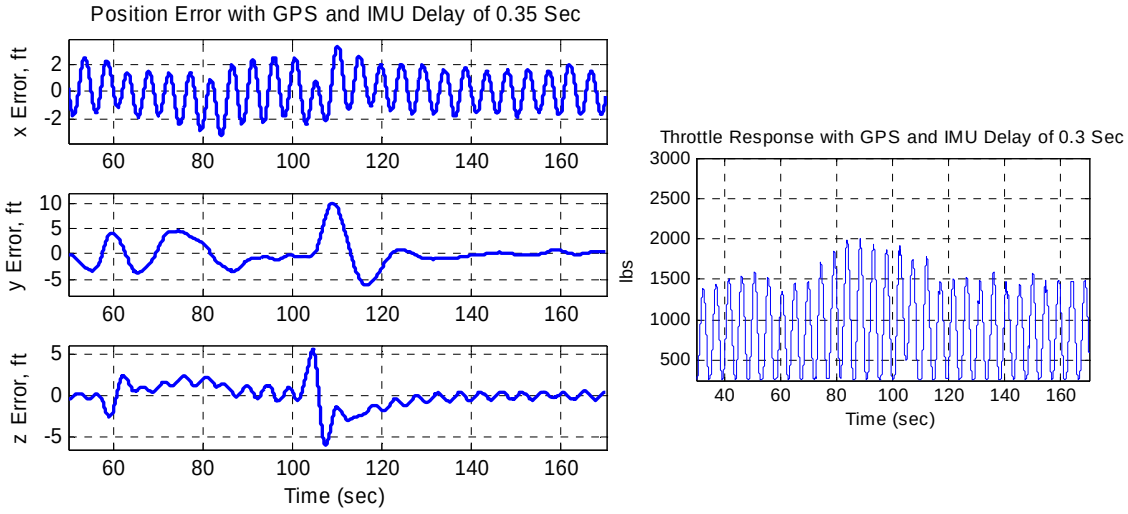

Figure 77. Limit Cycle Oscillations with GPS and IMU Delay of 0.35 Sec

The 0.2 Hz limit cycle oscillation dominates the longitudinal response in Figure 77, and the late, large throttle changes from idle to mid-range have coupled into the vertical channel, as the changes in speed cause the aircraft to climb and descend. This amount of time delay is obviously unsatisfactory, though the system is still stable.

The 0.06 second delay estimate for attitude signals internal to the VSS is probably too high. This is computational time delay only, with delays for actuators and physically moving parts already accounted for in the model. It is likely that the true delay is lower, but it was not measured. The same sensitivity technique was followed for VSS delay, and an increase to 0.12 seconds was found to be the limit of acceptable performance. The end conclusion is that with an increase of 2 times the estimated delay for the case of the VSS, or 3 times the estimated delay for the GPS and IMU signals, the system will have marginal performance. With any more delay, the performance is unacceptable, though it is still stable.

Turbulence.

The turbulence model was discussed in Chapter III. The robustness of the system to unexpected disturbances was investigated by increasing the severity. The system performance in the contact position with light turbulence is shown in Figure 78. The straight and level data presented back in Figure 51 shows the same simulation performed without turbulence. In comparison, Figure 78 shows that the position errors increase in all axes. The majority of turbulence is caused by air rising at different rates, so the most notable increase in error was intuitively in the vertical channel. The total errors are still well within the boom envelope limits, and do not raise questions about the

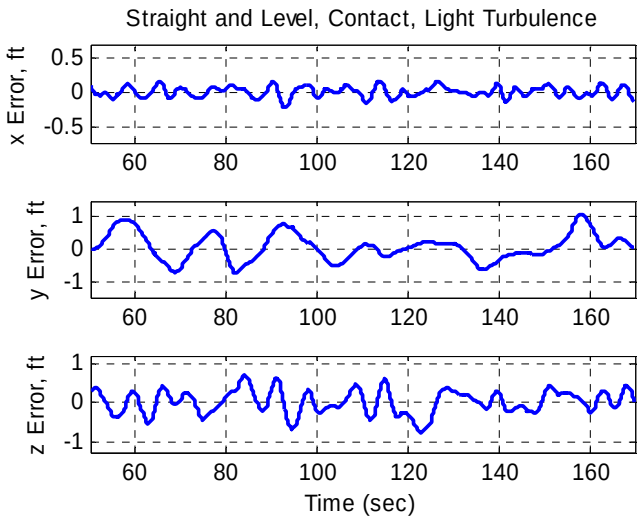

Figure 78. Straight and Level Simulation with Light Turbulence

suitability of the controller. For the extreme, thunderstorm level turbulence was applied in Figure 79. It is understood that Air Force aircraft are not permitted to operate in thunderstorms, much less attempt to refuel there. Unlikely circumstances, however, often occur eventually, and the effort was a good indicator of system robustness.

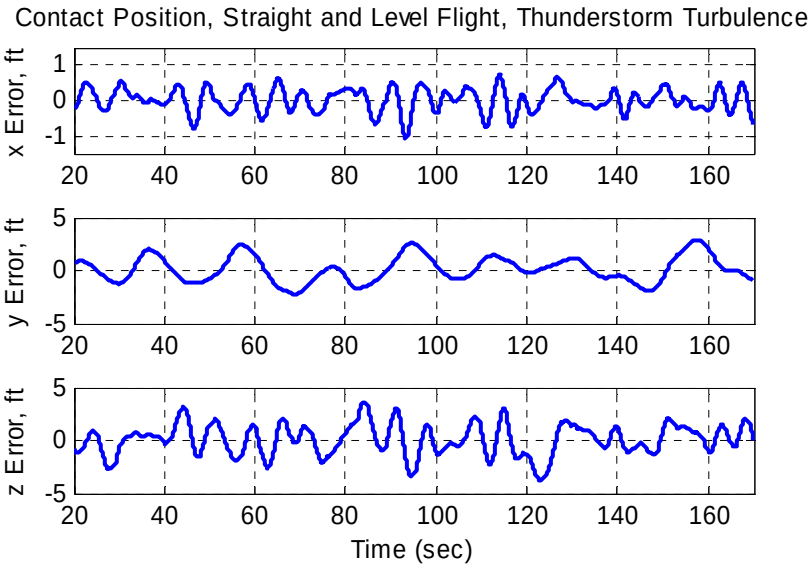

Figure 79. Straight and Level Simulation with Thunderstorm Level Turbulence

The simulation ran for over two minutes and all errors were contained within 5 feet. The greatest problems were caused in the vertical channel, but the controller still stays well within the boom envelope limits, as shown in a second run in Figure 80.

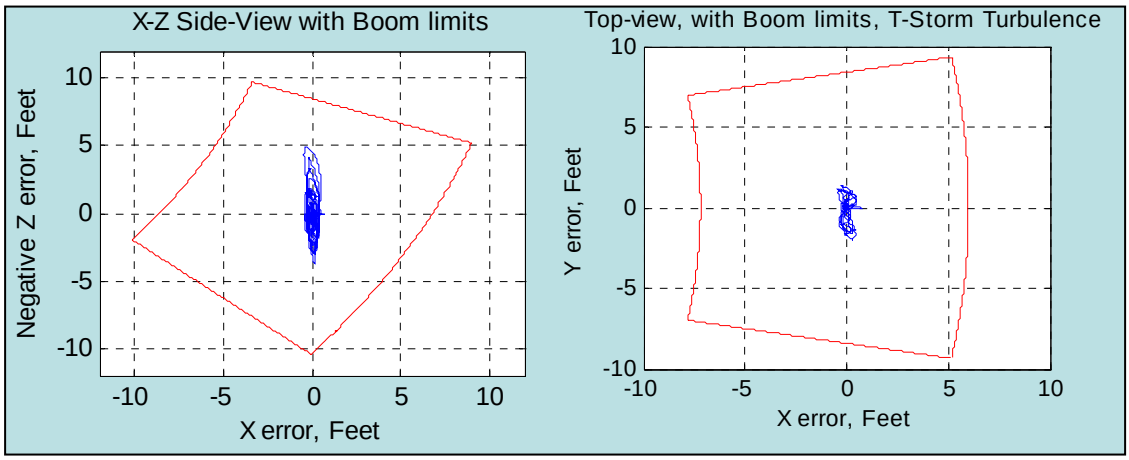

Figure 80. Boom Limits During Thunderstorm Level Turbulence

Bank Angle Increases.

The lead aircraft bank angle was increased next. Turns with 60 degrees of bank were investigated in each formation position. The most challenging place was the wing observation position, where the controller had to deal with a 97 foot vertical change in desired position in the time it took the lead aircraft to achieve its bank angle. Figure 81 shows the position errors, and Figure 82 shows parameters that help explain the motion. As the lead aircraft begins turning into the wingman at 55 seconds, the geometry of the formation changes to put the wing aircraft forward (positive x), right (positive y) and above (negative z) the desired position.

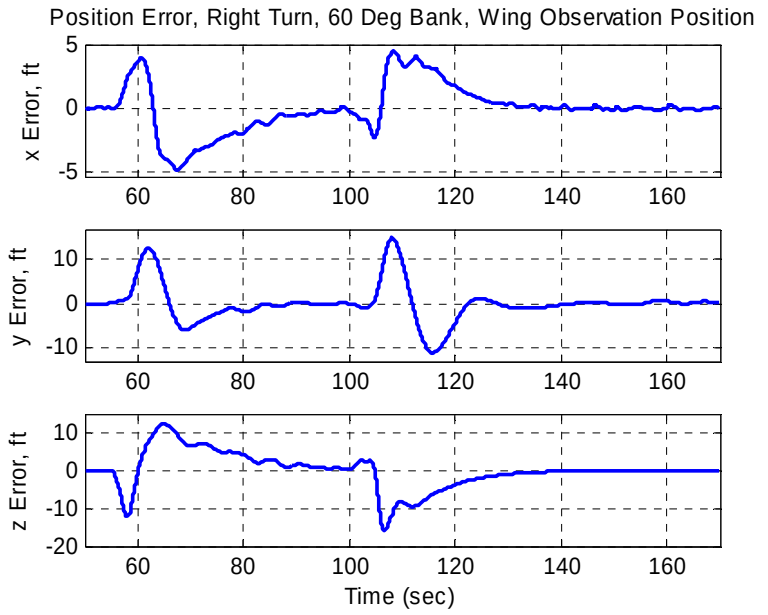

Figure 81. Simulated Right Turn, 60 Deg Bank, Wing Obs. Position

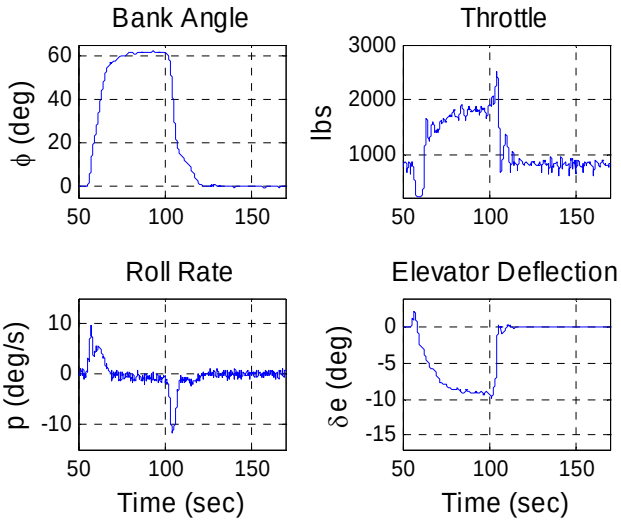

Figure 82. Selected Parameters During 60 Deg Bank Right Turn

Longitudinally, the throttle position plot in Figure 82 shows that idle power is initially selected, and then the integrator slowly feeds in power to overcome the increase

in induced drag at the high bank angles, eventually stabilizing in position. The slow effect of the integral control can be seen again in the roll out, and in the vertical channel, where the integral control takes time to move the elevator to the new steady state position required for the tight turn. Laterally, the position errors are exceptional for this angle and rate of turn, performed at a maximum of 10 deg/s.

For turns beyond 60 degrees of bank, the position errors start to increase notably, providing a good indicator of the controller's capability. The lead aircraft for flight test was a C-12, with a structural limit of 2.8 g's of normal acceleration. This occurs in a sustained turn at approximately 69 degrees. The lead profile was therefore set for a 70 degree turn. Obviously, this is well beyond the scope of a refueling controller, but it shows where stability comes into question. The controller had the closest approach to instability when on the outside of the turn in the wing observation position. The position errors are shown in Figure 83, with selected parameters in Figure 84.

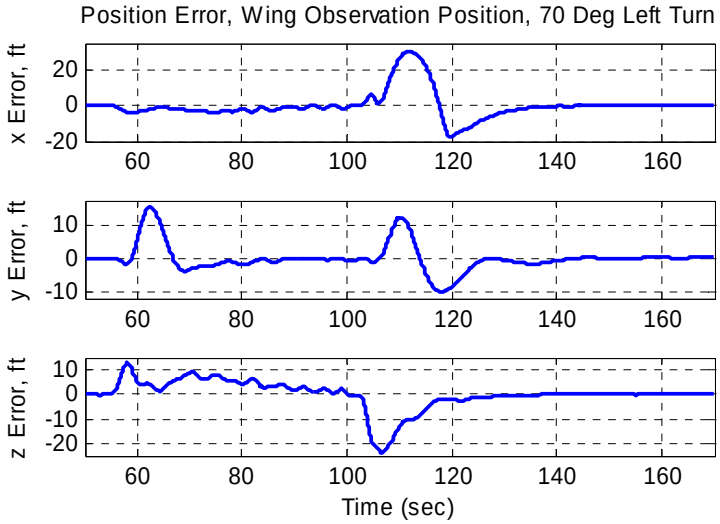

Figure 83. Simulated Left Turn, 70 Deg Bank, Wing Obs. Position

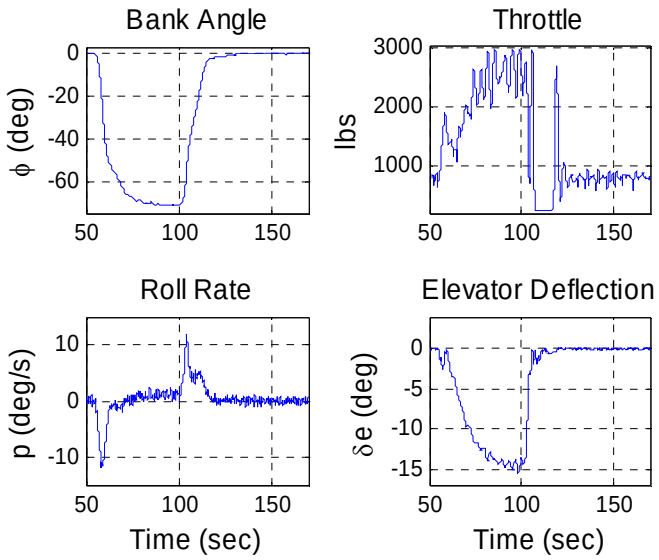

Figure 84. Selected Parameters, Left Turn, 70 Deg Bank

This turn is at the limits of the controller. Power is saturated at both military (maximum thrust) and idle at times, and gross position errors occur in the x-axis and z-axis as the wing aircraft cannot slow down quickly enough to regain equilibrium on the outside of the turn. In real flight, pilots would use the speed brake in this circumstance.

The end result of this portion of the investigation is that the controller is not exceptionally sensitive to total bank angles, and stability is not in question for turns up to 60 degrees of bank.

Roll Rate Increases.

The system is sensitive to roll rate increases. As the lead aircraft increases in roll rate, the desired position cue moves much faster, as if on the end of a stick connected to the lead aircraft. The most dramatic effects of this are seen in the wing observation position, where the wing aircraft is the farthest away. For a reference point, real tanker

roll rates with receivers in formation are between 2.5 and 3 deg/s. Much of the design work for this thesis was performed at 10 deg/s. In the contact position, if the tanker rolls to the left at more than 12 deg/s, the boom will exit the physical limits on the *inside* of the turn if the receiver does not initially move to the right.

The question is not whether an increase in roll rate will affect performance, this is guaranteed. The question is whether the system will show any signs of instability if subjected to unrealistically high roll rates. A lead profile was designed to rapidly roll (22 deg/s) to 30 degrees of bank, and then to reverse the turn direction rapidly (44 deg/s) before rolling out. The lead profile and error plots for the contact position are shown in Figure 85, and the results in the wing observation position are shown in Figure 86. These simulations were able to be accomplished because the lead aircraft model ended up being an F-16. The rates shown are impossibly high for a tanker, but they demonstrate that though the position errors are sensitive to roll rate changes, the stability of the system is not in question.

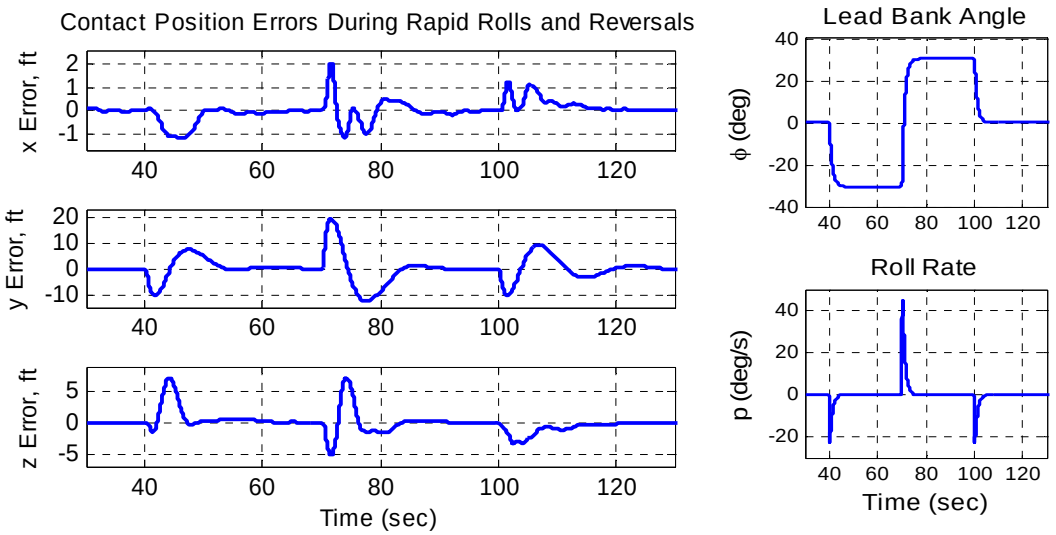

Figure 85. Simulated Performance in Contact Position at High Roll Rates

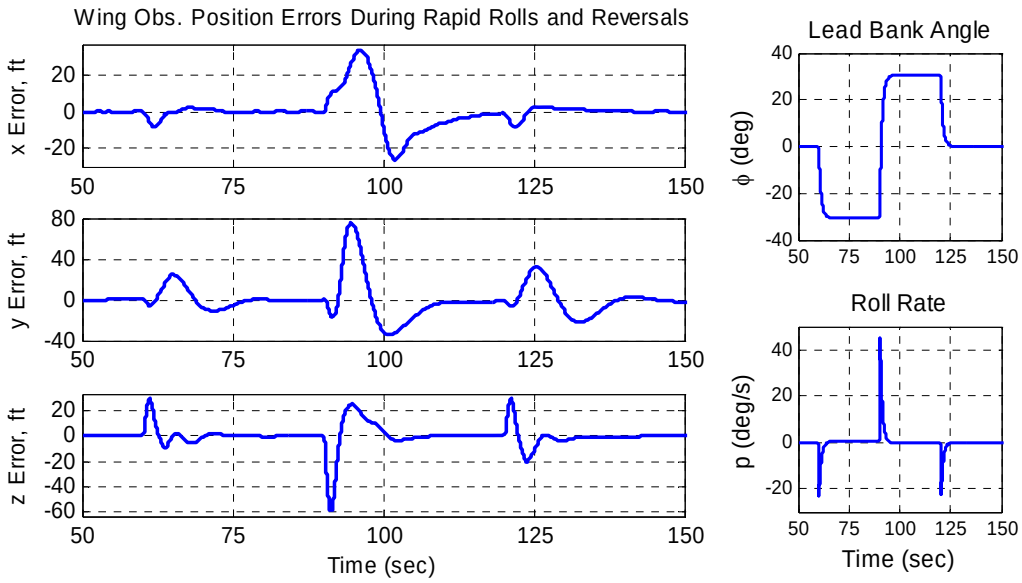

Figure 86. Simulated Performance in Wing Obs. Position During High Roll Rates and Reversals

The position errors in Figure 86 are ridiculously high for a close formation controller, and with those errors a mid-air collision would be all but unavoidable. The exercise, however, was to show stability under high roll rates, and therefore the shapes of the response are the most important. The controller exhibits a stable, well controlled, second order response to even extreme position errors.

Complex, Competing Commands.

Several experiments were performed with the simulator in an effort to force instability. Turbulence, high bank angles, turn reversals, and high roll rates were explored individually to get a feel for the robustness and sensitivity of the system. To ensure none of the effects compounded the problem if presented as a group, a series of

simulations were performed adding the effects of each of the variables. For brevity, only the most complex one is shown here. The wing aircraft is directed to change positions from contact to the wing observation position. During each leg of a position change, the wing aircraft accelerates and decelerates. The greatest dynamics occur in the middle of each segment, where the wing aircraft is moving at its highest rate of relative speed. At this point on the first segment, the lead aircraft quickly banks into a 30 degree turn. During the most difficult segment, the lateral leg from pre-contact to the back corner, the lead aircraft reverses its turn (60 degrees of total bank change with an 18 deg/s roll rate). The lead aircraft rolls out of bank as the wing aircraft nears the middle of the final leg of the position change. All of this is accomplished with thunderstorm level turbulence, and the results are shown in Figure 87.

Though large errors are caused by the dynamics of the maneuver, the controller tracks reasonably well and definitely shows positive stability. Again, this maneuver is well beyond the mission requirements for aerial refueling, and is only intended to excite the modes of the system in search instabilities. The entire investigation of sensitivity and robustness, however, has revealed that the system is very stable in the presence of faster than normal maneuvers, large position errors and unexpected disturbances like time delays and turbulence.

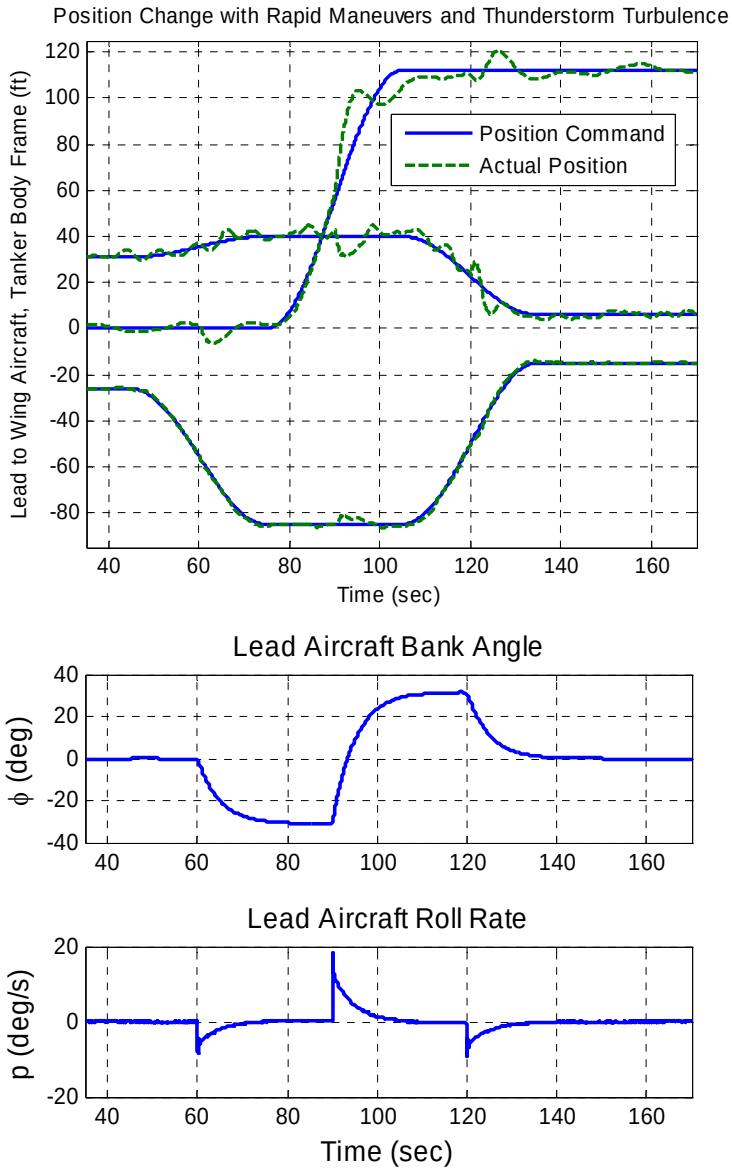

Figure 87. Simulated Position Change with Rapid Maneuvers and Thunderstorm Turbulence

VII. Flight Test Modifications

System Integration

The formation flight controller is one piece of a much larger framework of hardware required for aerial refueling. Besides controller development, much of the effort on this project was directed toward integrating all of the systems that were required to work together just to have the capability of testing it. The most obvious systems required were the aircraft themselves. A USAF C-12C Huron, owned by the Test Pilot School, was used for the lead aircraft, and Calspan's "Lear 2" LJ-25 Learjet was selected for the wing aircraft. Both are shown in Figure 88.

Figure 88. Test Aircraft

For attitude information, a 1.6 ounce, commercially available, Micro-Electrical Mechanical System Inertial Measurement Unit (MEMS IMU) was mounted to the C-12.

The MEMS IMU measures accelerations and integrates them for the C-12's velocities and Euler angles. The IMU is also GPS corrected with a single point solution to correct the grossly large amounts of drift the small device has on its own. The MEMS IMU represents one of the cost compromises necessary to actually get all of the systems required to demonstrate the controller. As mentioned previously, noise in the lead attitude system can significantly affect control of the wing aircraft, though several filtering techniques will be discussed that can mitigate or eliminate this. In addition, if bias exists in the attitude system, the wing aircraft will unknowingly fly to a position that is offset of the true desired location. For future precision guidance systems that rely on lead aircraft angles for positioning, high quality rate gyros would be more appropriate, but this test did prove that it can be accomplished even with cheaper sensors.

For position information, an AFIT Relnav carrier phase differential GPS system was used that was designed for another master's thesis by a fellow AFIT/TPS student, Captain Chris Spinelli. The system received GPS satellite information from the C-12 into a PC-104 computer manufactured by Diamond Systems Corporation. The GPS data were combined with attitude data from the MEMS IMU, stored in the PC-104 case shown in Figure 89.

Both the GPS and attitude signals were transmitted to the Learjet on a commercially available FreeWave Radio Modem datalink. The datalink transmitted at 1 Watt over an omni-directional datalink antenna at a frequency of 902 to 928 MHz, and could send attitude and position data at 20 Hz. A second PC-104 in the Learjet contained Captain Spinelli's algorithm. This unit added the Learjet's GPS data to the GPS data

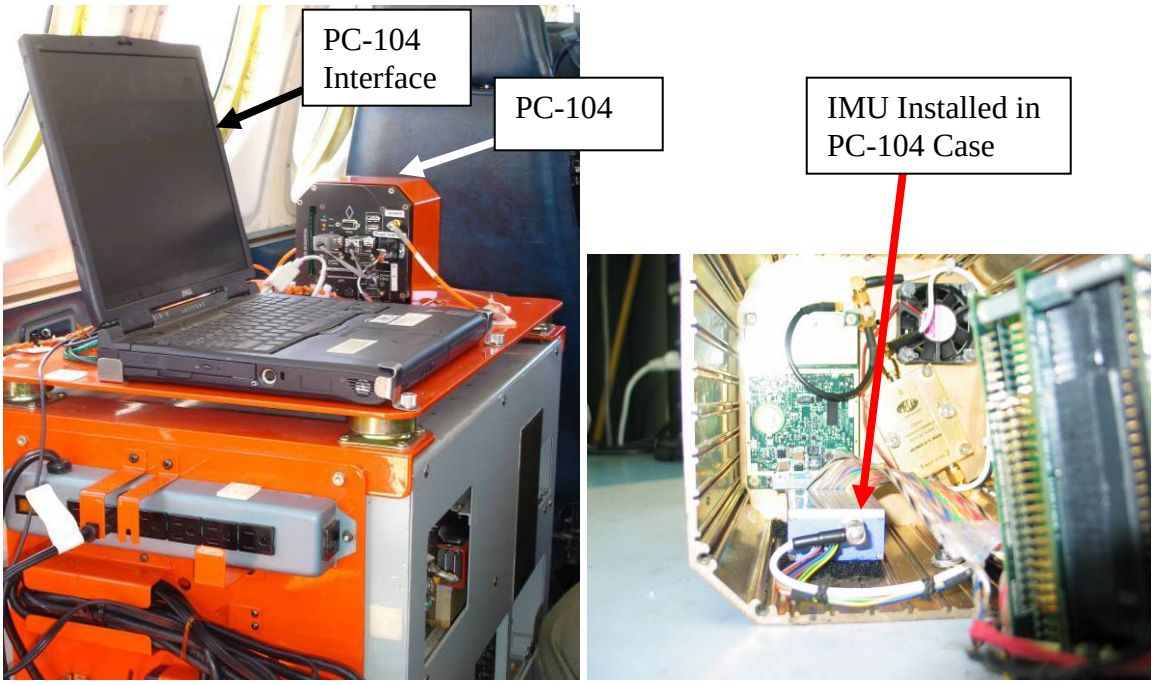

Figure 89. DGPS Hardware and IMU in C-12

from the C-12 and calculated the differential position solution. The relative position vector and the C-12 attitude data were then converted into MIL-STD-1553 formatting and placed on the data bus inside the Variable Stability System (VSS) computer. The Advanced Navigation Technology (ANT) center at AFIT provided all of the hardware and software required to get the signal to this point, including all DGPS requirements, the MEMS IMU, the datalink, and the 1553 conversion. The Calspan VSS then ran the controller, which determined appropriate control surface deflections and throttle settings to fly the Learjet.

The attitude and positioning system components are listed in Table 9.

Table 9. Positioning system components

Component	Model	Manufacturer
Datalink Transceiver	PCFW-104 OEM	Microbee Systems, Inc
DC Power Supply	HE104MAN-V8	Tri-M Engineering
Embedded PC	ATH-400 Athena	Diamond Systems, Inc
GPS Receiver Card	JNS100 OEM	Javad Navigation Systems
MEMS IMU	MIDG II INS/GPS	Microbiotics, Inc
UHF Datalink Antenna	P/N 6008	Haigh-Farr

Lead Aircraft Modifications

The C-12 used as the lead aircraft for this flight test was production representative, with the exception of a data acquisition system (DAS), telemetry system, and the hardware installed for this test. The hardware additions are shown in Figure 90.

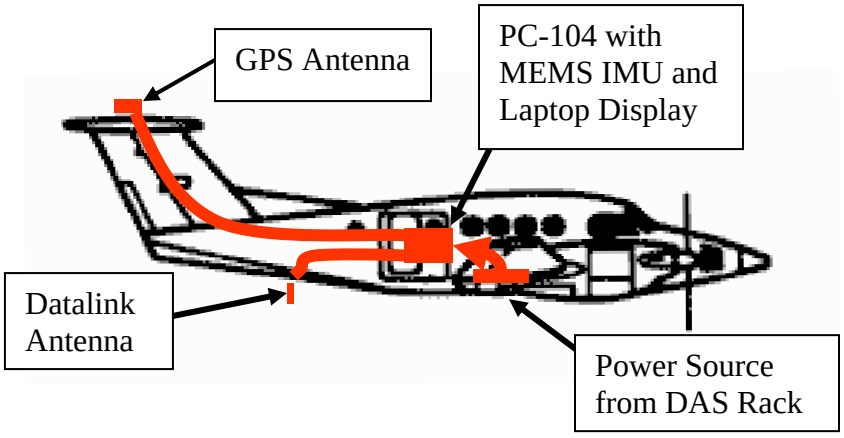

Figure 90. Hardware Configuration for C-12

For GPS measurements, the signal was spliced off of the production cable and GPS antenna, but the Javad receiver was new for this test and installed in the PC-104 case. The datalink antenna was mounted on a previously existing telemetry antenna base on the lower portion of the aft fuselage. A laptop display was installed on the DAS rack for user interface to the PC-104. The laptop also displayed the IMU output for pre-flight

checkout. The system was powered on and set up during ground operations, and left running until the end of each sortie. For more in-depth information on aircraft modification, the reader is directed to the Technical Report for this test [21] and the C-12 modification manuals [15 and 23].

Wing Aircraft Modifications

Calspan's Lear 2 is not production representative. The unique properties that affected this test included the VSS, with real-time access to flight parameters and the capability of driving strong control surface actuators, and an auto-throttle. The auto-throttle was installed for this test and difficulties precluded it from being used until the third test sortie. The Learjet had several GPS antennae, and the one selected for this test was on top of the fuselage, 15 feet back from the nose. The interior layout of the Learjet is shown in Figure 91.

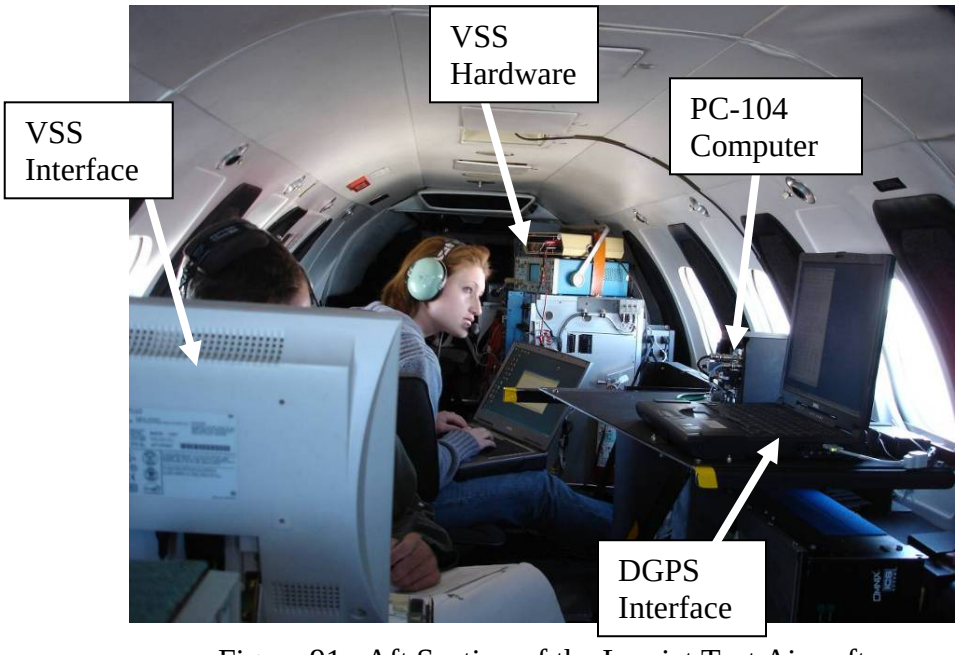

Figure 91. Aft Section of the Learjet Test Aircraft

The GPS and attitude information came into the VSS at 20 Hz, which ran the controller and scheduled the flight surfaces at 100 Hz. This led to the sampling problem discussed in Chapter III. The controller performed the coordinate transformation of the actual position vector and generated the desired position vector, based on the position command from the Flight Test Engineer (FTE). Both the desired and actual position vectors were sent to a pilot display on the right side of the Learjet cockpit. The display format is shown in Figure 92.

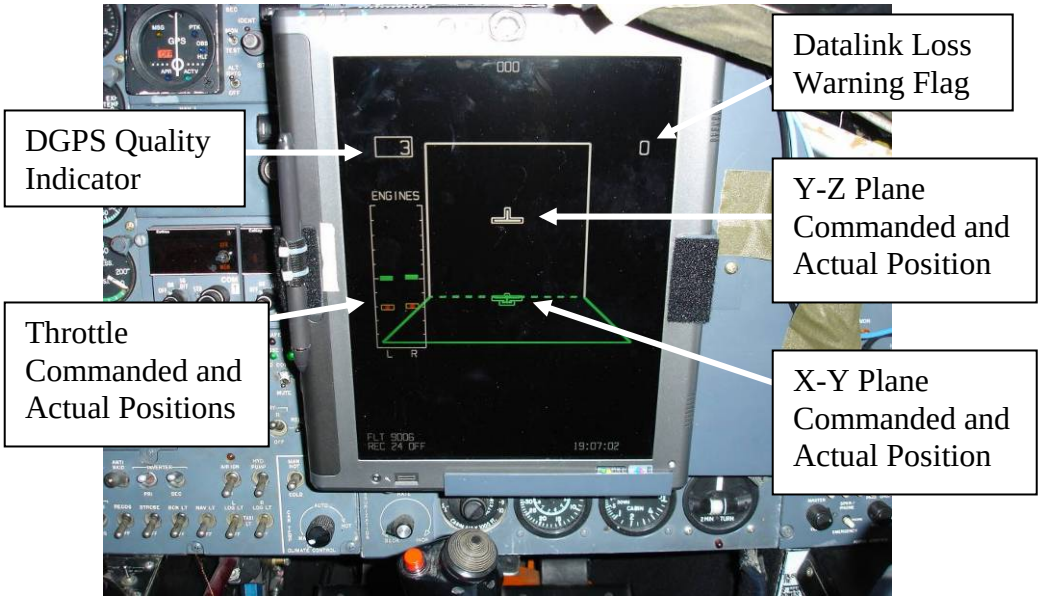

Figure 92. Pilot Display

The two central miniature aircraft symbols represent the tail view (the inverted "T") and the God's eye view of the wing aircraft and moved with the actual position vector. Though difficult to see, the outline of the symbols moved independently, representing the commanded position. When the symbol was centered in the outline, as

shown, there was zero position error. The throttle actual and commanded position blocks worked the same way. Difficulties with integration of the several systems precluded the DGPS quality indicator or the datalink loss warning flag from working during flight test.

Controller Software Modifications

No plan survives first contact with the enemy. Several modifications to the software plan were made from what has been presented in this thesis before successful achievement of autonomous flight. Using the C-12 as a lead aircraft was another cost compromise that drove the desired refueling speed of 250 KIAS (to replicate the J-UCAS refueling speed) down to 190 KIAS for this test. A question arose about the C-12's capability even to achieve the 190 KIAS design condition comfortably. Simulations for the controller were set up and run with slower speeds in 10 knot increments down to 160 KIAS for the contingency of a new design point. It was found that the normal gains selected were adequate, but not optimum, for the slower flight, which was undesirably slow in the Learjet without flap extension. A slight change was found for two feedback gains, but the effort ended up not being required for flight test. It is recommended, however, that future designers include airspeed and altitude flexibility in the simulator to find a gain schedule if the potential exists to operate significantly off the design point.

Derivative Blocks.

Due to a Matlab® limitation or a user error, the derivative filters were removed from the controller, and a word of caution is warranted for future designers. It was found that higher order ordinary differential equation solvers in Matlab® incorrectly propagated

the large, complex simulator. Figure 93 shows an output from a signal in the simulation that was recorded, and sent through a simple first order lag filter to simulate throttle actuator dynamics. The noise is magnified instead of smoothed, and the output does not track well.

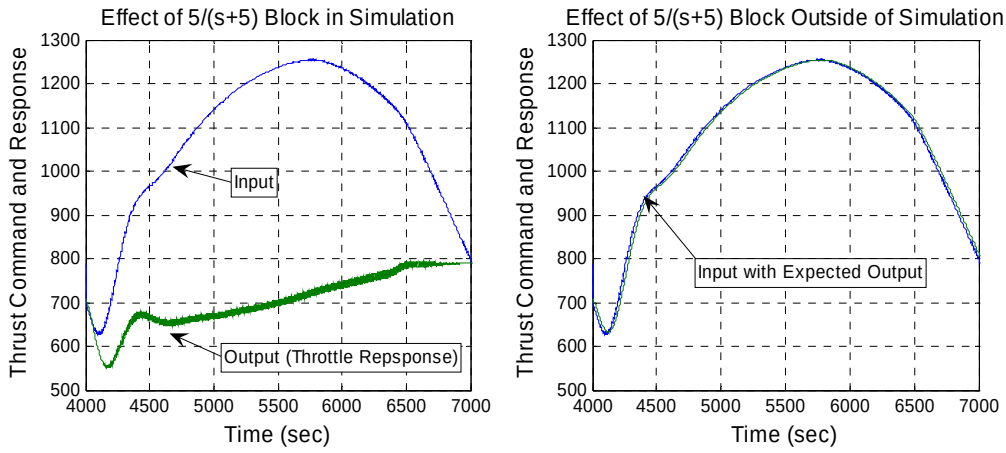

Figure 93. Higher Order Solver Difficulties

The second plot shows the exact same recorded input sent through the same filter with the same solver setup. The input, however, was placed in a fresh Simulink® file that contained only the signal and the filter without the overhead of the simulator in the background. The output was as expected, slightly smoothed with a small lag. The full simulator breaks down with higher order solvers, but runs well with a first order solver. This is potentially a difficulty with having both continuous elements such as the actuator dynamics blocks and discrete elements caused by the sampling errors between the VSS and the DGPS, but the true cause was never understood.

Unfortunately, the failure to understand the nature of this problem impacted the flight test. Tracking errors were noted across the derivative filters before the solver difficulty was understood. Recall that the transfer function $\frac{100^2 s}{(s+100)^2}$ was to be used for taking all derivatives, as discussed in the wing stability augmentation section of Chapter V. The intent was to get a derivative of the signal at low frequencies, while attenuating high frequency noise. Because the filter block output appeared incorrect (it was not understood that the blocks were fine, but the solver didn't work), all derivative filters were replaced by discrete derivative blocks $\left(\frac{\Delta\, signal}{\Delta\, time}\right)$. This decision was made in an effort to fix what ended up being the solver problem, and the advantages of the high frequency noise attenuation were lost. The true nature of the solver problem was found just prior to flight test months later, but the derivative filter blocks were not restored or used in the real aircraft. As noise from the derivative blocks was significant, the filtering may have been beneficial. With the benefit of hindsight, however, this was not a total loss. Due to inexperience with filters, the break frequency selected for the derivative filter (100 rad/s) was set far above where pilots normally operate. This decision was based on actuator capability, but inputs of only 3 rad/s are considered high bandwidth for pilot corrections [7]. It is likely that the filter would have been poorly tuned, failing to attenuate much of the noise, while still causing a small amount of the phase lag penalty inherent in any filtering.

IMU Failure and Heading Estimation.

The heading and pitch angle information from the MEMS IMU was unusable during flight test due to a hardware malfunction. On the first of the seven test sorties, the heading angle of the IMU swung rapidly from the correct heading to a value 30-40 degrees off during straight and level flight, as shown in Figure 94.

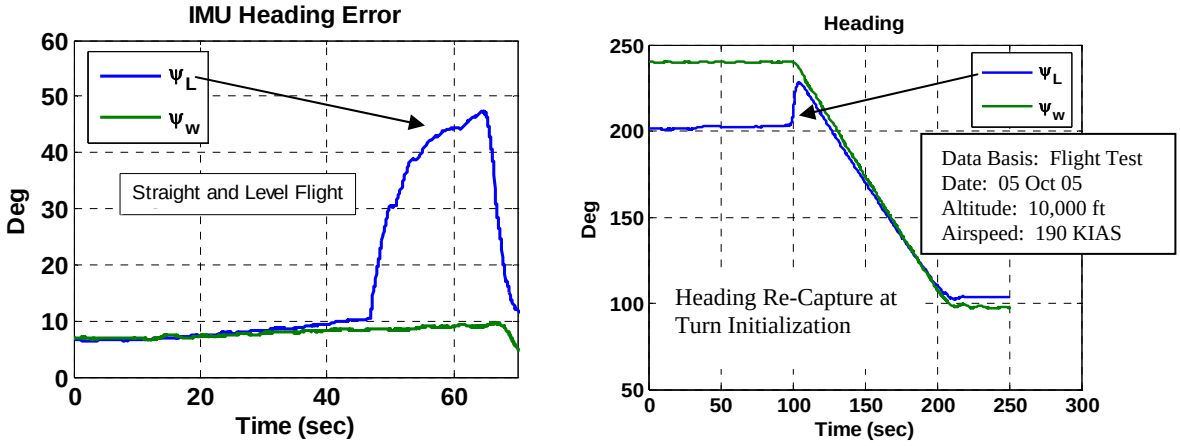

Figure 94. IMU Errors

A similar error occurred in the pitch angle. After consultation with the IMU manufacturer, a firmware option was found that adds magnetometer corrections to the heading and pitch data when reaching 8 degrees of heading uncertainty. Though this option was turned off, the data suggested there was a firmware error that was adding the "correction" anyway (and that the "correction" was adding the 30-40 degree error). This assumption was supported by the timing of the bias addition. The IMU was programmed to add GPS corrections to the measured heading angle in turns, but not in straight and level flight. After 45 to 60 seconds straight and level without correction, the uncertainty in the MEMS gyro most likely grew big enough to trigger the unwelcome magnetometer

"corrections". As the aircraft started to turn, however, the GPS corrections were added to the IMU's measured heading angle. Usually (though not in every case), the heading and pitch angles would re-capture as the turn started, as shown in Figure 94. The addition of the GPS corrections most likely moved the uncertainty below the 8 degree threshold and the magnetometer "corrections" were turned off. Recall that the controller had no way of knowing that the lead aircraft was not truly rotating, and it rapidly moved the Learjet to a position 40 degrees off of the tail of the C-12. With frequent random errors of such large magnitude, the heading and pitch angles were completely unsuitable for use in flight.

For the second test sortie, constants were used for the pitch and heading angles. Pitch angle varied only minutely in the C-12 for the entire flight. Some small transients were noted on the roll into bank, as well as an increase of less than 1 degree in the steady state pitch angle required for 30 degree banked turns. The lack of knowledge about the increase translated into the controller flying the Learjet to a steady state contact position that was approximately 4 inches too high during 30 degree banked turns. This was considered negligible. The required steady state value for pitch angle was dependent on the IMU installation, and was found by inspection of the IMU flight data (without magnetometer "corrections") and set in the controller as a constant.

Future designers should consider the feasibility of always using a constant for pitch angle, as you gain a lack of transients in turns and the reduction of an entire channel of attitude source noise, at a very small cost in terms of station keeping. This may be unfeasible for a real tanker where the pitch angle may change considerably due the large range of potential gross weights. Replacing pitch angle with a constant would also lead

to a larger steady state error if one desired to refuel in a climb or descent, a capability occasionally used by heavy-laden B-52s and A-10s.

Heading angle obviously could not be replaced by a constant, as it varied continuously in turns. For the second test sortie, no turns were allowed with the controller engaged. The heading angle from the compass in the C-12 was transmitted over the radio to the Learjet after every turn. This value was converted to true heading from magnetic, and then hard-coded by the FTE for each run. This is the exact configuration that NASA used for their formation demonstration [9].

By the third sortie, a heading estimator was designed to make up for the loss of the IMU. Several schemes were quickly built and flight tested, and the best one was kept for the remainder of the sorties. A constant g (32.2 ft/s^2) and a true airspeed (V_T) estimate of 371.5 ft/s was assumed based on the design point and the average daily temperature during the test days. The lead bank angle (φ_L) was then converted to turn rate (ω):

$$\omega = \frac{g \tan \varphi_L}{V_T} \tag{55}$$

The turn rate was integrated to produce a delta heading. For initialization, the FTE was provided with a "sync" button that was used before the first time the autopilot was engaged. The sync button stored the wing aircraft's current heading as the lead aircraft's initial heading, and the deltas from the turn rate equation were added to that. Special care was taken with magnetic heading (on the Learjet data bus) versus true heading (the expected IMU output), and in keeping the integrated solution between the values of 0-360 degrees, as expected for a compass value. Logic tools were created to

accomplish these efforts at the key points, and they are shown with the entire implementation of the heading estimator in Figure 121 through Figure 125 of Appendix A.

With mere turn rate integration alone, the heading solution was found to drift unacceptably. The bank angle that was measured by the IMU and integrated for turn rate varied from +5 to -4 degrees during straight and level flight. The errors in bank angle were due in large part to the poor MEMS IMU accuracy. There was also potentially some error contribution from IMU installation alignment and the differences in trim thrust between the C-12 engines. Actual in-flight thrust per engine was not measured or displayed to the pilot, but if the engines were not exactly matched, either bank or rudder would have been required to keep the aircraft from turning due to the asymmetric thrust. In the heading hold mode used during flight test, the C-12 autopilot would have used bank angle. Regardless of the source of the error, a random small bank angle was seen by the heading estimator and integrated into heading drift.

The heading of the lead aircraft during refueling is always very near that of the wing aircraft. During turns and position changes, the heading difference typically does not exceed more than 2 degrees. A correction factor ($\Delta\varphi_L$) was introduced that would keep the C-12 heading estimate (ψ_{L_est}) near the heading of the Learjet over time by slowly correcting the measured C-12 bank angle:

$$\Delta\varphi_L = 0.4(\psi_W - \psi_{L\_est}) \tag{56}$$

The correction to the lead aircraft's bank angle made the heading estimate correct over time without inducing undue responsiveness from the wing aircraft maneuvers. A

tool was created for use when both headings were near north, where one heading value may be 001 and the other may be 359. This tool ensures the heading difference remains correct despite the discontinuity in the heading past 359 degrees, and is shown in Figure 125 of Appendix A. The value of 0.4 was found empirically with recorded flight test data from the first two sorties. It is understood that traditional heading estimators would apply the heading difference correction to the actual heading estimate instead of changing the bank angle input. This solution minimized the impact of heading drift by eliminating the source of the drift—the bank angle bias.

With this short term fix, the flights were able to resume completely autonomously. One heading "sync" was performed prior to engaging the autopilot at the beginning of the sortie, and all systems were left on without further input beyond "go to" commands for position changes. There were some exceptions for an occasional VSS reboot or other "glitch", and the system averaged 1 or 2 power cycles across each 1.8 hour sortie for the second half of testing. The DGPS also required a 30 second reboot after each hour of use due to an initialization problem the test team was unable to fix. The heading estimation solution was adequate for flight test, but there was some "wander" in the data. Figure 95 shows characteristic performance. Further examples of the heading estimator performance are also shown in each maneuver of the flight test results in Appendix D. Figure 95 shows a general trend of staying on the right heading, with a slight wander of a couple of degrees during flight. The controller in the Learjet has no way to distinguish this from actual C-12 motion, so it attempts to maintain the moving position. Recall that a 1 degree error in heading results in the pre-contact

position moving 1.6 feet, and the motion adds dynamics that the controller must contend with. As such, an unknown (but likely small) portion of the lateral errors in the flight test results are due to the lack of a precise heading source.

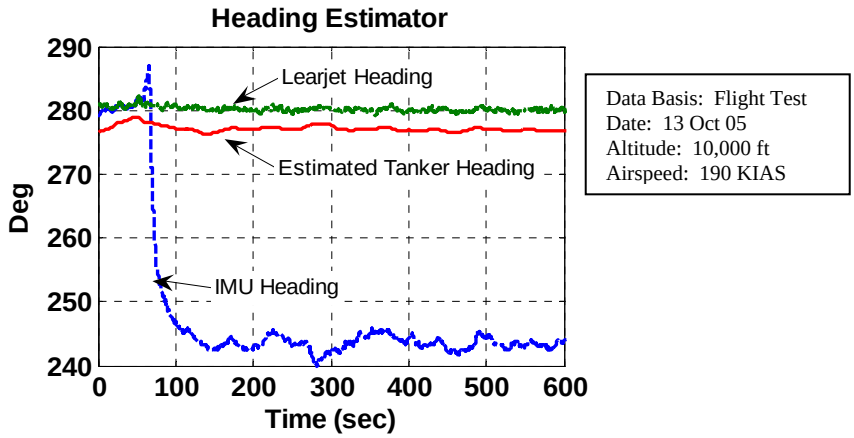

Figure 95. Heading Estimator During Ten Minute Straight and Level Run

Filter Requirements and Lateral Gain Reduction Error.

Originally, the formation simulation was built and the design gains were selected with very little filtering. The attitude and position information that entered the controller had a stair-step, zero-order-hold appearance due to the sampling rate change from the 20 Hz datalink into the 100 Hz VSS. This was smoothed with the simple averaging filter shown in Figure 119 of Appendix A that averaged the last 5 frames of data (0.05 seconds). This amount of smoothing, with the underestimated noise magnitudes from the IMU manufacturer, appeared to be sufficient. As mentioned, however, the real impact of the noise was found to be excessive during ground test. The situation was greatly exacerbated by a units error on the lead aircraft roll rate parameter. The roll rate

information from the IMU was translated into the MIL-STD 1553 format. During the conversion process the signal was unintentionally presented to the controller at 10 times the actual magnitude. This erroneously large amount of roll rate was fed forward directly into the aileron control channel, and the magnified noise on the signal could be seen in vibrations of the control yoke.

It was assumed that the feedback gains in the lateral channel were set far too high. The total loop gain, k_p_err, was decreased to one third of its intended value. This means that the actual controller tested in flight only used one third of the amount of planned aileron. The impact of the reduced gains on lateral control performance was obvious, and will be shown in the results section of the next chapter. Unfortunately, after the units error was identified and a gain was installed to adjust the roll rate signal to the true value, the lateral loop gain was not reset to the design value. This was due to another mis-analysis error of a DGPS update problem that also appeared like noise and will be explained shortly.

After the noise was seen in the control yoke, filter options were installed in every channel as the attitude and position information entered the controller, and as the commands exited the controller. The control surface commands that *exited* the controller were found in simulation to move very fast, and any significant delay raised the potential for instability during aggressive maneuvering. Therefore, all filtering on the commands exiting the controller was abandoned, and is not recommended. However, simulation showed that information *entering* the controller can be fairly heavily filtered with little effect. Due to the nature of refueling, the lead aircraft's heading, pitch, and bank angle

rates are limited to below about 3, near 0, and 4 degrees per second, respectively. The GPS position data was also easily filtered, as the data was differential and the rates between the two aircraft are extremely slow. The fastest intentional move is 6 feet per second. The fact that everything changes so slowly during refueling is what makes the level of filtering required to control with this paradigm acceptable, even with noisy sensors.

Filter Tuning.

All low pass filtering causes phase lag. As the break frequency of the low pass filter is decreased toward the frequency of the signal's actual motion, or as the order of the filter is increased, the filtering improves, but the phase lag gets worse. The break frequency and order of the filter for each channel on the controller were selected with a less-than-elegant manual tuning technique.

Several "best guess" options were provided for each of the 4 attitude channels (ψ_L, θ_L, φ_L, p_L), the 3 position channels (x, y, z), and the 2 wing feedback channels (φ_w, p_w). Each option increased the level of filtering by lowering the break frequency or increasing the order of the filter. A further option was provided to set the sensor input to a constant. During ground operations, the two aircraft were initialized and the data link was engaged. All controller inputs were set to constants first. Each input was then turned on individually. If any vibration was detectable in the control yoke, the next level of filtering was selected until the motion was gone. When the control yoke showed no motion, the next input was turned on. After each of the first few sorties, the flight data

from the IMU was run through simulation with more filters, and new options were provided for the next day's sortie until a good balance was found.

DGPS Update Errors.

After the filters were installed and the roll rate units problem was fixed, the loop gain on the aileron channel was temporarily restored to the design level and the system was engaged on the ground. Several small spikes were noted in the aileron position command of between 3 and 4 degrees. Noise was assumed, and the lateral loop gain was again reduced and left at the one third point, never to be actually flown as the controller was designed. The author failed to note that the spikes in the controls were rhythmic, and not random, and only late in the testing did the true nature of the problem emerge. Most of the suspected "noise problem" still remaining was due to a DGPS error. One position update per second was missed (and sometimes as many as 6 or 7 in a row, still at 1 Hz).

The exact cause of the missed updates was never determined. The DGPS Kalman filter updates at 1 Hz, and the datalink also has a 1 Hz logic cycle. The DGPS was more likely the cause, as the missed updates were not seen in the attitude data that also came across the datalink; however, the small missed updates could have been masked in the noisy MEMS IMU signals that were rounded off, resulting in many "flat spots" that could have been missed updates. Regardless of source, the impact of the missed updates went unnoticed while holding one position in flight. During position changes, however, a 1 Hz "kick" in the controls was obvious, annoying, and large enough to occasionally cause VSS safety disconnects when a command was too large or too fast. The "kicks" in the commands were in the aileron channel when moving laterally, and in the throttle

channel when moving forward or aft. One such disconnect is shown in Figure 96, and obviously the situation was unsatisfactory.

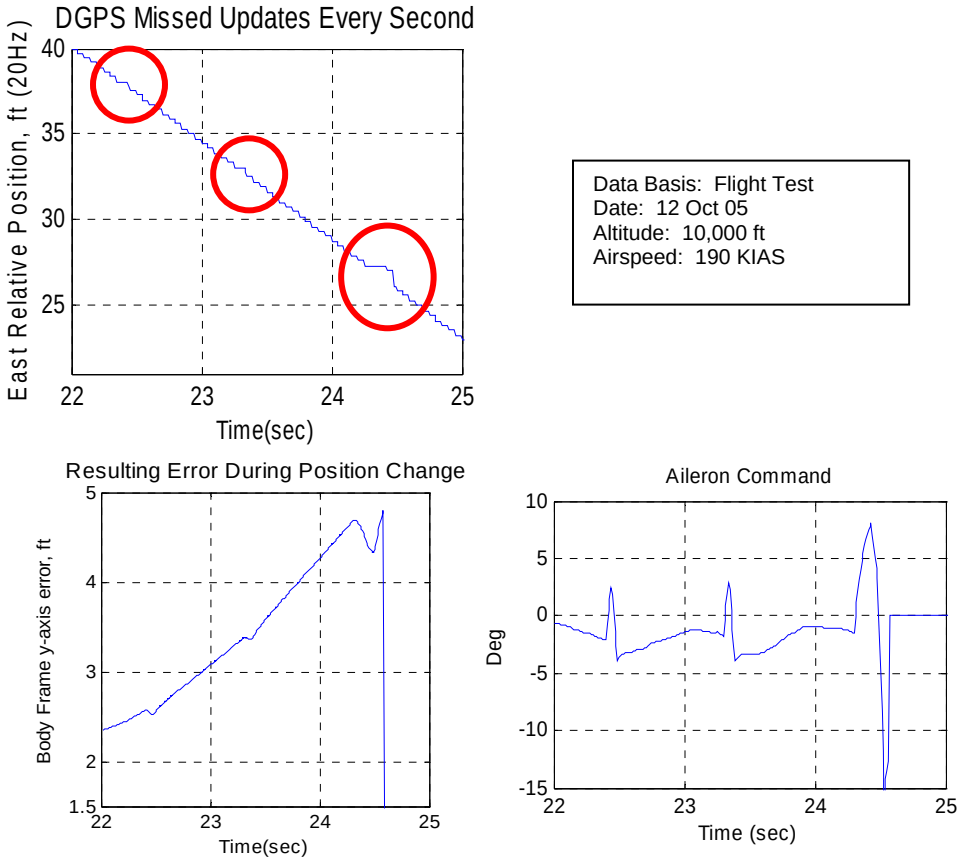

Figure 96. Differential GPS Missing Updates Causing Aileron "Kicks"

The fact that the effect was only noticeable while changing positions was the key to finding the error. The magnitude of the missed update, when stationary relative to the lead aircraft, only resulted in a "flat spot" in the position data that was filtered prior to reaching the derivative portion of the control laws. When the desired position vector was commanded to move for a position change, however, the "flat spots" became the "corners" shown in the lower left plot of Figure 96. The desired position vector was

continually updated, while the current position vector missed one update per second. To illustrate the problem, consider the wing aircraft moving from the pre-contact position to the back corner position. The desired position vector moves from one position to the other, and the wing aircraft has a certain offset behind the desired position that it is "catching up with" to correct. This offset is the error vector that is fed to the control laws. At the point where the actual position vector misses an update, it appears to the controller that the wing aircraft stopped moving, but the desired point continues to move away. The controller sees that the distance between the wing aircraft and the desired point is *increasing*, as a resulted of an opening rate of relative motion (the position error rate). At the next time epoch, the wing aircraft appears to move twice as far as it had been every epoch, as the DGPS makes up for the missed step. To the controller, it appears that the wing aircraft is now moving twice as fast toward the desired point, and the amount of position error to the control laws is *decreasing*. The apparent rate of closure changed twice, resulting in the "corners" of the error plot. As the derivative control operates on the rates of closure, seen in the changing slope of the position plot, it sends the "kick" into the ailerons. When the position change move is forward or aft, the "kick" goes to the throttles, as the error "corners" are in the longitudinal channel.

Two software patches were installed to mitigate the DGPS problem. First, Mr. Russ Easter of Calspan built a predictive filter that compared the average of the most recent 5 position epochs with the 5 epochs prior. Recall that with the sampling error difference between the DGPS and VSS, the position only updates once ever 5 VSS epochs. This causes the stair-step effect in the upper left plot of Figure 96. If the two

5-frame averages are exactly equal, the last position step did not update. A step is inserted in the same direction and magnitude as the last known position step. This limited the time of the exposure to position error that was generated by missing an update to one frame instead of 5, and reduced the effects of a single missed update. The predictive filter did nothing, however, when more than one update was missed in a row. The aileron "kicks" during position changes caused by single missed updates were annoying, but the large errors from several missed updates in a row were the cause of the VSS safety disconnects that had to be solved.

The filter structure was changed as shown in Figure 97.

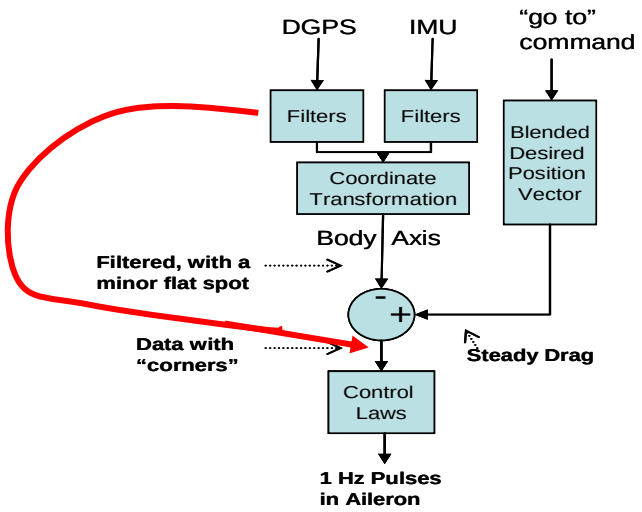

Figure 97. Filter Structure Change

It is imperative that the IMU filters be up front, as the attitude data is used to transform the position vector data into the tanker body frame. If that frame is jumping around with noise, it will appear that the position data is jumping around, and the noise in

the IMU will be amplified through the system. Recall that a small change in the attitude angles of the tanker body frame will move the components of the actual position extensively, based on how far the wing aircraft is from the center of the frame.

The small errors in the differential position from the DGPS, however, are not actually changed during the coordinate transformation. The error vector is exactly the same, only described by a different set of components. Therefore is no requirement to filter them early, as the noise effects do not change. Delaying this filtering until after the current and desired position vectors have been subtracted allowed the filters to operate on the "corners" that were a result of the subtraction of the moving vectors. This greatly alleviated the update problem. The single missed updates were no longer noticeable, and the large missed updates were small enough to be an occasional nuisance.

Filter Summary.

The values for each filter were found by hand tuning them to actual flight data after each of the first few sorties, and then simulating the controller extensively to determine any undesirable effects from delay. The final configuration consisted of the 4 tuned lag filters in Table 10 and the predictive filter built by Mr. Easter. The IMU data from the lead aircraft (roll rate and bank angle), and the wing aircraft feedback parameters of roll rate and bank angle were filtered immediately upon entering the controller. No filtering was required on heading or pitch angle from the lead aircraft due to the IMU failure. The DGPS data was filtered after the subtraction of the desired and actual position vectors.

Table 10. Filter Summary

Data Type:	Filter:
DGPS Data:	
x,y,z position	$\frac{10}{s+10}$
IMU Data:	
φ_L	$\frac{10^3}{(s+10)^3}$
p_L	$\frac{7^3}{(s+7)^3}$
Wing Aircraft Data:	
φ_w, p_w	$\frac{15}{(s+15)}$

The requirement to install filters was driven by vibrations that could be seen in the control yoke. Some of the vibration was caused by legitimate noise that required filtering, and some was due to the units error on the lead aircraft's roll rate and the DGPS update problem. All of the sources, however, were initially attributed to excessive lateral feedback gains, and the total loop gain was decreased. Unfortunately, by the time the filters were installed, the units error was fixed, and the DGPS update problem was understood and resolved, the test team did not have time to return the lateral loop gain up to the design value. Any gain change required a new start of the safety buildup process and a repeat of the entire test matrix. The options available to the test team were to complete the test matrix with a "dumbed down" controller, or to fix the controller, but have insufficient time to complete the flight test. The former option was selected, and the result was a loss of dynamic rolling performance that will be shown in the test results section of the next chapter.

VIII. Flight Test Results

Flight Test Overview

Flight test to evaluate the performance of the controller and to prove the concept that close formation flight could be autonomously controlled well enough to air refuel was completed in October, 2005 at Edwards AFB, CA as a Test Management Project for the USAF Test Pilot School. The overall objective of the test was to demonstrate the performance of the control algorithm in an operationally representative environment. This overall goal was divided into three sub-objectives: to demonstrate that the system was capable of maintaining the pre-contact, contact, and wing observation positions; to demonstrate that the system was capable of properly moving between the three positions; and to record parameters in the system during maneuvering that were used in troubleshooting the system and in presenting the results for this paper [21].

All objectives were met, and the system performed quite well. In the controller's final configuration, it demonstrated the ability to fly formation well enough to autonomously refuel an aircraft during straight and level flight, or when established in turns with up to 30 degrees of bank. Rolling maneuvers, however, did not meet expectations and are discussed in this chapter. All position changes were performed correctly and efficiently. Safety and stability were never in question.

Chronology and Test Flow

Approximately 6 hours of ground test to verify system functionality were conducted prior to flight test. Seven formation sorties consisting of 12.6 hours on the Learjet and 13.1 hours on the C-12 were flown in the R-2508 complex to accomplish the objectives. The design flight condition was 10,000 ft MSL and 190 KIAS. All flights were accomplished there except flight number 5, which was moved to 12,000 ft MSL in an effort to reduce turbulence. A summary of program chronology is shown in Table 11.

Table 11. Flight Test Chronology

Date	Testing Accomplished
29-Aug-05	Ground checkout of C-12 DGPS and datalink
3-Oct-05	Ground checkout of C-12 and Learjet--Full system integration
5-Oct-05	Flight #1, System Calibration: Auto-throttles inoperative, Inertial Measurement Unit unreliable with large swings in heading and pitch
6-Oct-05	Flight #2 System Calibration: IMU heavily filtered or inputs replaced with constants, auto-throttles inoperative
11-Oct-05	Flight #3, Test Flight: Auto-throttles operational, IMU heading and pitch angle replaced with estimators; turning capability incorrect due to Calspan Simulink code translation error
12-Oct-05	Flight #4, Test Flight: Heading estimator and filters modified, turning correct
12-Oct-05	Flight #5, Test Flight: Filters modified – Configuration stable, fully capable
13-Oct-05	Flight #6, Test Flight: Stable configuration - Performance data collected
14-Oct-05	Flight #7 Test Flight: Stable configuration – Completed data collection

The first two sorties did not use the auto-throttle. Instead, a test pilot used a display to manually match the current throttle position to what was commanded by the controller. The entire system was fully autonomous by the third sortie, meaning there was no user input or involvement with any part of the entire system except for a numeric

command of what position to fly to. Additional hardware and software problems led to modifications of the controller during the flight test window. The configuration of the aircraft and the controller was in flux the latter half of test flight #5. At that point, the test matrix was restarted, and all of the planned maneuvers were repeated in the frozen configuration, which unfortunately included a reduced total aileron loop gain. The key results are discussed in this chapter, and the supporting data from the final configuration runs are in Appendix D.

The test point matrix was planned using a safety buildup approach, flying positions that were farthest away first, increasing maneuver difficulty and decreasing range as the system performed acceptably. Station keeping and position changes were accomplished in straight and level flight first, then turns of 15, and eventually 30 degrees of bank were performed as the tasks were repeated. Most data runs were recorded for 60 seconds. Finally, position changes were performed with rolls initiated and completed during each leg. For safety considerations, an intermediate position was added in between contact and pre-contact for the opportunity to further measure the performance of the controller in close formation before pulling all the way into the contact position, where only 5 feet of nose-tail clearance existed between the aircraft.

Objective 1: Station Keeping

The fundamental requirement of the air refueling controller was station keeping. The three positions of contact, pre-contact, and wing observation were each maintained as shown again in Figure 98.

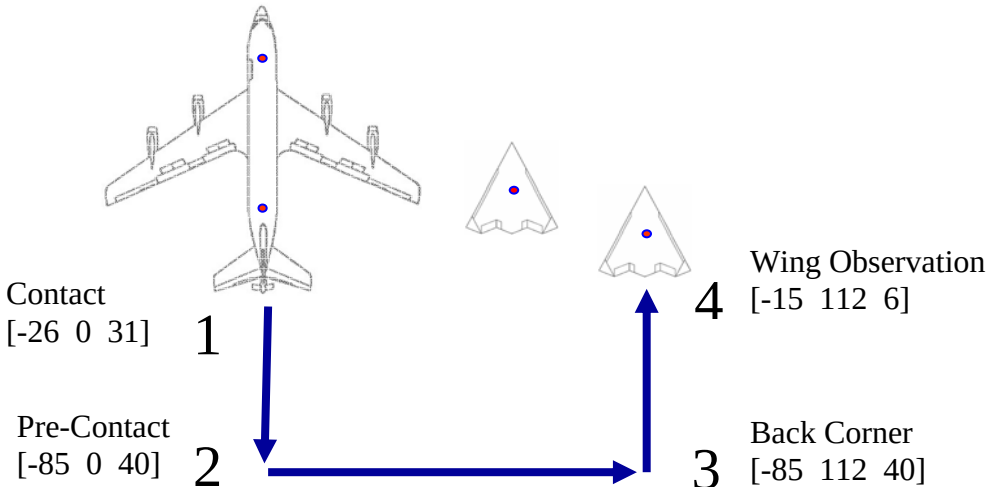

Figure 98. Formation Positions and Position Change Path

Station Keeping in Straight and Level Flight.

The controller's performance in the contact position, where it would actually be connected to the lead aircraft, is obviously the most critical and is presented first. To successfully refuel, the wing aircraft must not only maintain this position within the refueling boom envelope limits, but it also must be stable enough that a human operator can fly the boom to the wing aircraft's refueling receptacle. Figure 99 shows the contact position as it appeared during flight test. At no time in the straight and level flight runs did the system exit a notional boom envelope. The longest data run recorded was for 10 minutes, and is shown in Figure 100. The dashed lines represent an average KC-135 boom envelope (the smaller of the two possible tanker options), the limits of which change as the controller moves in the x-body direction. Since the longitudinal axis is

tightly controlled, this is conservative, as the limits are the greatest when the boom is centered longitudinally.

Figure 99. Test Aircraft in Contact Position

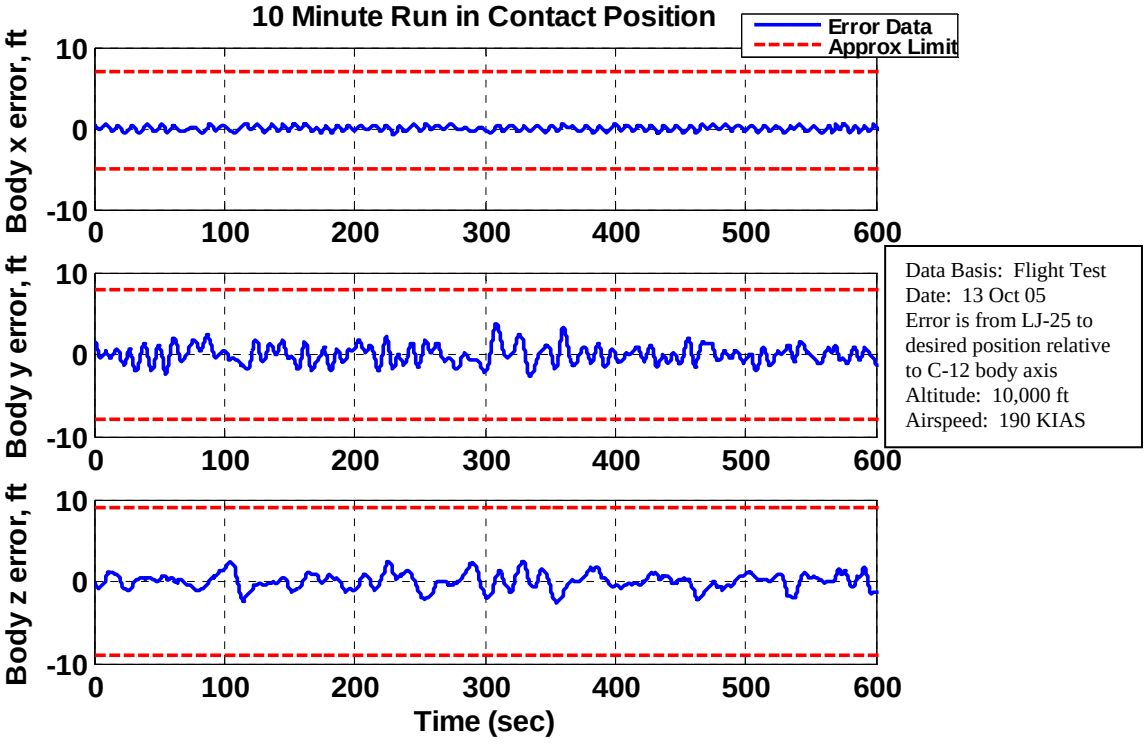

Figure 100. Contact Position Station Keeping, Straight and Level Flight

Combining the data in all three axes, the mean radial error for this 10 minute run was 1.33 feet, with a maximum radial error of 3.9 feet. Considering all data runs in the contact position, the mean radial error was 1.29 feet, with no change in maximum error. This is completely acceptable for air refueling. The error traces appear to have high frequency content only due to the greatly compressed time scale.

The performance in Figure 100 represents the core requirement of the controller, and an important end result of the thesis—the controller can hold position well enough to refuel for long periods of time in straight and level flight.

For the pre-contact and wing observation positions, the control of the aircraft is theoretically more difficult due to the effects of noise and random lead aircraft motion being magnified by a longer lever arm from the lead aircraft. This is offset by the fact that the wing aircraft does not have to compete with the disturbed airflow around the C-12, as it does in the contact position. Station keeping performance in all positions was essentially equivalent, as shown in Figure 101 and Figure 102. The boom limits were removed, as they do not exist outside of the contact position, and the goal of this research was to maintain these positions within 10 feet in all directions. Again considering all of the data runs together, the mean radial position error for the pre-contact position in straight and level flight was 1.54 feet, with a maximum radial error of 3.34 feet. For the wing observation position, the mean radial position error in straight and level flight was 1.57 feet, and again the maximum radial error was 3.34 feet.

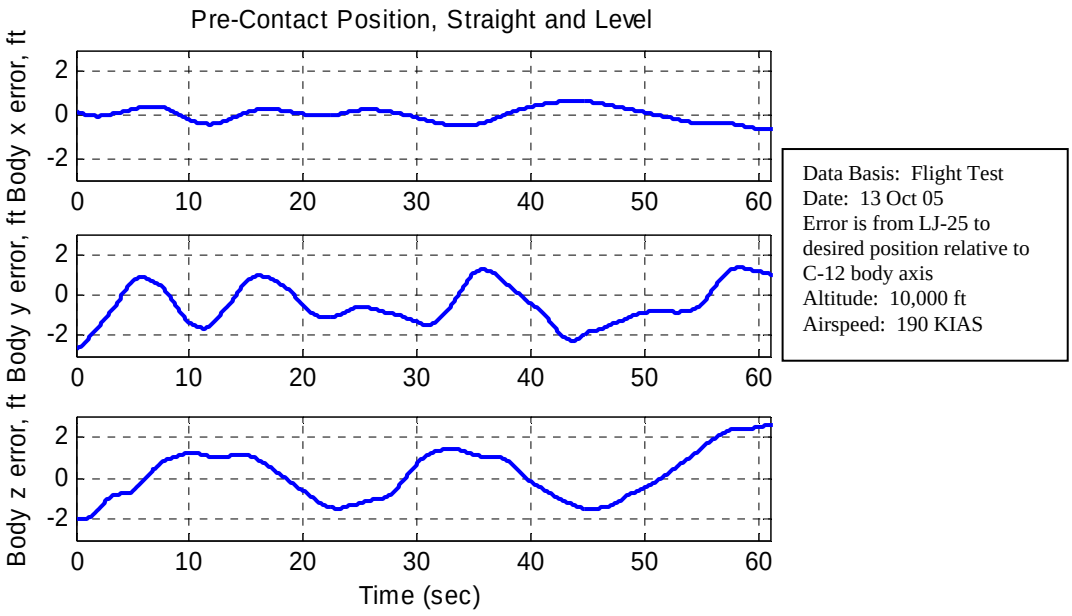

Figure 101. Pre-Contact Position Station Keeping, Straight and Level Flight

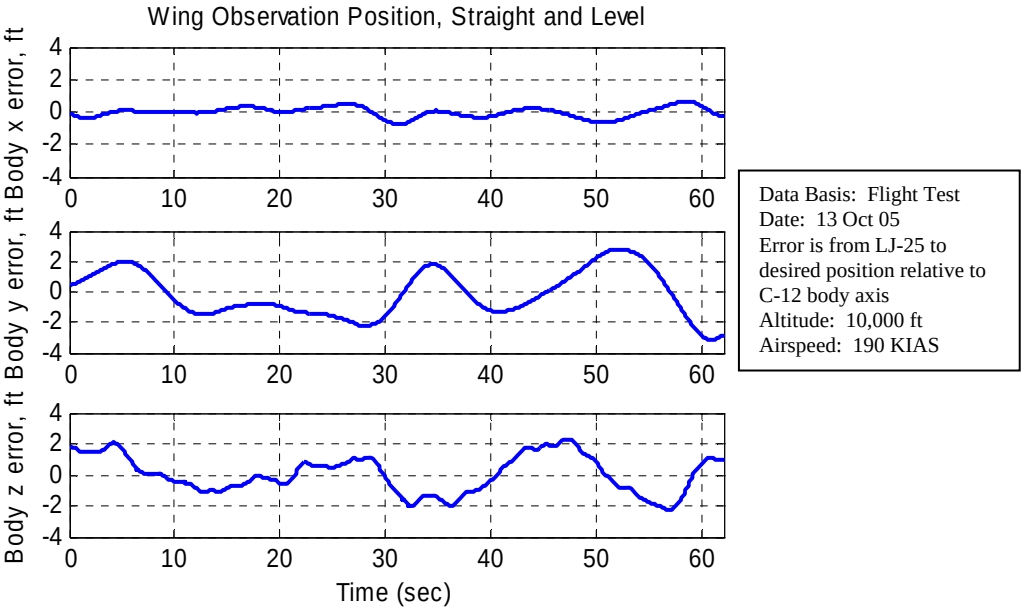

Figure 102. Wing Observation Station Keeping, Straight and Level Flight

Though the straight and level station keeping capability of the controller was satisfactory, it did not match up to the predictions from the simulator, and the

discrepancy between the predicted and actual results increased with the dynamics of maneuvers. Some of this discrepancy was from the increase in noise from the MEMS IMU over what was predicted by the manufacturer. The majority of the increased errors were due to the reduction of the total aileron loop gain. Additionally, a small part of the unforeseen error was due to a poor throttle servo.

Throttle Asymmetry.

The servo that operates the fuel control unit on the right engine of the Learjet was receiving a low quality RPM signal. In effect, this caused a "sticky throttle" that did not move until a large signal was input. Large hysteresis effects were also noted. When a throttle reduction was commanded by the controller, the left throttle would move back farther than the right (the right throttle did not fully comply with the command). This caused a thrust asymmetry which resulted in left yaw. In addition, the aircraft did not move back as fast as planned, since the total reduction of thrust was less than commanded. This had the capacity to drive an overshoot, as the integral control demanded an even larger throttle reduction. As the aircraft reached the desired point, the controller commanded that the power be increased once again. This time, however, the "sticky throttle" caused the left throttle to move farther *forward* than the right throttle, causing a yaw back to the right. The throttle asymmetry and hysteresis effect had the capacity to achieve a very slow, sustained oscillation, as shown in Figure 103.

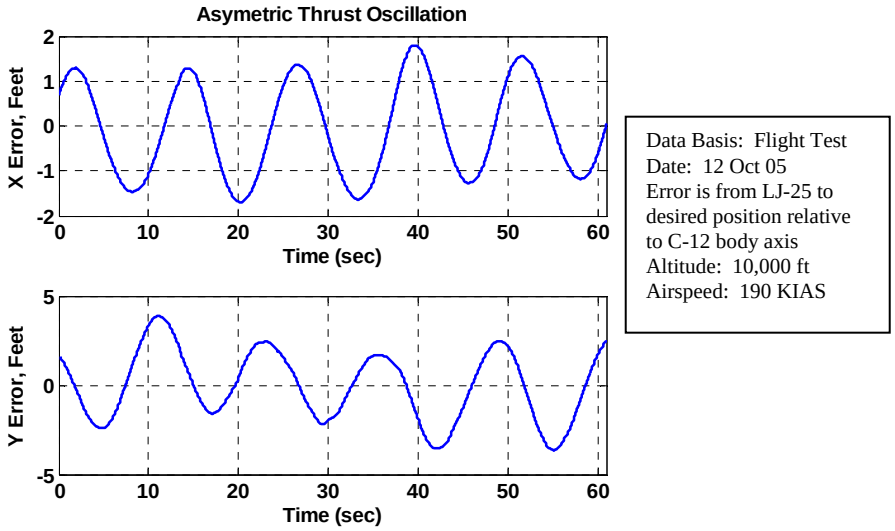

Figure 103. Oscillation Due to Bad Throttle Servo

Figure 103 illustrates an extreme example that was only noted twice during the two weeks of flight testing. The throttle problem was always a factor at some level, however, and some of the position error in every data run is most likely due in part to the bad servo. This was always the case during dynamic maneuvers, because throttle adjustments were unavoidable and unfortunately not symmetric. In the steady state positions, throttle asymmetry contributions are likely culprits when a small sustained error oscillation in the longitudinal axis is noted at the same frequency as a lateral oscillation.

Station Keeping in Turns.

As discussed in Chapter I, the standard refueling track is planned for sustained turns at 15 degrees of bank, with the option of using up to 30 degrees of bank for unforeseen circumstances. A typical tanker roll rate was estimated during flight testing

to be approximately 2.5 to 3 deg/s. The performance of the flight controller was directly impacted by the roll rate and smoothness of the lead aircraft. Maneuvers with abrupt stops or abrupt roll initiation increased the lateral overshoot. Once a turn was established, the controller stayed within the boom position limits with small enough deviations to easily refuel. During the rolling portion of the maneuver, however, the lateral error exceeded the limits on one of the 15 degree banked turns, and most of the 30 degree banked turns. Figure 104 shows an example of a smooth turn with acceptable performance in the contact position.

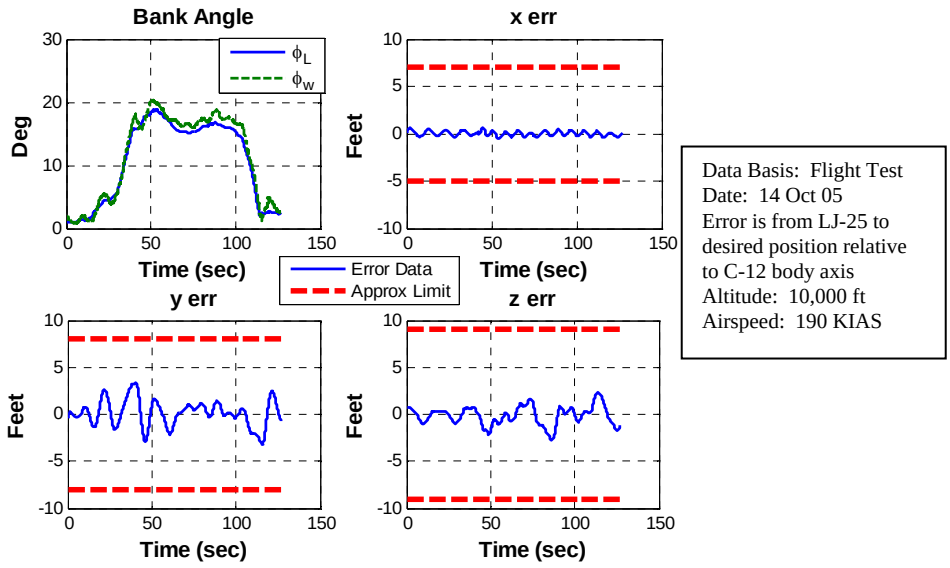

Figure 104, Contact Position, Smooth 15 Degree Right Turn, Acceptable Performance

Figure 105, however shows a maneuver where the controller exceeded the notional boom limits.

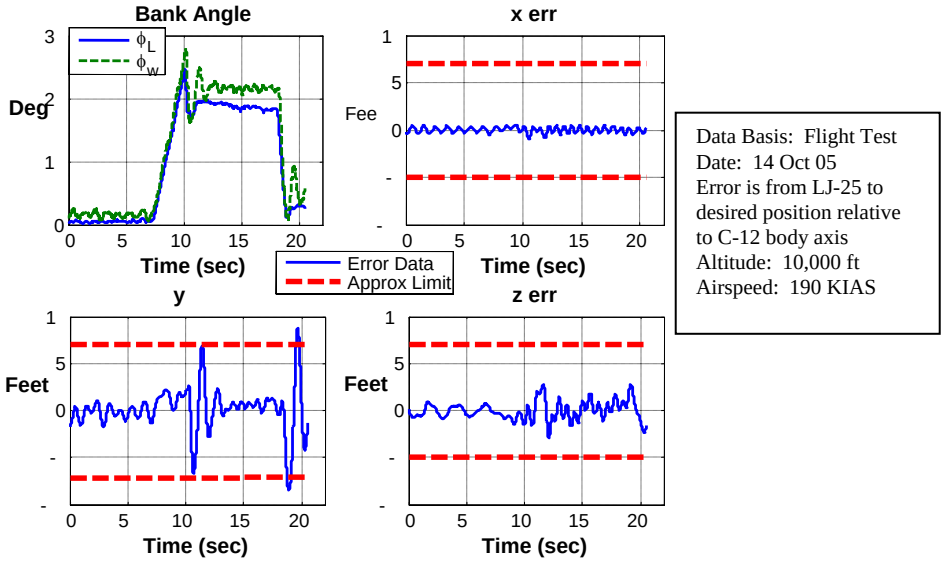

Figure 105. Nineteen Degree Banked Turn with Lead Aircraft Overshoot and Rapid Roll Out; Unacceptable Performance

For the maneuver in Figure 105, the C-12 autopilot was malfunctioning, and the pilot was only able to attain an extremely slow roll in, which overshot and corrected back rapidly to a steady state value higher than intended (approximately 19 degrees). The roll out was performed with a different autopilot command technique which had a faster roll rate and another slight overshoot. The controller was not able to acceptably maintain position laterally during the dynamic portions, though it was solid once established in the turn. It should be noted that this turn was not the smooth, predictable roll expected of a tanker with a receiver on the boom. Technically, the maneuver should be classified as a "no test", but it is possible that a UAV might see similarly unusual conditions at some point, and it represents a good limit to what the controller can handle in the configuration tested.

The same performance trend characterized the controller during the dynamic portions of flight, including up to 30 degree banked turns. The controller typically exceeded the boom envelope limits slightly during the roll in and roll out, but had solid performance when established in the turn. Additional examples are shown in Appendix D.

The majority of the difference between the expected and actual controller performance is due directly to the reduction in the total aileron loop gain to 33% of the design value. As mentioned in Chapter VII, a misunderstanding of a DGPS update problem led to a gain reduction in an attempt to reduce what was thought to be random noise seen in the ailerons. The error was found and fixed with a filter structure change, but it was too late in testing to reset the controller to the design values. The end result was that the lateral channel did not have the aileron authority it needed to get the aircraft rolling fast enough to stay with the lead aircraft in the dynamic portion of the turns.

Performance in the pre-contact and the wing observation positions during turns was not significantly different than in contact, though the errors were slightly larger. The design goal was to stay within 10 feet in each axis, and the controller generally met that, but had some small excursions laterally during the rolling dynamics of some of the turns, based on the roll rate of the lead aircraft. Figure 106 shows an example of a 15 degree right turn in the wing observation position, and Figure 107 shows the same turn taken to 30 degrees of bank for comparison.

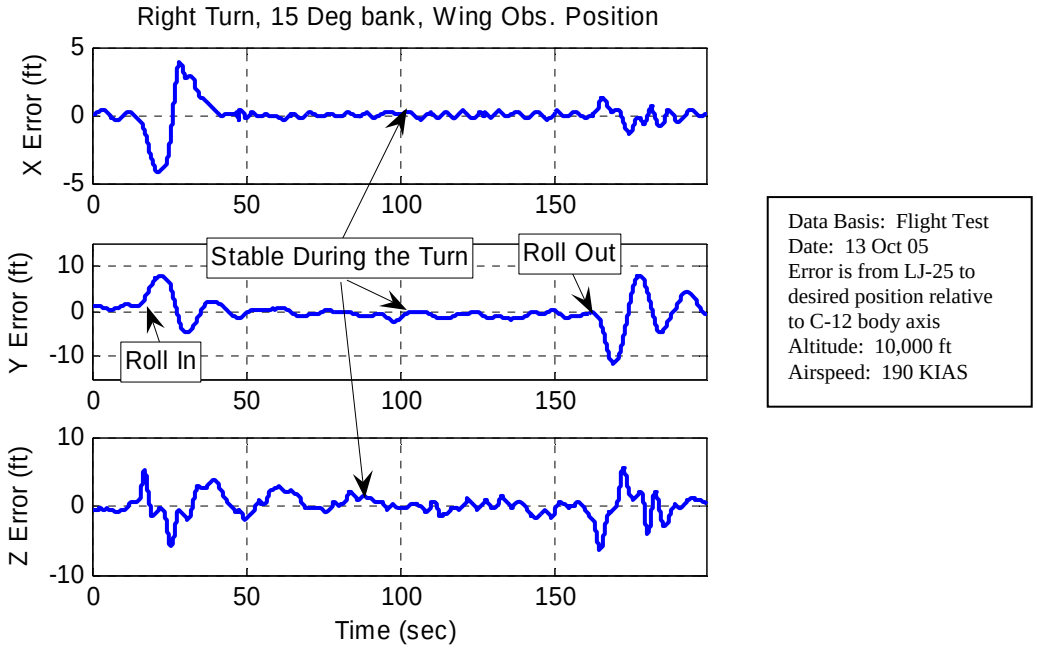

Figure 106. Station Keeping in 15 Deg Turn, Wing Observation Position

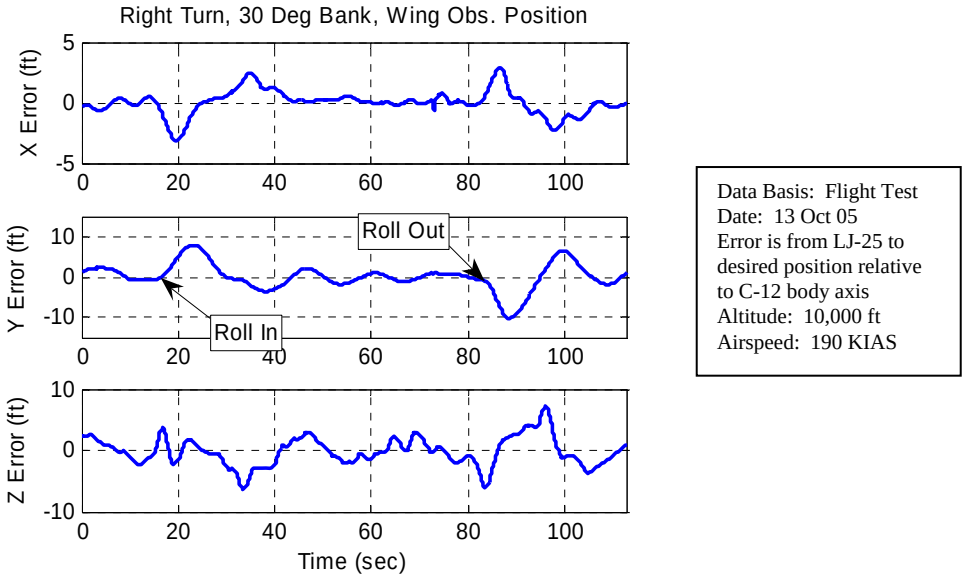

Figure 107. Station Keeping in 30 Deg Turn, Wing Observation Position

Even though there were moments where the controller exceeded the 10 foot thesis design goal, the overall station keeping performance in the pre-contact and wing

observation positions in straight and level flight and turns was satisfactory for safely accomplishing the required elements of air refueling.

In summary of objective 1, Table 12 shows the station keeping performance of the controller during flight test. A separate analysis was performed for established turns and for turns that included the dynamic rolling portion, since that represented a clear difference in performance.

Table 12. Station Keeping Performance Summary

Position	Avg. Absolute Error (ft)			Max Absolute Error (ft)			Avg Radial Error (ft)	Max Radial Error (ft)
	x	y	z	x	y	z		
Straight and Level Flight								
Contact	0.26	0.85	0.73	0.81	3.85	2.71	1.29	3.92
Precontact	0.27	0.97	1.07	0.65	2.69	2.57	1.54	3.34
Wing Obs.	0.24	1.08	0.90	0.74	3.15	2.30	1.57	3.34
Established in 15° bank								
Contact	0.22	0.78	0.83	0.55	2.20	2.84	1.27	2.92
Precontact	0.26	1.23	0.79	1.02	4.44	2.30	1.65	4.47
Wing Obs.	0.17	0.68	0.71	1.13	2.30	2.85	1.15	2.92
15° turn with roll dynamics								
Contact	0.23	1.40	0.91	0.72	9.3	3.09	1.87	9.3
Precontact	0.29	2.64	0.83	1.02	10.39	2.67	2.95	10.41
Wing Obs.	0.45	1.66	1.00	4.18	11.60	6.36	2.25	11.62
Established in 30° bank								
Contact	0.32	1.33	1.61	1.75	6.12	7.31	2.36	7.57
Precontact	0.33	2.25	1.52	0.92	5.83	4.16	2.94	7.07
Wing Obs.	0.28	0.87	1.43	2.49	3.58	6.38	1.86	6.70
30° turn with roll dynamics								
Contact	0.32	1.93	1.52	2.44	15.19	7.52	2.82	15.21
Precontact	0.34	3.21	1.52	1.17	13.39	4.16	3.85	13.47
Wing Obs.	0.45	1.84	1.55	3.13	11.14	7.20	2.82	11.35

The overall station keeping capability of the controller was good, but not sufficient for operational use. Performance during straight and level flight in any

position was satisfactory, as was performance in established turns tested up to 30 degrees of bank. Performance during rolling maneuvers was also satisfactory and safe for the pre-contact and the wing observation positions, but not for the tighter limits required of the contact position. The controller exceeded the boom limits on the rolling portion of one 15 degree banked turn, and on most of the 30 degree banked turns. The primary cause of the failure was a lack of aileron authority due to a reduction in total loop lateral gain.

During actual air refueling, an aircraft is automatically or manually disconnected from the refueling boom before exceeding its limits. Once established back within the limits and stable, an operator reconnects the boom. If this controller was used for actual refueling, the potential exists for disconnects during the rolling maneuvers, obliging the tanker to reconnect after the bank angle was established.

Objective 2: Position Changes

The horseshoe path of a position change during air refueling was shown in Figure 98. The ability to move between the required positions around the tanker is a core requirement to efficiently refuel in an environment with multiple receivers. This will be the case for future UAVs, which conceptually will employ with other manned and unmanned aircraft in formation. Position changes were first tested in straight and level flight for every leg and in both directions (clockwise or counter clockwise). The process was then repeated in established left and right turns of 15 degrees of bank, and again in 30 degrees of bank. Finally, dynamics were added by rolling into and out of turns while the wing aircraft was in transit between positions. All position changes were performed

correctly, and were found to be safe and efficient. The formation is shown during a position change in Figure 108.

Figure 108. Position Change over Edwards AFB

A known VSS problem with Simulink® memory blocks intermittently caused unexpected position sequencing from the horseshoe logic. The controller and the VSS were investigated to ensure that the source of the error was indeed the known memory block problem on the Learjet, and the horseshoe logic was not invoked further. This problem also surfaced with the heading sync option, which used the same type of memory block and also typically required 3-4 identical inputs before one "took." The only effect this had on operations was that for a position change from contact (position 1) to wing observation (position 4) the FTE would type "2,3,4" instead of commanding "4" directly. This circumvented the problem entirely, and the actual control of the aircraft

did not change. The horseshoe logic itself is still solid and is recommended as a safety feature for future controllers.

The speed of the maneuver was set for 30 seconds per leg of the position change. The test team intended to experiment with faster leg times, but it was found that 30 seconds per leg was already an appropriate speed for an unmanned aircraft in the controlled environment of air refueling. The tested speed was in no way taxing on the controller, but it was already operationally representative without acceleration.

Performance closely matched predictions from the simulator, and no surprises were found during position changes during flight test. Therefore, for brevity, only one direction in each major case is presented. In addition, only complete changes from contact to wing observation or back are shown as they encompass all of the required control aspects of the individual leg changes that may be commanded independently. More examples of position changes are shown in Appendix D. The straight and level performance is shown in Figure 109. The difference between the commanded and actual positions is hard to distinguish, so a total radial error plot is included to show that the magnitude is insignificant.

The position blending logic supplied the correct position change commands to guide the wing aircraft around the formation while ensuring that it would not encroach on any airspace that may be occupied by the tanker or other potential receivers. The controller then stayed very near the commanded path, with the only notable errors in the lateral channel during the move from the back corner to the pre-contact position. The

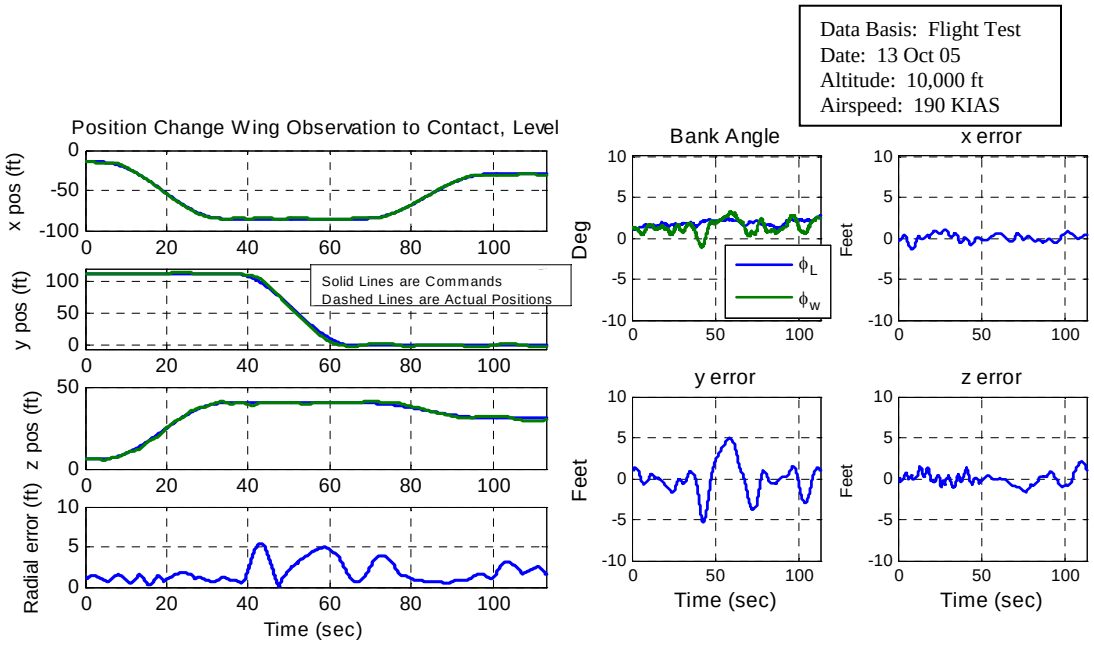

Figure 109. Position Change, Wing Observation to Contact, Straight and Level Flight

magnitude of the position error was small, and since there is no truly defined path that an aircraft must follow exactly to safely change positions, the errors were completely transparent in flight. The most critical portion of the position change, the approach to the boom, was well controlled in path and rate, and desirably slowed as the range between the aircraft decreased.

Position changes while in established turns were also well performed. The more difficult 30 degree banked turn is shown in Figure 110, and the performance in the 15 degree banked turn was slightly better.

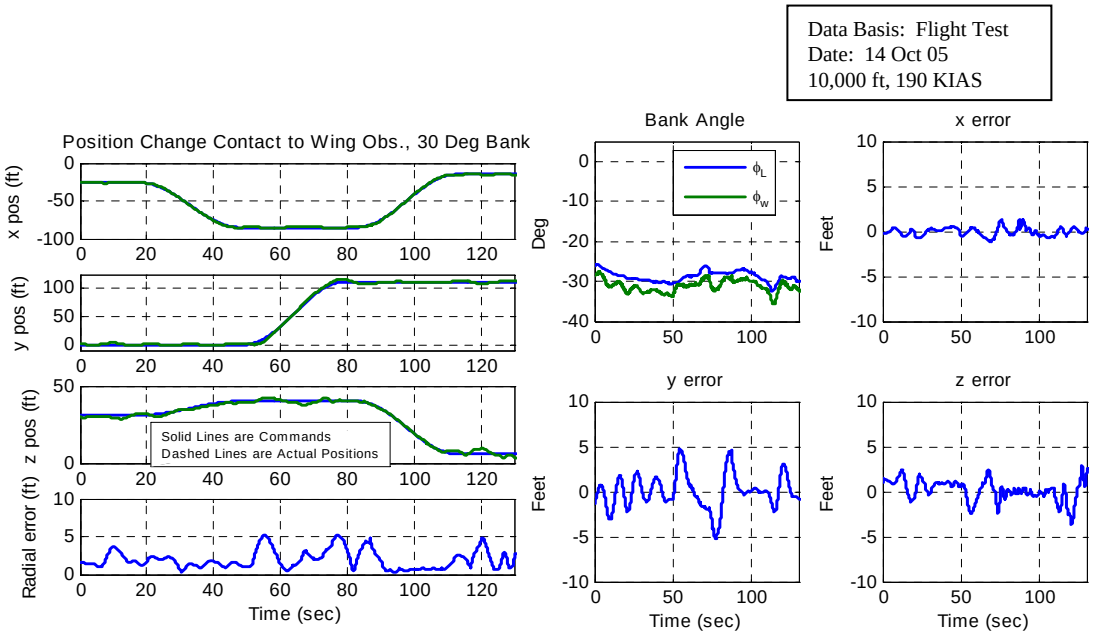

Figure 110. Position Change, Contact to Wing Observation, Left Turn, 30 Deg Bank

The final step in the position change investigation was to create a scenario where the tanker initiates or completes a turn while the wing aircraft is in transit between positions. This represents the greatest level of dynamics that would be induced on a formation controller during air refueling. Figure 111 represents the most inopportune timing and direction of those dynamics from the wing aircraft's perspective. A position change is performed from the wing observation position to the contact position, and as the wing aircraft is at the back corner, the farthest point inside and aft of the tanker, the tanker turns into the wingman with 30 degrees of bank. This forces the wing aircraft to simultaneously deal with the problems of the position change, the new turn, and the closure generated by the tanker "stuffing" the wingman on the inside of the turn.

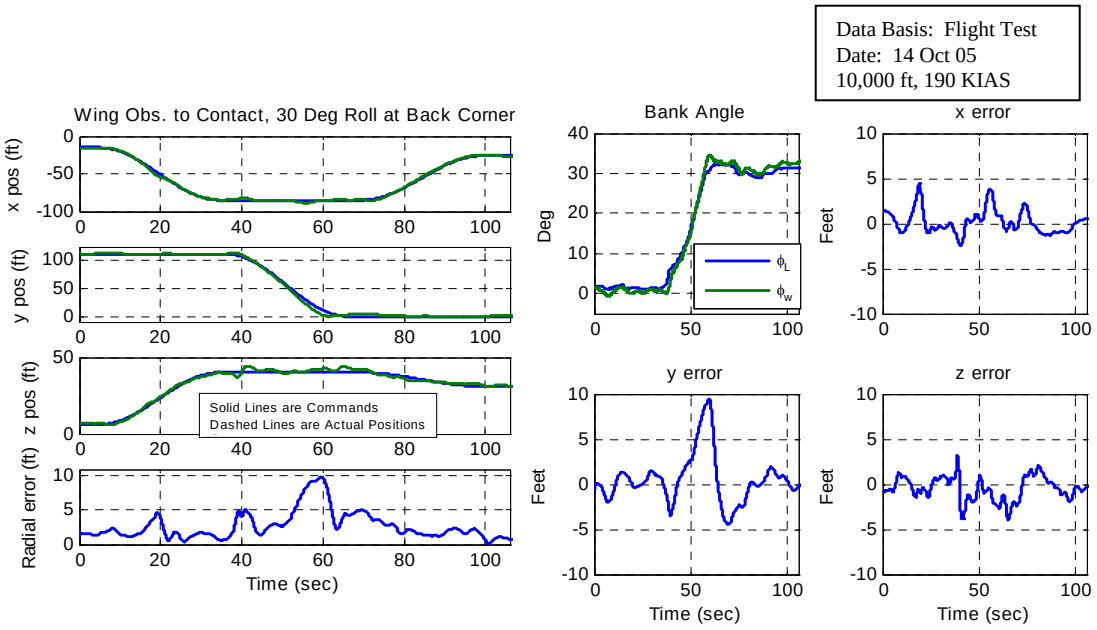

Figure 111. Position Change, Wing Observation to Contact, 30 Deg Roll at Back Corner

Again, the errors in Figure 111 are small enough to be insignificant on the arbitrarily defined path of a position change that is well behind the tanker and other receivers. Turns of 15 and 30 degrees of bank did not present difficulty to the controller, even when the timing of the dynamic portion of the rolls caused closing or opening velocity problems to the wing aircraft. In summary of the second objective, the position change capability of the controller was found to be satisfactory for air refueling.

Objective 3: Data Recording

The third objective of the flight test was merely to collect the data that were used to troubleshoot the controller during flight test and to analyze the results. A list of the majority of the parameters recorded is attached in Appendix E. Several other internal

parameters were recorded that pulled individual signals out of the controller in several places to analyze specific changes as the signal propagated through. All of the data collected during flight test is archived with the flight test report at the Test Pilot School, Edwards AFB, CA, TPS/EDT [21].

Summary of Results

The controller demonstrated the ability to fly close formation well enough to autonomously refuel an aircraft during straight and level flight, or when established in turns with up to 30 degrees of bank. During the dynamic portion of the turns, however, the aircraft control was characterized by an excessive position overshoot as the lead aircraft rolled into or out of turns. The magnitude of the overshoot was acceptable for the pre-contact and the wing observation positions, but it exceeded the boom envelope limits required in the contact position during most of the 30 degree banked turns and one turn to 15 degrees of bank. The loose lateral channel control was attributed to an erroneous aileron loop gain reduction. Position changes in both directions were performed in straight and level flight and in turns, including rolling while the wing aircraft was in transit. All position changes were performed correctly and efficiently. Safety and stability were never in question.

IX. Conclusions and Recommendations

Automated air refueling is a short-term Air Force goal that is currently under research for unmanned vehicles. Implementation of AAR will strengthen US global strike capability, increasing range and station time of unmanned assets. Success in the AAR program will be dependent on the correct integration of positioning and control systems which represent a significant departure from the control schemes of current autopilots.

This research encompassed the entire journey from a paper theory of single aircraft modeling and control to a fully automated close formation flight control system. The end result was the first-ever formation flight test of a fully autonomous system that demonstrated the concept of close formation control, and proved that the knowledge and technology required to achieve performance suitable for air refueling are currently attainable.

To accomplish this, aircraft models were developed for the lead and wing aircraft independently, and both models were stabilized. An autopilot was then designed for the lead aircraft, and profiles were built to simulate the problems that a receiving aircraft will be faced with during operational air refueling. A formation simulator was designed to track the relative motion of the individual aircraft in order to produce the signals available to the wing aircraft controller in flight. These signals were then conditioned with modeled disturbances of noise, turbulence, time delays, and real-life hardware limitations such as differing sample rates.

With the formation simulator built, theories of wing aircraft control were developed and investigated, and a concept of controlling the wing aircraft to a point defined relative to the lead aircraft's position and attitude was pursued. An error vector was produced between the desired and actual positions of the wing aircraft, and presented to the controller in terms of the tanker body frame. The controller used elements of PID control in each axis to minimize position error and fed parameters forward to match the lead aircraft's bank angle and roll rate, while applying a penalty for varying from an equilibrium pitch attitude.

Extensive modifications to the controller were required to make the leap from paper theory to real-life hardware, including mechanization to transfer control of the aircraft to the autopilot at initialization. Built-in functions were also required to properly generate a command path that moves the wing aircraft between several formation positions in response to a real-time input from the flight crew. With the controller in a flight-ready configuration, simulations were performed for the tasks required in air refueling, and sensitivity and robustness were investigated.

The controller was installed on Calspan's LJ-25, and received DGPS position data with MEMS IMU attitude data from a C-12 lead aircraft. Seven formation flight test sorties were accomplished to evaluate the capability of the controller. Several changes were made to the controller during flight test, the most significant being the creation of a heading estimator and the modification and expansion of the filter structure. A misanalysis of a DGPS update problem led to an erroneous reduction in the total aileron loop gain to one third of the design value.

The controller was capable of air refueling. The performance was found to be satisfactory in straight and level flight in all formation positions, as well as in established turns of 15 and 30 degrees of bank. Performance during rolling maneuvers, however, was characterized by a slightly sluggish lateral response that led to a lateral position overshoot. This was found to be acceptable in the pre-contact and wing observation positions, but not in the contact position where tighter position limits were required. The lateral difficulty was attributed in small part to a wandering heading estimate due to IMU failure and to throttle asymmetry caused by a bad throttle servo. The vast majority of the error, however, was a result of a lack of aileron authority caused by the lateral gain reduction. Position changes in both directions were performed in straight and level flight and in turns, including rolling while the wing aircraft was in transit between positions. All position change maneuvers were found to be satisfactory.

The flight test verified and validated not only the theory of control developed in the thesis, but also the complicated implementation techniques required to create a fully "hands off" system. Numerous lessons were learned along the way that are directly applicable to the current and future research for AAR. The future for this research is clear--another controller will be designed to perform the same purpose, only better. As such, some key notes are summarized in terms of control theory, mechanization, and flight test lessons.

Future Close Formation Flight Control Theory

There are several top-level methods that can be used to control close formation. The one pursued in this research was shown to be tenable. The formation position to fly

to was selected as if it were a rigid part of the tanker that moves and rotates with it just as the real refueling boom does. This paradigm is the most instinctive from the pilot's perspective, and the strengths include the direct application to the controls, the simplicity of design, and zero steady state position error without a requirement for trimming functions. The weakness of this paradigm is the reliance on the lead aircraft attitude to determine the right position to fly to. Noise in the attitude signals from the lead aircraft results in motion of the desired flight position, exacerbated by the lever arm between the GPS antennae on the two aircraft. Real life considerations of poor attitude sensors must be overcome to use this paradigm cheaply. The key that makes it work is that the actual rates of rotation during operational air refueling are very slow, allowing filtering to stabilize poor sensor signals without significantly degrading control.

The tanker body frame was selected as the reference frame used to present error to the controller. The weakness of this decision is the fact that when the attitude of the tanker and receiver are not aligned, some amount of control will be misapplied. The advantage of the frame is that the tanker and receiver are very nearly aligned during all of air refueling, but the tanker is not maneuvering to fight for position. The tanker body frame effectively operates as an "average" wing body frame, dividing almost all of the error signal to the right channels while having no sensitivity to the required motion of the wing aircraft.

For the control laws, PI control was attempted and found to be insufficient for control in any channel. The fluid environment of flight requires lead compensation, and this was provided with PID control on each channel. Additional damping is

recommended in the pitch channel, and feedback of the difference in pitch from equilibrium was found to be effective. The lateral channel was by far the most difficult to control. Matching the bank angle and the roll rate of the lead aircraft is recommended. Four recommendations are provided for future flight control concepts:

1. The requirement for a tight positioning system is significant for the full AAR program. However, this requirement can be eliminated. The refueling boom on all tankers is already instrumented. The azimuth, elevation, and extension of the boom are displayed to the operator. In addition, the wiring for communication already exists in the refueling boom, as pilots are able to talk to the operator over intercom. If a military GPS system is used, or an optical system that can just get the aircraft within 5 feet or so, the human boom operator can make the connection. Once the connection is made, the control laws can center the boom instead of working with a datalink to get a highly accurate DGPS position solution. This eliminates all concerns for communication emissions, which can easily be tracked in today's electronic battlefield. In addition, the concern for horizon shielding of the receiver's GPS antenna by the tail of the tanker is also eliminated.

2. Lateral position station keeping could be very easily improved by feeding back lateral error to the rudder channel. It is recommended to use a technique similar to that of Osteroos to avoid using rudder for large corrections [13].

3. Control may be improved with the simple addition of an aileron-rudder-interconnect by feeding aileron commands into the rudder channel. As only one flight condition is required, an ARI gain schedule is not required.

4. Consider turning off the integrators at key times. When the tanker rolls into bank, the feed forward element of roll rate causes the wing aircraft to roll with the tanker, even though the desired position is now outside of the turn relative to the wing aircraft. Though this is desired, the error integrator counts up the false error outside of the turn, and as the turn is established and the wing aircraft seeks to "catch" the desired position, the false error in the integrator causes an overshoot to the outside of the turn. The opposite effect happens on roll outs. Consider logic implementation that would hold the current value in the integrator any time the tanker exceeds a roll rate threshold. Throttle integration should likewise be held to avoid addition of excessive errors when the throttles are on the physical limits, which occasionally occurred in aggressive maneuvers in simulation.

Future Formation Flight Controller Mechanization

Some of the mechanization ideas used for this research will be required in all future controllers. The following key points should be replicated in some form:

1. Position Blending Logic. Multiple techniques are available for commanding position changes. Slowly blending the command from one position to another is much more effective than the obvious technique of instantly changing a position command as a waypoint. To adjust the speed of the position blending, a cosine wave driven with an integrator timer was used which resulted in a slow acceleration and slow deceleration, with no overshoots. This was much more effective than a linear ramp command.

2. Horseshoe Logic. A dangerous situation will occur if some sort of logic is not implemented to prevent a UAV commander from selecting a direct flight path to the

contact position from the wing observation position. The horseshoe logic developed in this research is one option that will prevent this.

3. Initialization. A “hold position” option with control trimming and balancing is recommended to zero out all position error to the controller as the system is initialized. A reset function of some sort is also required to set the position error integrators back to zero at the moment aircraft control changes over to the autopilot in order to prevent any control surface motion at the instant the system is turned on.

4. Failure States. Due to the MEMS IMU failure, it was shown in this research that close formation flight with this control paradigm can be accomplished without reference to the lead aircraft pitch or bank angle. If this system were to employ operationally, it is not unlikely that the lead aircraft’s attitude source would fail at some point. A back-up mode is recommended with the heading estimator designed in this research. This will ensure full capability if only bank angle and rate are available, as well as full capability in straight and level flight if no attitude signals are available at all.

5. Pitch angle. Future designers should consider the feasibility of always using a constant estimate for lead aircraft pitch angle. The benefits include a lack of transients in turns and the reduction of an entire channel of attitude source noise, at a very small cost in terms of station keeping. This does not apply if considering refueling in a climb or descent, or if the pitch changes of a real tanker are excessive due to the large range of gross weights and would result in unacceptable steady state error.

6. DGPS Missed Updates and Filtering. Missed datalink or DGPS updates were not expected to cause difficulty with the controller, but ended up being responsible for

large control spikes. Future controllers should allow for this with predictive filters and a filter structure which operates on the signal after the desired position is subtracted from the actual position. The IMU signals must be filtered before the coordinate transformation to the control frame to prevent signal noise from being magnified in position error, and filtering of the fast signals from the controller to the actual flight control surfaces is not recommended. The filtering process in this research represents a weak point of the controller, and a researcher with some education or experience with filtering and rate limiting could certainly improve on the author's work.

Flight Test Lessons Learned

The results of this research represent a major milestone in the advancement of close formation flight control. The effort could not have been undertaken without the experience and expertise of several flight test experts. Nevertheless, several flight test lessons were (re)learned and are presented here as guidance for future designers:

1. Modeling, Simulation, and System Flexibility. The impact of modeling and simulation for the success of this project cannot be overstated. Several complete "show stoppers" occurred which were overcome with software fixes and patches. The heading estimator was completely designed in the midst of testing with actual flight data pulled into the simulator. The filter structure changes, gain changes, and DGPS fixes were all found and fixed with late night simulation before the next sortie. Without a simulator and the ability to modify the controller as errors were found, the test project would never have flown. The ability to adjust parameters in flight, especially filter settings and gains, is highly recommended. The Calspan variable stability Learjet was ideal for this.

2. Time Compression. From the time the Learjet arrived at Edwards, the test team had 9 work days to install the system and antenna, ground test all systems for their first integration (including the new auto-throttles, which were still shutting down engines when the aircraft arrived), and complete the seven sorties. This short time interval included a four day down period while a broken DGPS unit was shipped back to Ohio for repair, and daily Test Pilot School syllabus sorties unrelated to this flight test. Analysis errors, such as the reduction of the lateral control gains due to a misunderstanding of the DGPS failure, directly impacted the performance of the controller. Future testing must have analysis time between sorties to achieve peak performance of the system.

3. Commercial-Off-the-Shelf (COTS) Products. The MEMS IMU was already a cost compromise from a high quality rate gyro, and it ended up not providing heading or pitch angle at all. This emphasized the importance of individual component testing whenever possible, even for COTS products.

4. On Site System Expertise. At some point during flight test, every piece of hardware failed. Having experts on site who were familiar with, or who actually built, each system was instrumental in keeping testing going when the many unavoidable unknowns occurred.

It was the author's intent to make the lessons learned for this project understandable, and the work required for a real controller repeatable. If these recommendations are incorporated into future controllers, they will be well on the way to fully autonomous close formation flight.

Appendix A. Matlab Simulink® Model

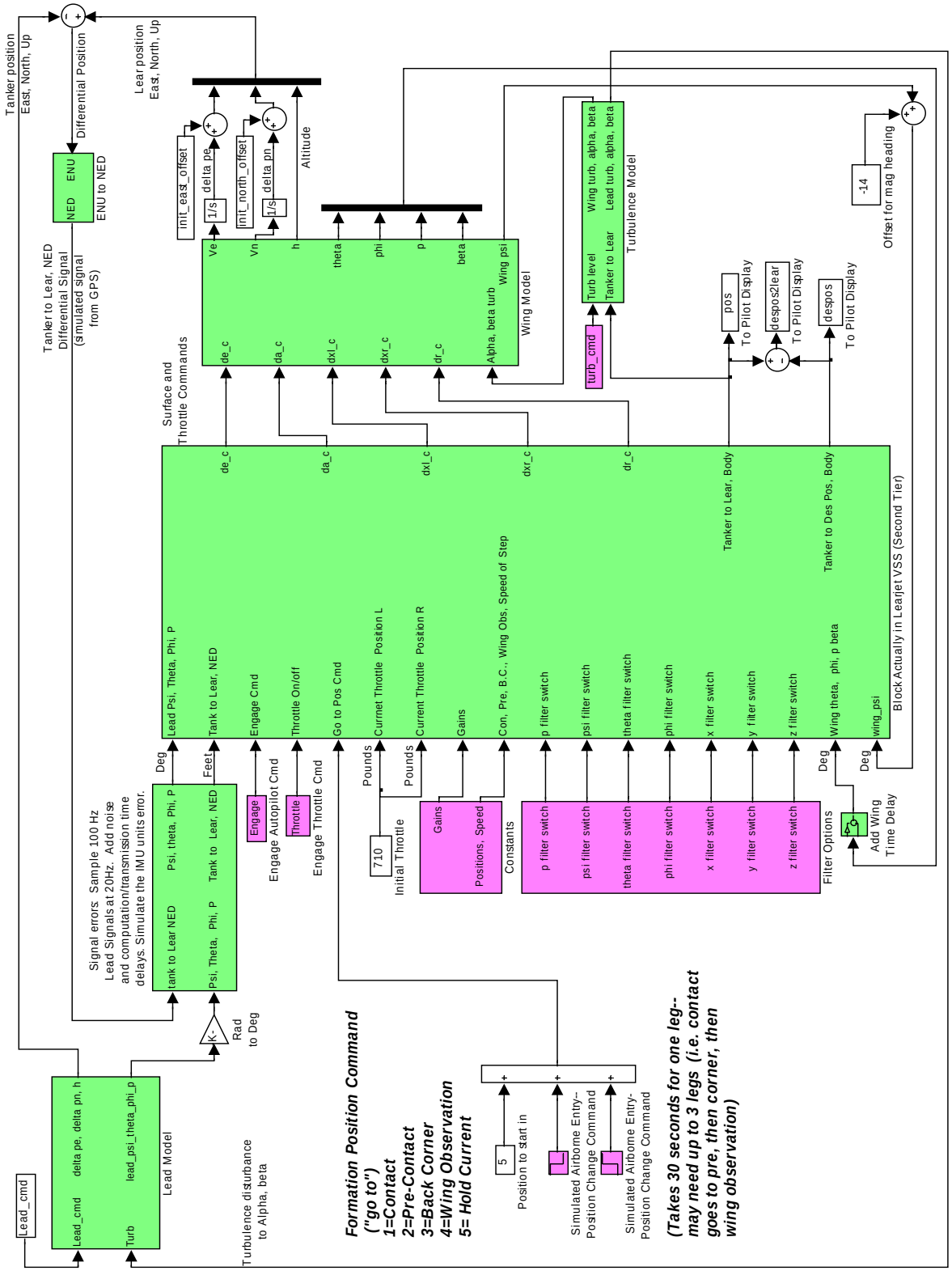

Figure 112. Formation Simulation Model (Top Tier)

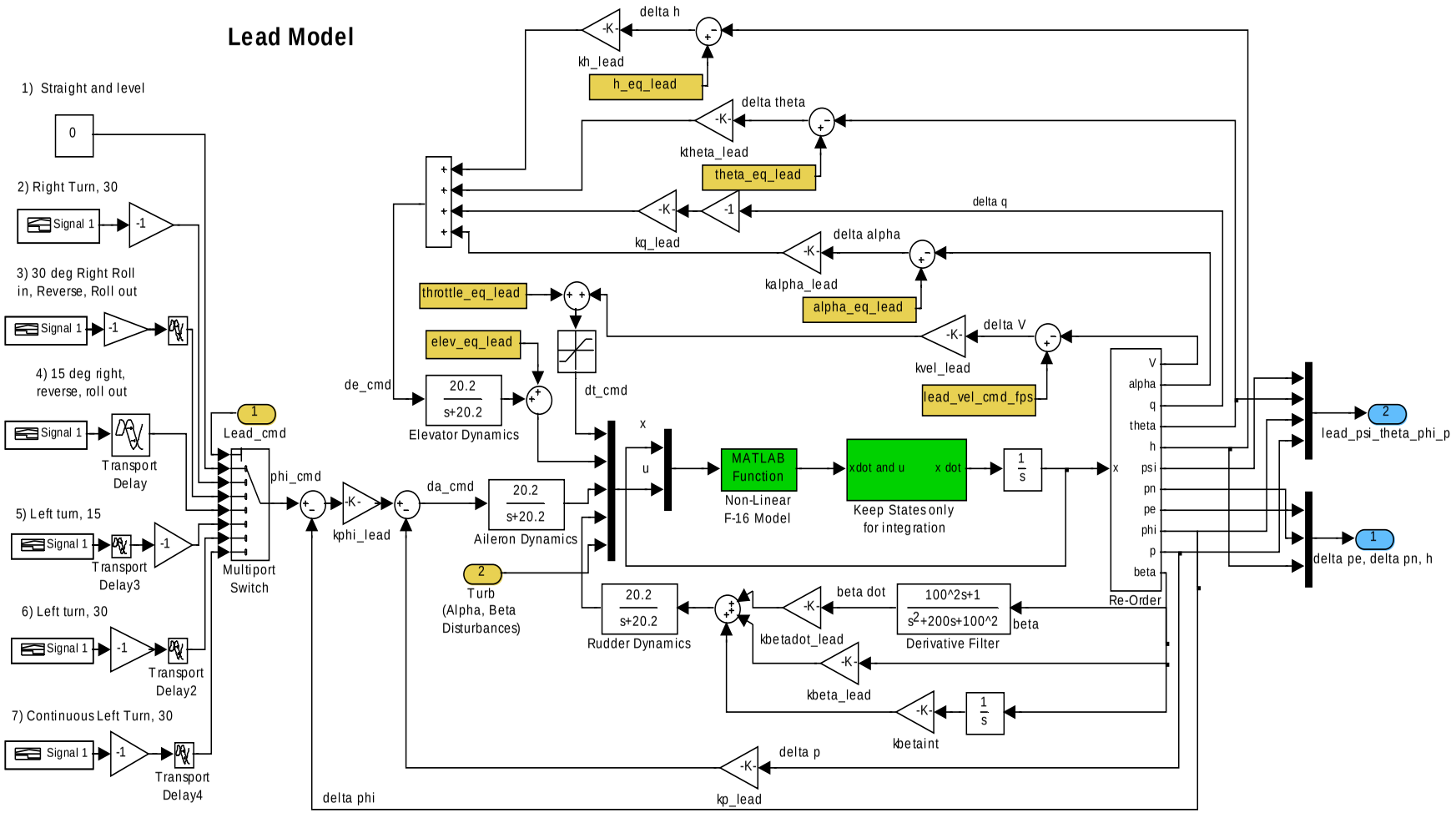

Figure 113. Lead Aircraft Model (From Top Tier)

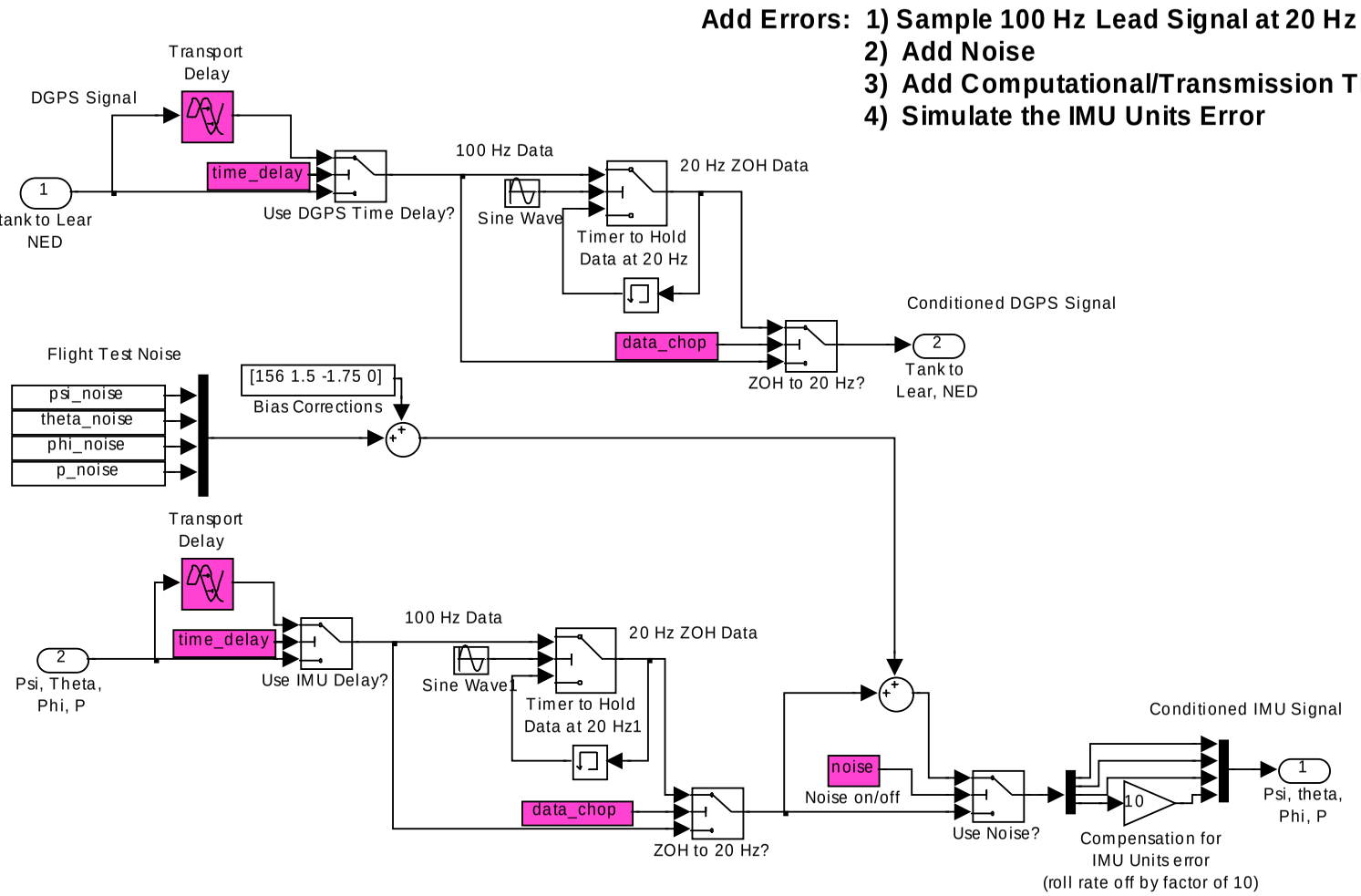

Figure 114. Signal Error Model (From Top Tier)

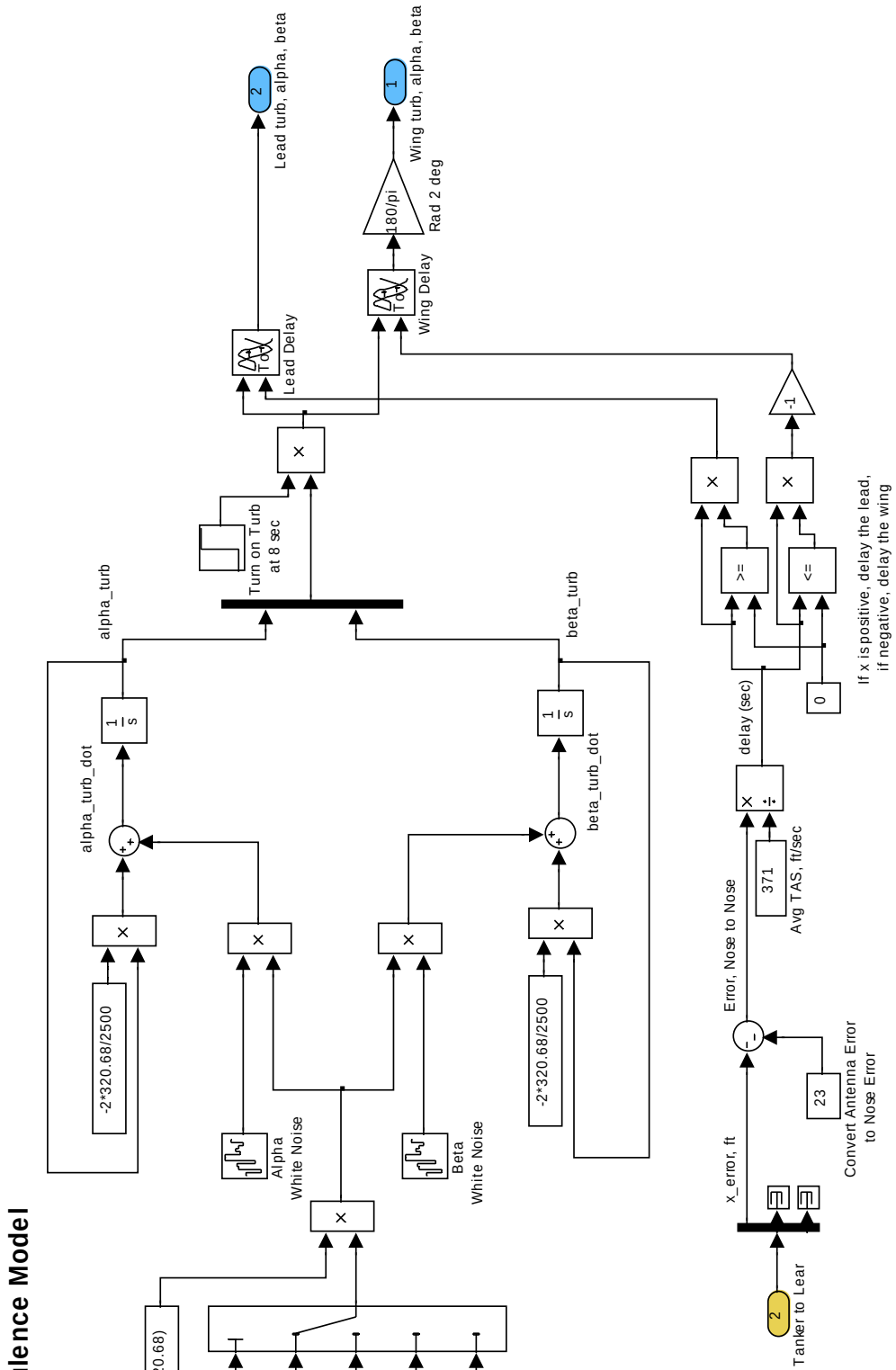

Figure 115. Turbulence Model (from Top Tier)

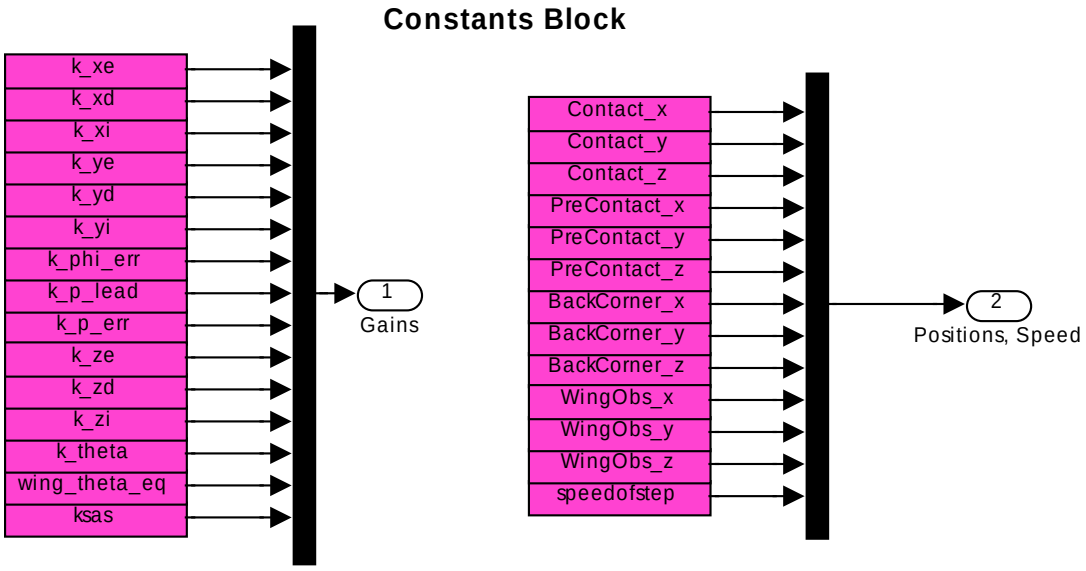

Figure 116. Constants Adjustable In Flight (From Top Tier)

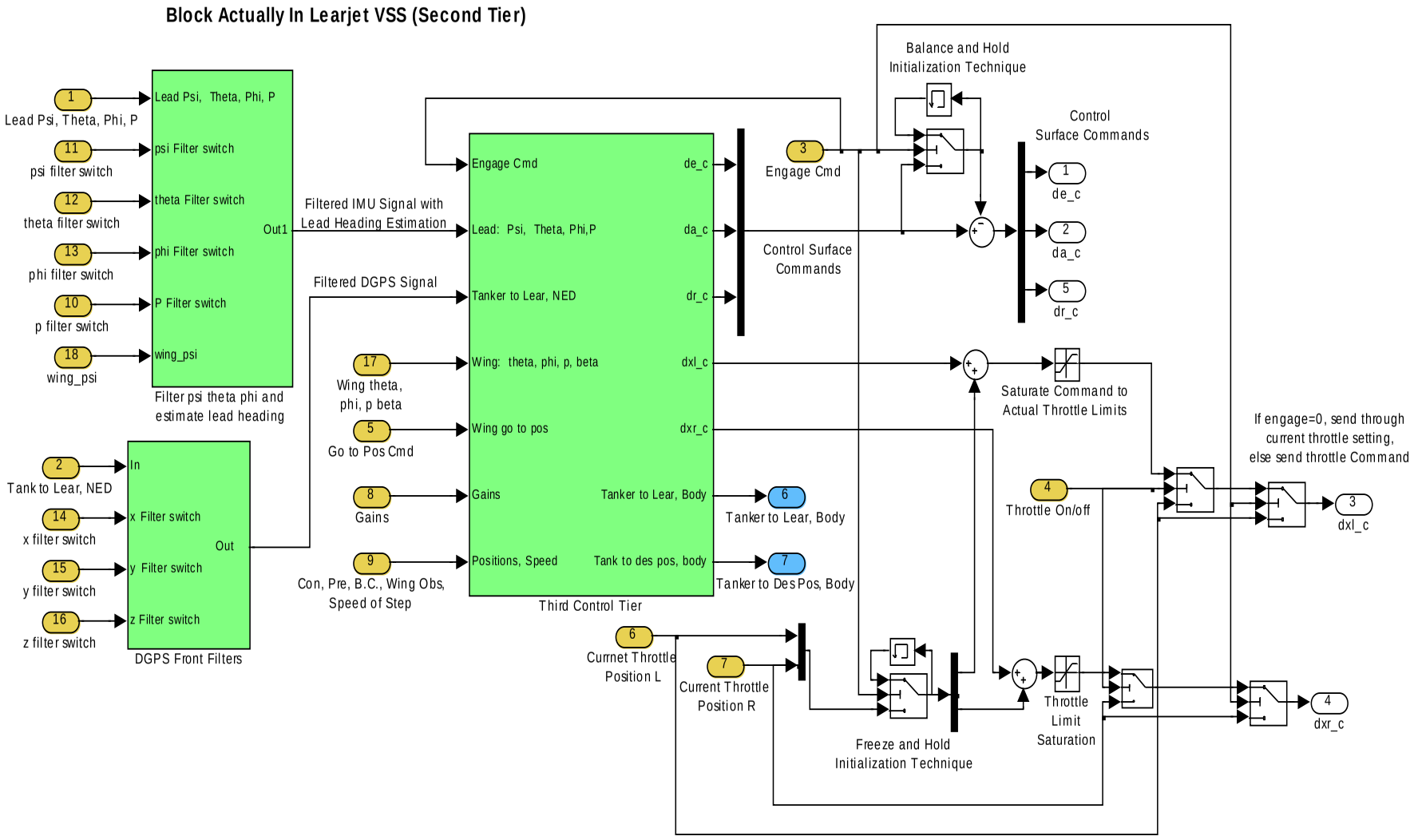

Figure 117. Second Control Tier, the Block Actually In the Learjet VSS

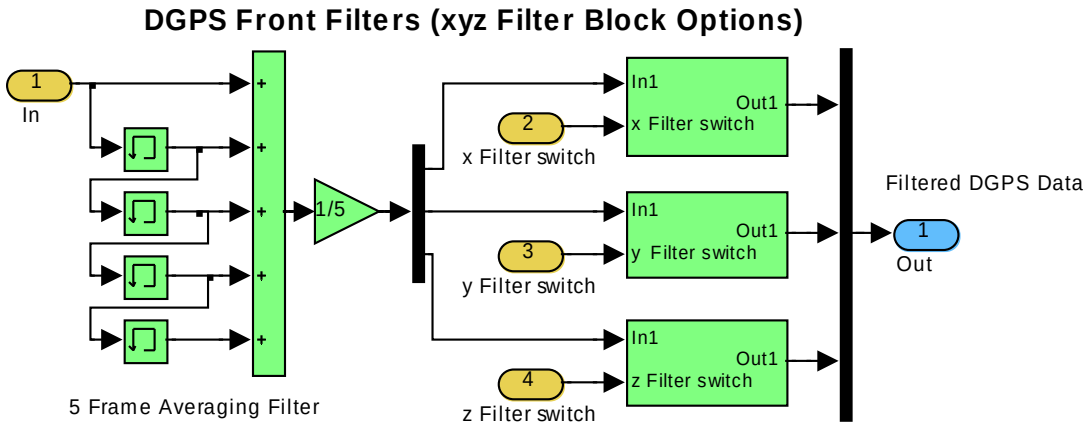

Figure 118. DGPS Filter (from Second Tier)

Note: After the 1 Hz cycling problem was identified (the last two test sorties), these filters were selected to pass through the original data (unfiltered) and similar filters were used in their place further down the data path.

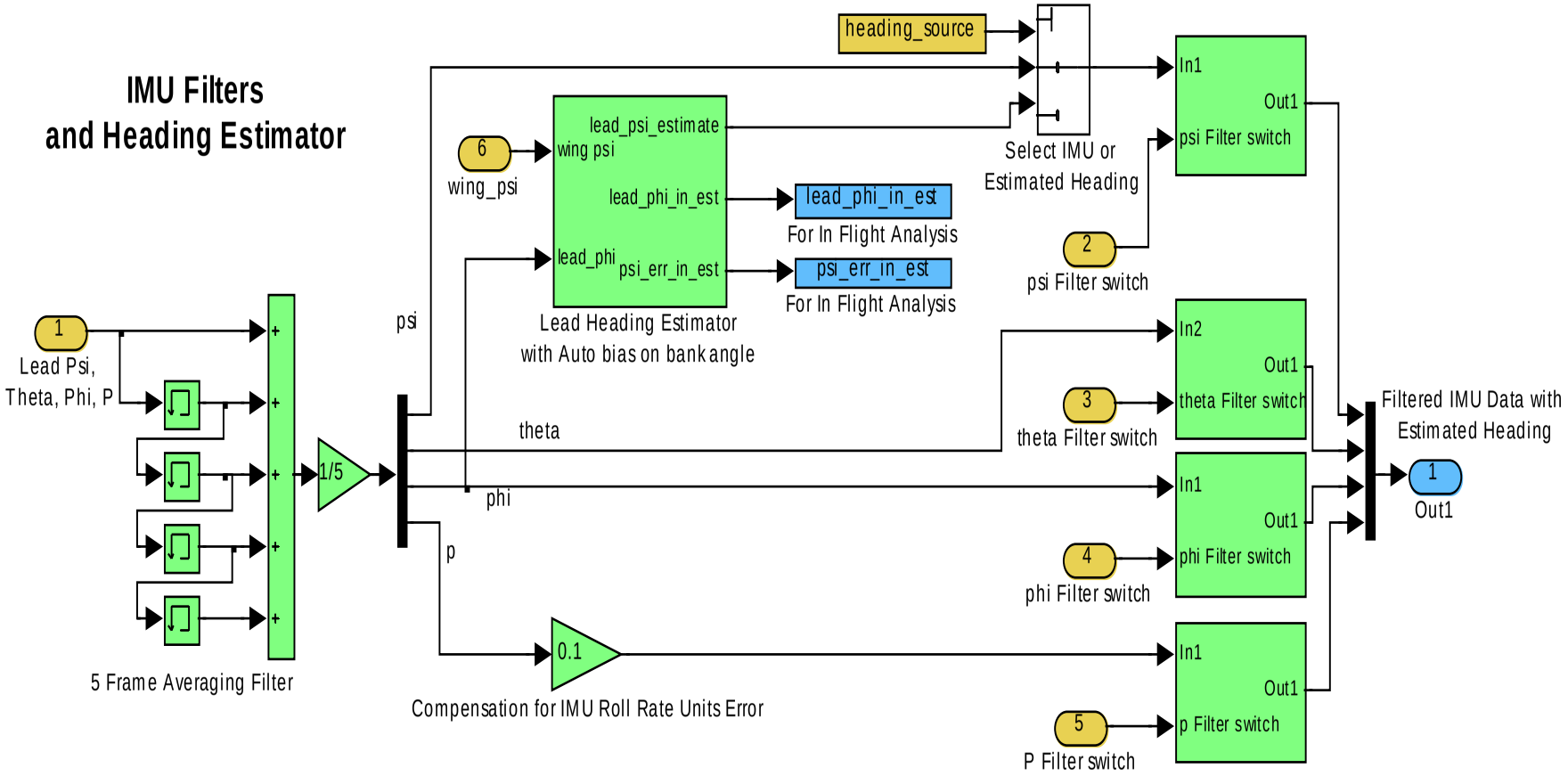

Figure 119. IMU Filters and Heading Estimator (from Second Tier)

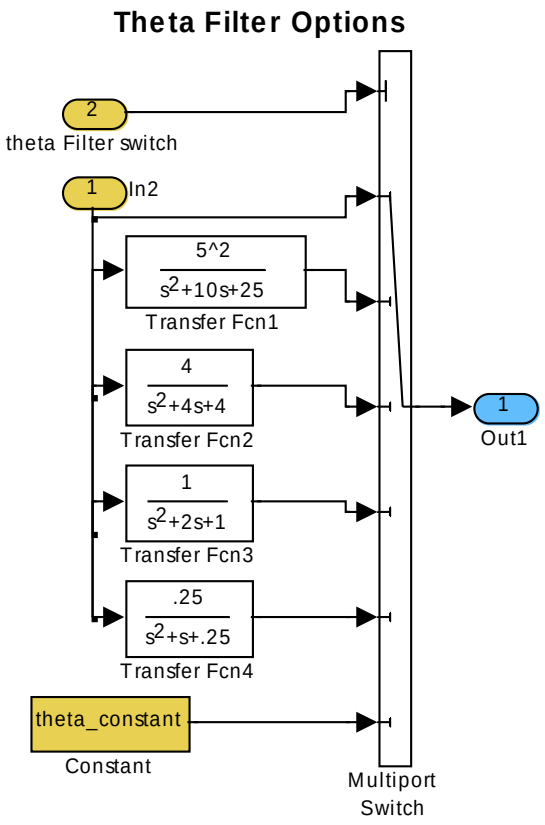

Figure 120. Example Filter Option Block (from IMU Filters and Heading Estimator)

Note: Figure 120 is only an example, each filter option block contained different filter selections every sortie. The order of the filters and the break frequencies were adjusted daily based on hand tuning of flight data for each of the Euler angles, the DPGS axis errors (xyz), and the wing aircraft feedback parameters. The filter options for each sortie were then investigated during ground operations and in flight.

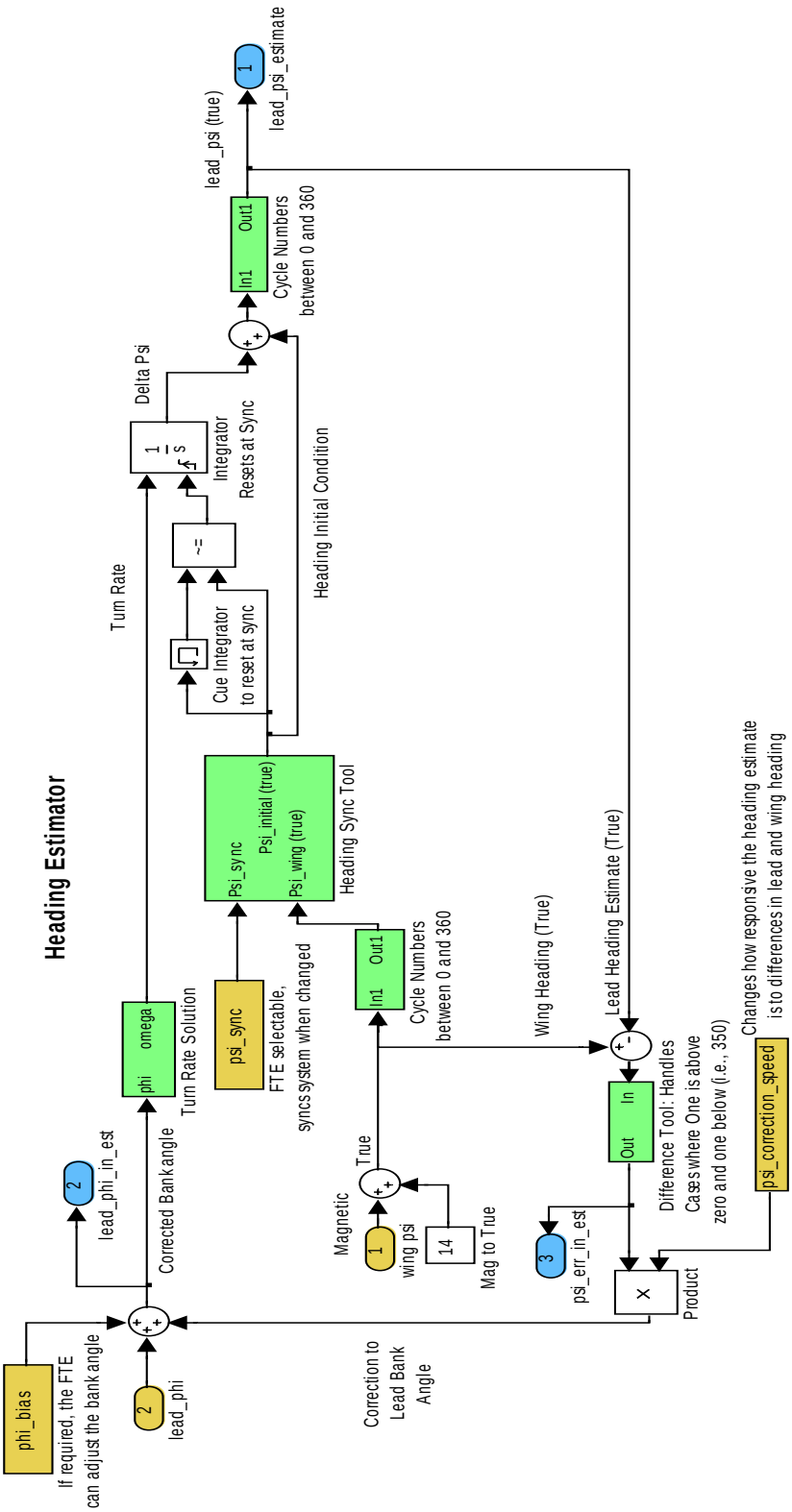

Figure 121. Heading Estimator

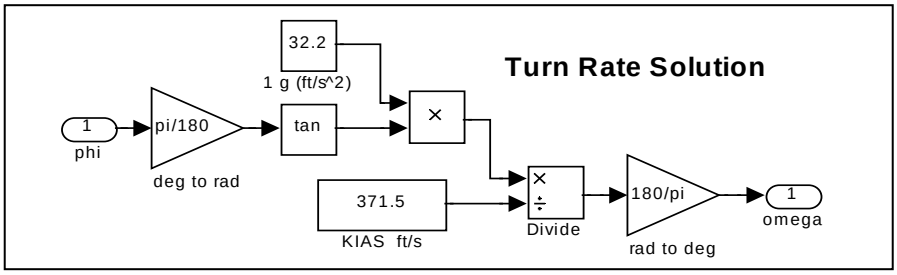

Figure 122. Turn Rate Estimation Tool (from Heading Estimator)

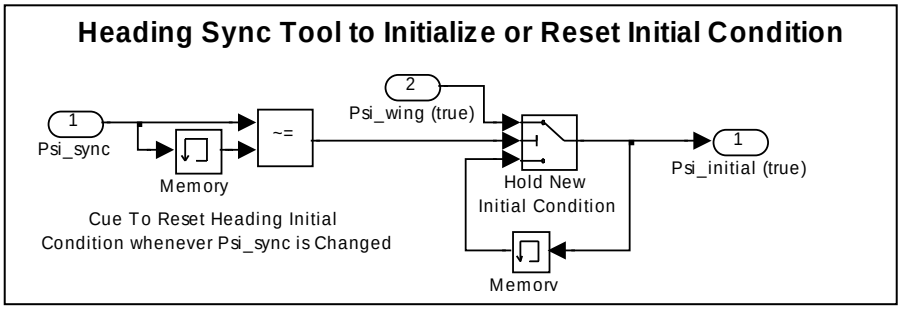

Figure 123. Heading Sync Tool (from Heading Estimator)

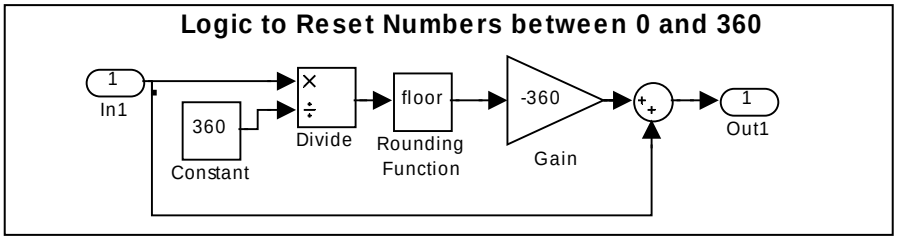

Figure 124. Zero to 360 Tool (from Heading Estimator)

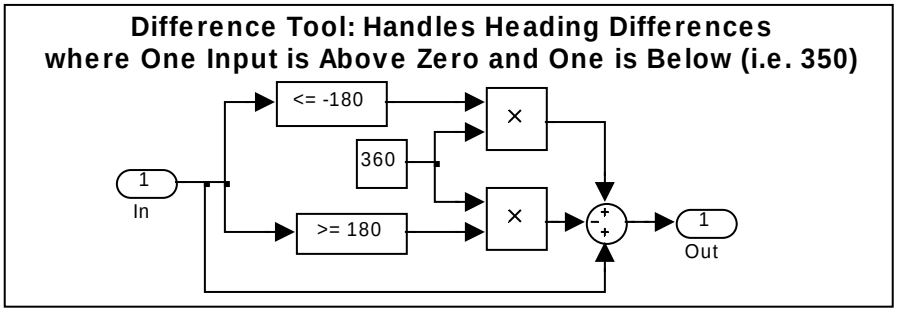

Figure 125. Differencing Tool (from Heading Estimator)

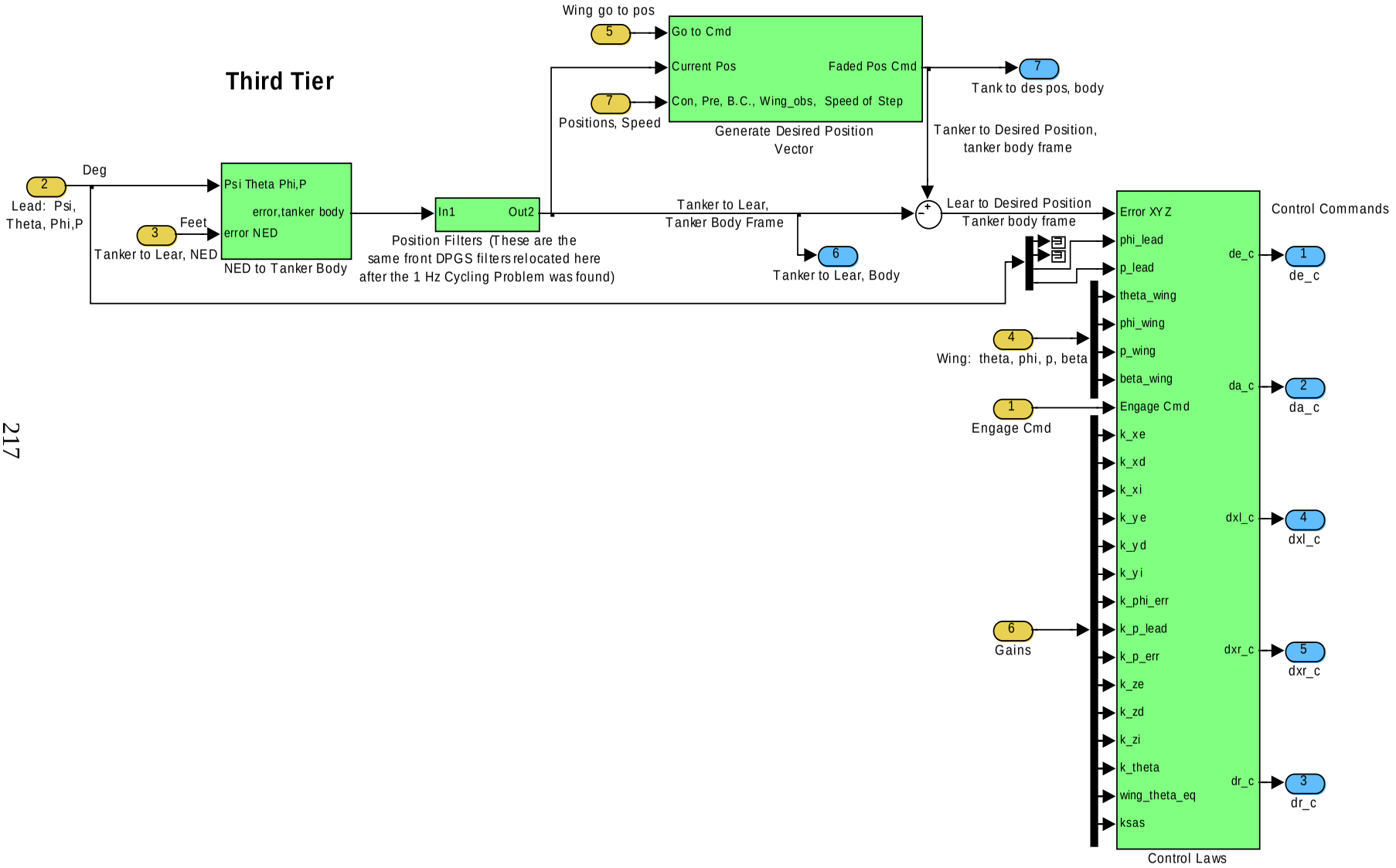

Figure 126. Third Control Tier

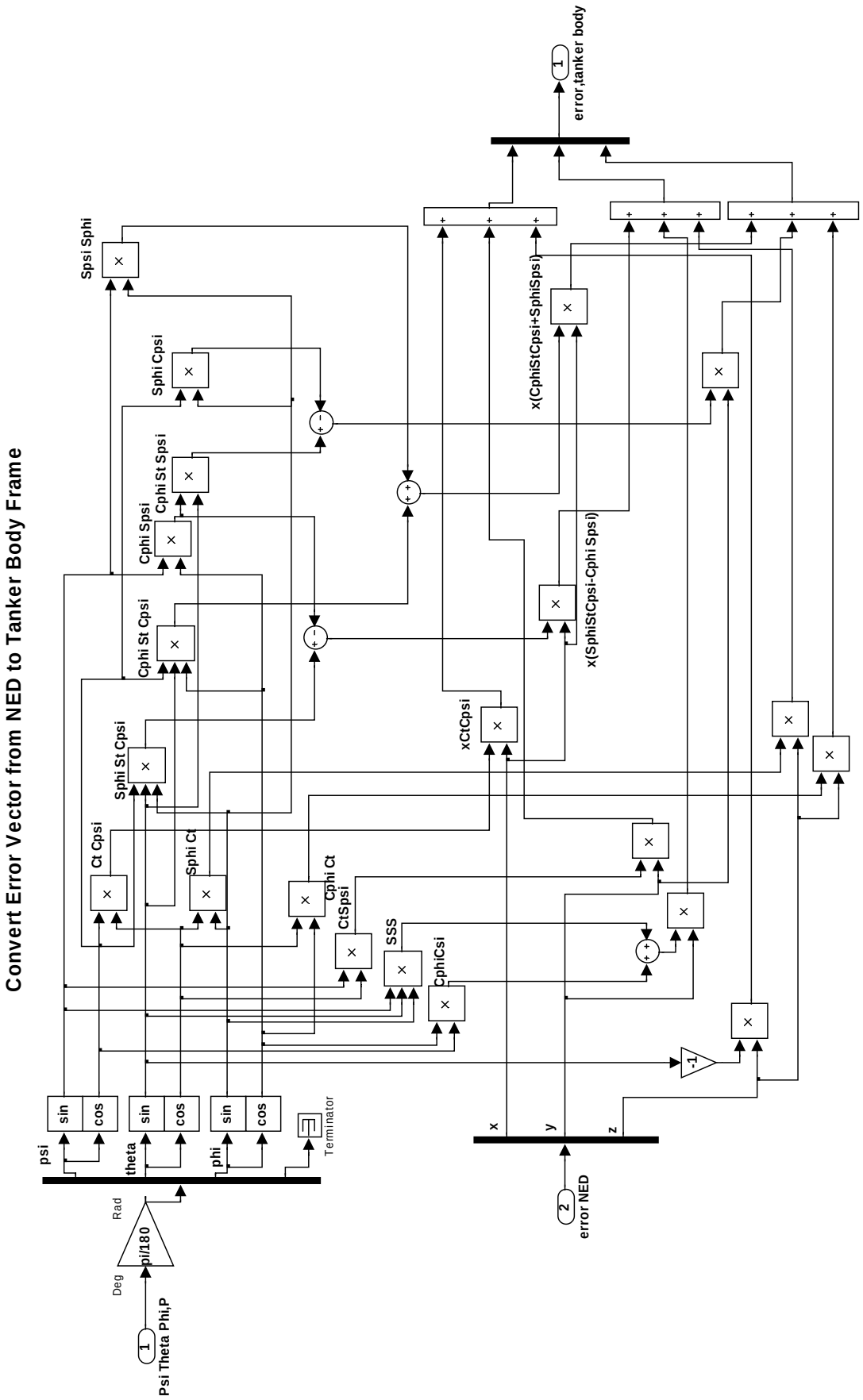

Figure 127. Transformation from NED to Tanker Body Frame (from Third Tier)

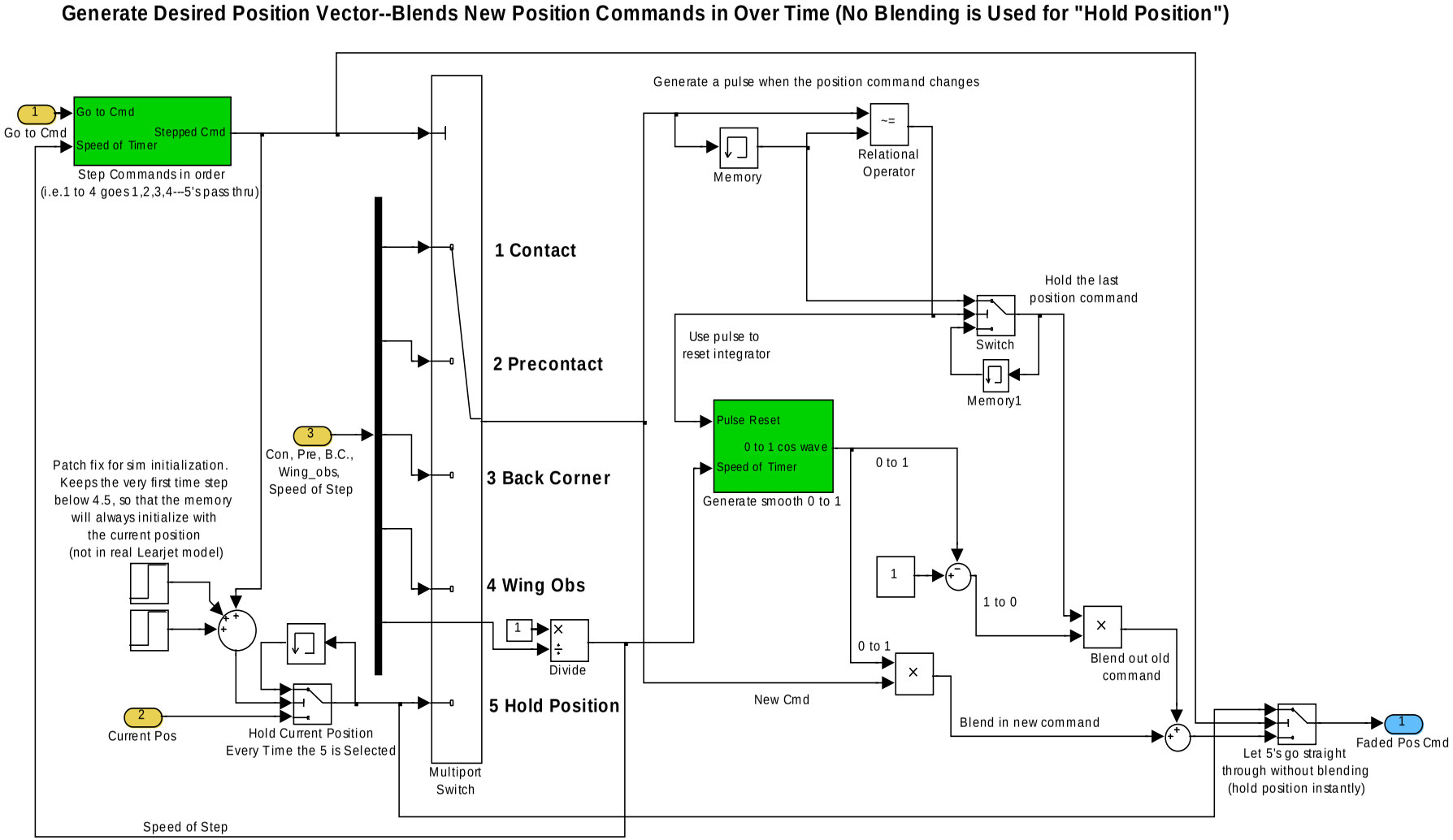

Figure 128. Model to Generate Desired Position Vector (from Third Tier)

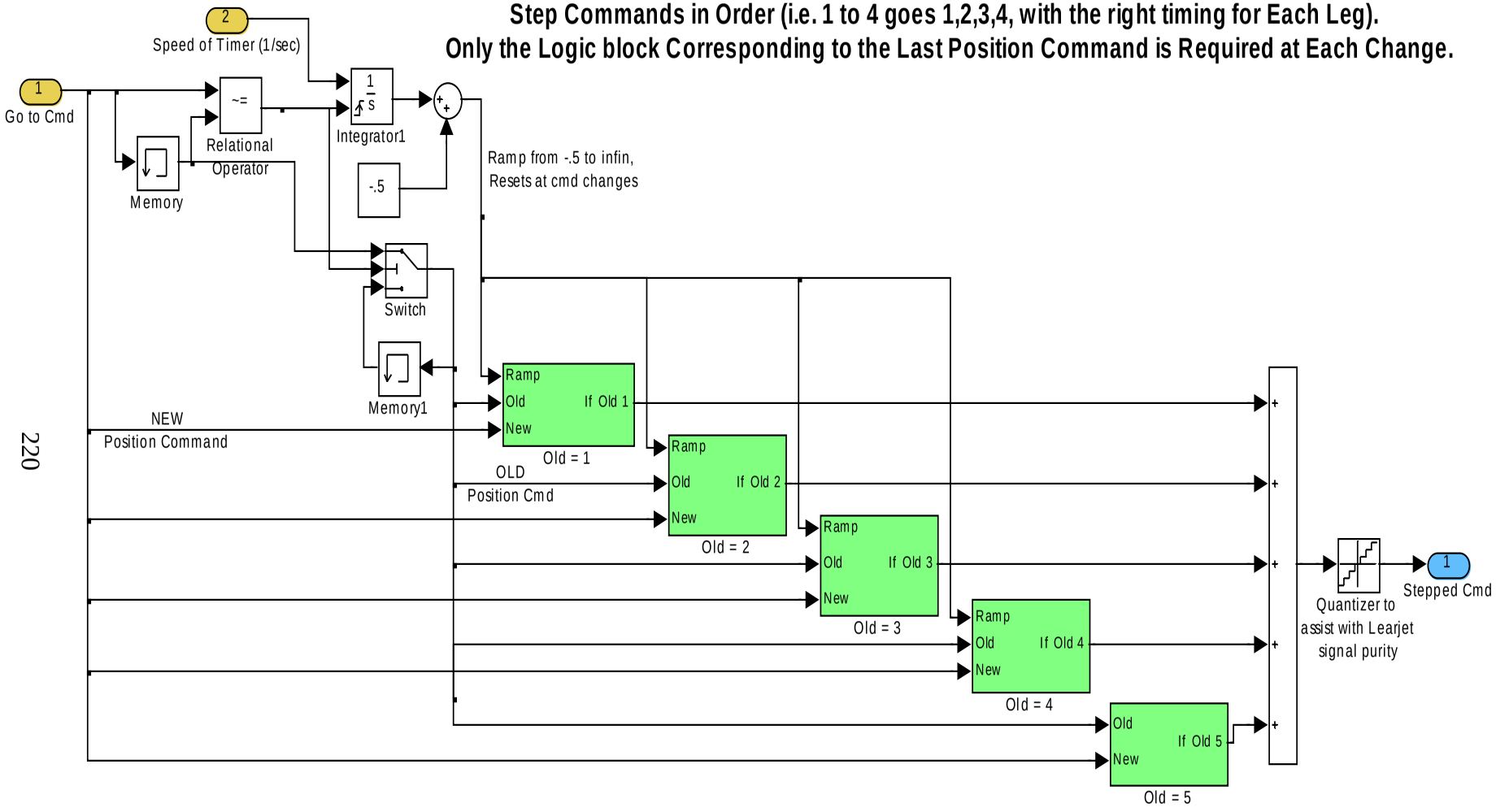

Figure 129. Model to Step Position Commands in Order (from Figure 128, Generate Desired Position

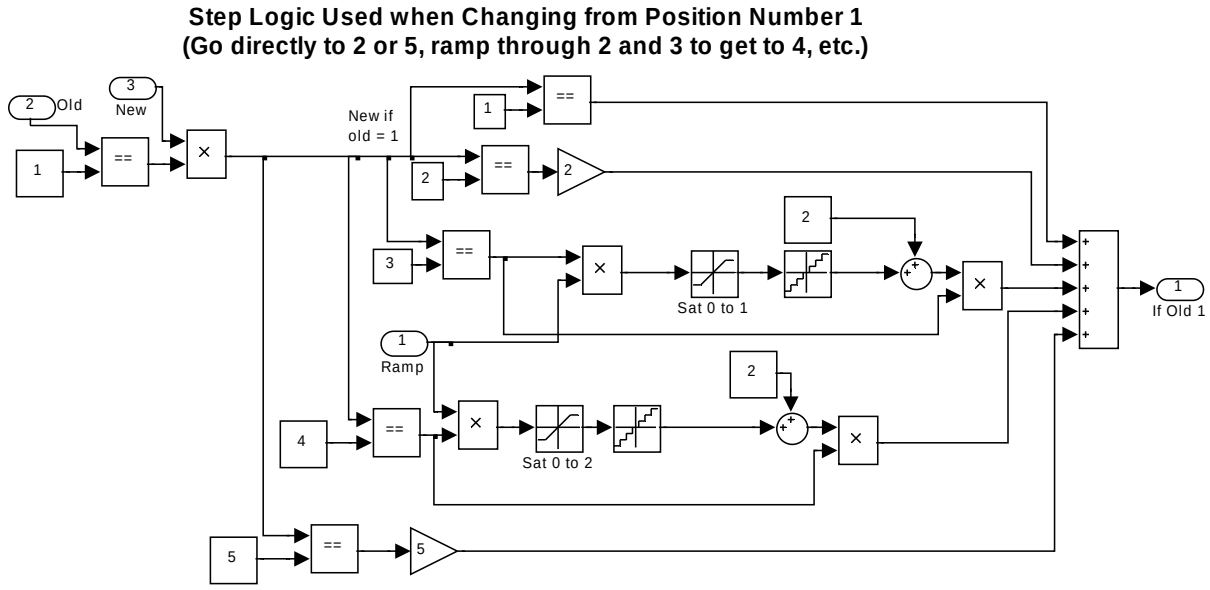

Figure 130. Step Logic Used when Changing from Position Number 1 (from Figure 129)

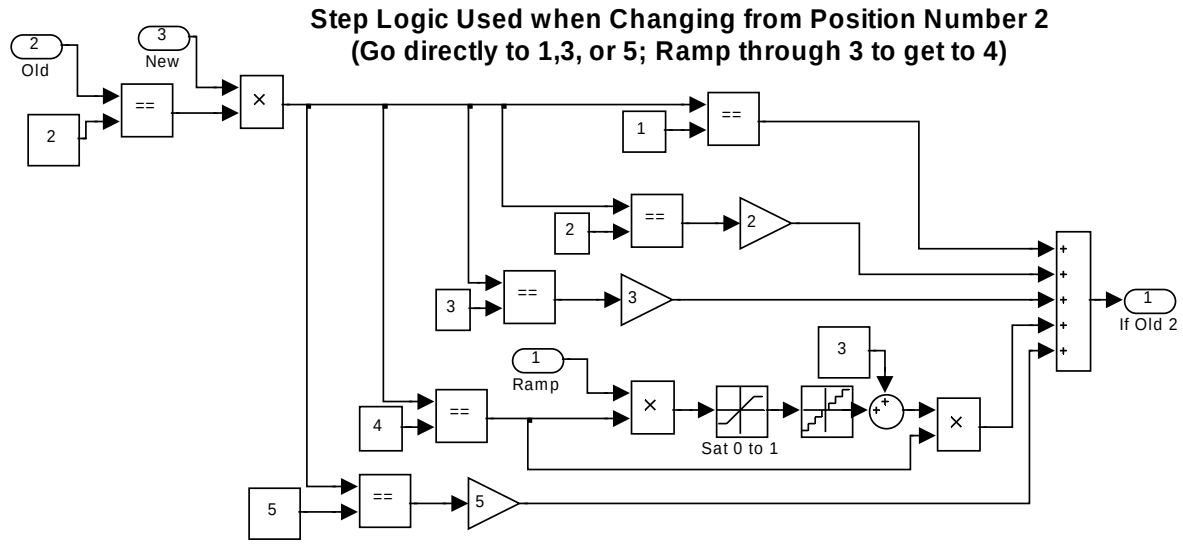

Figure 131. Step Logic Used when Changing from Position Number 2 (from Figure 129)

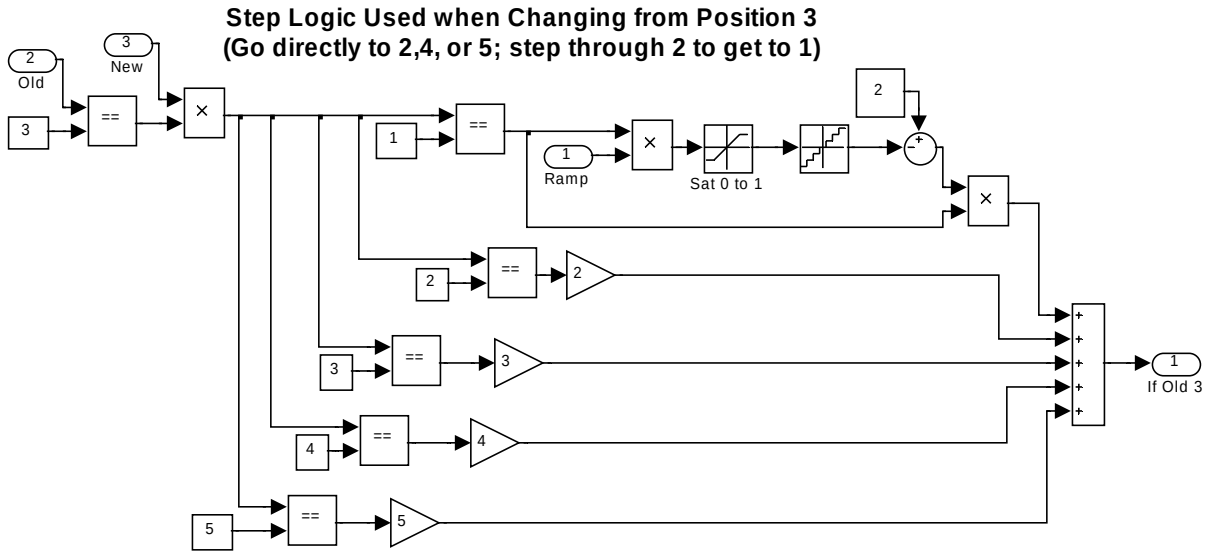

Figure 132. Step Logic Used when Changing from Position Number 3 (from Figure 129)

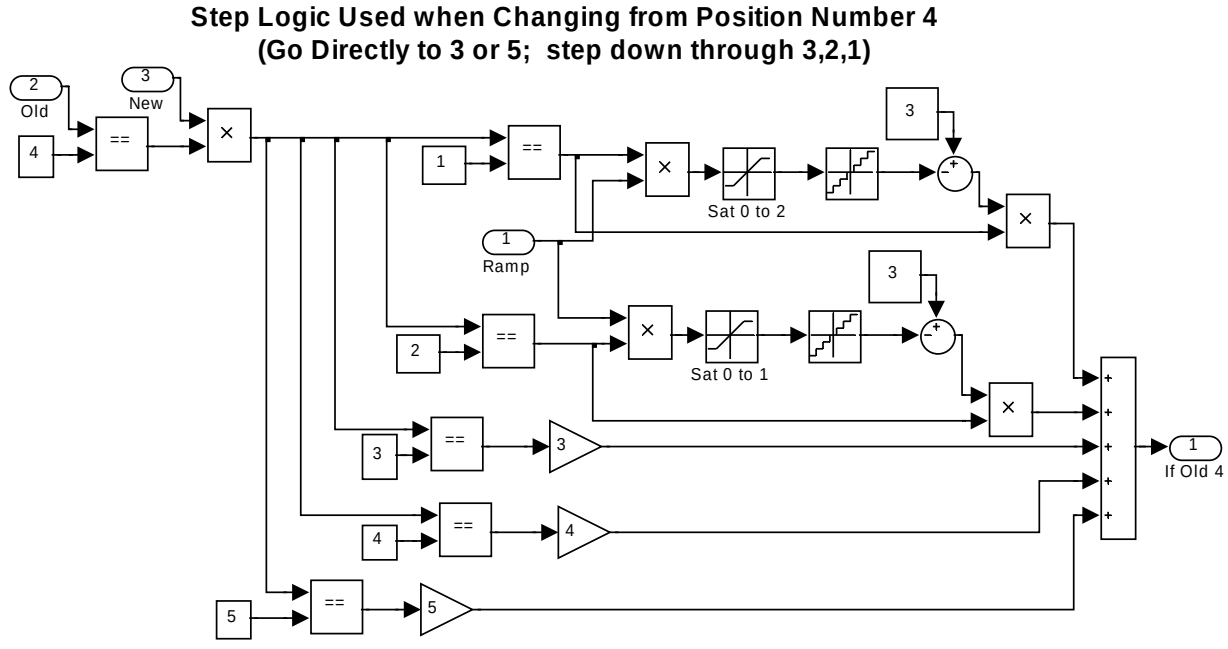

Figure 133. Step Logic Used when Changing from Position Number 4 (from Figure 129)

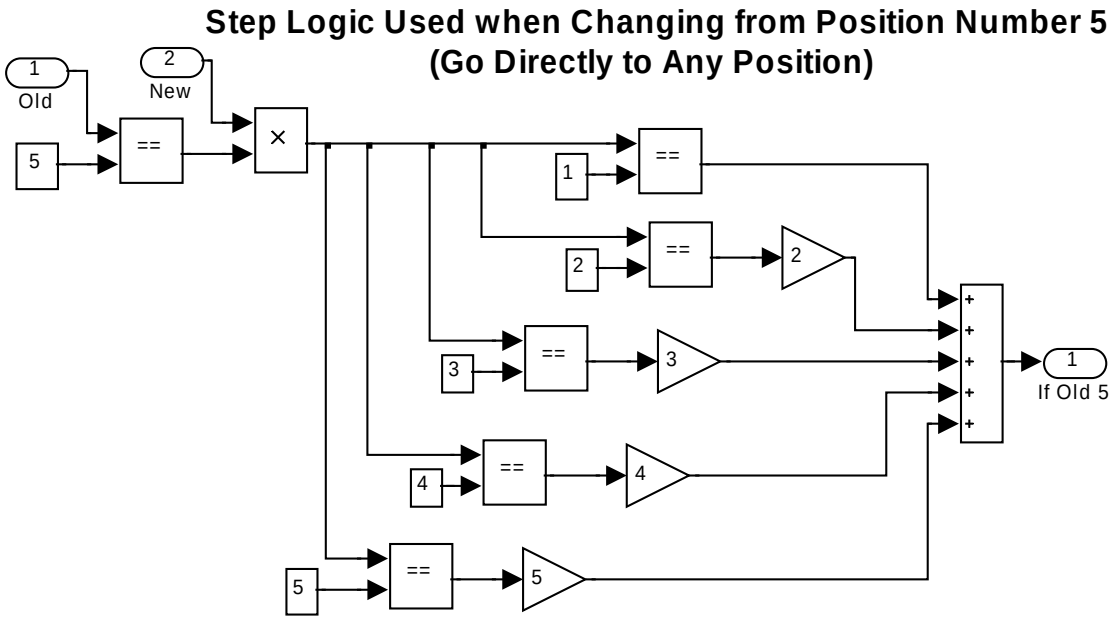

Figure 134. Step Logic Used when Changing from Position Number 5 (from Figure 129)

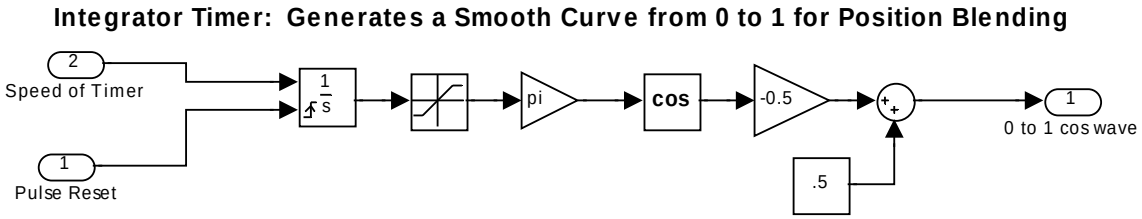

Figure 135. Integrator Timer to Generate a Smooth Curve from 0 to 1for Position Change Timing (from Figure 128, Generate Desired Position Vector)

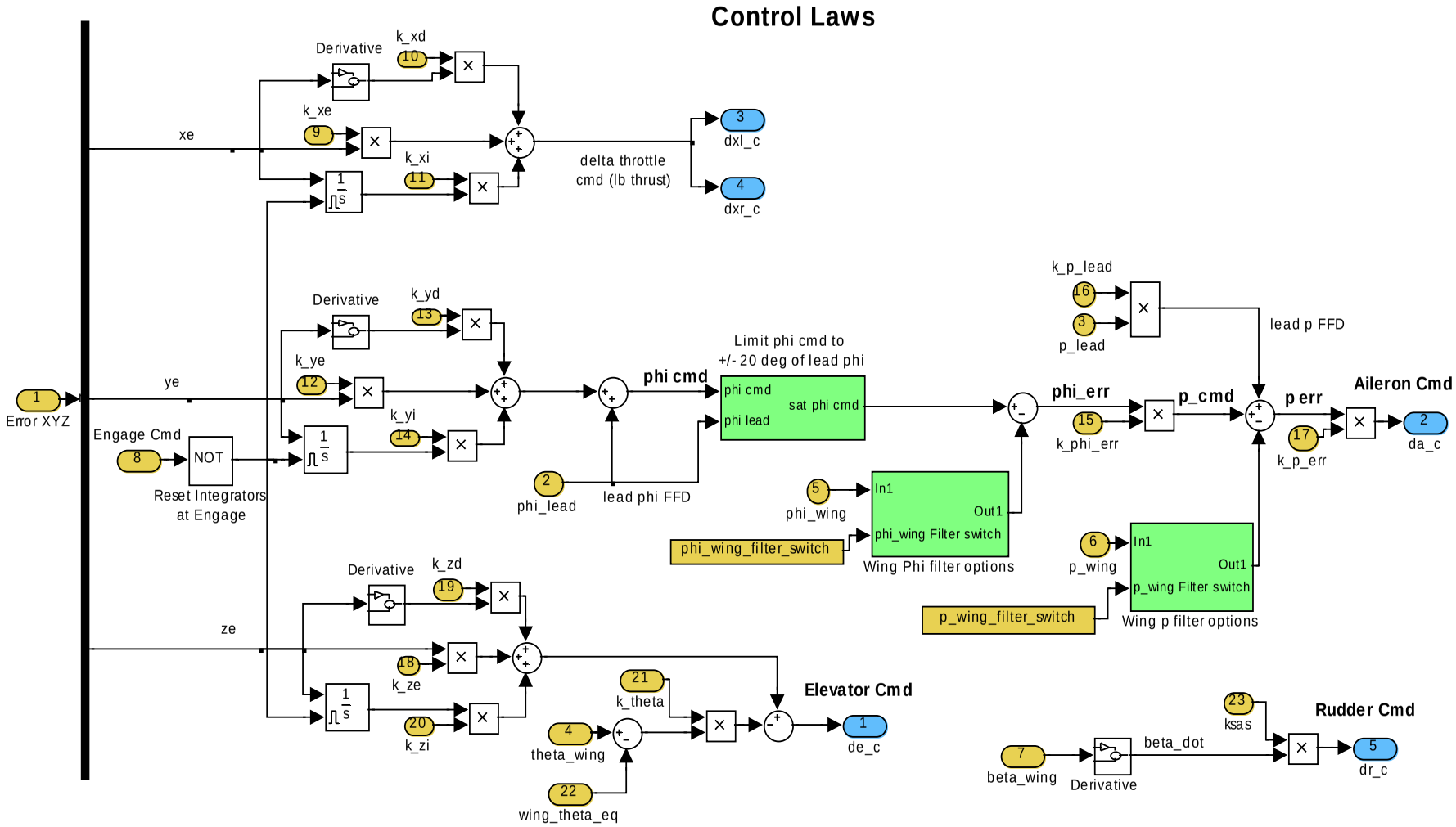

Figure 136. Control Law Model (from Third Tier)

Appendix B. Matlab Initialization Code

Simulator Initialization M-file

```
%%%%%%%%%%  Initializes the Simulator. %%%%%%%%%%%%%%%
clear
clc

%%%%%%%%%%  Disturbances %%%%%%%%%%%%%%%%%%

%% NOISE

   noise=1;                          %% Noise on =1  Noise off=0

   noise_choice=1;                   %0=C-12 noise  1=C172 noise

   load C172noise2.mat               %Load to use C-172 noise injection
   load IMU_noise_on_C12.mat         %Load noise from our flight test on C-12


%% TIME DELAY
   time_delay=1;                     %%Delay on=1  no delay=0

   %% Set delay values in seconds
   time_delay_GPS=.1;      %.1
   time_delay_IMU=.1;      %.1
   time_delay_VSS=.06;     %.06


%%SAMPLING ERRORS
   data_chop=1;         %%Chop IMU and GPS data from lead to 20 Hz  Yes=1 No=0


%% TURBULENCE
   turb_cmd=1;          %%  1=none 2=norm  3=cumulous  4=Thunderstorm


%%%%%%%%%%%%%% Initialization Routine %%%%%%%%%%%%%%%%%%

Lead_cmd=3;
%Lead_cmd: 1=strt&lvl                2=Rt 30deg for 180 deg
%         3=30 deg rt turn 90/reverse   4=15deg rt turn/reverse
```

```
%       5=Left 15 deg, in, out       6=Left 30 in, out
%       7=Continuous left turn, 30 deg
   %%% Change any Turn Direction with -1 on Lead Model


%initialize wing sim

speedflag=2;          %1=160 KCAS  2=190 KCAS  3=180 KCAS  4=170 KCAS
gs_init_burns
ACT_INIT

%%% Set a random start spot
GS_init_h=9950;
init_east_offset=10;   %10
init_north_offset=-25;  %-25

lear1_switch = 0;     %0=stab deriv's for Lear 2, else=Lear 1
zero_fuel_weight = 9000;
fuel_total    = 5000;
fuel_fuselage = 500;
use_computed_wt_and_inertias = 1;
WEIGHT = 13500;
CG = .21;
IXX = 28000;
IYY = 28000;
IZZ = 54000;
IXZ = 2000;

%%%%%%%%%%%%%%%    Lead model initiation    %%%%%%%%%%%%%%%

% Lead Speed options:
if speedflag==1
   VT_lead=323.12;
elseif speedflag==2
   VT_lead=383.2;
elseif speedflag==3
   VT_lead=363.21;
elseif speedflag==4
   VT_lead=343.18;
end

% Lead Equilibrium Condition
x_eq_lead =[VT_lead .1284892793 0 0 .1284892793 0 0 0 0 0 0 10000 11.2039114414];
throttle_eq_lead=.172527;                %percent
```

```
elev_eq_lead=-.568695/180*pi;       %radians
h_eq_lead=x_eq_lead(12);            %feet
theta_eq_lead=x_eq_lead(5);         %radians
alpha_eq_lead=x_eq_lead(2);         %radians
lead_vel_cmd_fps=x_eq_lead(1);      %ft/s

% Lead Autopilot Gains
kp_lead=57.3*-2.3
kq_lead=-.192*57.3;
ktheta_lead=-3*57.3;
kalpha_lead=-.56*57.3;
kvel_lead=.1;
kh_lead=-.8;
kphi_lead=-.5*57.3;
kbeta_lead=-4*57.3;
kbetadot_lead=-5*57.3;
kbetaint=-1*57.3;

%initialize gains and positions
final_VSS_gains_init
final_VSS_positions_normal_init
```

VSS Initialization M-File (run for both aircraft or simulator)

```
%%final_vss_gains_init

%%%%%%%%%%  Initializes the VSS gains constants.  Run this
%% in the VSS during ground operations prior to flight.  For
%% the simulator, run this after the sim init (also run
%% positions init)

k_xe=150;
k_xd=300;
k_xi=20;

k_ye=.3;
k_yd=.8;
k_yi=.03;
k_phi_err=2.5;
k_p_lead=1.5;
k_p_err=-3; %ran -1 for flight, neg for aileron convention
```

```
k_ze=.6;
k_zd=.25;
k_zi=.08;
k_theta=-2
wing_theta_eq=9.05;

ksas=-1.2;

speedofstep=30; %sec. Sets speed of the ramps
                %for the cmd blend & fade

engage_autopilot=1;

engage_throttle=1;

psi_filter_switch=1;
theta_filter_switch=1;
phi_filter_switch=1;          %should be 3 for flight
p_filter_switch=1;            %should be 3 for flight
x_filter_switch=1;
y_filter_switch=1;
z_filter_switch=1;
de_c_filter_switch=1;         %only use for gnd test
da_c_filter_switch=1;         %only use for gnd test
dr_c_filter_switch=1;         %only use for gnd test
dxl_c_filter_switch=1;        %only use for gnd test
dxr_c_filter_switch=1;        %only use for gnd test

p_wing_filter_switch=1;       %should be 2 for flight
phi_wing_filter_switch=1;     %should be 2 for flight
p_wing_constant=0;
phi_wing_constant=0;


theta_constant=-1.5 %Doesn't match sim—empirical from flight
                    % test data—IMU installation error
psi_constant=0;
phi_constant=0;
p_constant=0;


%Contstants for heading estimator
heading_source=1;   %1=IMU  2=Estimated, auto correct phi
                    %3=Estimated,manual correct only--should
                    %be 2 for flight
psi_correction_speed=.4;
phi_bias=0;
psi_sync=0;
```

```
x_body_filter_switch=1;   %should be 2 for flight
y_body_filter_switch=1;   %should be 2 for flight
z_body_filter_switch=1;   %should be 2 for flight
```

Position Initialization (run for both aircraft and simulator)

```
%final_vss_positions_normal_init

%%%%%%%%%%  Initializes the VSS Positions. Run this after
the sim init %% (also run the gains init)

Contact_x=-26;
Contact_y=0;
Contact_z=31;

PreContact_x=-85;
PreContact_y=0;
PreContact_z=40;

BackCorner_x=-85;
BackCorner_y=112;
BackCorner_z=40;

WingObs_x=10;
WingObs_y=112;
WingObs_z=6;
```

Appendix C: Earth Centered, Earth Fixed (ECEF) Frame Considerations

Earth Centered, Earth Fixed (ECEF) Frame

The GPS differential vector that initially drove the controller was expressed in the ECEF frame. Future designs that use GPS for positioning will have to go through this frame at some point. The ECEF frame is a rotating reference frame (with respect to inertial space) with the origin at the center of mass of the Earth. The ECEF z-axis, Z, is directed from the origin through the Conventional Terrestrial Pole. The ECEF x-axis is orthogonal to the z-axis, and directed through the reference Greenwich Meridian on the Earth at zero longitude. The y-axis is orthogonal to both and completes a right-handed x-y-z system.

The simulator was originally designed to convert the position displacement signal from each aircraft models in the NED frame, into ECEF frame. The position vectors were then subtracted to yield the relative position vector in ECEF coordinates, as it was originally to be presented to the controller. In the controller, the ECEF vector was converted back to NED before the Euler angles could be used to transform the position vector into the tanker body frame. The coordinate transformation process followed is taken from Raquet, and is outlined here to repeat the process for future designs [17].

Transformation from ECEF to Local Frame [17]

To transform coordinates from the ECEF frame $[X\ Y\ Z]^T$ to error coordinates in the local frame, geodetic coordinates of longitude (long), latitude (lat), and altitude (alt)

are required. The center of the local frame was defined with longitude and latitude (respectively) in degrees as:

$$p_o = \begin{bmatrix} -117.8909 & 34.91799 & 0 \end{bmatrix}^{\mathrm{T}}$$

To begin the transformation, the ECEF coordinates of the local origin are found by defining the semi-major axis of the Earth (a) and the square of its eccentricity (e) to be:

$$a = 6378137 \qquad e^2 = 0.00669437999013$$

The ECEF position is found with the following relations:

$$r_n = \frac{a}{\sqrt{1 - e^2 \sin^2(lat)}} \tag{57}$$

$$R_{eqiv} = (r_n + alt)\cos(lat) \tag{58}$$

$$\mathbf{ECEF}_{pos} = \begin{bmatrix} R_{eqiv}\cos(long) & R_{eqiv}\sin(long) & ((1-e^2)r_n + alt)\sin(lat) \end{bmatrix}^{\mathrm{T}} \tag{59}$$

The ECEF coordinates of the local origin are now defined as:

$$\mathbf{p}_0 = \begin{bmatrix} X_0 & Y_0 & Z_0 \end{bmatrix}^{\mathrm{T}} \tag{60}$$

The error vector from the desired position to the local origin, expressed in ECEF is:

$$\mathbf{p}^E = \begin{bmatrix} X - X_0 & Y - Y_0 & Z - Z_0 \end{bmatrix}^{\mathrm{T}} \tag{61}$$

The rotation can now be performed with a direction cosine matrix (DCM):

$$\mathbf{p}^G = \mathbf{C}_E^G \mathbf{p}^E \tag{62}$$

where:

$$\mathbf{C}_E^G = \begin{bmatrix} -\sin(long) & \cos(long) & 0 \\ -\sin(lat)\cos(long) & -\sin(lat)\sin(long) & \cos(lat) \\ \cos(lat)\cos(long) & \cos(lat)\sin(long) & \sin(lat) \end{bmatrix}$$

and:

$$\mathbf{p}^G = \begin{bmatrix} East\ error & North\ error & Alt\ error(MSL\ Altitude) \end{bmatrix}^{\mathrm{T}}$$

The transformation from geodetic coordinates to local coordinates was also required for simulation, and is found with another equivalent radius (r_m):

$$r_m = \frac{a\left(1-e^2\right)}{\left(1-e^2\sin^2\left(lat\right)\right)^{3/2}} \tag{63}$$

This radius is combined with the differences between the coordinates [long lat alt] and the origin [$long_0$ lat_0 alt_0]:

$$East\_error = \left(r_n + alt\right)\cdot \Delta long \cdot \cos\left(lat\right) \tag{64}$$

$$North\_error = \left(r_m + alt\right)\cdot \Delta lat \tag{65}$$

$$Alt\_error = \Delta alt \tag{66}$$

where:

$$\Delta long = long - long_0$$
$$\Delta lat = lat - lat_0$$
$$\Delta alt = alt - alt_0$$

The resulting vector is the displacement of position in the NED frame, used in the simulator.

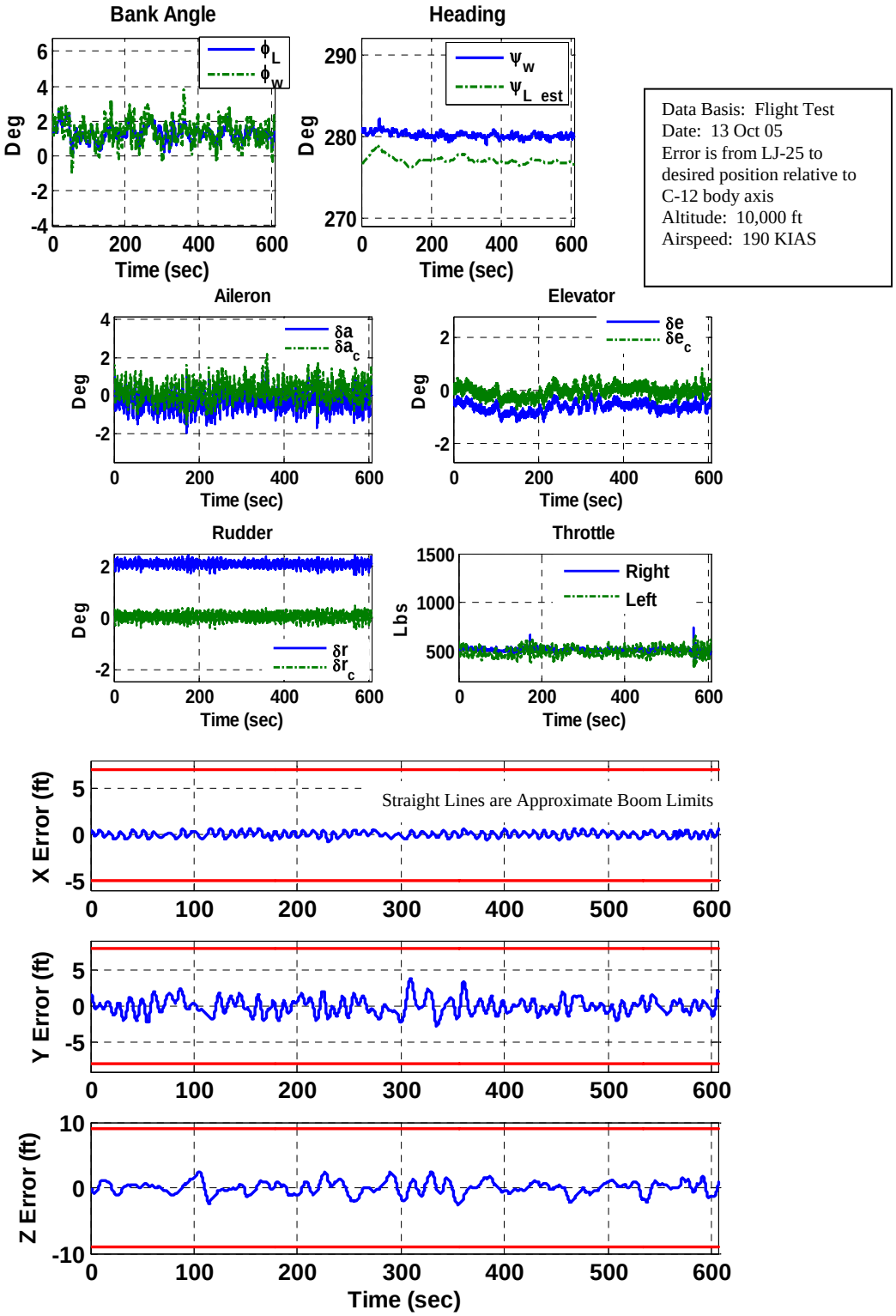

Figure 137. Ten Minutes in Contact Position, Straight and Level

In positions other than contact, the boom position limits have been removed.

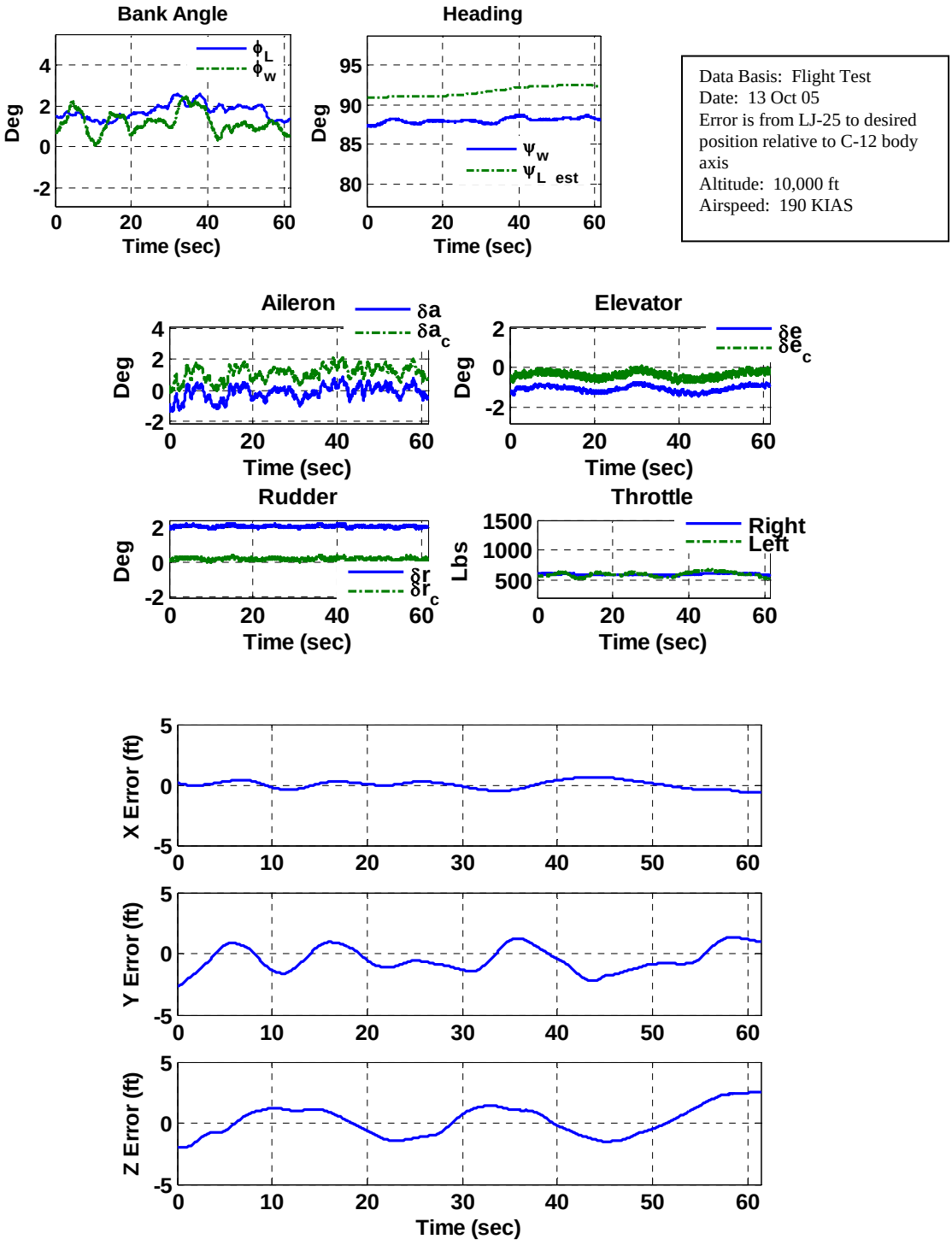

Figure 138. Pre-contact Position, Straight and Level Flight

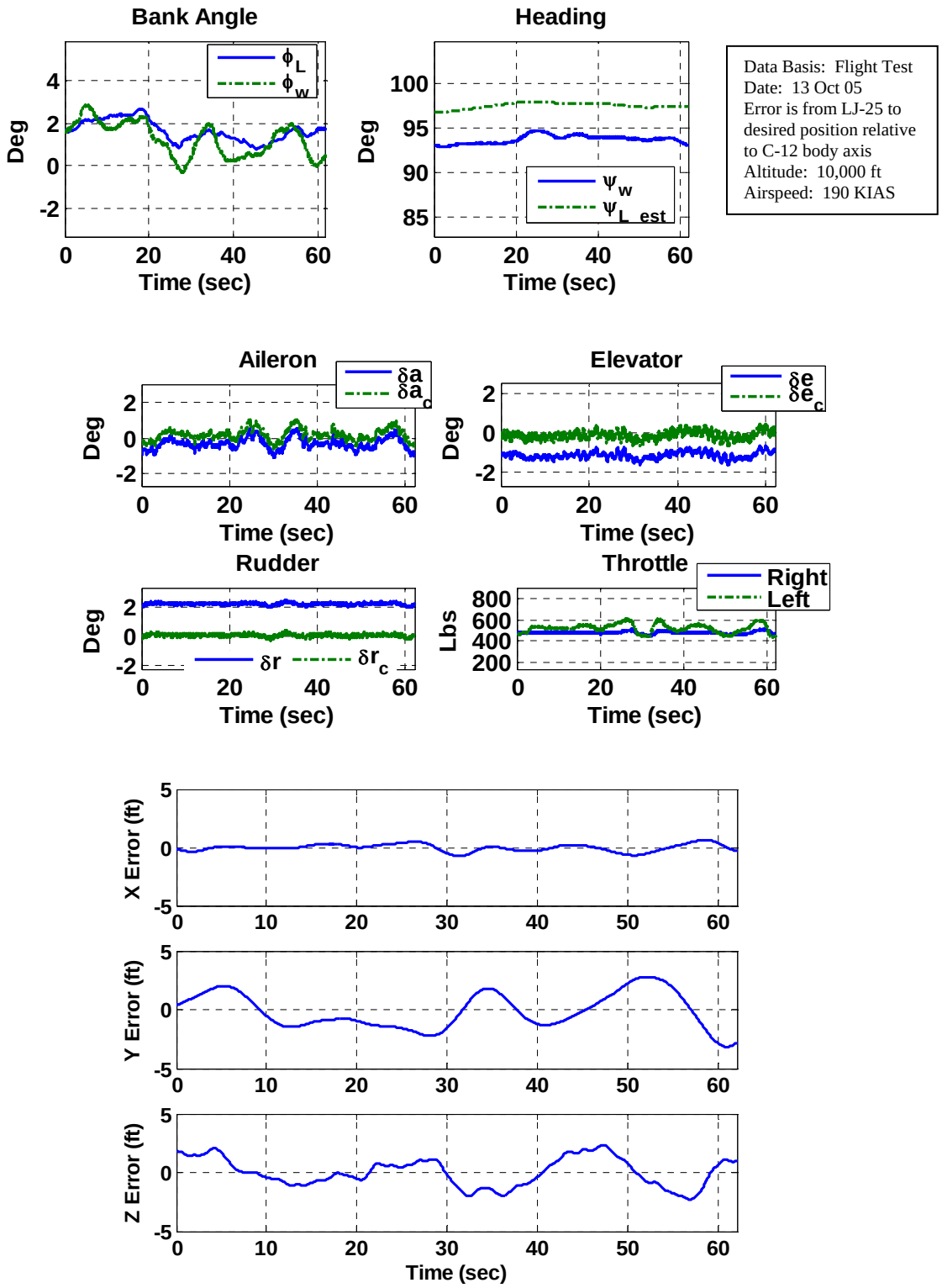

Figure 139. Wing Observation Position, Straight and Level Flight

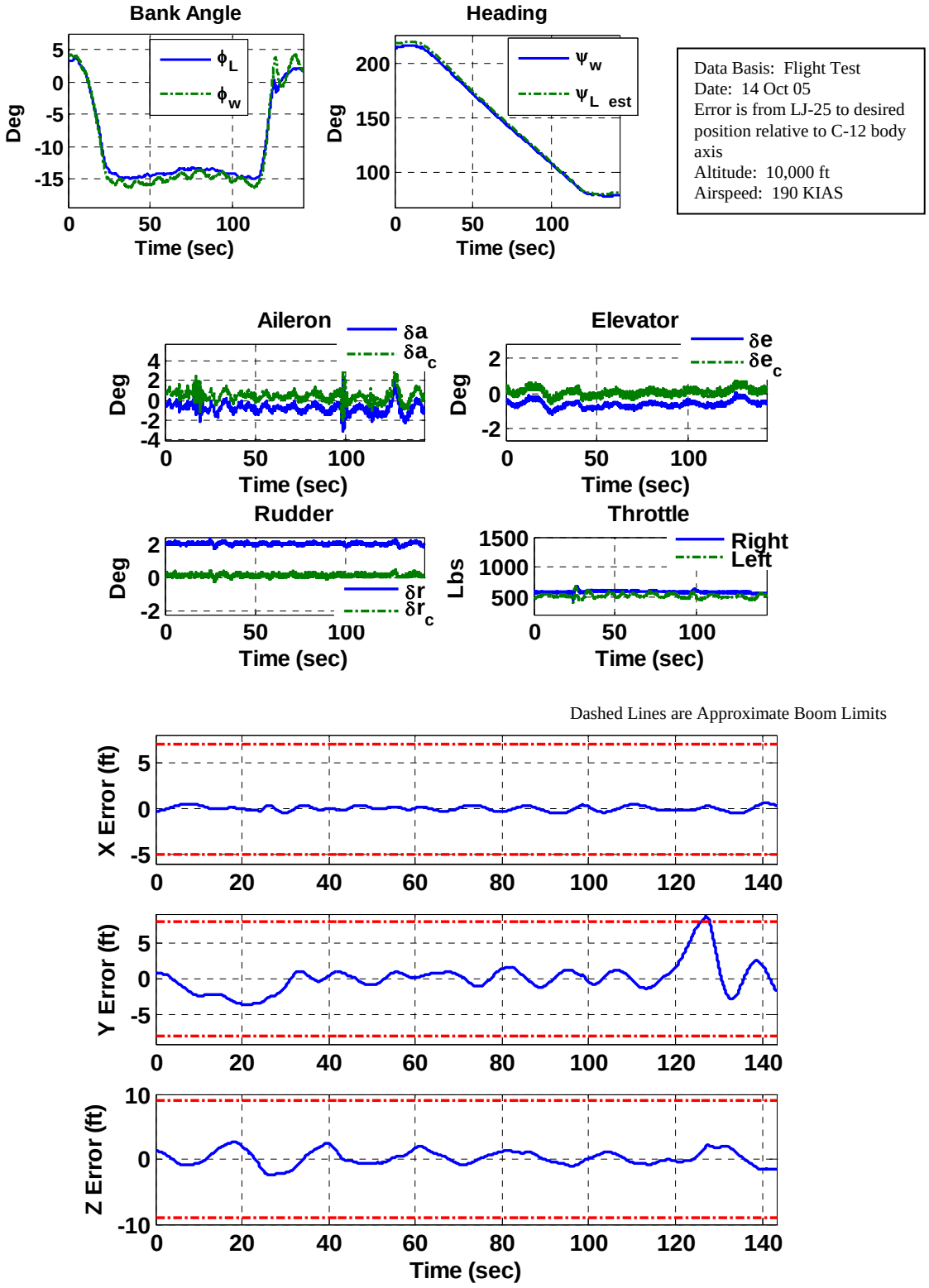

Figure 140. Contact Position, 15 Deg Bank Left Turn

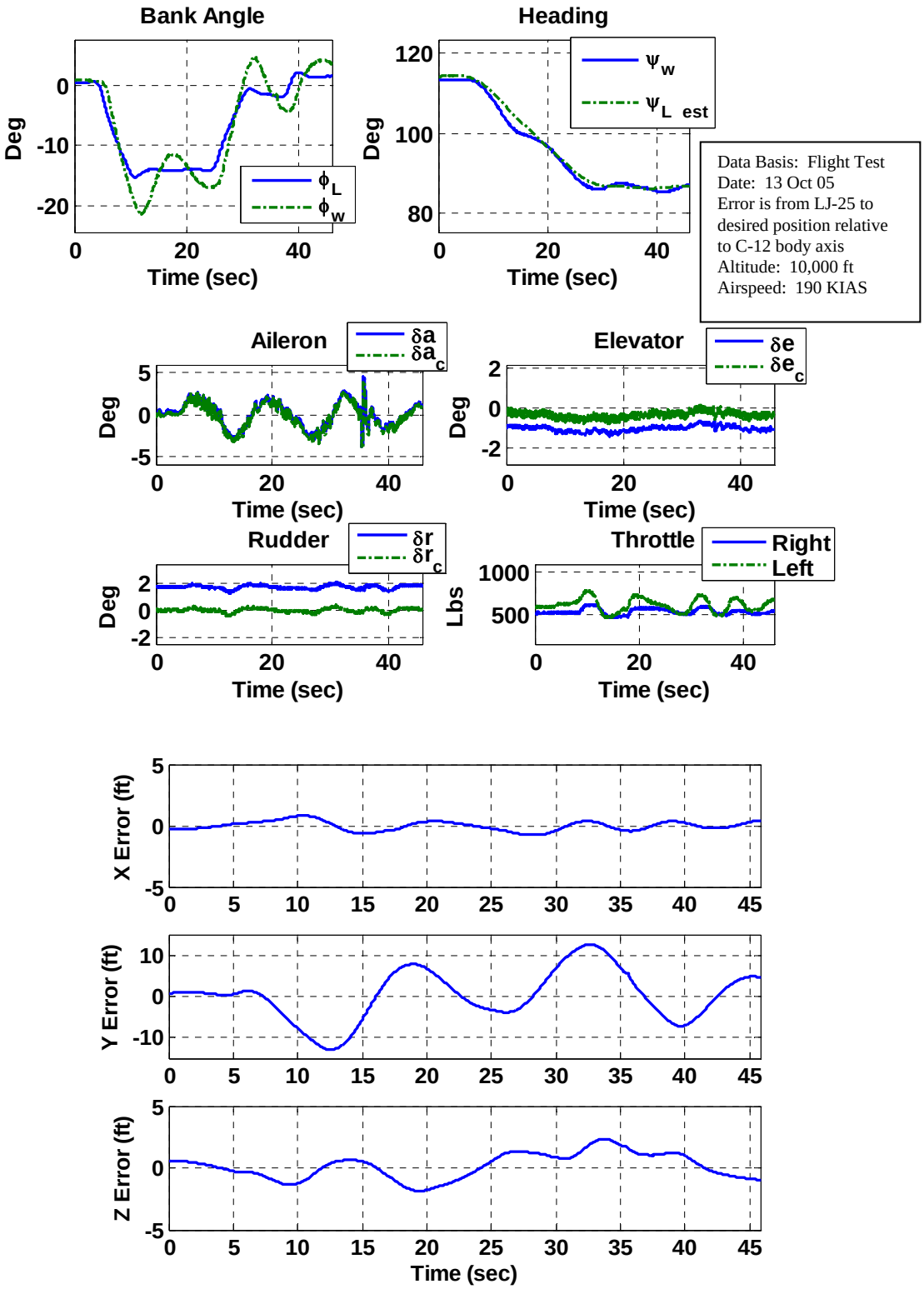

Figure 141. Pre-contact Position, 15 Deg Bank Left Turn

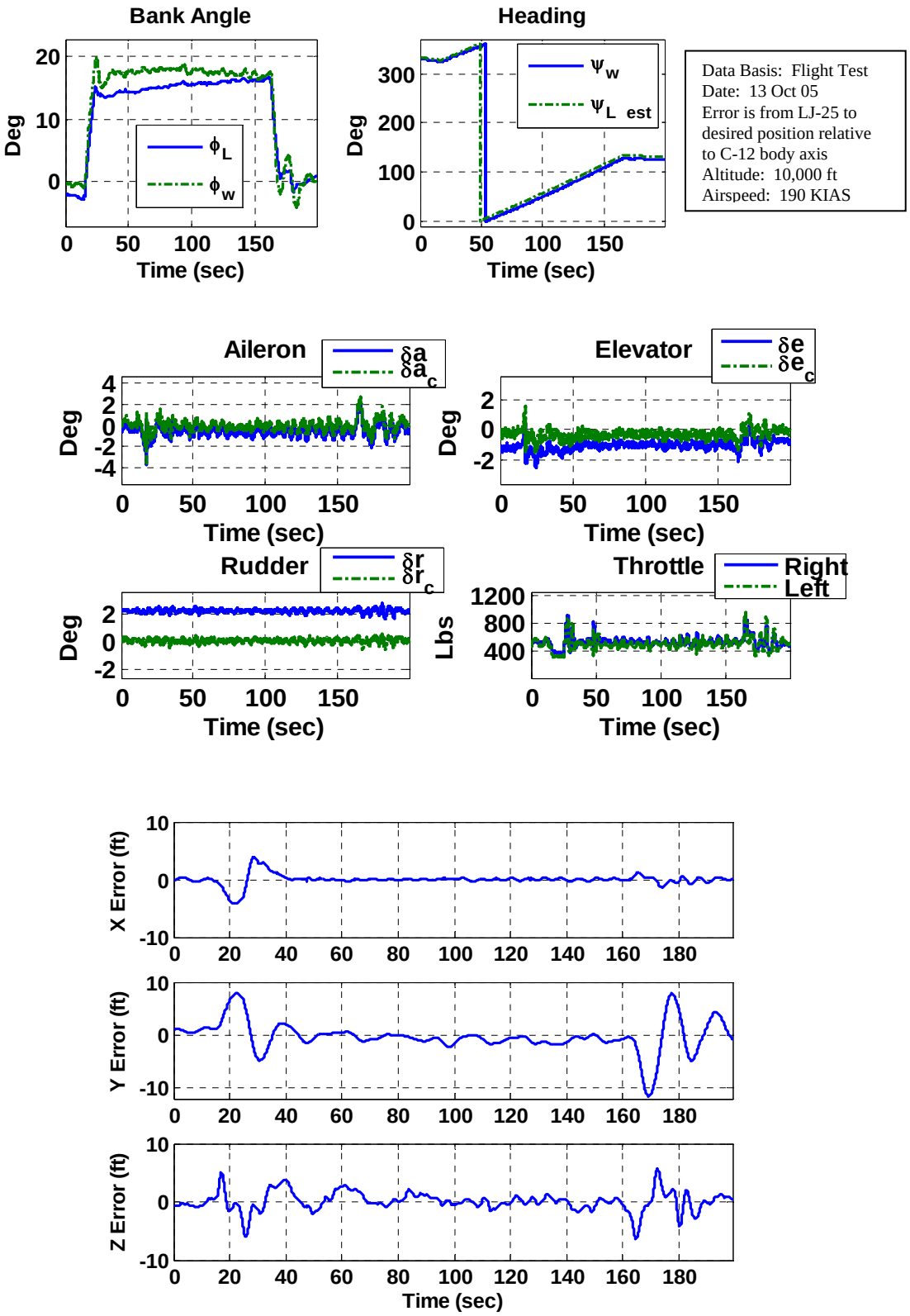

Figure 142. Wing Observation Position, 15 Deg Bank Right Turn

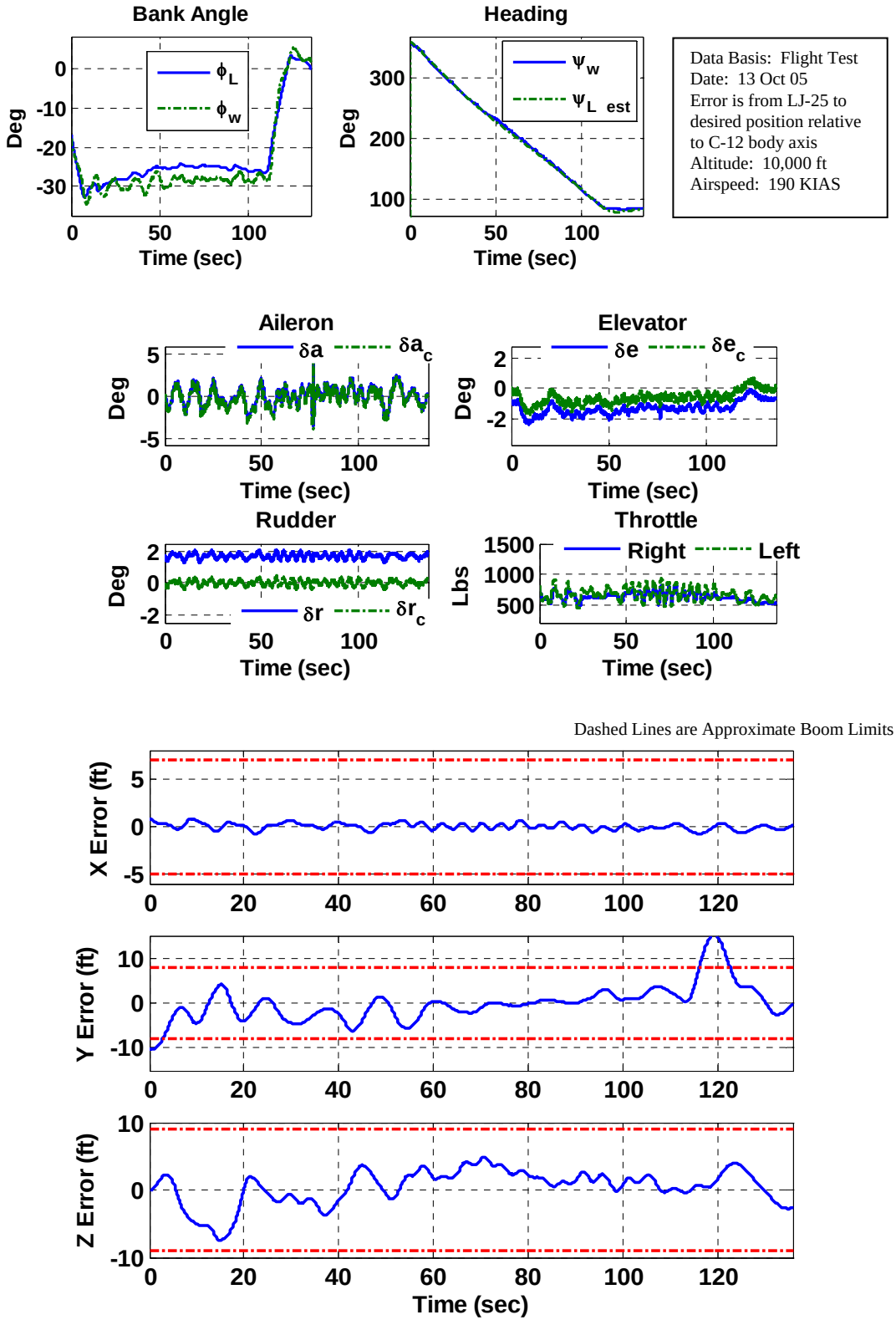

Figure 143. Contact Position, 30 Deg Bank Left Turn

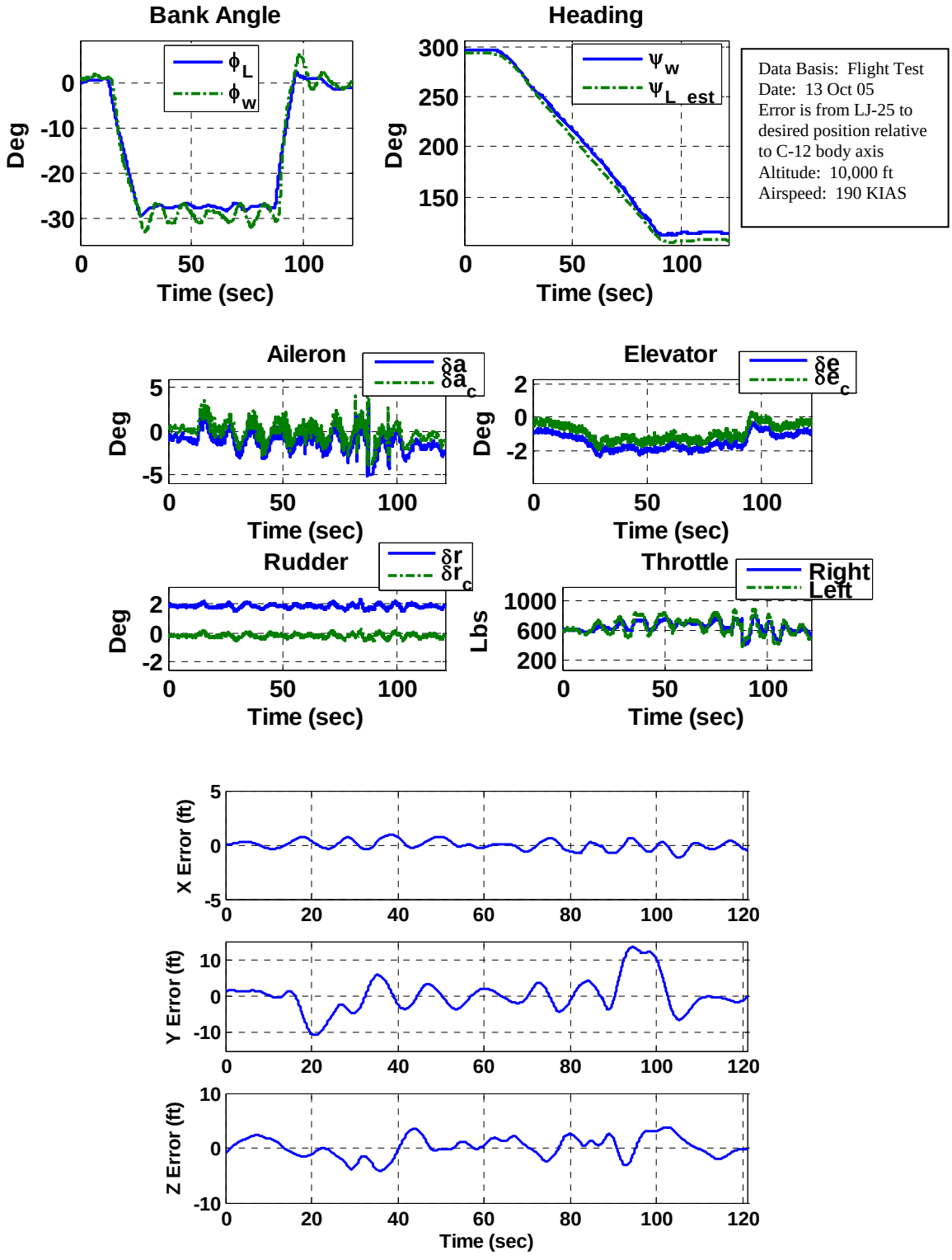

Figure 144. Pre-contact Position, 30 Deg Bank Left Turn

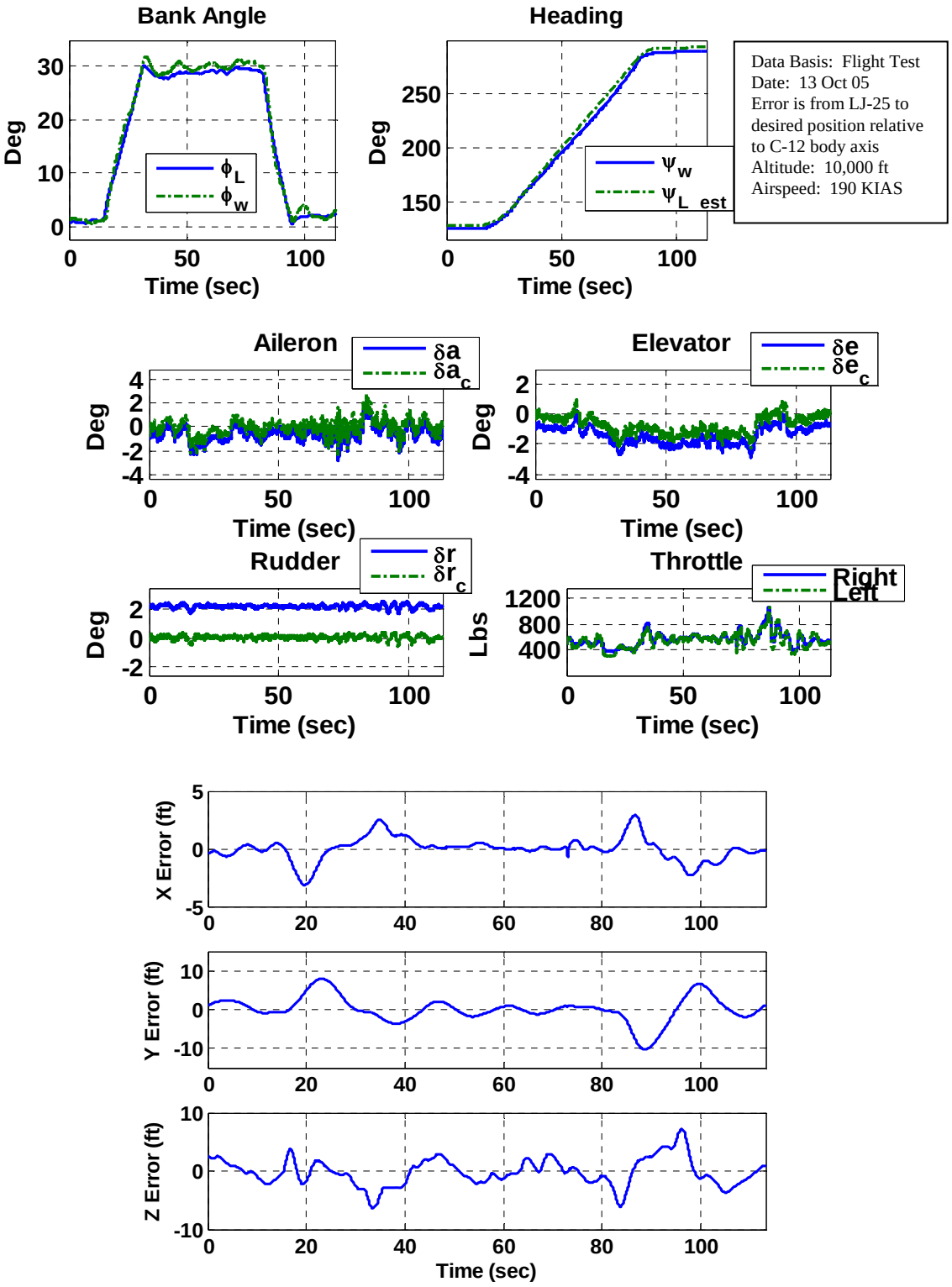

Figure 145. Wing Observation Position, 30 Deg Bank Right Turn

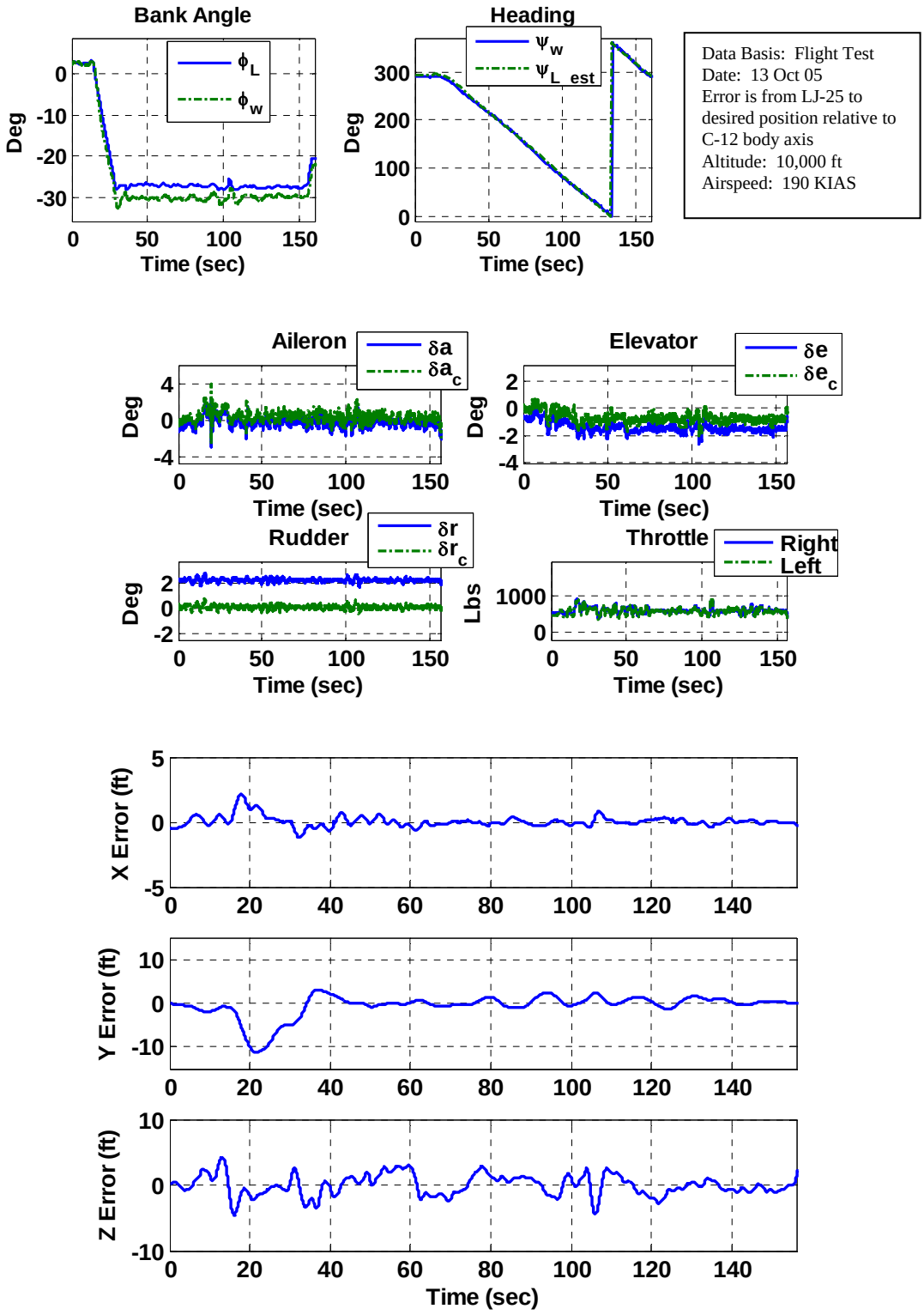

Figure 146. Wing Observation Position, 30 Deg Bank Left Turn

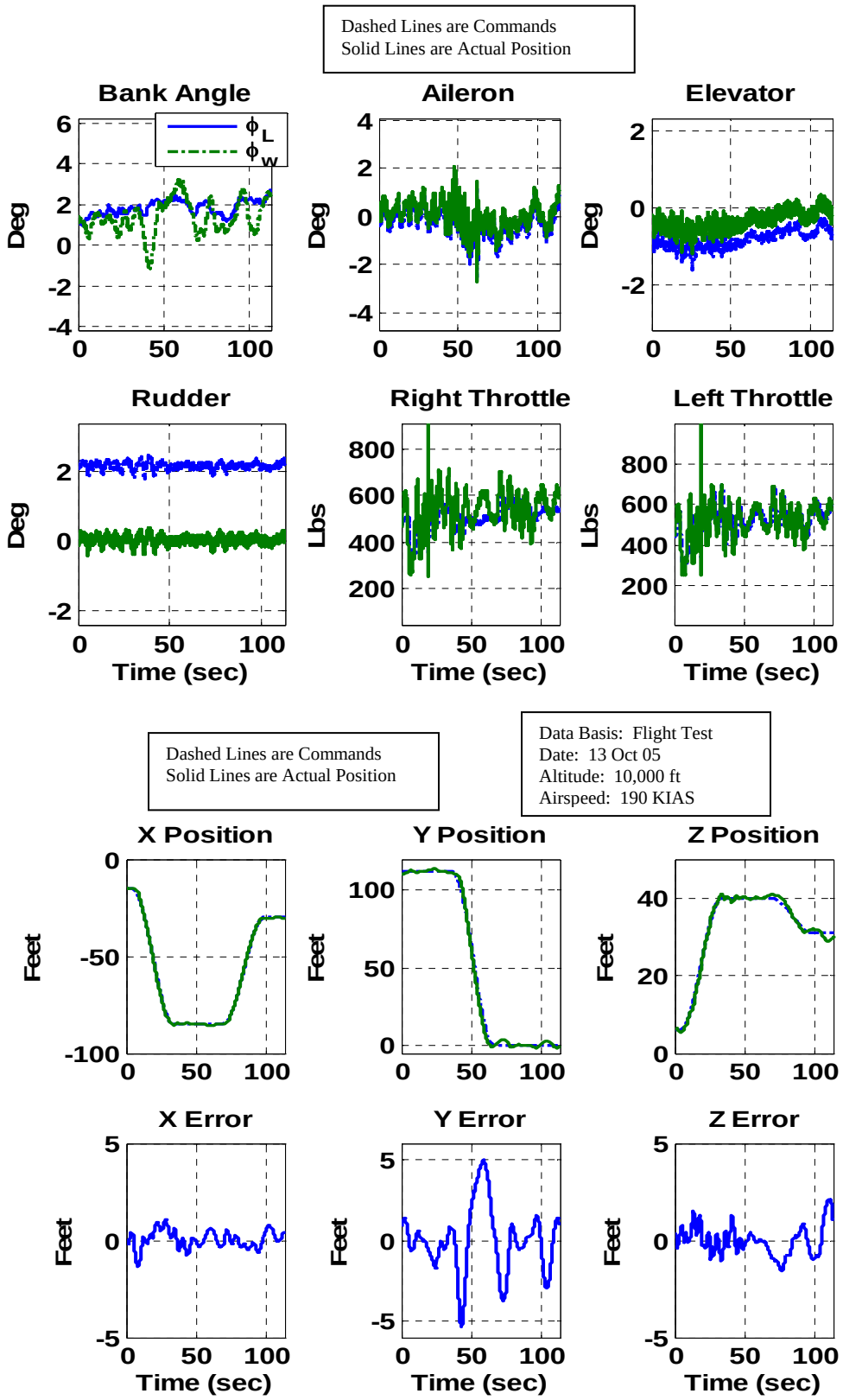

Figure 147. Position Change from Wing Obs. to Contact, Straight and Level.

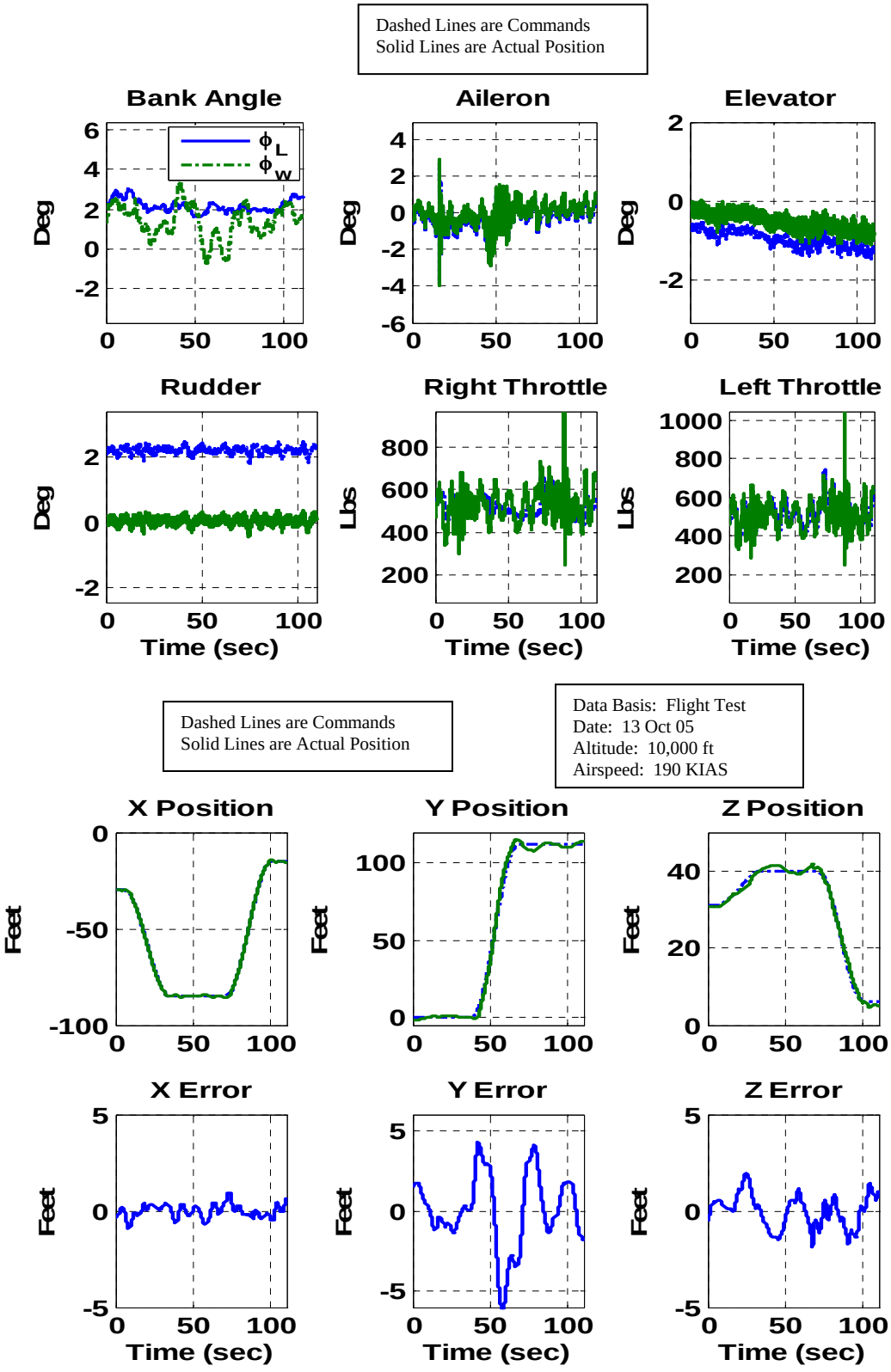

Figure 148. Position Change from Contact to Wing Obs., Straight and Level

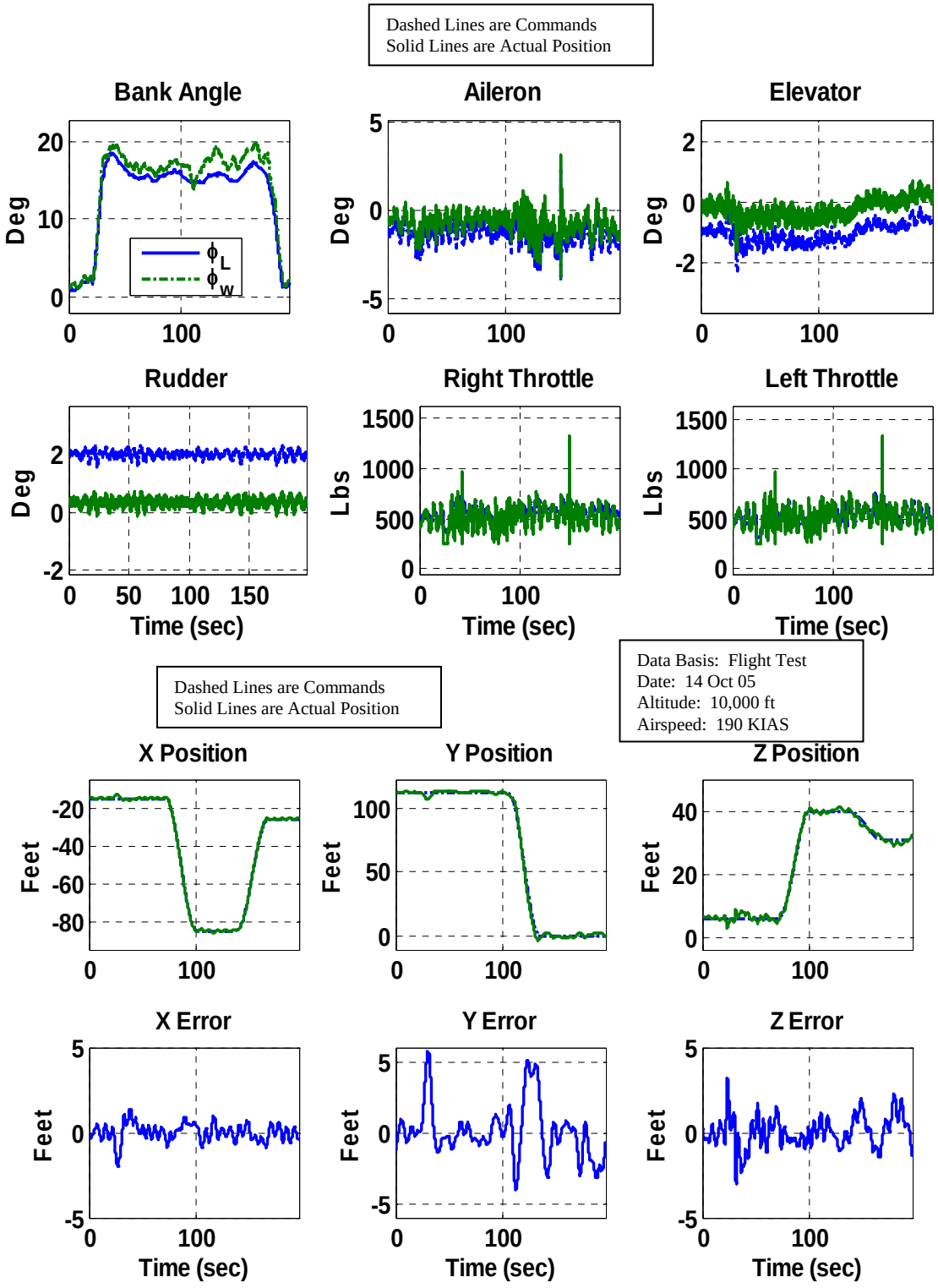

Figure 149. Position Change from Wing Obs. to Contact, 15 Deg Right Bank

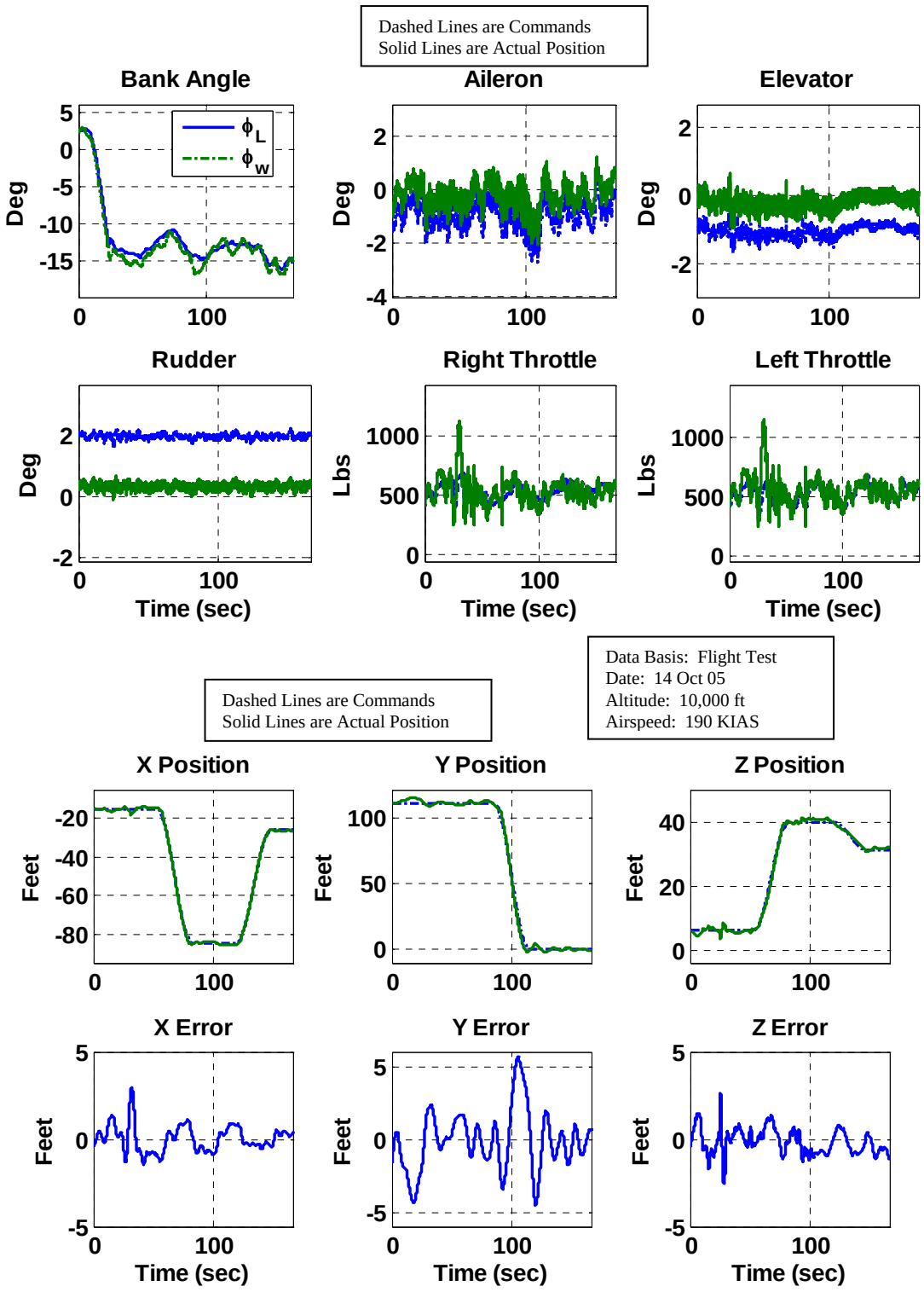

Figure 150. Position Change from Wing Obs. to Contact, 15 Deg Left Bank

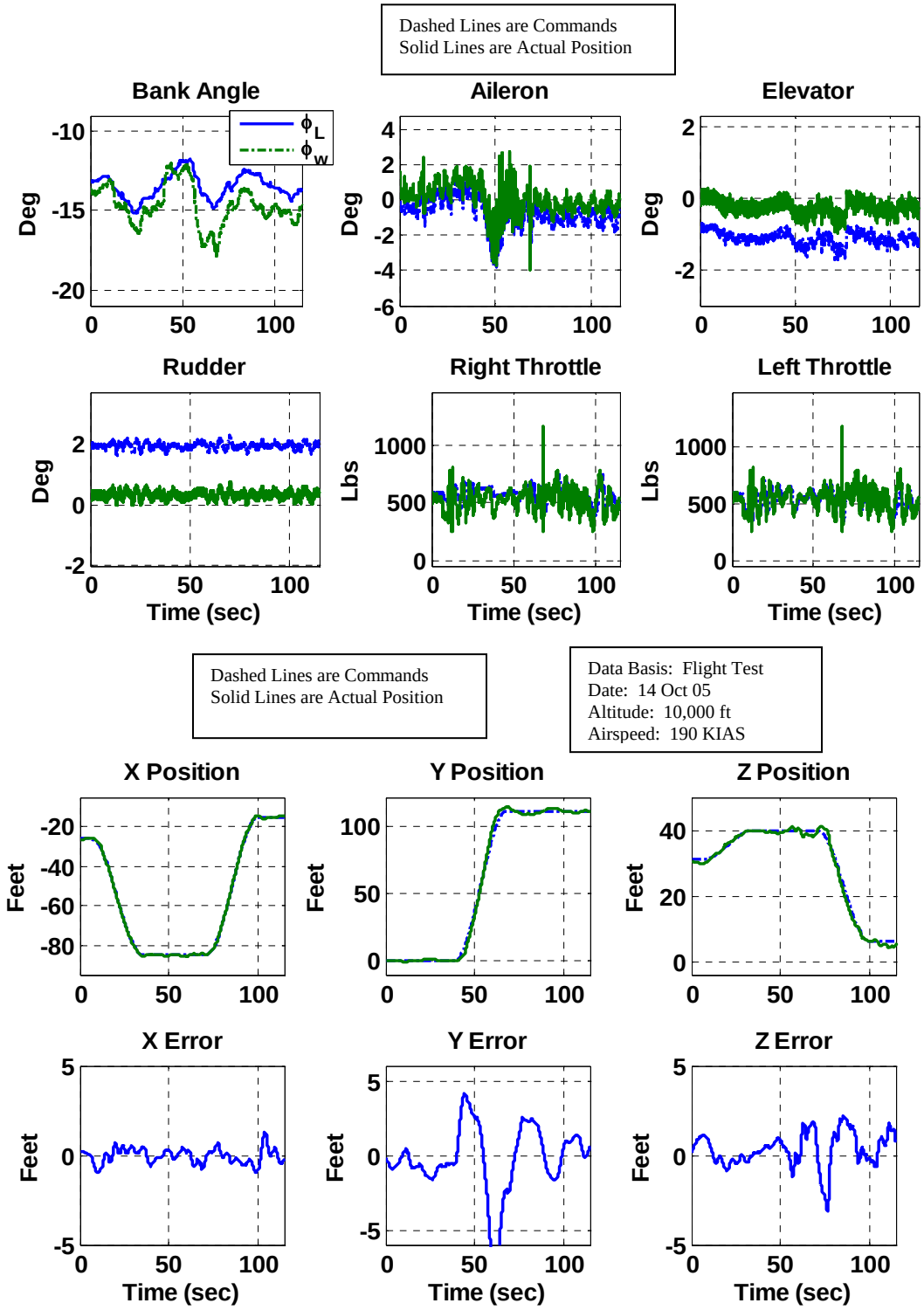

Figure 151. Position Change from Contact to Wing Obs., 15 Deg Left Bank

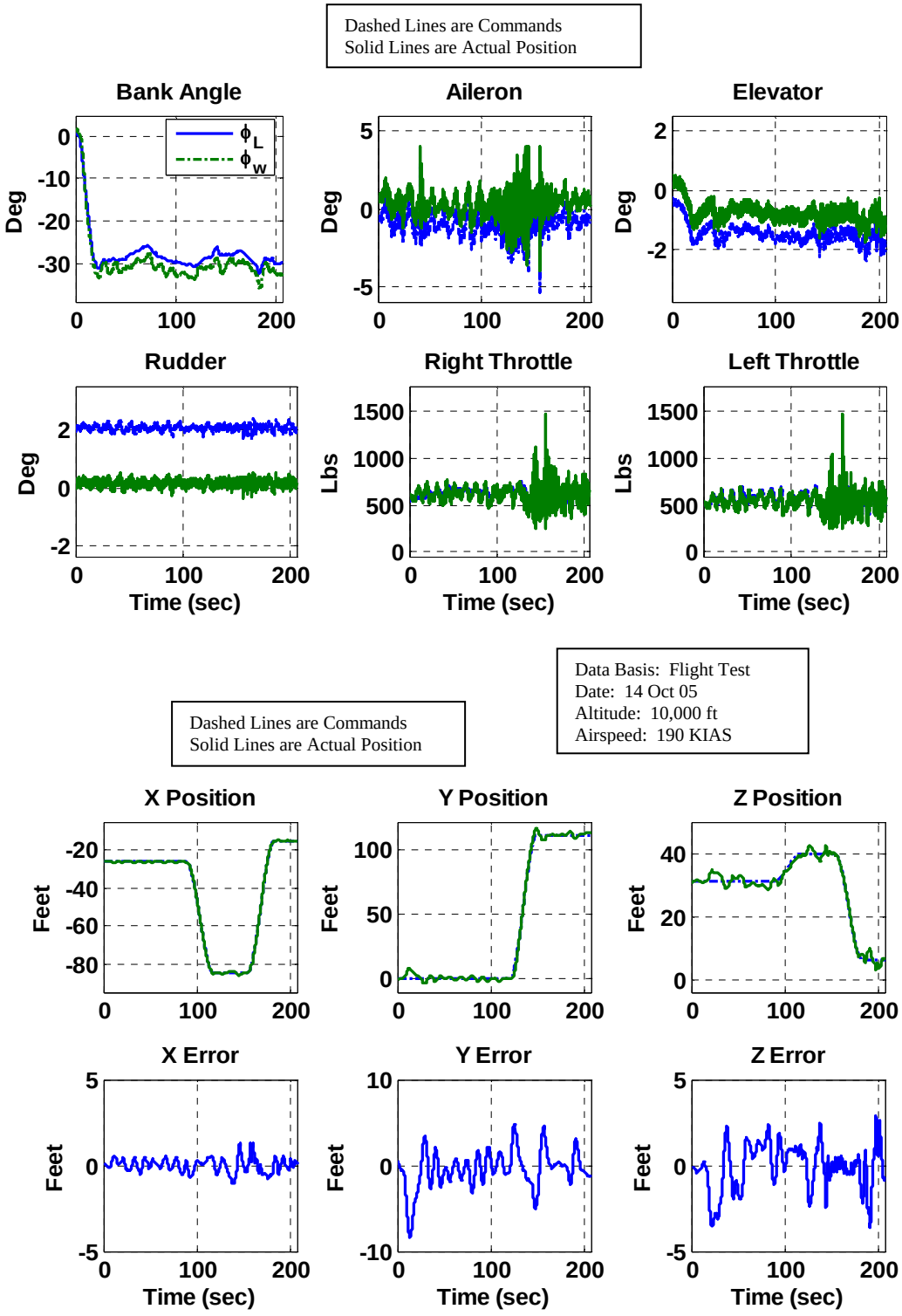

Figure 152. Roll to 30 Deg Left Bank, Position Change from Contact to Wing Obs.

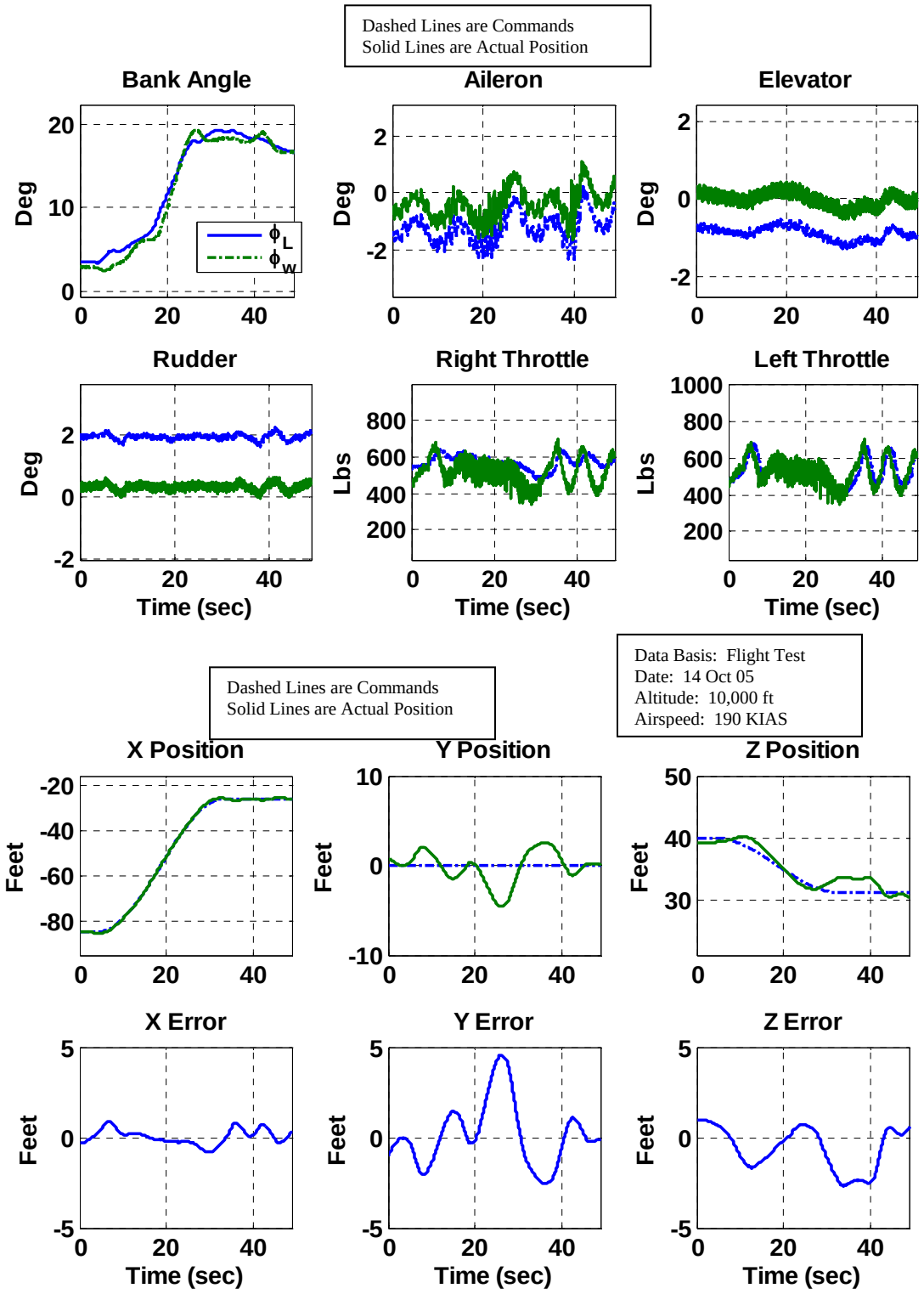

Figure 153. Right Turn Initiated and Stopped while Moving from Pre-contact to Contact

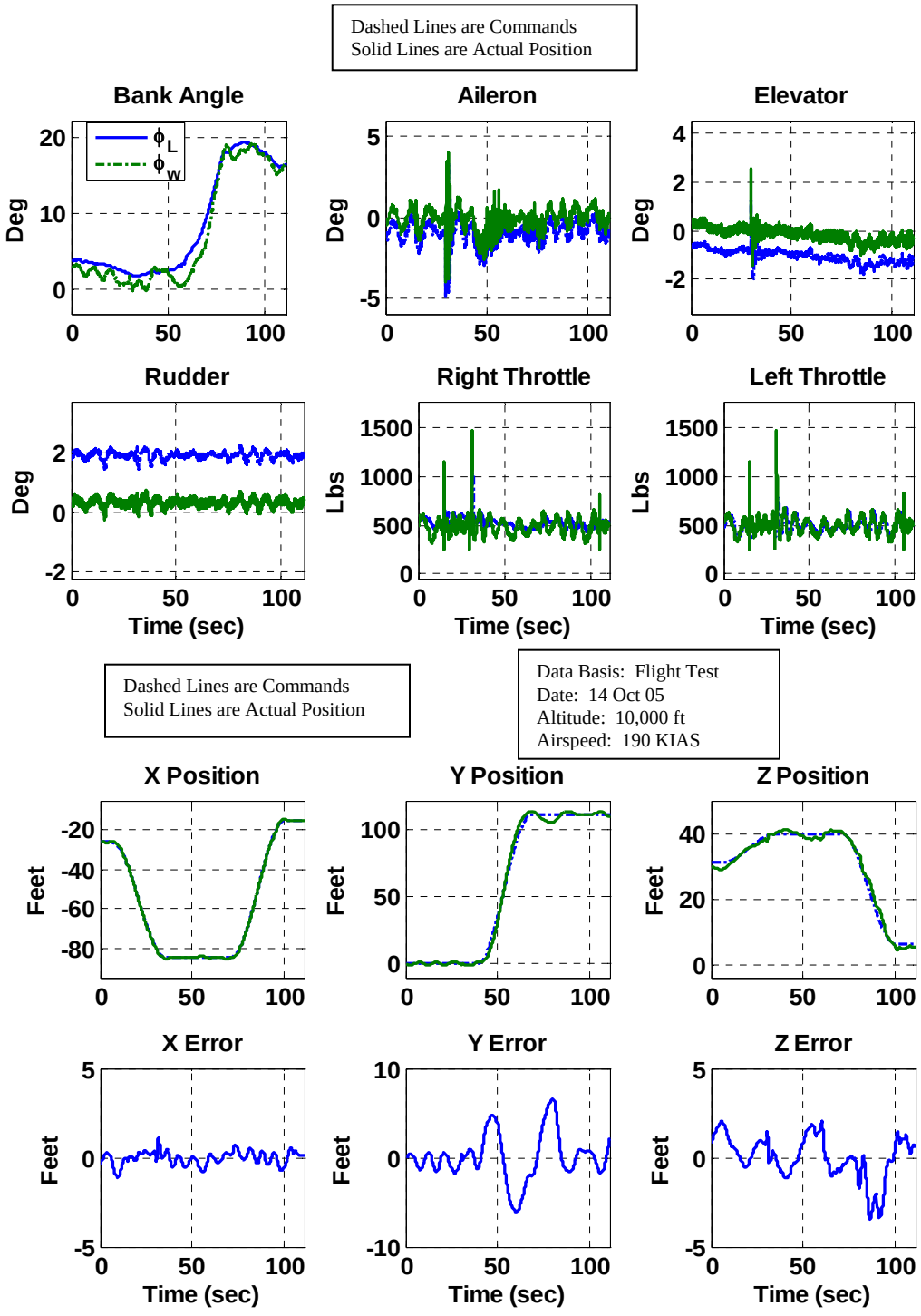

Figure 154. Position Change from Contact to Wing Obs., with Roll at "Back Corner"

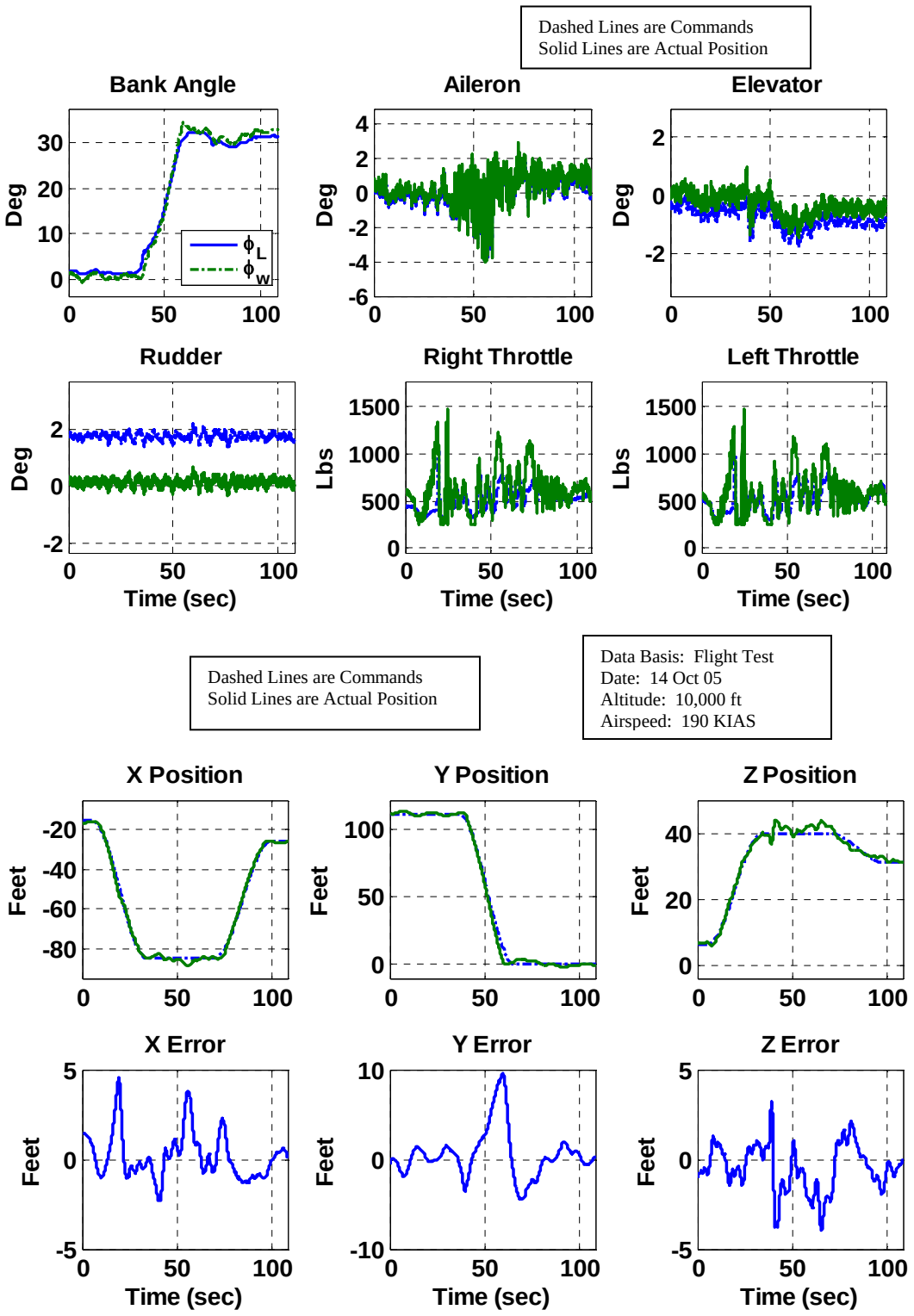

Figure 155. Position Change from Wing Obs. to Contact with 30 Deg Roll into the Wingman at the "Back Corner"

Appendix E: Recorded Parameter List

Table 13. Lead Aircraft Recorded Parameters

No.	Parameter Name	System	Units	Resolution	Sample Rate (Hz)	Media
1	IRIG Time	DAS	Sec	0.001	1000	8mm Tape
2	Event	DAS	-	1	-	8mm Tape
3	Indicated Airspeed	DAS	Knots	1	10	8mm Tape
4	Indicated MSL Altitude	DAS	Feet	1	10	8mm Tape
5	Angle of Attack	DAS	Deg	0.04	76.88	8mm Tape
6	Angle of Sideslip	DAS	Deg	0.04	76.88	8mm Tape
7	Outside Air Temperature	DAS	^{o}C	0.01	10	8mm Tape
8	Roll Angle	DAS	deg	0.03	76.88	8mm Tape
9	Pitch Angle	DAS	deg	0.02	76.88	8mm Tape
10	Time of Day	GAINR	HMS	0.001	10	PCMCIA
11	Time of Day	GAINR	sec	0.001	10	PCMCIA
12	Latitude	GAINR	deg	0.00001	10	PCMCIA
13	Longitude	GAINR	deg	0.00001	10	PCMCIA
14	Ellipsoid Height	GAINR	feet	0.1	10	PCMCIA
15	MSL Altitude	GAINR	feet	0.1	10	PCMCIA
16	Ambient Temperature	GAINR	^{o}C	0.1	10	PCMCIA
17	True Airspeed	GAINR	ft/s	0.1	10	PCMCIA
18	Ψ - PSI - Angle WRT North	GAINR	deg	0.1	10	PCMCIA
19	Θ - THETA - Pitch Angle	GAINR	deg	0.1	10	PCMCIA
20	Φ - PHI – Roll Angle	GAINR	deg	0.1	10	PCMCIA
21	X Pos - N,E,U Coordinates	GAINR	feet	0.1	10	PCMCIA
22	Y Pos - N,E,U Coordinates	GAINR	feet	0.1	10	PCMCIA
23	Z Pos - N,E,U Coordinates	GAINR	feet	0.1	10	PCMCIA
24	X Pos - Geocentric	GAINR	feet	0.1	10	PCMCIA
25	Y Pos - Geocentric	GAINR	feet	0.1	10	PCMCIA
26	Z Pos - Geocentric	GAINR	feet	0.1	10	PCMCIA
27	GPS Time of week	SUT	sec	0.001	20	Laptop File
28	Lead Yaw - Ψ - PSI	SUT	deg	0.001	20	Laptop File
29	Lead Pitch - Θ - THETA	SUT	deg	0.001	20	Laptop File
30	Lead Roll - Φ - PHI	SUT	deg	0.001	20	Laptop File
31	Lead Roll Rate – p	SUT	deg/s	UNK	20	Laptop File
32	Raw GPS Data	SUT	-	N/A	20	Laptop File
33	Transmitted datalink signal	SUT	-	-	20	Laptop File

Note: Not all parameters were available on every flight

Table 14. Wing Aircraft Recorded Parameters

No.	Parameter Name	Units
1	Cockpit communications	Not applicable
2	Time	Sec
3	Learjet Heading (psi)	Degrees
4	Learjet Pitch Angle (theta)	Degrees
5	Learjet Bank Angle (phi)	Degrees
6	Learjet Roll Rate (p)	Degrees/sec
7	Learjet Angle of Attack (alpha)	Degrees
8	Learjet Angle of Sideslip (beta)	Degrees
9	Learjet Z-axis acceleration (Nz)	G's
10	Learjet Indicated Velocity	KIAS
11	Learjet Altitude	Feet
12	Outside air temp	Celsius
13	C-12 Heading (psi)	Degrees
14	C-12 Pitch Angle (theta)	Degrees
15	C-12 Bank Angle (phi)	Degrees
16	C-12 Roll Rate (p)	Degrees/sec
17	GPS Differential Vector, North	Feet
18	GPS Differential Vector, East	Feet
19	GPS Differential Vector, Down	Feet
20	Engage Autopilot Command	None
21	Engage Throttle Command	None
22	Go To Command	None
23	Elevator Command	Degrees
24	Elevator Position	Degrees
25	Aileron Command	Degrees
26	Aileron Position	Degrees
27	Rudder Command	Degrees
28	Rudder Position	Degrees
29	Left Throttle Command	Pounds
30	Left Throttle Position	Pounds
31	Right Throttle Command	Pounds
32	Right Throttle Position	Pounds
33	Speed of Position Change	None
34	k_xe (proportional gain, throttle)	None
35	k_xd (derivative gain, throttle)	None
36	k_xi (integral gain, throttle)	None
37	k_ye (proportional gain, aileron)	None
38	k_yd (derivative gain, aileron)	None
39	k_yi (integral gain, aileron)	None
40	k_phi_err (cmd vs actual bank angle gain)	None
41	k_p_lead (feed forward roll rate gain)	None

42	k_p_err (cmd vs actual roll rate penalty)	None
43	k_ze (proportional gain, elevator)	None
44	k_zd (derivative gain, elevator)	None
45	k_zi (integral gain, elevator)	None
46	k_theta (non-equilibrium pitch penalty gain)	None
47	k_wing_theta_eq (equilib theta estimate)	Deg
48	k_sas (yaw damper gain)	None
49	Contact Position x-body axis	Feet
50	Contact Position y-body axis	Feet
51	Contact Position z-body axis	Feet
52	Pre-Contact Position x-body axis	Feet
53	Pre-Contact Position y-body axis	Feet
54	Pre-Contact Position z-body axis	Feet
55	Back Corner Position x-body axis	Feet
56	Back Corner Position y-body axis	Feet
57	Back Corner Position z-body axis	Feet
58	Wing Observation Position x-body axis	Feet
59	Wing Observation Position y-body axis	Feet
60	Wing Observation Position z-body axis	Feet
61	Tanker to Lear Vector, body axis, x	Feet
62	Tanker to Lear Vector, body axis, y	Feet
63	Tanker to Lear Vector, body axis, z	Feet
64	Tanker to Desired Position, body axis, x	Feet
65	Tanker to Desired Position, body axis, y	Feet
66	Tanker to Desired Position, body axis, z	Feet
67	Post Filter Data, C-12 heading (psi)	Degrees
68	Post Filter Data, C-12 pitch angle (theta)	Degrees
69	Post Filter Data, C-12 bank angle (phi)	Degrees
70	Post Filter Data, C-12 roll rate (p)	Degrees/sec
71	Post Filter Data, Tanker to Lear, North	Feet
72	Post Filter Data, Tanker to Lear, East	Feet
73	Post Filter Data, Tanker to Lear, Down	Feet

Note: All parameters were recorded at 100 Hz, and downloaded from the VSS internal memory after each sortie.

Bibliography

1. Adams, Charlotte. "Automated Refueling of UAVs," *Avionics Magazine*, 30:38-41 (January 2006).

2. Athens, Michael and others. "The Stochastic Control of the F-8C Aircraft Using a Mu ltiple Model Adaptive Control (MMAC) method—Part I: Equilibrium Flight," *IEEE Transactions on Automatic Control*, Vol AC-22, No 5. October 1977.

3. Buzogany, Louis E., *Automated Control of Aircraft in Formation Flight*, MS thesis, A AFIT/GE/ENG/92D-07, School of Engineering, Air Force Institute of Technology (AFIT), Wright-Patterson AFB OH, December, 1992.

4. Dargan, John L., *Proportional Plus Integral Control of Aircraft for Automated Maneuvering Formation Flight*, MS thesis, AFIT/GE/ENG/91D-14, School of Engineering, Air Force Institute of Technology (AFIT), Wright-Patterson AFB OH, December, 1991.

5. Davis, Brooke. *First Ever Coordinated UAV Flight Makes History*, AFMC News Service Release 0825, Air Force Flight Test Center Public Affairs, 16 Aug 2004. http://www.afmc.wpafb.af.mil/organizations/HQ-AFMC/PA/news/archive/2004/August/0825-04.htm

6. Department of Defense. *Flying Qualities of Piloted Aircraft*. MIL STD 1797A. Washington: Government Printing Office, 1990.

7. Department of Defense. *USAF Test Pilot School Flying Qualities Phase Textbook, Part IV*. Air Force Flight Test Center, Edwards AFB CA, 20 February 2002.

8. Hall, James K., *Three Dimensional Formation Flight Control*, MS Thesis, AFIT/GAE/ENY/00M-06, School of Engineering, Air Force Institute of Technology (AFIT), Wright-Patterson AFB OH, March, 2000.

9. Hanson, Curtis E. and others. *An Overview of Flight Test Results for a Formation Flight Autopilot.* NASA/TM-2002-210729. Edwards CA: NASA Dryden Flight Research Center, 2002.

10. McCamish, Sean J., *Advanced Formation Flight Control*, MS thesis, AFIT/GE/ENG/95D-16, School of Engineering, Air Force Institute of Technology (AFIT), Wright-Patterson AFB OH, December, 1995.

11. Nelson, Robert C., *Flight Stability and Automatic Control* (2nd Edition), Boston: McGraw-Hill Companies, Inc, 1998.

12. Ogata, Katsuhiko. *Modern Control Engineering* (Fourth Edition). Upper Saddle River NJ: Prentice Hall, Inc., 2002.

13. Osteroos, Ryan K. *Full Capability Formation Flight Control*, MS thesis, AFIT/GAE/ENY/05-M16, School of Engineering, Air Force Institute of Technology (AFIT), Wright-Patterson AFB OH, February, 2005.

14. Osteroos, Ryan, and others. *Limited Evaluation of the Automatic Formation Flight Controller (Project SOLO FORM)*, AFFTC-TIM-04-08, Air Force Flight Test Center, Edwards AFB CA, December 2004.

15. Peters, Patrick J. *Modification Operational Supplement: C-12C, Serial Number 73-1215*, Department of Defense, Edwards AFB CA, 21 March 2005.

16. Proud, Andrew W., *Close Formation Flight Control*, MS thesis, AFIT/GE/ENG/99M-24, School of Engineering, Air Force Institute of Technology (AFIT), Wright-Patterson AFB OH, March, 1999.

17. Raquet, John F. Class notes, EENG 533, Global Positioning System. School of Electrical Engineering, Air Force Institute of Technology, Wright-Patterson AFB OH, Spring Quarter 2004.

18. Reyna, Vincent P., *Automation of Formation Flight Control*, MS thesis, AFIT/GE/ENG/94M-01, School of Engineering, Air Force Institute of Technology (AFIT), Wright-Patterson AFB OH, March, 1994.

19. Rohs, Paul R., *A Fully Coupled, Automated Formation Control System for Dissimilar Aircraft in Maneuvering, Formation Flight*, MS thesis, AFIT/GE/ENG/91M-03, School of Engineering, Air Force Institute of Technology (AFIT), Wright-Patterson AFB OH, March, 1991.

20. Roskam, Jan. *Airplane Flight Dynamics and Automatic Flight Controls, Part I.* Ottawa, KS: Roskam Aviation and Engineering Corporation, 1982.

21. Ross, Steven and others. *Demonstration of Control Algorithm for Autonomous Aerial Refueling (AAR) (Project NO GYRO)*, AFFTC-TIM-05-10, Air Force Flight Test Center, Edwards AFB CA, December 2005.

22. Stevens, Brian L. and Frank L. Lewis. *Aircraft Control and Simulation* (2nd Edition). New Jersey: John Wiley & Sons, Inc., 2003.

23. Taschner, Michael J. *Modification Flight Manual: C-12C Serial Number 73-215*, Department of Defense, Edwards AFB CA, 23 September 2002.

24. Veth, Michael J., *Advanced Formation Flight Control*, MS thesis, AFIT/GE/ENG/94D-30, School of Engineering, Air Force Institute of Technology (AFIT), Wright-Patterson AFB OH, December, 1994.

Vita

Captain Steven M. Ross was raised in Sacramento, California, and entered undergraduate studies at the United States Air Force Academy (USAFA) in 1992, where he graduated with a Bachelor of Science degree in Engineering Sciences and a minor in Japanese Language Studies. He was commissioned as a Second Lieutenant and recognized as the Outstanding Student in Japanese Studies and a Distinguished Graduate of USAFA's Class of 1996.

Shortly after graduation, Captain Ross married his wonderful wife, and they enjoyed a casual status assignment as a sailplane instructor pilot at the Academy. Shortly thereafter, they moved to Sheppard AFB, Texas for pilot training in the Euro-NATO Joint Jet Pilot Training (ENJJPT) course. Captain Ross completed the course as a Distinguished Graduate, and was assigned to fly the F-15C. After a 6 month conversion course at Tyndall AFB, Florida, he and his wife moved to Kadena AFB, Japan, where he served as a combat fighter pilot.

Captain Ross returned to Sheppard AFB at the end of 2001, where he served as an instructor pilot in the T-37 for two student classes, and was recognized by both as the Outstanding Instructor. While at Sheppard, Captain Ross was graced with a daughter, and in 2003 was selected for the Air Force Institute of Technology/Test Pilot School (AFIT/TPS) program. While taking classes at AFIT, he was blessed again with a son. Captain Ross has completed the TPS portion of the program as a Distinguished Graduate and upon graduation from AFIT will be assigned to Eglin AFB, Florida as a test pilot in the F-15.

REPORT DOCUMENTATION PAGE	Form Approved OMB No. 074-0188

1. REPORT DATE *(DD-MM-YYYY)*	2. REPORT TYPE	3. DATES COVERED *(From – To)*
23-03-2006	**Master's Thesis**	Aug 03 – Mar 06

4. TITLE AND SUBTITLE

Formation Flight Control for Aerial Refueling

5a. CONTRACT NUMBER

5b. GRANT NUMBER

5c. PROGRAM ELEMENT NUMBER

6. AUTHOR(S)

Ross, Steven, M., Captain, USAF

5d. PROJECT NUMBER

5e. TASK NUMBER

5f. WORK UNIT NUMBER

7. PERFORMING ORGANIZATION NAMES(S) AND ADDRESS(S)
Air Force Institute of Technology
Graduate School of Engineering and Management (AFIT/EN)
2950 Hobson Way
WPAFB OH 45433-7765

8. PERFORMING ORGANIZATION REPORT NUMBER

AFIT/GAE/ENY/06-M35

9. SPONSORING/MONITORING AGENCY NAME(S) AND ADDRESS(ES)
TPS/EDT
Gary Aldrige
220 S. Wolfe Ave Bldg 1220
Edwards, CA 93524-6485

10. SPONSOR/MONITOR'S ACRONYM(S)

11. SPONSOR/MONITOR'S REPORT NUMBER(S)

12. DISTRIBUTION/AVAILABILITY STATEMENT
APPROVED FOR PUBLIC RELEASE; DISTRIBUTION UNLIMITED.

13. SUPPLEMENTARY NOTES

14. ABSTRACT

A close formation flight controller is designed for automated air refueling and was flown in the first fully autonomous close formation flight. A formation simulator is designed with independent models, a lead aircraft autopilot, and disturbance models from flight and actual hardware limitations. Formation flight control theory and control laws are developed for the controller, as well as mechanization issues such as initialization techniques and command logic to drive position changes to the contact, pre-contact, and wing observation positions. The controller is simulated with an investigation of sensitivity and robustness. Flight test results are presented from seven formation sorties of a C-12 and a LJ-25 under fully autonomous control simulating air refueling. Close formation flight control lessons are discussed for control theory and flight test.

15. SUBJECT TERMS
No Gyro C-12 Aircraft LJ-25 Aircraft Autonomous Aerial Refueling Automatic Air Refueling DGPS (Differential GPS) IMU (Inertial Measurement Unit) Autopilot MEMS (Micro Electrical Mechanical System) Learjet Unmanned Aerial Vehicle (UAV) Joint Unmanned Combat Air Systems (JUCAS) Flight Testing Automated Formation Flight Test Controller Control Laws

16. SECURITY CLASSIFICATION OF:			17. LIMITATION OF ABSTRACT	18. NUMBER OF PAGES	19a. NAME OF RESPONSIBLE PERSON
REPORT	ABSTRACT	c. THIS PAGE			Dr. David R. Jacques AFIT/SYE
U	**U**	**U**	**UU**	280	**19b. TELEPHONE NUMBER** *(Include area code)* (937) 255-3355 x3329